



NATIONAL TECHNICAL UNIVERSITY OF ATHENS

**Examination of suitability of the Strut and Tie model, for the
design of reinforced concrete elements**

UNDERGRADUATE THESIS MSC

Analysis and Design of Earthquake Resistant Structures

PAUL TOURATZIDIS

Advisor

Konstantionos V. Spiliopoulos
Professor at institute for Structural Analysis &
Antiseismic Research (ISAAR)
School of Civil Engineering, NTUA

Athens, October 2021

Contents

Chapter 1

Intoduction

1.1 The Strut and Tie model

1.2 The structure's B- and D-regions

1.3 Principles of strut-and-tie model design

1.4 Modelling of individual D-regions

1.5 Dimensioning the struts, ties and nodes

1.6 Applications

Chapter 2

AStrutTie model

2.1 Introduction

2.2 *ModelingofMemberGeometry*

2.3 *Templates of AStrutTie*

2.4 *ApplicationofLoads*

2.5 *StructuralAnalysisforESO&StressFlow*

2.6.1 *StrutTypes*

2.6.2 *TieTypes*

2.6.3 *NodeTypes*

2.7 *Elements of the templates*

Chapter 3

FEM Programm FE77

3.1 Introduction

3.2 *Concrete modeling*

3.3 *Reinforcement steel modeling*

3.4 *Failure criterion*

3.5 Proposed Numerical strategy

Chapter 4

Abaqus Damage Plasticity Model (DPM)

4.1 Introduction

4.2 Mechanical behavior

4.3 Uniaxial tension and compression stress behavior

4.4 Multiaxial behavior

4.5 Reinforcement

4.6 Defining tension stiffening

4.7 Postfailure stress-strain relation

4.8 Fracture energy cracking criterion

4.9 Implementation

4.10 Defining compressive behavior

4.11 Defining damage and stiffness recovery

4.12.1 Tensile damage

4.12.2 Compressive damage

4.13 Concrete plasticity

Chapter 5

Solution of beams with different ratios $\frac{a}{d}$ and $\frac{l}{h}$ with the Strut and Tie model

5.1 Case 1, $\frac{a}{d}=1.0$

5.2 Case 2, $\frac{a}{d}=1.0$

5.3 Case 2, $\frac{a}{d}=1.0$, with Canadian Standards(1984)

5.4 Case 3, $\frac{a}{d}=1.5$

5.5 Results from Strut and Tie modeling

5.6 Deep beam with Fe77 and with Strut and tie model, and comparisons

5.7 Flexural beam with Fe77 and comparison with Strut and tie model.

Chapter 6

Nonlinear Cyclic Truss Model for Reinforced Concrete Structures

6.1 Introduction

6.2 Nonlinear truss modeling approach

6.3 Constitutive stress-strain relationships

6.4.1 Concrete Model for Vertical and Horizontal Truss Elements

6.4.2 Concrete Model for Diagonal Truss Elements

6.5 Model validation

6.6 Wall details

6.7 Results and discussion

Bibliography

Chapter 1

1.1 Introduction

Certain parts of structures are designed with almost exaggerated accuracy while other parts are designed using rules-of-thumb or judgment based on past experience. However, all parts of a structure are of similar importance and must be carefully designed. A unified design concept, which is consistent for all types of structure and all their parts, must be based on realistic physical models. Strut-and-tie models, a generalisation of the well-known truss analogy for beams, are proposed here as the appropriate approach for designing structural concrete, which includes both reinforced and prestressed concrete structures. ACI codes, Eurocodes and other international codes, allow the use of these models, in certain cases.

It was actually at the turn of the last century, when Ritter and Morsch introduced the truss analogy, for concrete beams that are cracked, and so the theory of elasticity is not valid. This method was later refined and expanded by Leonhardt, Kupfer, and others, and Marti and Mueller created its scientific basis for a rational application in tracing the concept back to the theory of plasticity. Collins and Mitchell further considered the deformations of the truss model and derived a rational design method for shear and torsion.

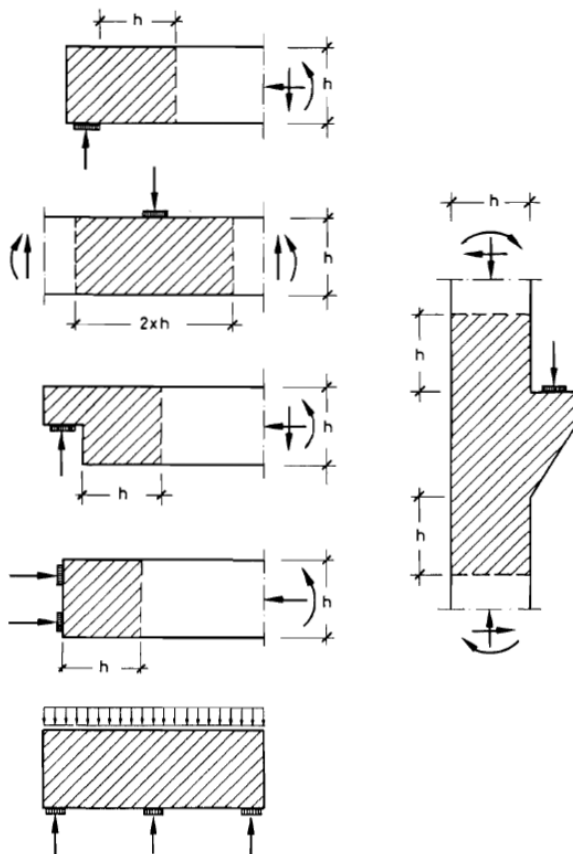
In various applications, Bay, Franz, Leonhardt, Kupfer had shown that strut-and-tie models could be usefully applied to deep beams and corbels.

The method is applied to a few new examples, using also the Commercial Programm "AStrutTie" that is based in the strut-and-tie model, including some comparison with test results. Comparison is done also with the results of FE programmes, that are "Abaqus Cae", and FE77. The main features of these programs, are discussed later. Some of the examples that are given, show that the strut-and-tie method is useful not only in dimensioning given members but also in developing an adequate conceptual design for a critical detail.

1.2 The structure's B- and D-regions

Reinforced concrete may be divided into regions that are called B-regions and D-regions. Those regions of a structure, in which the Bernoulli hypothesis of linear strain distribution is assumed valid, will be referred to as B-regions (where B stands for beam or Bernoulli). As a result, plane sections remain plane, before and after the bending. Their internal forces or stresses can be derived from moments, shear and axial forces analysed by means of the statical system of beams, frames, plates, etc. If uncracked, the stresses are calculated using the bending theory for linear elastic material. For cracked B-regions the truss-analogy models or the

standard methods of codes apply. These standard methods are not applicable to the other regions and details of a structure, where the strain distribution is significantly non-linear, e.g. near concentrated loads, corners, bends, openings and other discontinuities (Fig 1). Such regions will be called D-regions, where D stands for discontinuity, disturbance or detail. The internal flow of forces in D-regions can be reasonably well described by Strut-and-Tie models. Not much accuracy is necessary in determining the dividing sections between B- and D-regions. These sections can be assumed to lie approximately in a distance h from the geometrical discontinuity or the concentrated load, where h is equal to the depth of the adjacent B-region (Fig 1). This assumption is justified by Saint-Venant's principle. This principle states that the stress due to axial load and bending approach a linear distribution at a distance approximately equal to the overall depth of the member, h , away from a discontinuity. Therefore, St. Venant's principle does not apply to sections located closer than distance ' h ' from a discontinuities in the applied load or geometry.



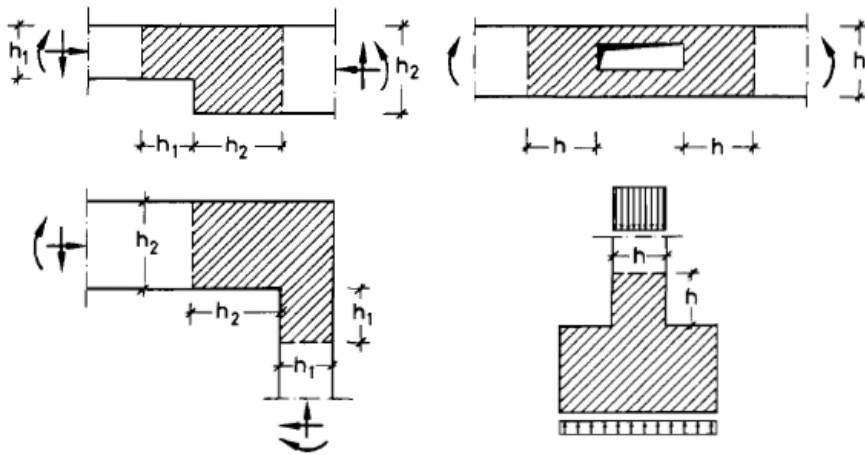


Figure 1. D-Regions due to statical or geometrical discontinuities

1.3 Principles of strut-and-tie model design

Strut-and-tie modeling is currently the most rational and simple method for designing non-flexural members, that contain significant extend of D-regions. The Strut-and-Tie modeling is based on the lower-bound theorem of plasticity. According to this theory, the actual capacity of a structure is always less than the actual capacity of the structure if the following requirements are met:

- (a) The truss is in equilibrium
- (b) Sufficient deformation capacity exists to distribute forces according to the assumed truss model
- (c) The stresses applied to the elements do not exceed their yield or plastic flow capacity

Like a real truss, a strut-and-tie model consists of some struts and some ties. In a strut-and-tie model the struts represent concrete stress fields with prevailing compression in the direction of the strut. Accordingly, the ties normally represent one or several layers of tensile reinforcement. However, model ties can occasionally also stand for concrete tensile stress fields. This is evident from models of practically approved details, the structural safety of which can be explained only if concrete ties are assumed in places where no reinforcement is provided. Typical examples are slabs without stirrups or bar anchorages without spiral or transversal reinforcement.

As far as struts are concerned, they are frequently idealized as prismatic or uniformly tapering members as shown in *figure 2*. This is because the

concrete stress fields are wider at the midlength of the strut than at the ends. These struts are sometimes called *bottle-shaped*. If a suitable model of a D-region is known, the forces of the struts and ties will be calculated, thereby satisfying equilibrium between applied loads checked to carry the inner forces, as described later. This method implies that the structure is designed according to the lower bound theorem of the theory of plasticity. However, since structural materials, in particular concrete, permit only limited plastic deformations, the internal structural system (the strut-and-tie model) has to be chosen in a way that the deformation capacity is not exceeded at any point, before the assumed state of stress is reached in the rest of the structure. In highly stressed regions, this ductility requirement is fulfilled by adapting the struts and ties of the model to the direction and size of the internal forces as they would appear from the theory of elasticity.

In normally or lightly stressed regions the direction of the struts and ties in the model may deviate considerably from the elastic pattern without exceeding the structure's ductility. The ties, and hence the reinforcement, may be arranged according to practical considerations. The structure adapts itself to the assumed internal structural system.

This method of orientating the strut-and-tie model along the force paths indicated by the theory of elasticity obviously neglects some ultimate load capacity which could be utilised by a pure application of the theory of plasticity. On the other hand, it has the major advantage that the same model can be used for both the ultimate load and the serviceability check.

If, for some reason, the purpose of the analysis is to find the actual ultimate load, the model can easily be adapted to this stage of loading by shifting its struts and ties in order to increase the resistance of the structure. In this case, however, the rotation capacity of the model has to be considered.

Strut-and-tie modelling obviously provides the structural analyst with some freedom of choice which can be used to aim either at the safest or at the cheapest or at an otherwise optimised solution. Modelling therefore requires some design experience as does the choice of a representative overall statical system or of a reasonable finite element net.

The modelling process also covers much of what is normally called detailing and therefore requires considerable knowledge about practicable reinforcement layout; on the other hand, it is just in this field where strut and-tie models replace experience and guesswork by a more systematic and understandable design.

1.4 Modelling of individual D-regions

Before modelling of a D-region begins, all the forces and reactions acting on the D-region must be evaluated (Fig 2). The forces or stresses in sections bounded by B-regions are taken from B-region design.

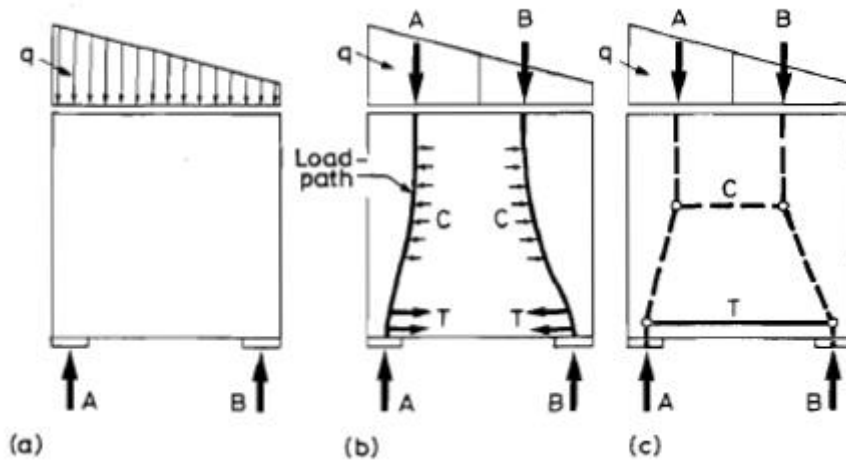


Figure 2. The Structure with its loads, the load path and the strut-and-tie model.

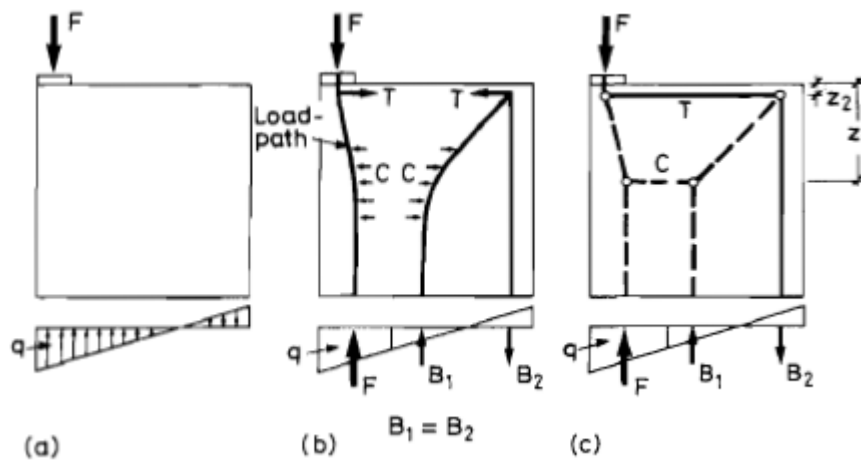


Figure 3. The Structure with its loads, the load path and the strut-and-tie model, for concentrated load.

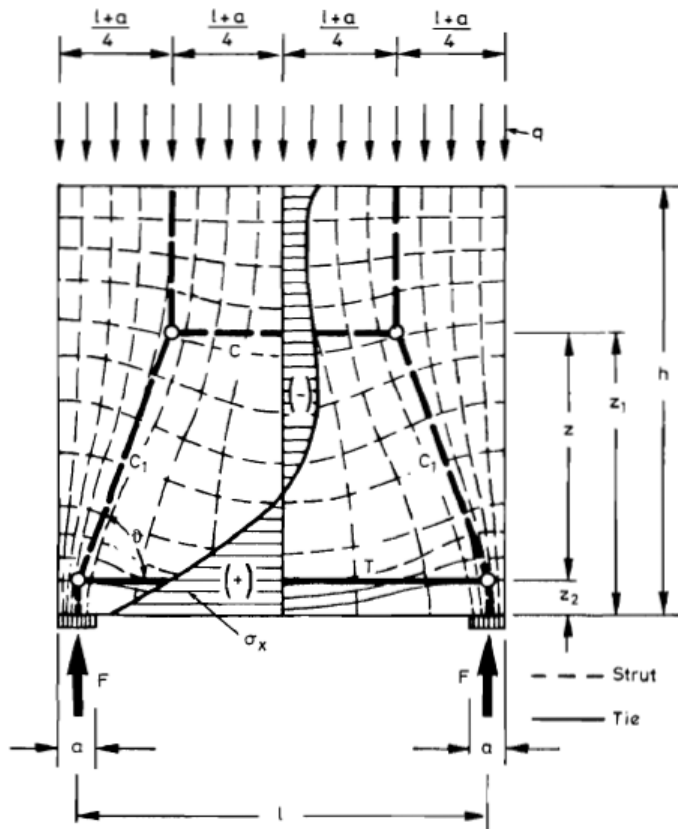


Figure 4. Distribution of elastic stresses, and the strut-and-tie method model.

New strut-and-tie models can be systematically developed by tracing the flow of forces through the structure, using the 'load path' method.

After the selection of an STM, defining the geometry of the nodal regions is required to calculate stresses on each nodal face. Nodal geometry is an idealization of regions in the STM where struts and ties are equilibrated. The stress diagrams of all the forces applied to the D-region boundaries are subdivided in such a way that the individual stress resultants on opposite sides of the D-region correspond in magnitude and can be connected by streamlined 'load paths' which do not cross each other

(Fig 2). After sketching the load paths smoothly curved and replacing them by polygons, further struts and ties must be added for transverse equilibrium (Fig 2).

Obviously, in some cases the stress diagrams or the loads are not completely balanced with the load paths described; then the load path for the remaining forces enters the structure and leaves it after a U-turn on the same side (Fig 3).

Developing a model of a D-region is much simplified if the elastic stresses and principal stress directions are available from an elastic FEM analysis. The direction of struts can then be taken in accordance with the mean and main direction of principal compressive stresses, or the more important struts and ties can be located at the center of gravity of the stress diagram of typical sections (Fig 4).

When modelling, the angles between struts and ties, in particular those with relatively high forces, should be chosen larger than 45° (better 60°) in order to avoid incompatibility problems.

The resulting models are quite often kinematic, which means that the geometry of such a model is strictly related to a particular load configuration and cannot be used for other loads without modification. Therefore, the governing load combinations have to be investigated. This disadvantage is not a peculiarity of the strut-and-tie method but is inherent to the non-linear material properties of cracked concrete.

So, the layout of a strut-and-tie model follows the rules below:

Equilibrium

1. The STM model must be in equilibrium with the external loads.
2. The ties cannot cross or overlap, because this would contradict the distribution of elastic stresses, while ties can cross struts.
3. The STM model should be compatible with the flow of forces from loads through the D-regions, that may come from a FEA.
4. Because ties consist of an arrangement of steel bars, that are always placed orthogonally in the member, there is a restriction on the conformance of ties with tensile stress trajectories.
5. It is generally assumed that the structure will have enough plastic deformation capacity to adapt to the directions of the struts and ties chosen in design if they are within $\pm 15^\circ$, according to the ACI recommendations. In addition, ties should give a practical reinforcement layout
6. The loads try to follow the path with the least forces and deformations. Due to the fact that the tensile ties are more deformable than the struts, the model should have the least and the shortest ties. Figure (6), shows two different types of a STM model, the correct and the noncorrect.

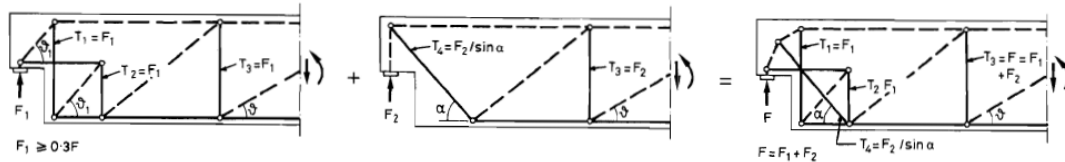


Figure 5. Combination of two different strut-and-tie models

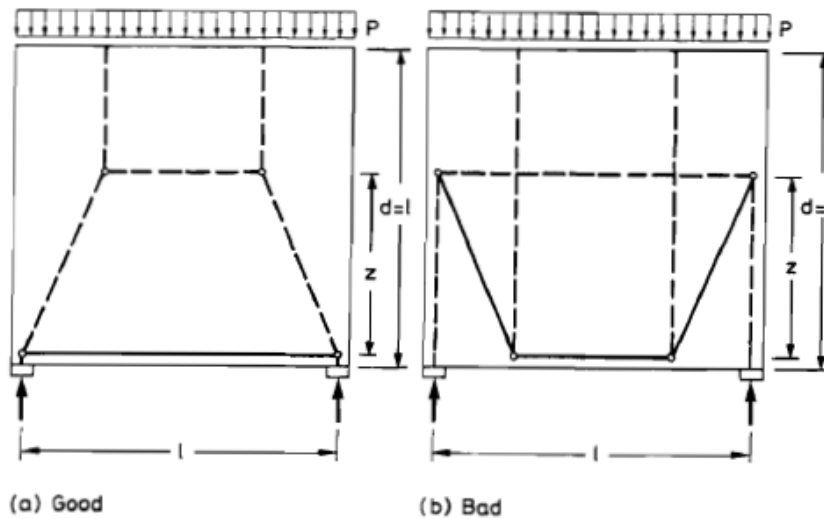


Figure 6. The appropriate strut-and-tie model(a),and the non-appropriate one(b).

Accordingly, superposition of two models is possible only if the combined model satisfies the requirements on reasonable angles between struts and ties. By combining two simple models it is sometimes possible to develop much better but rather complicated models (Fig 5). Instead of investigating such a hyperstatic model with representative stiffnesses of the struts and ties, it is normally more adequate to immediately allow the loads to the two simple models with an eye on the expected stiffness ratio of the individual models.

Doubts could arise as to whether the correct model has been chosen out of several possible ones (Fig 6). In selecting the model, it is helpful to realise that loads try to use the path with the least forces and deformations. Since reinforcement ties are much more deformable than concrete struts, the model with the least and shortest ties is the best.

Next, we will show what is the difference between the different types of the STM, that can be chosen.

1.5 Dimensioning the struts, ties and nodes

Reinforced and unreinforced ties

Normally tie forces are carried by reinforcement. Its cross-section follows from the tie force in the ultimate limit state and the design yield strength of the steel. For crack distribution the reinforcement shall be distributed over the tensile zone. Crack widths can be analysed if the reinforced tie is considered as a prismatic reinforced bar with an effective concrete area. The tensile strength of concrete should be utilised for equilibrium forces only if no progressive failure must be expected and if local failure zones are assumed. Thereby restraint forces and microcracks have to be taken into account even in 'uncracked' concrete. Further, some positive experience with similar details and loading should be available.

Concrete struts or compression stress fields

To cover all cases of compression stress fields, three typical configurations are sufficient.

(a) The fan-shaped stress field (Fig 7(a)) is an idealisation of a stress field with negligible curvature. It does not develop transverse stresses.

(b) The bottle-shaped stress field (Fig 7(b)), with its bulging stress trajectories, develops considerable transverse stresses: compression in the bottle neck and tension further away. The transverse tension can cause longitudinal cracks and initiate an early failure. It is therefore necessary to reinforce the stress field in the transverse direction or to consider the transverse tension when determining the failure load of the strut. The transverse tension can be determined from a strut-and-tie model of the stress field. Diagrams simplify its dimensioning (Fig 8).

(c) The prismatic or parallel stress field (Fig 7(c)) is a frequent special case of the preceding two stress fields. The fan-shaped and the bottle-shaped stress fields are frequently found in D-regions where concentrated loads are introduced into a structure and spread out. The prismatic stress field is typical for B-regions.

The strength of the concrete in compression stress fields depends to a considerable extent on the multiaxial state of stress and on disturbances from cracks and reinforcement. For practical dimensioning of all kinds of stress fields, the following simplified design strength values $f_{cd,1}$ are proposed:

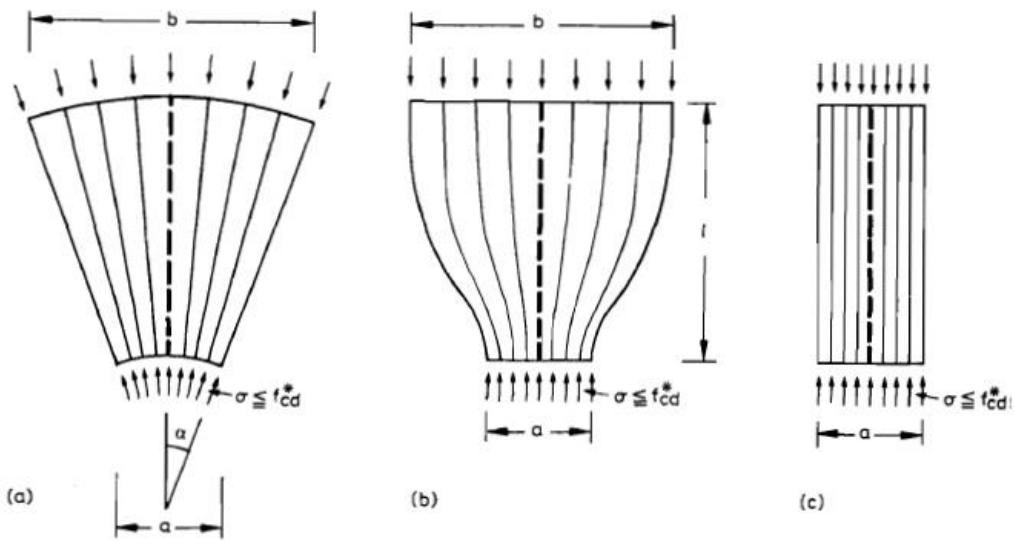


Figure 7. The basic compression fields

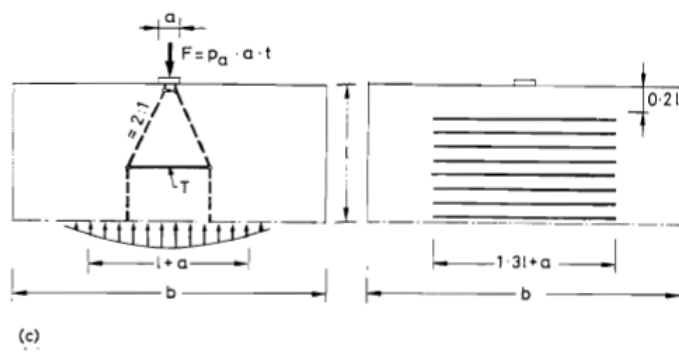
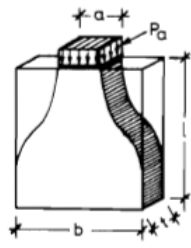
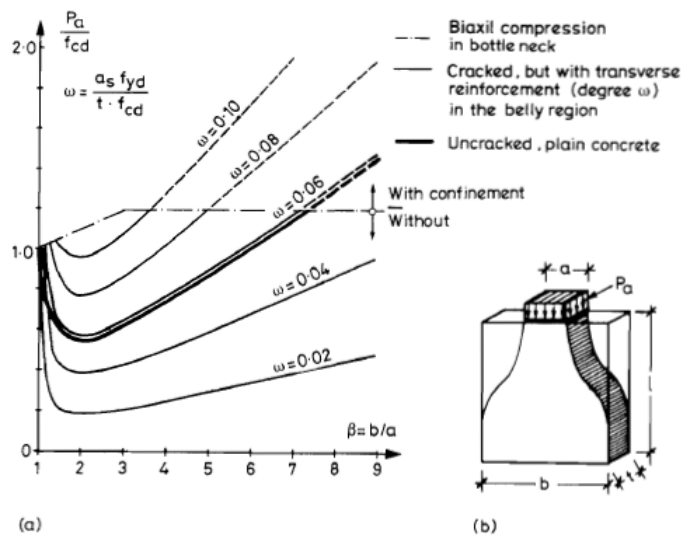


Figure 8. Combination of two different strut-and-models

$f_{cd,1} = 1.0 f_{cd}$ for an undisturbed and uniaxial state of stress

$f_{cd,1} = 0.8 f_{cd}$ for compression fields with cracks parallel to the compression stresses

$f_{cd,1} = 0.6 f_{cd}$ for compression fields with skew cracks where f_{cd} denotes the concrete compressive design strength for uniaxial compression according to the Code of Practice.

The design values given above for cracked concrete are meant for structural concrete, whose crack widths are limited in the usual manner. The values for cracked concrete shall also be applied for concrete with transverse tension below the expected tensile strength and if tensile reinforcement is crossing the stress field. Skew cracks are not expected if the theory of elasticity is closely followed during modelling. However, skew cracks may also be left over from a previous loading case with a different stress situation. The increase in strength due to 2- or 3-dimensional states of compressive stresses may be taken into account if the simultaneously acting transverse compressive stresses are reliable. Before deciding on one of the given strength values, both transverse directions must always be considered.

The nodes

The nodes are in reality, regions where forces are deviated over a certain length and widths. The 'smeared' or 'continuous' nodes, where wide concrete stress fields join each other or with closely distributed reinforcing bars, are not critical; it is sufficient to ensure safe anchorage of the reinforcing bars in the smeared node and to catch the outermost fibers of the deviated compressive stress field with reinforcement (Fig 9).

On the other hand, where concentrated forces are applied the deviation of forces is locally concentrated in 'singular' or 'concentrated' nodes. These have to be carefully designed in order to balance the oncoming forces of the struts and ties without excessive deformations resp. cracks.

Though numerous cases of different singular nodes exist, in most cases their forces balance each other in the node region through direct compressive stresses. Also bond is essentially a load transfer via compressive stresses which are supported by the ribs of the steel bar and by radial pressure in bent bars. However, in many cases also concrete tensile stresses develop transverse to the model plane ('third direction'). The stress distribution in singular nodes is mostly so complicated that it cannot be analysed individually with bearable expenditure. But experience

shows that some types of nodes and detail are repeated again and again in quite different structures and can be designed safely by simplified rules:

(a) The geometry of the node has to be tuned with the applied forces. Therefore, reinforcement anchored in the node should be distributed over a certain height u with due regard to the widths of the oncoming stress

fields and the magnitude of their forces; further, it should be adequately distributed in the transverse direction in order to keep transverse tensile stresses low.

(b) The average compressive stresses in the node region boundaries have to be checked to be less than

$f_{cd,1} = 1.1f_{cd}$ in nodes where only compression struts meet, thus creating a 2- or 3-dimensional state of compressive stresses in the node region

$f_{cd,1} = 0.8f_{cd}$ in nodes where tensile bars are anchored and an allowance in strength must be made for bond action

Suitable node region boundaries and the corresponding compression stresses can easily be determined, as shown in the typical nodes in figures 10-13. As for all nodes, also the stresses of the oncoming struts have to be checked as described earlier.

(c) Safe anchorage of ties in the node has to be assured: minimum radius of bent bars and anchorage lengths of bars are selected following the Code. The anchorage must be located within and 'behind' the node (Figs 11 and 13). The anchorage begins where the transverse compression stress trajectories meet the bar and are deviated. The bar must extend to the other end of the node region. If this length is less than required by the Code, the bar may be extended beyond the node region and introduce some of its forces from behind.

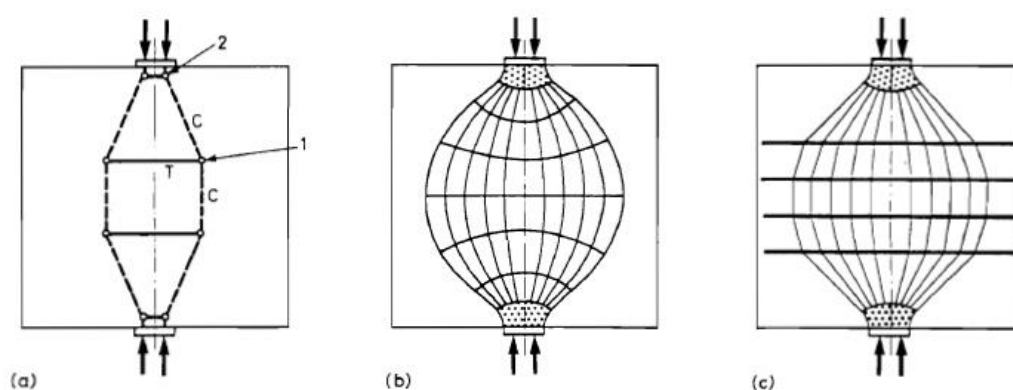


Figure 9. Smeared Nodes, (a) Strut-and-tie model, (b), (c) Stress fields and node regions

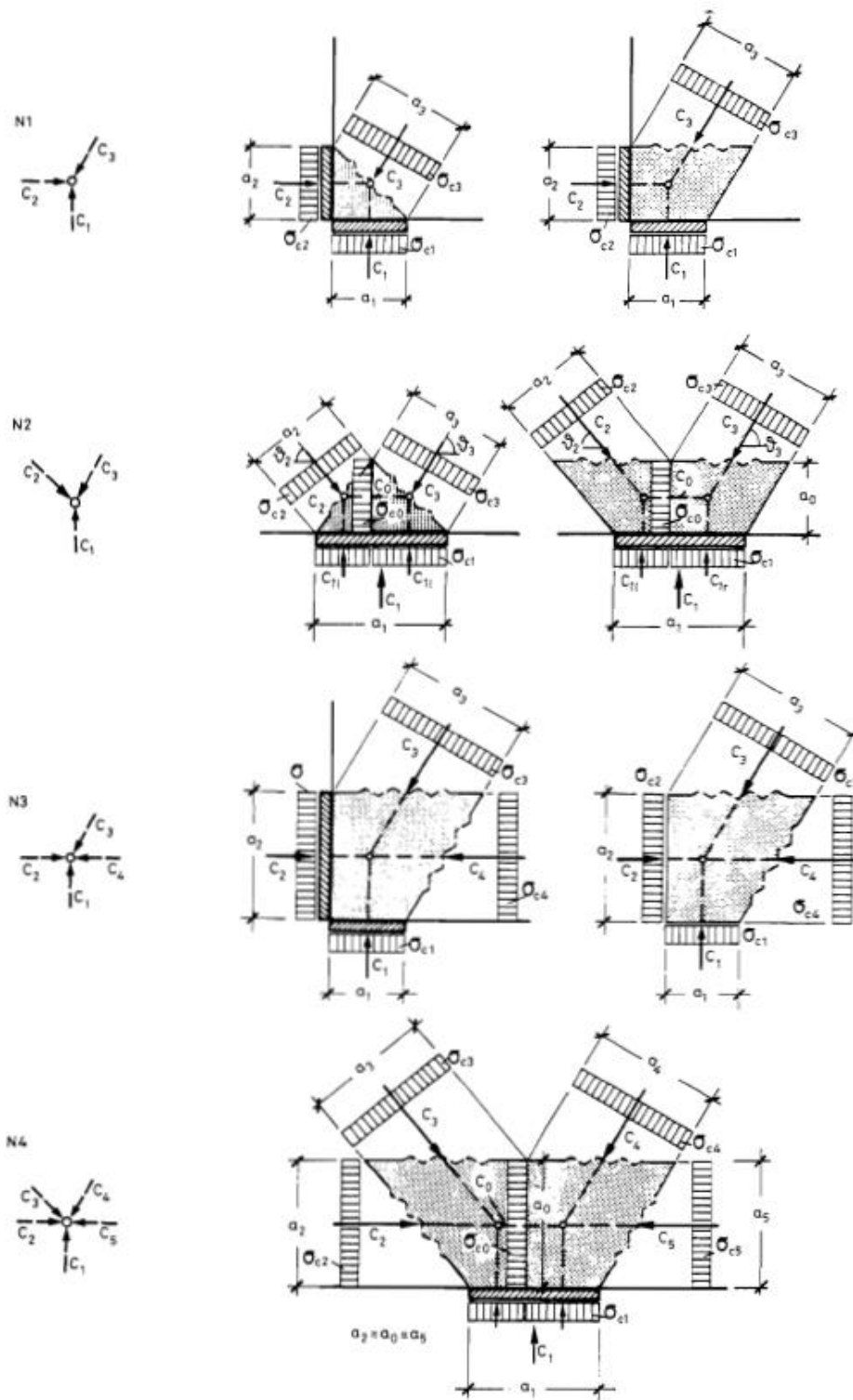


Figure 10. Nodes with anchorage of reinforcement

Node N1 (Fig 10) is typical for a node of compression struts in a corner. Two alternative node region boundaries are shown for the same node, both leading to the same results. The node is safe, if

$$\sigma_{c1}, \sigma_{c2}, \sigma_{c3} \leq 1.1f_{cd}$$

Node N2 (Fig 10) is a combination of two nodes N1. It is realistic and convenient to choose a_0 large enough,

$$a_0 \geq a_1 \cos \theta_2 \sin \theta_2 = a_1 \cos \theta_3 \sin \theta_3$$

in order that the bearing pressure $\sigma_{cl} \leq 1.1 f_{cd}$ governs the node's design.

Nodes N3 and N4 (Fig 10) are typical for loads or support forces applied to the edge of a structure with a chord force running parallel to this edge through the node. Normally, the concrete compressive stresses σ_{co} and $\sigma_{cl} \leq 1.1 f_{cd}$ govern to the design.

Node N5 (Fig 11) applies to the anchorage of ties far from the edges, i.e. inside the structure in the plane of the model. As for all nodes with ties, the anchorage length must be checked.

Node N6 (Fig 11) is typical for end supports. The height u in deep beams should be chosen

$$u \cong 0.15h \leq 0.2h \leq 0.2l$$

where h is the height of D-region and l is the span of deep beam. Single-layer reinforcement shall be placed near the lower edge, where the deviation forces are largest. Checks include

$$\sigma_{c1}, \sigma_{c2} \leq 0.8 f_{cd}$$

Node N7 (Fig 11) is typical in the tension chord of beams or deep beams. Thin, well-distributed bars shall be chosen as reinforcement for tie T_2 and they shall embrace tie T_1 . Concrete stresses $\sigma_c \leq 0.8 f_{cd}$ will rarely be decisive.

Node N8 (Fig 11) is a mixture of the nodes N1 and N6, and therefore maximum compression stresses between those of both node types are proposed:

$$\sigma_{c1}, \sigma_{c2} \leq f_{cd}$$

Besides, the rules for typical node N6 apply.

Node N9 (Fig 11) is composed of two nodes N5; checks are accordingly. This node is typically over the support of continuous beams and normally also covered by the Code rules (check the beam's cross-section for M , N and V , bearing pressure, anchorage of chord reinforcement).

Node N10 (Fig 12) is checked via the admissible radius of the bent bar. In nodes with local pressure ($a < t$, fig. 13), the transverse tension in the third direction must be covered by transverse reinforcement designed for

$$T = 0.25 \times \frac{t-a}{t} \times C_1$$

Local pressures σ_{c11} may be tolerated up to

$$\sigma_{c11} = \frac{C_1}{a_t a_1} \leq \frac{t}{a_t} f_{cd,1} \leq 3.3 f_{cd}$$

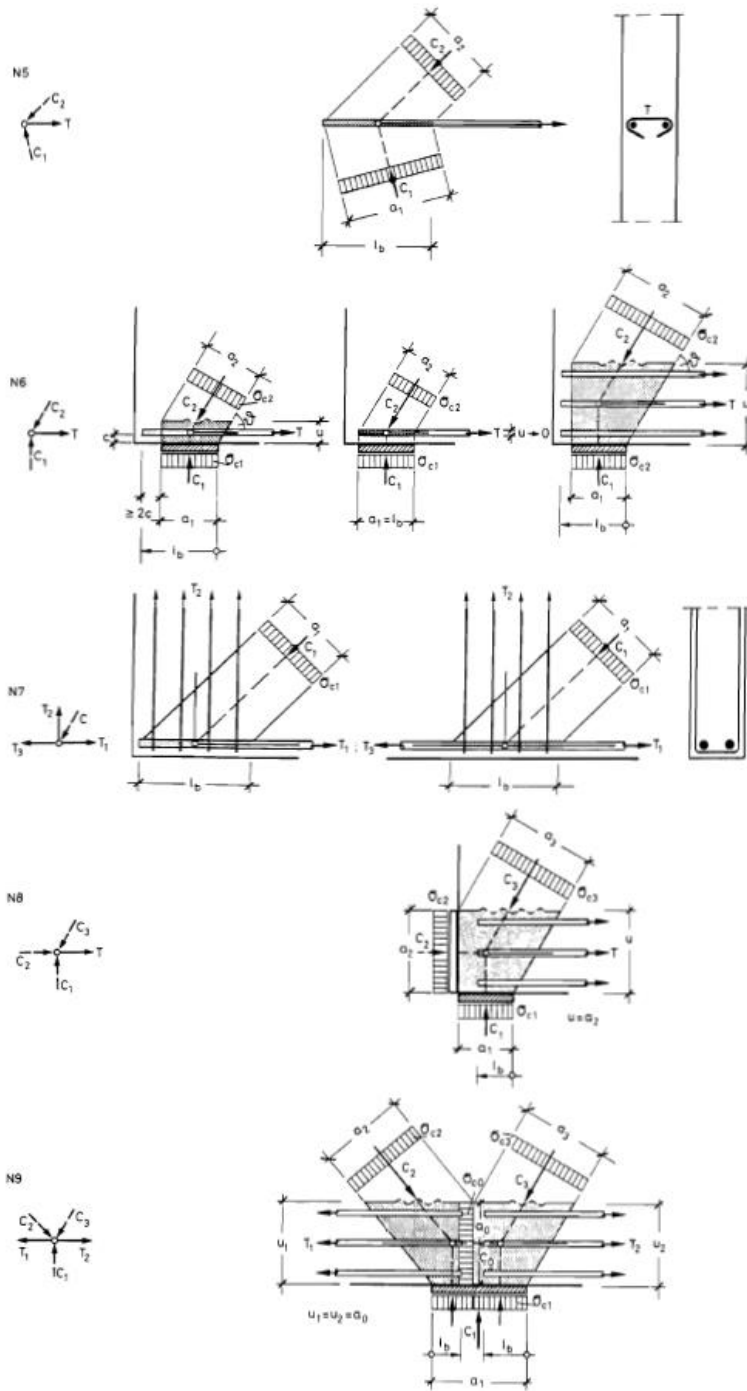


Figure 11. Nodes with anchorage of reinforcement

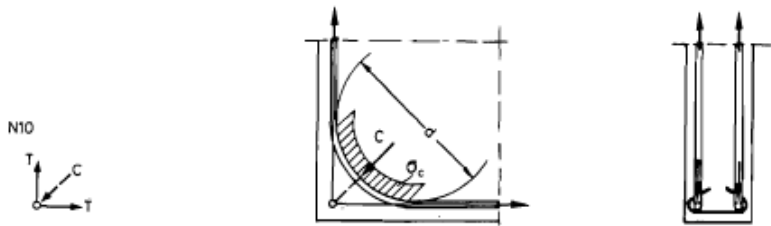


Figure 12. Nodes with anchorage of reinforcement

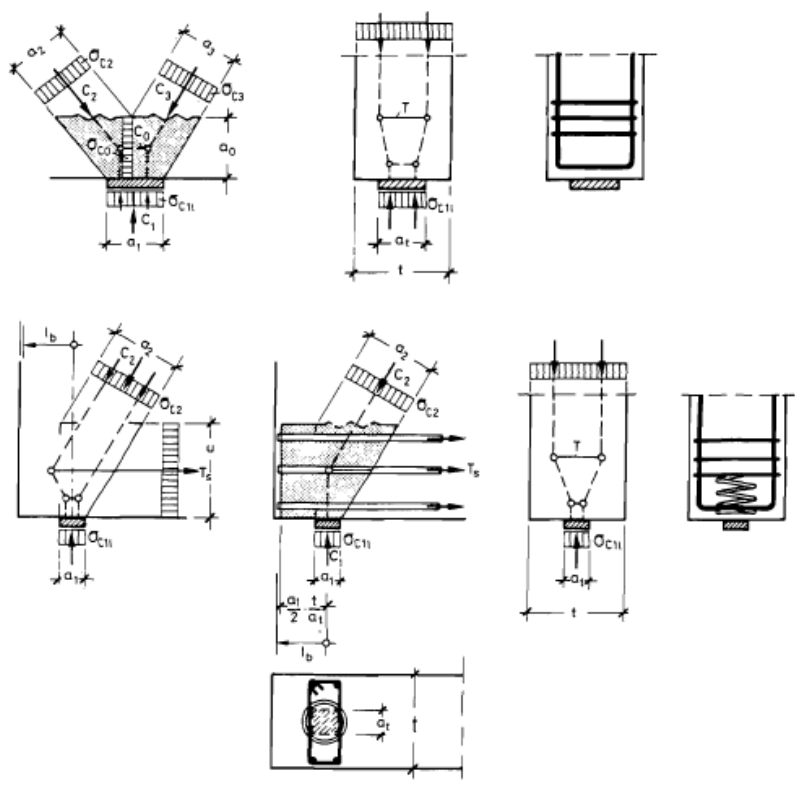


Figure 13. Nodes with anchorage of reinforcement

General rule

Sincesingularnodesarebottlenecksofthestresses,itcanbeassumedthat an entire D-region is safe, if the pressure under the most heavily loaded bearing plate or anchor plate is less than $0.6f_{cd}$ and if all significant tensile forces are resisted by reinforcement and further if sufficient development lengths are provided for thereinforcement. Only if this rule does not lead to a satisfactory result, more sophisticated analysis, as described earlier, is required.

1.6 Applications

Only a few applications of the strut-and-tie method can be shown here; many more can be found in refs. 1 and 12.

Corbels

Corbels are D-regions for which strut-and-tie models are applied successfully for a long time. For a check of the method and the design rules given above, a test specimen will be analysed and the results compared with the test results. In order to include also the potential concrete failure in the checks, one of those rare test specimens is selected for which yielding of the main tie is not the obvious failure criterion.

The test specimen representing two symmetrical corbels was tested upside down (Fig 14(a)). The crack pattern depicts quite well the internal flow of forces (Fig 14(b)), condensed in the simplified model (Fig 14(c) left side). This model can easily be derived by the load path method. However, the precise model geometry is known only after the nodes are dimensioned.

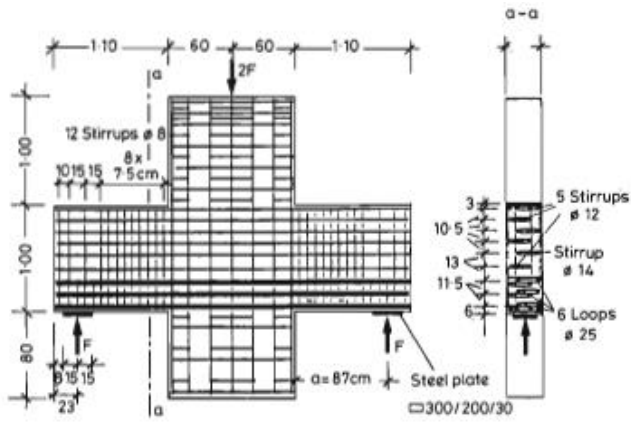
Taking a strut angle $\theta = 33^\circ$ from a first sketch of the model, the following internal forces are derived for the recorded failure load $F_u = 1.425 \text{ MN}$:

$$T = C_4 = F_u / \tan \theta = 2.19 \text{ MN}$$

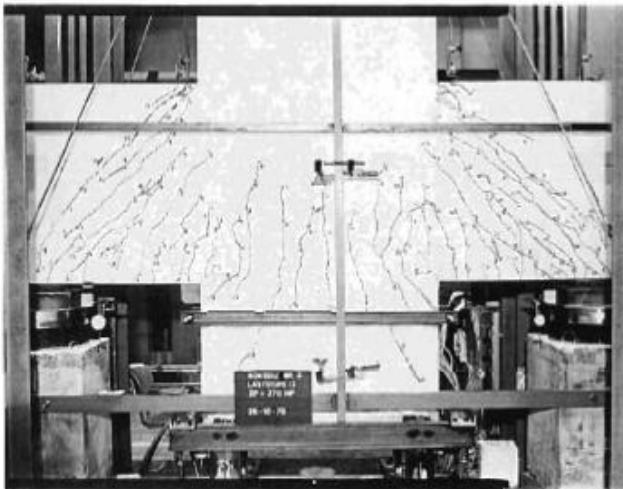
$$C_2 = F_u / \sin \theta = 2.62 \text{ MN}$$

Tie T:

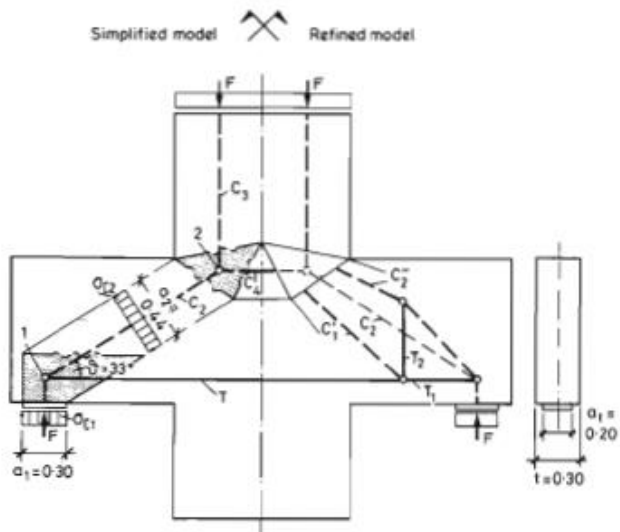
$$\sigma_s = \frac{T}{A_s} = 359 \text{ N/mm}^2 < f_u = 452 \text{ N/mm}^2$$



(a)



(b)



(c)

Figure 14. Corbel, test specimen

Node 1:

$$\sigma_{c1} = \frac{F_u}{a_t \times a_1} \leq 23.8 \text{ N/mm}^2 < \frac{t}{a_s} \times f_u = 31.6 \text{ MPa}$$

Transverse tension from local pressure is covered by loops and stirrups.
Anchorage and distribution of reinforcement in the node region is adequate.

$$\sigma_{c2} = \frac{C_u}{a_2 \times t} \leq 19.8 \text{ N/mm}^2 < 0.8 \times f_u = 21.0 \text{ MPa}$$

Node 2.

The concrete stresses in this pure compression node (similar to typical node N2) cannot be critical,

$$\sigma_{c2} < 1.1 \times f_c = 21.0 \text{ MPa}$$

if the stresses in the adjacent stress fields are satisfactory.

Strut C₂

The diagram for bottle-shaped stress fields (Fig 8) will be used. Reinforcement ratio: vertical $\omega_y = 0.08$, horizontal $\omega_x = 0.08$.

For $\omega = 0.08$ the diagram predicts a minimum capacity

$$p_a = 0.75 f_c = 19.7 \text{ N/mm}^2$$

which almost exactly coincides with the pressure $\sigma_{c2} = 19.8 \text{ N/mm}^2$ determined for node 1 in the ultimate condition. Indeed, the strut C₂ failed in the test after yielding of the vertical reinforcement. The same width a_2 is necessary in the other bottle neck of the stress field where it joins node 2. This determines the geometry of node 2 and finally that of the simple model. However, it must be pointed out that the strut angle $\vartheta = 33^\circ < 45^\circ$ indicates a rather poor orientation of the simple model at the elastic behaviour. A refined model is given in Fig 14(c), right side. This model immediately explains the forces in the yielding vertical stirrups (tie T) and leads to reduced stresses and anchor forces in node 1, which therefore cannot be critical. The geometry and the checks for node 2 are unchanged if the resultant C₂ of struts c.; and C₁' is considered. Stresses in the diagonal struts are not higher than in the simple model.

Deep beam

The deep beam tested by Leonhardt & Walther ¹⁴ shall be evaluated using the strut-and-tie method. Dimensions and reinforcement layout are given in Fig 15(a).

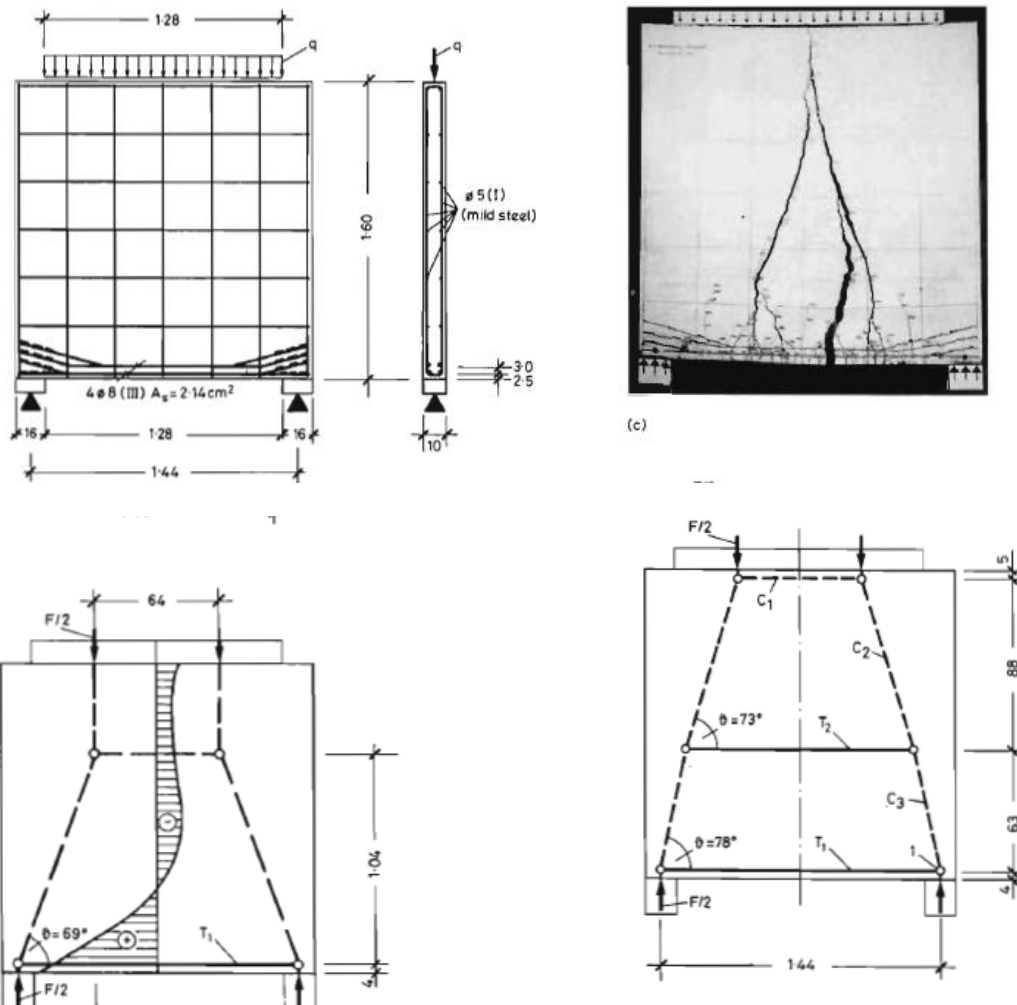


Figure 15. Deep beam, test specimen

$f_c = 30.2 \text{ N/mm}^2$ concrete prism strength

$f_{sy} = 428 \text{ N/mm}^2$ yield strength of main reinforcement

$f_{su} = 547 \text{ N/mm}^2$ rupture strength of main reinforcement The test specimen failed at a total load $F_u = 1195 \text{ kN}$ after rupture of the principal reinforcement.

For a first approximation the model from Fig 4 will be used (Fig 15(b)), neglecting the deviation of bars near the support and the mesh

reinforcement. The lever arm of the chord is assumed to be not much larger than expected from the theory of elasticity:

$$z = 0.72 l = 1.04 \text{ m}$$

When the tension chord begins to yield,

$$T_{1y} = A_s x f_y = 2.14 \times 42.8 = 91.6 \text{ kN}$$

$$F_y = \frac{2 \times T_{1y} \times z}{e} = \frac{2 \times 91.6 \times 1.04}{0.4} = 476 \text{ MPa}$$

This is already more than the usual design would predict, but only 40% of the measured failure load. However, for an explanation of the recorded ultimate load, the model must be adapted to the real behaviour (Fig 15(c)) by shifting the compression chord to the upper end of the deep beam (Fig 15(d)). If further the rupture strength of the main reinforcement is introduced ($T_{1u} = 117.1 \text{ kN}$) and if also the mild steel mesh reinforcement is taken into account (assuming $\sigma_s = 340 \text{ N/mm}^2$, $T_{2u} = 53.4 \text{ kN}$), 94% of the real ultimate load is explained. The rest can be attributed to friction in the supports.

This example shows that, with strut-and-tie models, the real behaviour of cracked structures can be analysed much better than by the theory of elasticity and that considerable 'redistribution' is possible in deep beams. Nevertheless, it is recommended not to depart too much from the theory of elasticity with respect to crack width in the serviceability limit state.

To complete the check of the tested deep beam, also the compression struts and the nodes have to be looked at.

Strut C_1 , can easily be chosen as a prismatic stress field deep enough not to exceed $\sigma_c = f_c$.

Following the earlier description, the bearing pressure $0.8 f_{ed}$ in the support allows an ultimate design load

$$F = 2A = 2ta\sigma_{cA} = 2 \times 0.10 \times 0.16 \times 0.8 \times 30.2 = 0.773 \text{ MN}$$

which is only 65% of the failure load in the test. This can be explained by transverse compression in the concrete due to friction in the bearing plates and to the reinforcement loops. These loops also provide safe anchorage over the support.

Concrete stresses in the support node boundary adjacent to strut C_3 are smaller than σ_{cA} since there reinforcement is very well distributed in the node region over a considerable height u .

Deep beam example

In the first example, we solve a deep beam ,with the following information and geometry of the *figure 1*:

Beam's of width: 0,35m

Column's width: 0,4m

Compressive strength of concrete: 23,5MPa

Yield modulus of steel: 400MPa

Concentrated load: 1000KN

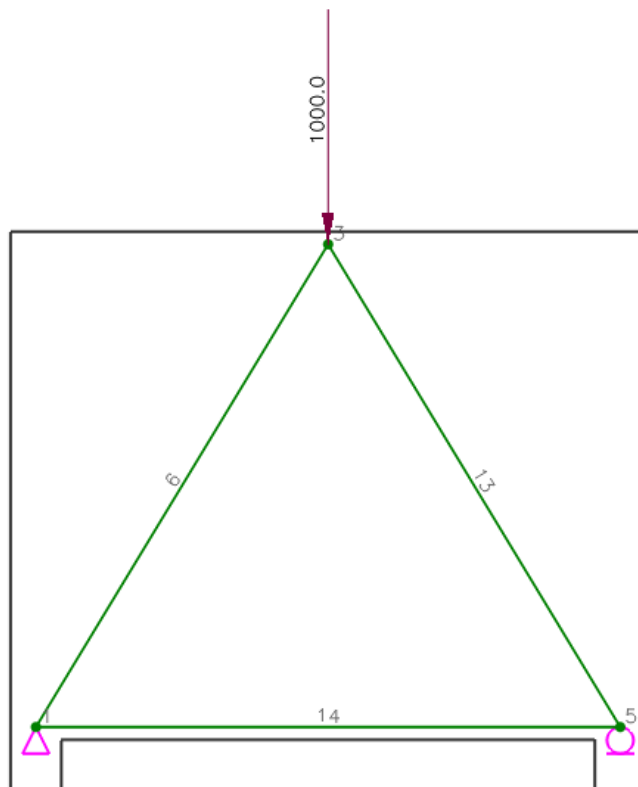


Figure 16. Deep beam(a) geometry

The bars 6,13 are the two concrete struts, while the bar 14 is the tie, that represents the steel bars. Using the program AStrutTie, the solution of the truss, gave the following results:

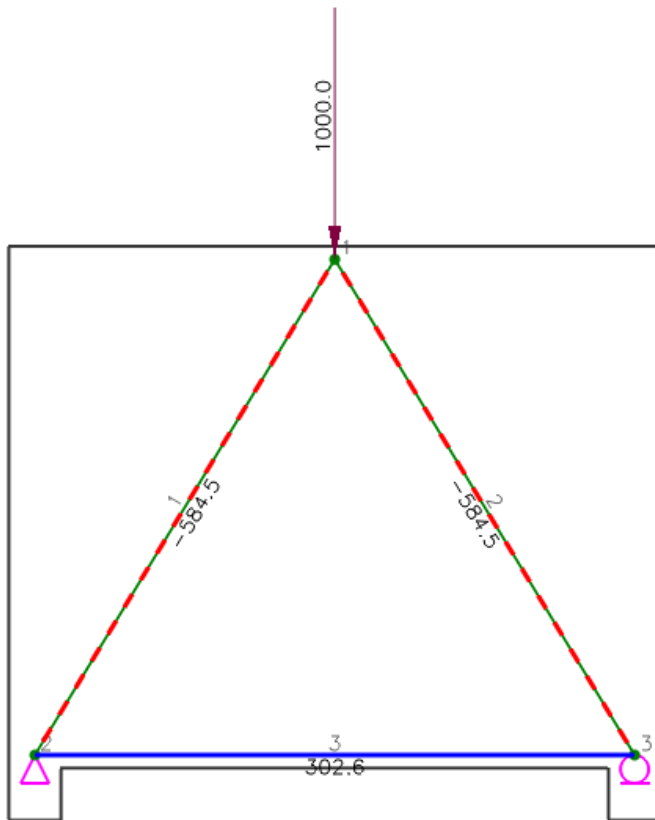


Figure 17. Deep beam, analysis results

Using the program, we can see if the beam is safe or not. So, it can be seen from figure 3 if there is enough reinforcement, and if the w_{prov} is greater than the w_{req} .

| Tie No. | Types | Fu (kN) | theta (deg.) | Rebars | As.req (mm ²) | As.used (mm ²) | Note |
|---------|--------|---------|--------------|--------|---------------------------|----------------------------|------|
| 5 | Bottom | 302.63 | 0.0 | 8-#4 | 681 | 1013 | O.K |

| Strut No. | Type | theta | Fu (kN) | b (mm) | Wreq (mm) | Wprov (mm) | Note |
|-----------|------|-------|---------|--------|-----------|------------|------|
| 1 | 2 | 58.8 | 584.5 | 350.0 | 96.2 | 445.8 | O.K |
| 4 | 1 | 58.8 | 584.5 | 350.0 | 52.2 | 445.8 | O.K |

Figure 20. Calculations of rebar and strength of struts

Form the tables of figure 20, it is shown that the beam is safe.

Next, the same beam is solved using a different STM, in order to show the difference in the results. In figure 4 shows the STM model

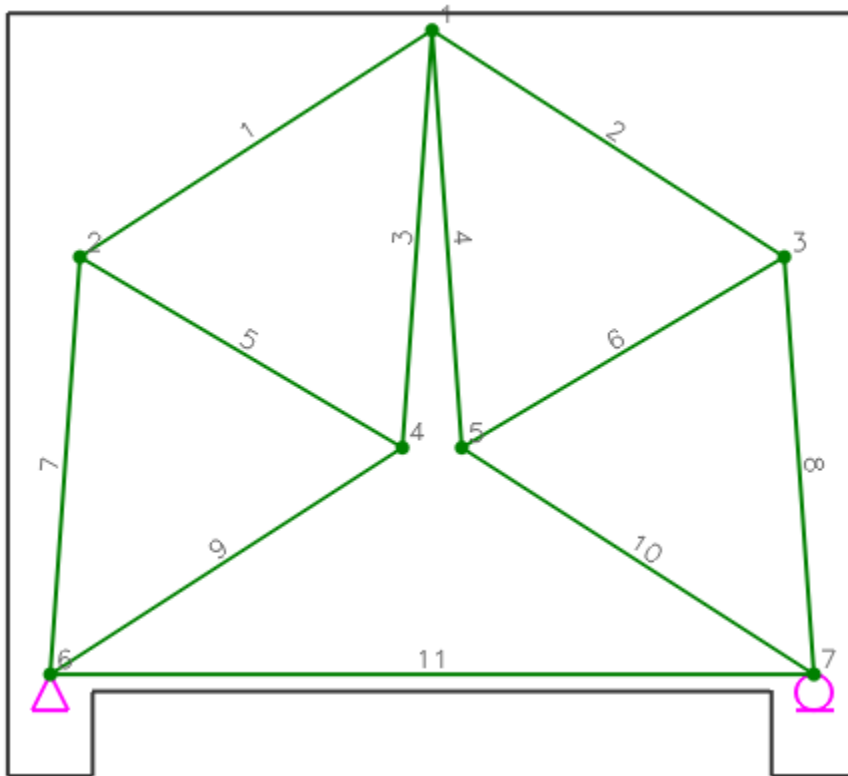


Figure 19. Deep beam(b),test specimen

Here, bars 1,2,3,4,7,8,9,10 represent the concrete struts, while the tensile bars 5,6 represent the steel bars that may be grid reinforcement, horizontal and vertical, that may be placed also for crack control. The tensile bar 11 represent the tie, that is the main reinforcement of the beam. The solution of the bar gives the following result, in figure 21:

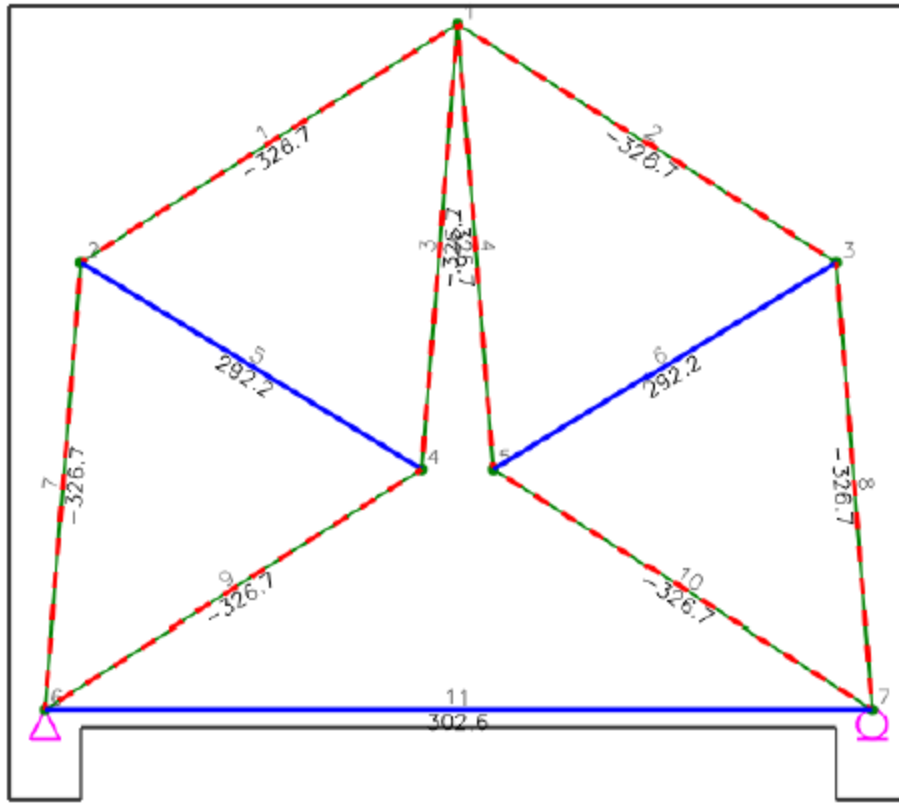


Figure 21. Analysis results for truss(b)

In the same way, it can be seen from figure 22 if there is enough reinforcement, and if the w_{prov} is greater than the w_{req} .

| Tie No. | Types | Fu (kN) | theta (deg.) | Rebars | As.req (mm ²) | As.used (mm ²) | Note |
|---------|--------|---------|--------------|--------|---------------------------|----------------------------|------|
| 5 | Top | 292.23 | 31.2 | 8-#4 | 769 | 1013 | O.K |
| 11 | Bottom | 302.63 | 0.0 | 8-#4 | 681 | 1013 | O.K |

| Strut No. | Type | theta | Fu (kN) | b (mm) | Wreq (mm) | Wprov (mm) | Note |
|-----------|------|-------|---------|--------|-----------|------------|------|
| 1 | 1 | 32.2 | 326.7 | 350.0 | 29.2 | 382.6 | O.K |
| 2 | 1 | 32.2 | 326.7 | 350.0 | 29.2 | 382.6 | O.K |

| | | | | | | | |
|----|---|------|-------|-------|------|-------|-----|
| 3 | 1 | 85.4 | 326.7 | 350.0 | 29.2 | 414.8 | O.K |
| 4 | 1 | 85.4 | 326.7 | 350.0 | 29.2 | 414.8 | O.K |
| 7 | 1 | 85.4 | 326.7 | 350.0 | 29.2 | 414.8 | O.K |
| 8 | 1 | 85.4 | 326.7 | 350.0 | 29.2 | 414.8 | O.K |
| 9 | 1 | 32.2 | 326.7 | 350.0 | 29.2 | 382.6 | O.K |
| 10 | 1 | 32.2 | 326.7 | 350.0 | 29.2 | 382.6 | O.K |

Figure 22. Calculations of rebar and strength of struts

Form the tables of figure 22, it is shown that the beam is safe.

Then, we use the STM of figure 23, to solve the beam. The current model is the same with the pervious, with two more bars, so the corresponding truss is two times indetermined. Hear in figure 7 is the model:

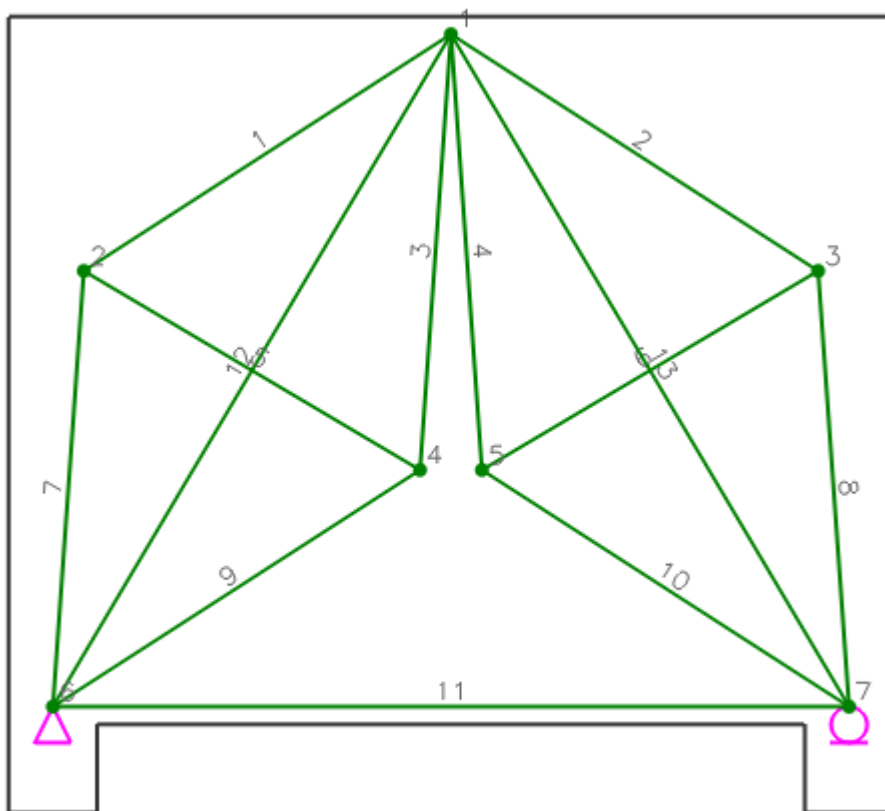


Figure 23. Deep beam(c), test specimen

Hear, the struts are the same as before, with the additional 5,6 bars. The solution of the bar gives the following result, in figure 5:

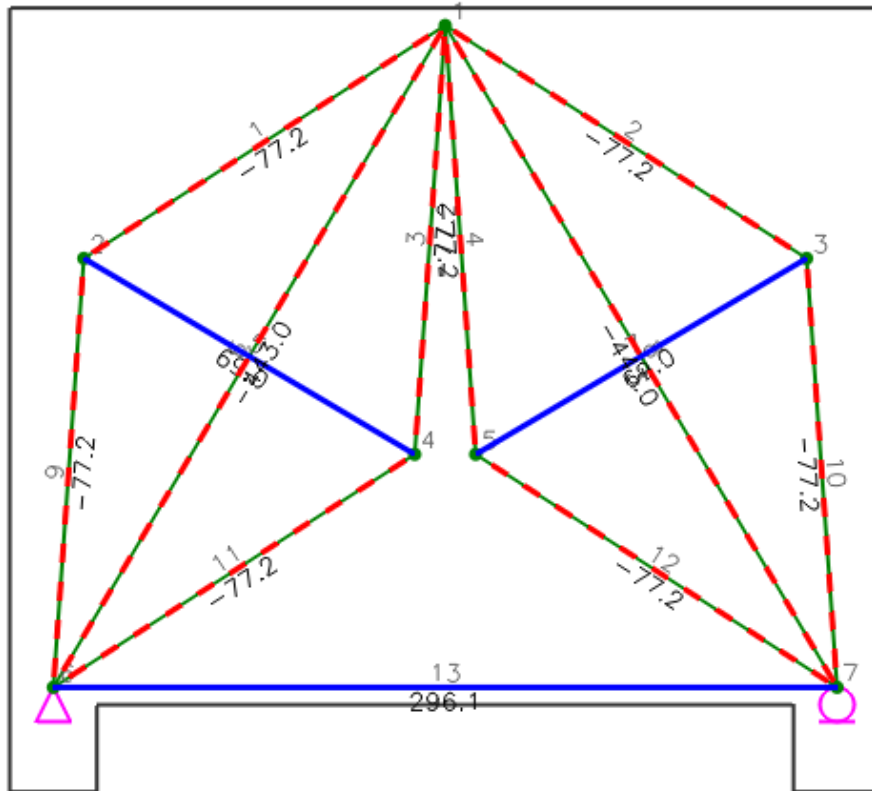


Figure 24. Analysis results for truss(c)

| Tie No. | Types | Fu (kN) | theta (deg.) | Rebars | As.req (mm ²) | As.used (mm ²) | Note |
|---------|--------|---------|--------------|--------|---------------------------|----------------------------|------|
| 5 | Top | 69.44 | 31.2 | 8-#4 | 183 | 1013 | O.K |
| 13 | Bottom | 302.63 | 0.0 | 8-#4 | 681 | 1013 | O.K |

| | | | | | | | |
|----|---|------|-------|-------|------|-------|-----|
| 2 | 1 | 32.2 | 77.6 | 350.0 | 6.9 | 382.6 | O.K |
| 3 | 1 | 85.4 | 77.6 | 350.0 | 6.9 | 414.8 | O.K |
| 4 | 1 | 85.4 | 77.6 | 350.0 | 6.9 | 414.8 | O.K |
| 6 | 1 | 58.8 | 445.6 | 350.0 | 39.8 | 445.8 | O.K |
| 8 | 1 | 58.8 | 445.6 | 350.0 | 39.8 | 445.8 | O.K |
| 9 | 1 | 85.4 | 77.6 | 350.0 | 6.9 | 414.8 | O.K |
| 10 | 1 | 85.4 | 77.6 | 350.0 | 6.9 | 414.8 | O.K |
| 11 | 1 | 32.2 | 77.6 | 350.0 | 6.9 | 382.6 | O.K |
| 12 | 1 | 32.2 | 77.6 | 350.0 | 6.9 | 382.6 | O.K |

Figure 25. Calculations of rebar and strength of struts

Form the tables of figure 25,it is shown that the beam is again safe.

Finally, we solve the beam δοκού with the above model of figure 26:

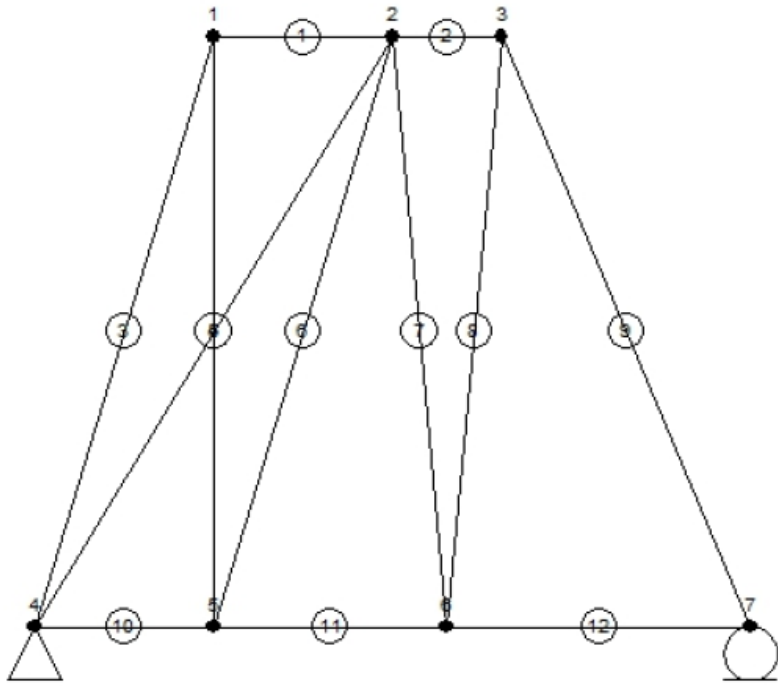


Figure 26. Truss model (d) for the deep beams

By solving the truss, we take the following forces of the bars:

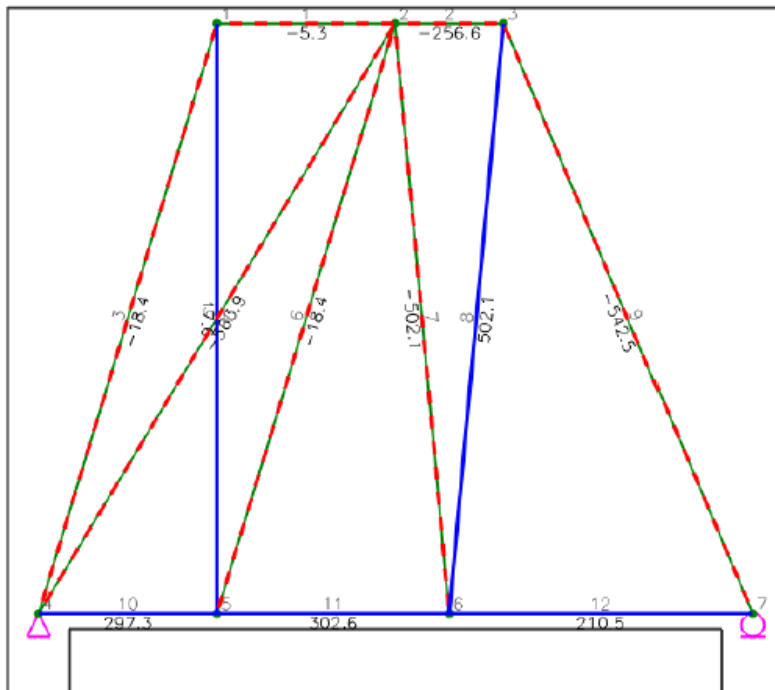


Figure 27. Analysis results for truss(d)

Form the tables of figure28,we have the results of design.

| Tie No. | Types | Fu (kN) | theta (deg.) | Rebars | As.req (mm ²) | As.used (mm ²) | Note |
|---------|--------|---------|--------------|--------|---------------------------|----------------------------|------|
| 10 | Bottom | 297.31 | 0.0 | 8-#4 | 669 | 1013 | O.K |
| 11 | Bottom | 302.63 | 0.0 | 8-#4 | 681 | 1013 | O.K |
| 12 | Bottom | 210.53 | 0.0 | 8-#4 | 474 | 1013 | O.K |

| Tie No. | Fu (kN) | theta (deg.) | Rebars | W _{eff,tie} (mm) | S _{prov} (mm) | phi F _n (kN) | Note |
|---------|---------|--------------|--------|---------------------------|------------------------|-------------------------|------|
| 4 | 17.57 | 90.0 | 4-#4 | 1150.0 | 200.0 | 1294.9 | O.K |
| | | | 4-#4 | 1150.0 | 200.0 | | |
| 8 | 502.12 | 84.7 | 4-#4 | 416.7 | 200.0 | 1193.9 | O.K |
| | | | 4-#4 | 975.0 | 200.0 | | |

Figure 28. Calculations of rebar and strength of struts

From figure28, we get that the beam is again safe.

In all the four truss models, we try to present the differences between the results of each case. These differences are shown form the values of compressive stresses, on compressive struts, and also the required reinforcement. By comparison of the compressive stresses of the trusses **a** and **b**, we can see that both the W_{req} ,and W_{prov} are less than before. As for the ties, the requirement is the approximately the same, because the forces in the main tie remains the same.

Corbel design

In the second example, we design a corbel, that has the following information of materials and geometry of *figure 29*:

Properties

Width of corbel: 1,00m

Width of columns: 0,4m

Concrete compressive stress : 35MPa

Yield stress of steel : 400MPa

Concentrated load : 700KN

Geometry

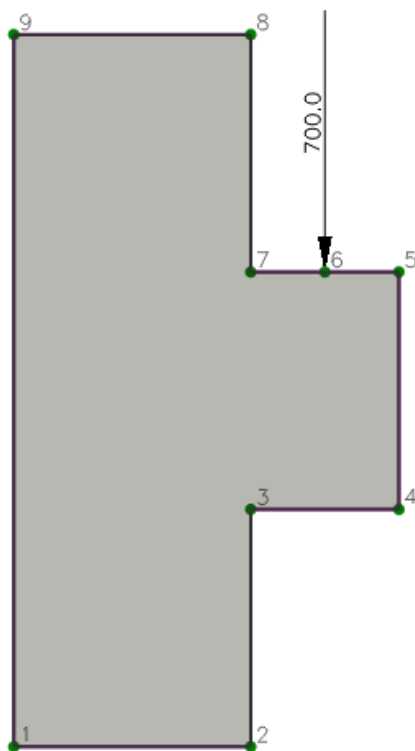


Figure 29. Geometry of the corbel

Following the same procedure as with the deep beam, we solve the corbel with three different STM.

Firstly, we assume the model below, in figure 30:

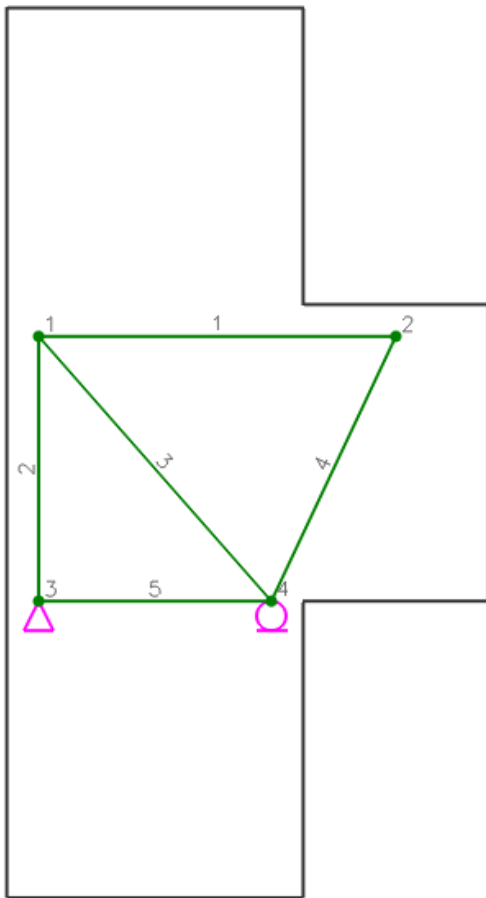


Figure 30. Truss model(a) for the corbel

The bars 4,5 are the two concrete struts, while the bar 1 is the tie, that represents the steel bars. Using the program, the solution of the truss, gave the following results:

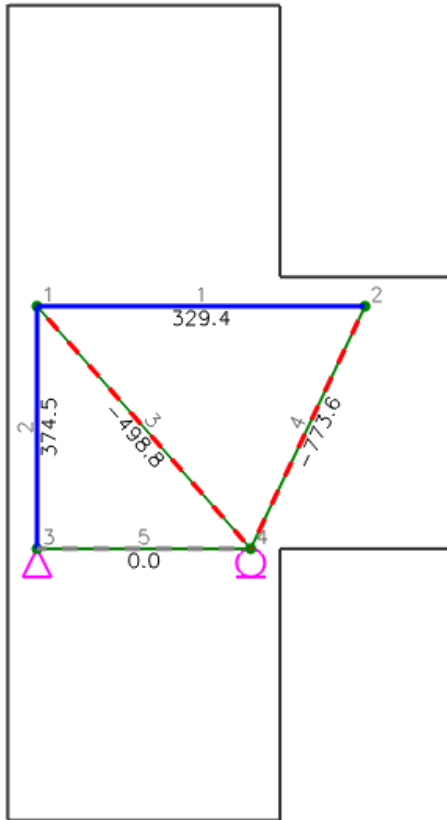


Figure 31. Analysis results for truss(a)

Using the program, we can see if the beam is safe or not. So, it can be seen from figure 31 if there is enough reinforcement, and if the w_{prov} is greater than the w_{req} , so the compressive struts are adequate.

| Tie No. | Types | Fu (kN) | theta (deg.) | Rebars | As.req (mm ²) | As.used (mm ²) | Note |
|---------|-------|---------|--------------|--------|---------------------------|----------------------------|------|
| 1 | Top | 329.41 | 0.0 | 4-#3 | 741 | 285 | N.G |

| Tie No. | Types | Fu (kN) | theta (deg.) | Rebars | As.req (mm ²) | As.used (mm ²) | Note |
|---------|-------|---------|--------------|--------|---------------------------|----------------------------|------|
| 2 | Outer | 374.52 | 90.0 | 4-#3 | 843 | 285 | N.G |

| Strut No. | Type | theta | Fu (kN) | b (mm) | Wreq (mm) | Wprov (mm) | Note |
|-----------|------|-------|---------|--------|-----------|------------|------|
| 3 | 2 | 48.7 | 498.8 | 1000.0 | 20.7 | 114.5 | O.K |
| 4 | 2 | 64.8 | 773.6 | 1000.0 | 32.1 | 95.0 | O.K |

Figure 32. Calculations of rebar and strength of struts

Form the tables of figure 32,it is shown that the beam is safe.

Next, the same beam is solved using a different STM, in order to show the difference in the results. In figure 33 shows the STM model. The model is the same, with one more bar, that is the strut bar 7. So the truss now is one time indetermined.

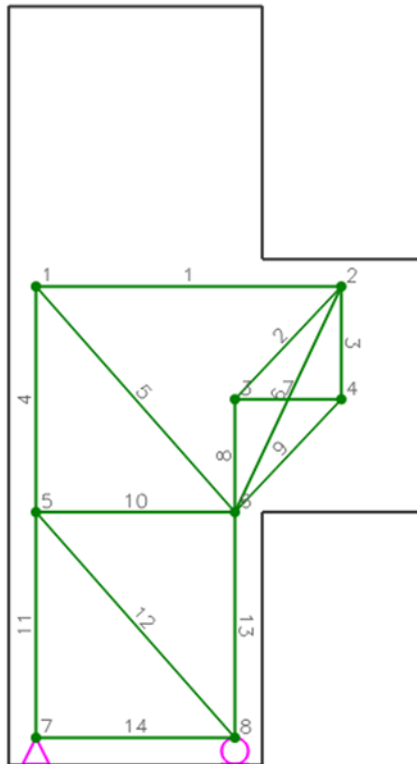


Figure 33. Truss model(b) for the corbel

The bars 2,3,7,8 are the two concrete struts, while the bar 1,6 are the ties. Using the program, the solution of the truss, gave the following results:

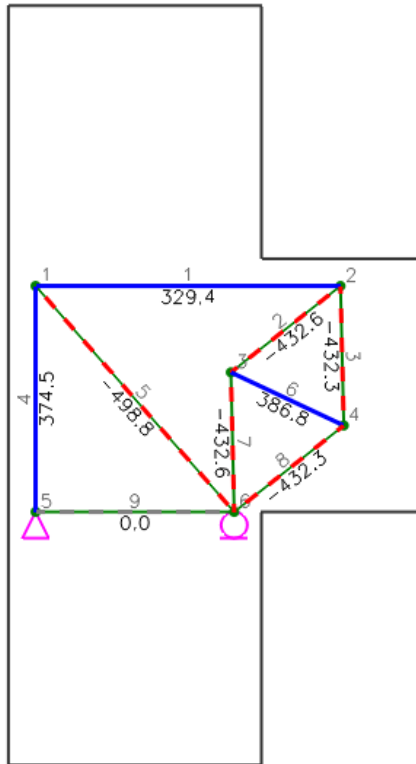


Figure 33. Analysis results for truss(a)

The results are the following:

| Strut No. | Type | theta | Fu (kN) | b (mm) | Wreq (mm) | Wprov (mm) | Note |
|-----------|------|-------|---------|--------|-----------|------------|------|
| 2 | 1 | 38.2 | 432.6 | 1000.0 | 9.3 | 173.8 | O.K |
| 3 | 1 | 88.6 | 432.3 | 1000.0 | 9.3 | 176.4 | O.K |
| 5 | 2 | 48.7 | 498.8 | 1000.0 | 20.7 | 114.5 | O.K |
| 7 | 1 | 88.6 | 432.6 | 1000.0 | 9.3 | 86.0 | O.K |
| 8 | 1 | 38.2 | 432.3 | 1000.0 | 9.3 | 69.5 | O.K |

| Tie No. | Types | Fu (kN) | theta (deg.) | Rebars | As.req (mm ²) | As.used (mm ²) | Note |
|---------|-------|---------|--------------|--------|---------------------------|----------------------------|------|
| 1 | Top | 329.41 | 0.0 | 6-#6 | 741 | 1710 | O.K |

| Tie No. | Types | Fu (kN) | theta (deg.) | Rebars | As.req (mm ²) | As.used (mm ²) | Note |
|---------|-------|---------|--------------|--------|---------------------------|----------------------------|------|
| 4 | Outer | 374.52 | 90.0 | 8-#6 | 843 | 2280 | O.K |
| 6 | Outer | 386.82 | 25.2 | 8-#6 | 2044 | 2280 | O.K |

Figure 34. Calculations of rebar and strength of struts

So, the beam is safe.

Finally, considering a more complicated model, we have the following results of the analysis of the truss:

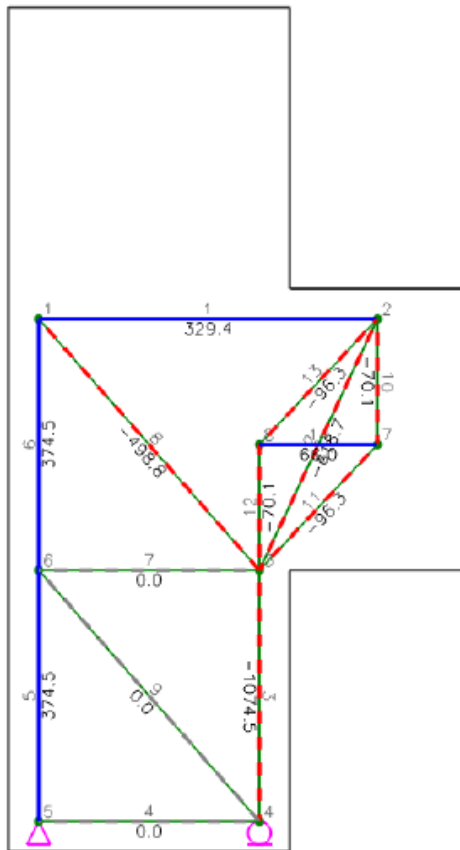


Figure 35. Analysis results for truss(b)

The results are the following:

| Tie No. | Types | Fu (kN) | theta (deg.) | Rebars | As.req (mm ²) | As.used (mm ²) | Note |
|---------|-------|---------|--------------|--------|---------------------------|----------------------------|------|
| 4 | Outer | 374.52 | 90.0 | 6-#7 | 843 | 2328 | O.K |

| Tie No. | Fu (kN) | theta (deg.) | Rebars | Weff,tie (mm) | Sh (mm) | phi Fn (kN) | Note |
|---------|---------|--------------|--------|---------------|---------|-------------|------|
| 7 | 90.02 | 0.0 | 3-#4 | 178.5 | 250.0 | 100.5 | O.K |

| Strut No. | Type | theta | Fu (kN) | b (mm) | Wreq (mm) | Wprov (mm) | Note |
|-----------|------|-------|---------|--------|-----------|------------|------|
| 2 | 2 | 46.7 | 131.3 | 1000.0 | 5.5 | 79.9 | O.K |
| 3 | 2 | 90.0 | 95.6 | 1000.0 | 4.0 | 84.0 | O.K |

| | | | | | | | |
|----|---|------|--------|--------|------|-------|-----|
| 5 | 2 | 48.7 | 498.8 | 1000.0 | 20.7 | 114.5 | O.K |
| 6 | 2 | 64.8 | 562.2 | 1000.0 | 23.3 | 76.0 | O.K |
| 8 | 2 | 90.0 | 95.6 | 1000.0 | 4.0 | 84.0 | O.K |
| 9 | 2 | 46.7 | 131.3 | 1000.0 | 5.5 | 72.0 | O.K |
| 13 | 1 | 90.0 | 1074.5 | 1000.0 | 23.0 | 86.0 | O.K |

Figure 36. Calculations of rebar and strength of struts

In figure 36, all the results of the analysis of the beam are presented, and so the beam is safe.

Chapter 2

A Strut Tie model

2.1 Introduction

A Strut Tie is a strut-tie model analysis/design software for concrete members with disturbed stress region(s). It enables users to design corbel (bracket), abutment/pier footing, bridge pier coping (pier cap), frame corner, anchorage zone, deep beam, etc. The software supports U.S (ACI, ASHTO) and Europe (EuroCode2) Codes and Specifications.

A concrete member can be classified into B-region(s) and D-region(s). D-regions are parts of structure in which the strain distribution is highly nonlinear. Most design practices for D-regions are mostly based on empirical approaches. The strut-tie model approach promotes a better understanding of load transfer mechanisms and structural behavior

and it improves the designers' ability to handle unusual circumstances including D-regions.

A Strut Tie is a powerful and practical analysis/design software for concrete members with D-region(s). The most appropriate strut-tie models can be constructed by considering the principal stress flows and/or evolutionary structural optimization (ESO) results. A specialized solver capable of handling any types of internally/externally (in) determinate strut-tie models is associated. The strut-tie model provisions of ACI 318-14 (2014), AASHTO LRFD (2014), and EC2 (2004) are applied. For fast and efficient strut-tie model designs, multirole templates are provided for corbel (bracket), abutment footing, pier footing, bridge pier coping (pier cap), frame corner, anchorage zones with inclined and straight tendons, and deep beams with concentrated and distributed

loads. Advanced element sets representing truss mechanism, truss and arch mechanism, and fan action are provided. A Strut Tie provides various automated design checks regarding the conditions for rebar requirement and strength verification of struts and nodal zones. Visual verifications of strength conditions are possible, too. A structural design report is generated automatically, and design results are examined by previewing the report.

Uncertainty in the construction of an appropriate strut-tie model due to lack of general and comprehensive specifications. Inefficiency in the construction of strut-tie models representing load transfer mechanisms for multiple load combinations.

Enormous time and efforts for examining the suitability of a constructed strut-tie model that satisfies the strength conditions of struts and nodes.

The strut-tie model approach has been recognized as an efficient methodology for the design of all types of structural concrete with D-regions, and accepted in design codes globally. However, the design of a structural concrete with the approach requires many iterative numerical structural analyses, numerous graphical calculations, enormous time and efforts, and designer's subjective decisions in terms of the construction of an appropriate strut-tie model, determination of required areas of struts and ties, and verification of strength conditions of struts and nodal zones.

Han Gil has developed a design software A Strut Tie that enables the analysis and design of structural concrete efficiently and professionally by overcoming the aforementioned limitations of the strut-tie model approach. In the software, all the numerical programs that are essential in the strut-tie model analysis or design of a structural concrete, including finite element analysis programs for the plane truss and solid problems with all kinds of boundary conditions, a program for evaluating the axial rigidities of struts and ties

of statically determinate and indeterminate strut-tie models, a program for determining, and a program for the graphical verification of strut-tie model's appropriateness by displaying various geometrical shapes of struts and nodal zones, are loaded. Great efficiency and convenience during the application of the strut-tie model approach may be provided by the various graphics environment-based functions of the software.

2.2 Modeling of Member Geometry

The geometrical shape of concrete member is constructed in the Beginning Mode. The geometrical shape is constructed by, direct drawing, importing a file, or using a Template. The boundary lines and truss model of the concrete member are regenerated by importing a file. The geometrical shape, evolutionary structural optimization, stress flow, and truss model can be generated automatically by using a Template. In the following pictures in figure 37, shows the previous.

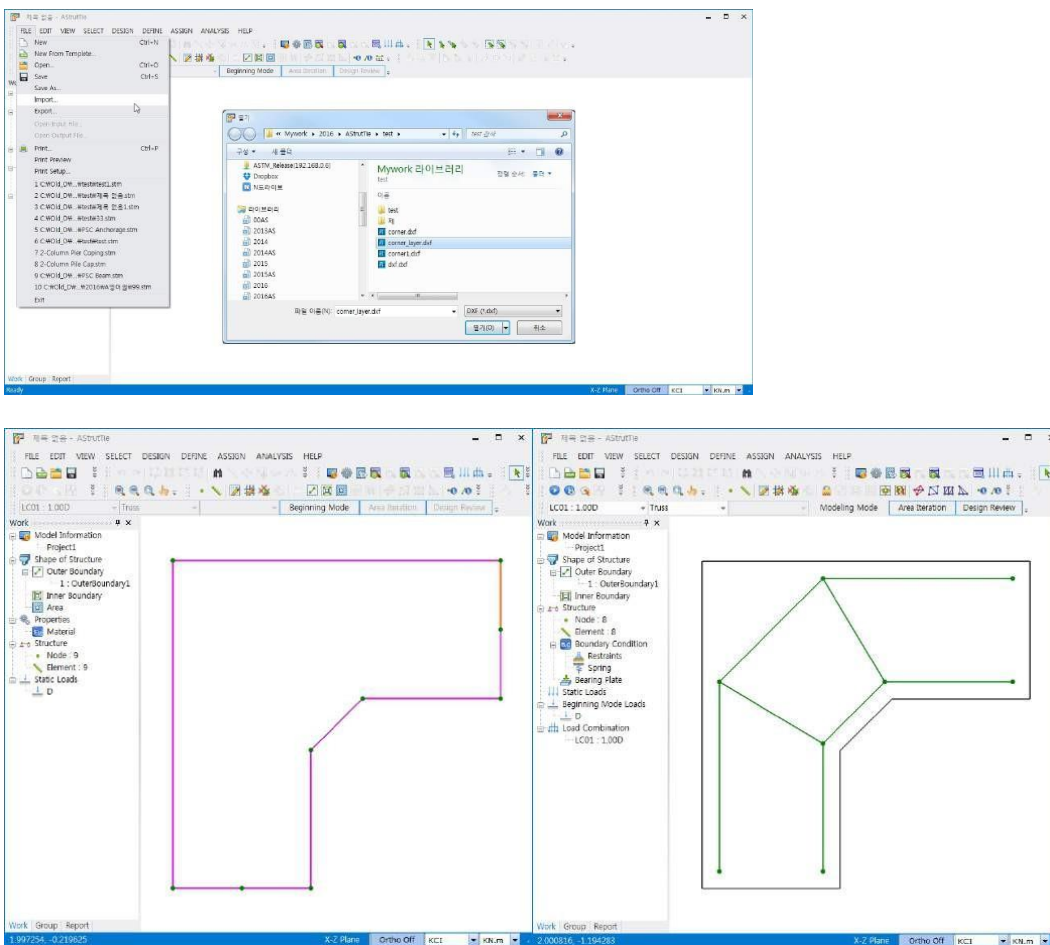


Figure 37. Geometry of a corbel

2.3 Templates of AStrutTie

The geometrical shape of concrete member and truss model are generated by New From Template and selecting one of the provided templates shown in figure below. The basic information on the geometrical shape including thickness, width, and height must be input. The figure 38, shows the templates that the program provides to the users.

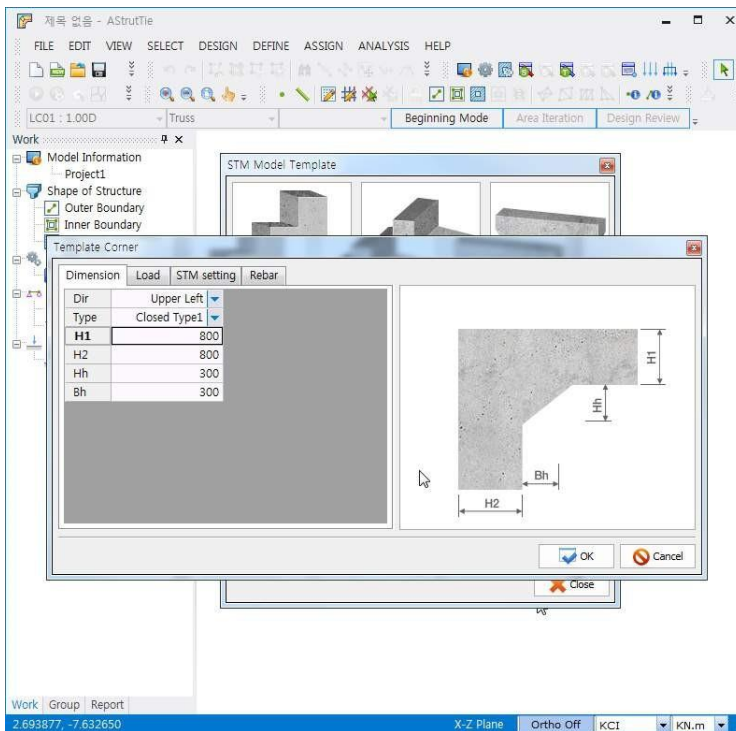
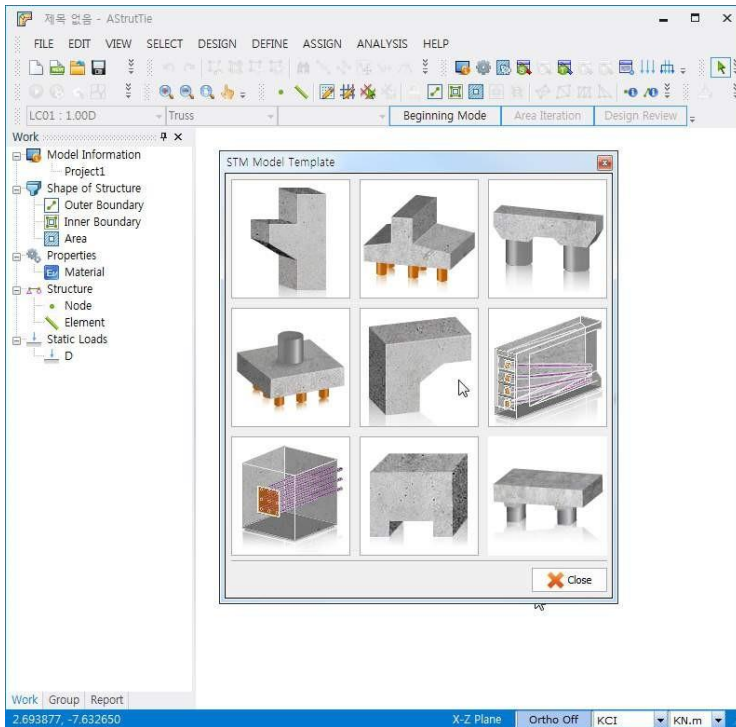


Figure 38. Templates of the program

2.4 Application of Loads

Two methods for applying loads are provided in the program.

Node Static Loads

External loads are assigned by Assign-Static Load. After selecting nodes and elements, the following figure appears. Here, in figure 38, the loads applied in a corbel are shown.

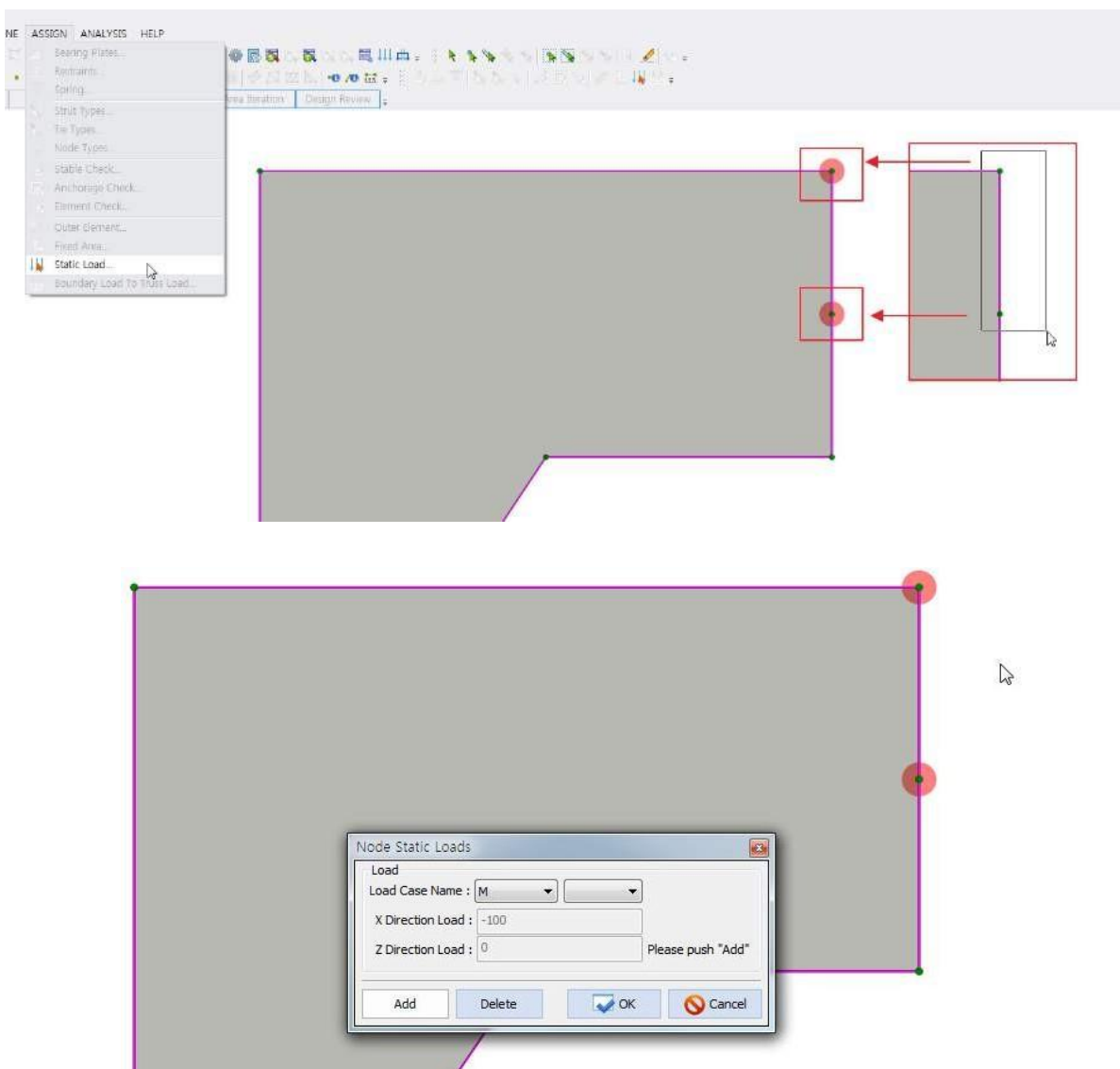
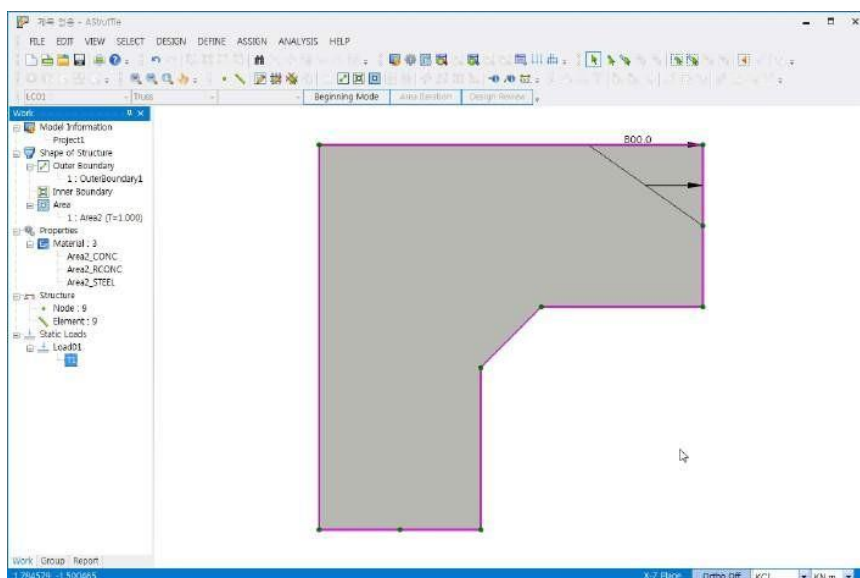
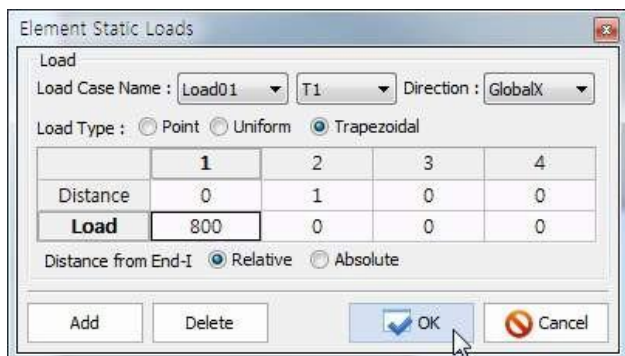


Figure 38. Application of the loads

And then, the direction of load and load type must be selected. Three load types (point load, uniform load, and trapezoidal load) are available. An example for inputting trapezoidal load is shown below.



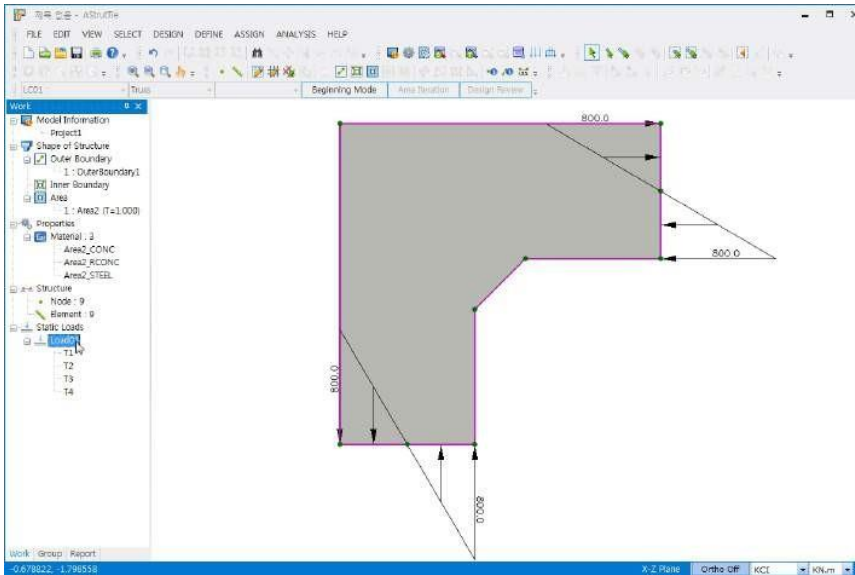
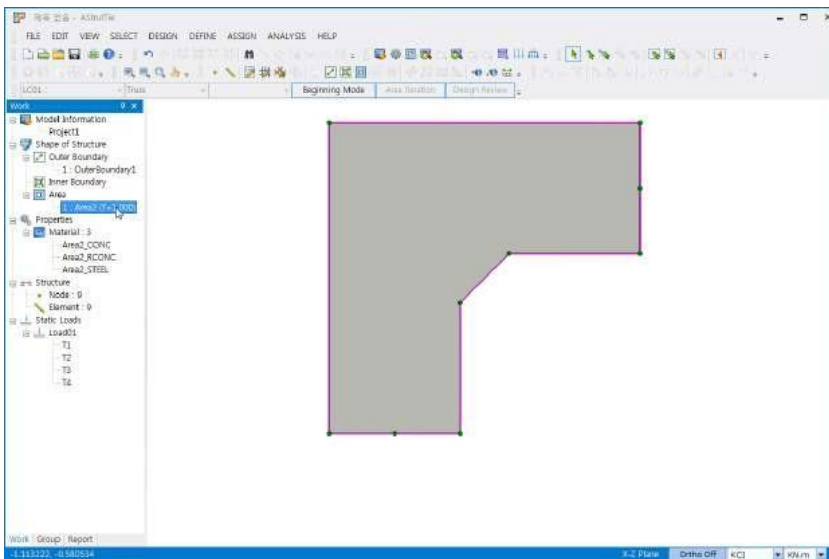


Figure 39. Trapezoid load in a corbel

The material properties can be altered in Area Properties, as shown in figure 40.



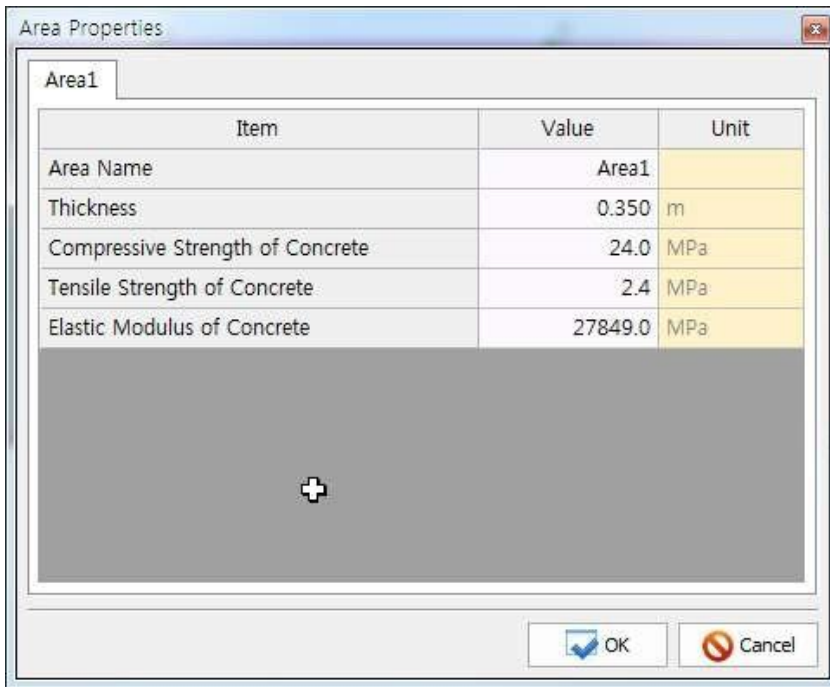
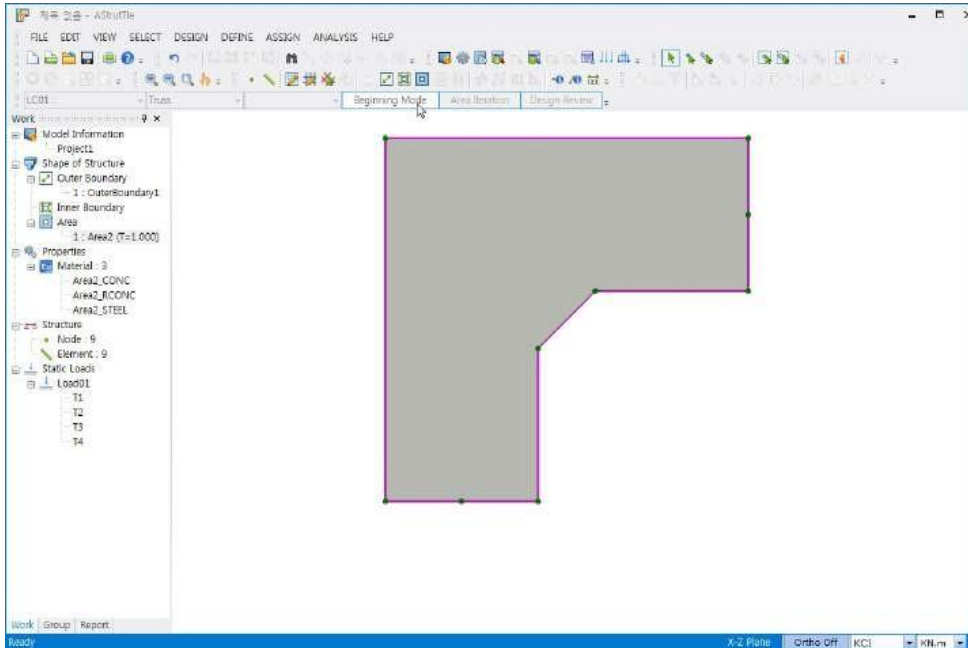


Figure 40. Properties of the corbel

2.5 Structural Analysis for ESO & Stress Flow

The window transforms to the Modeling Mode for numerical structural analysis after imposing loads on a concrete member. The Modeling Mode consists of ESO, Stress Flow, and Truss. The finite element model of a concrete member for ESO and Stress Flow analyses is constructed by using a mesh generator. The mesh size is setup by clicking DEFINE-Project Information. Followings are the figures that illustrate the finite element modeling of a concrete member. After clicking Beginning Mode and selecting Modeling Mode-Stress Flow, DEFINE-Project Information(Dialog) need to be activated to alter the mesh size. The loads inserted by clicking Static Load are



switched to nodal forces automatically. Figure 41 shows such a mesh.

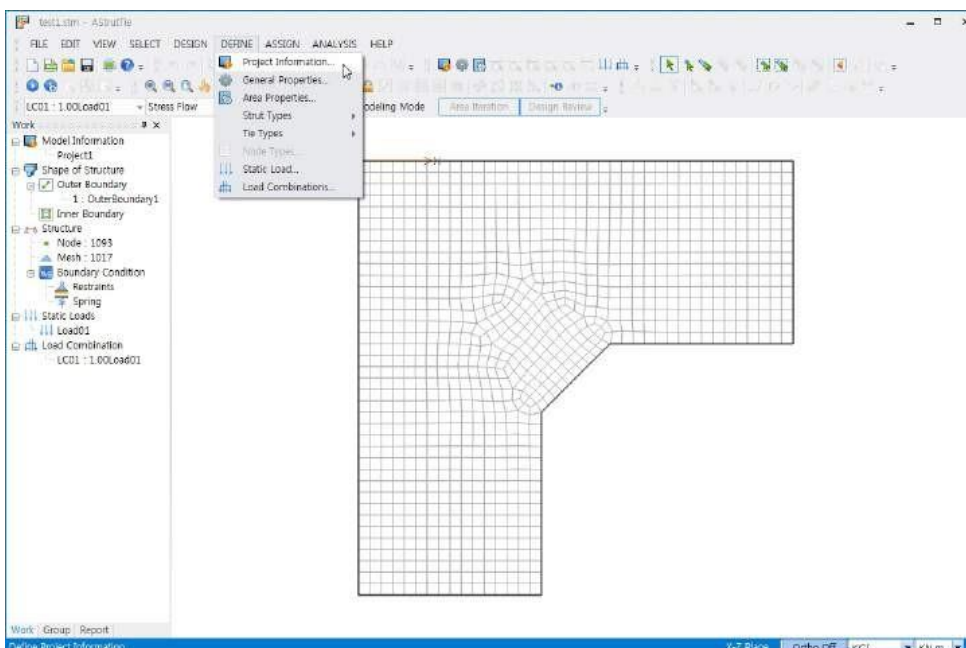


Figure 41. Mesh of the area

If the mesh size is changed, the boundary conditions must be updated.

After selecting the nodes on which restraints must be imposed, the boundary conditions are set up by clicking ASSIGN-Restraints. This can be seen in the figure 42.



Figure 42. Assigning restrains.

And then, by clicking ANALYSIS-Run Analysis the finite element linear elastic analysis is conducted for checking the compressive principal stress trajectories. The left figure shown below is an example showing the stress trajectories. In the same way, by clicking ESO (instead of Stress Flow) and completing the necessary modifications and inputs in DEFINE-Project Information (Dialog) and ASSIGN-Restraints, the finite element analyses are conducted for checking the approximate load paths by the evolutionary structural optimization technique. The right figure 8 shown below is an example showing the results of the optimization.

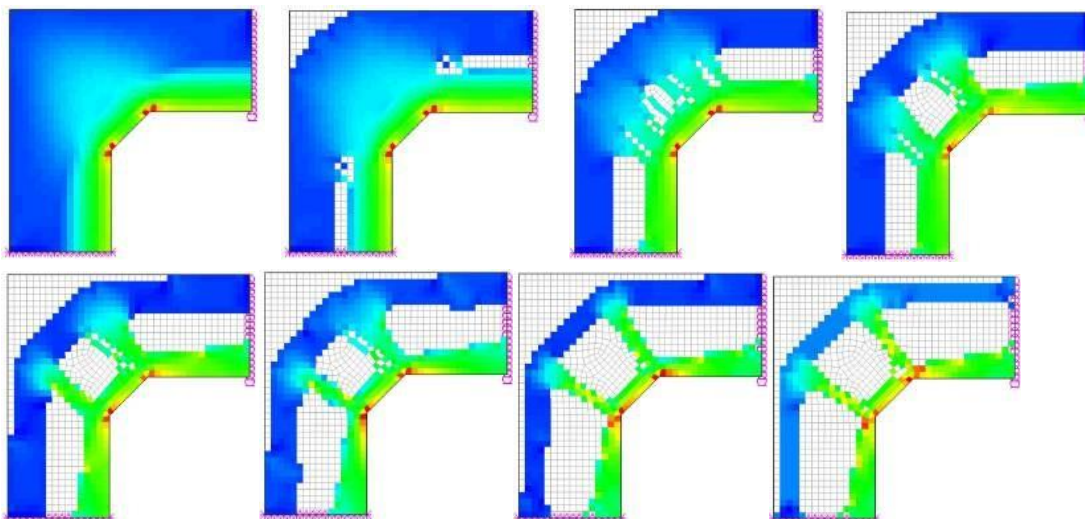
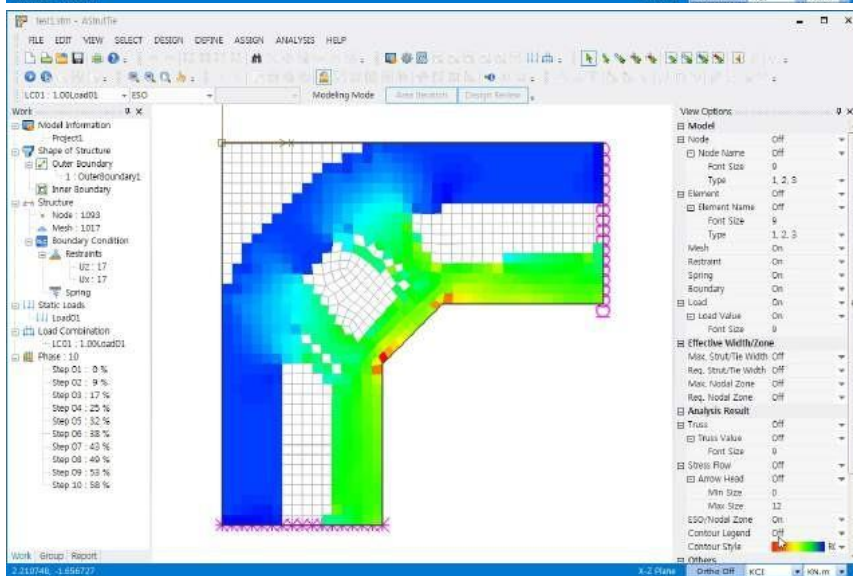
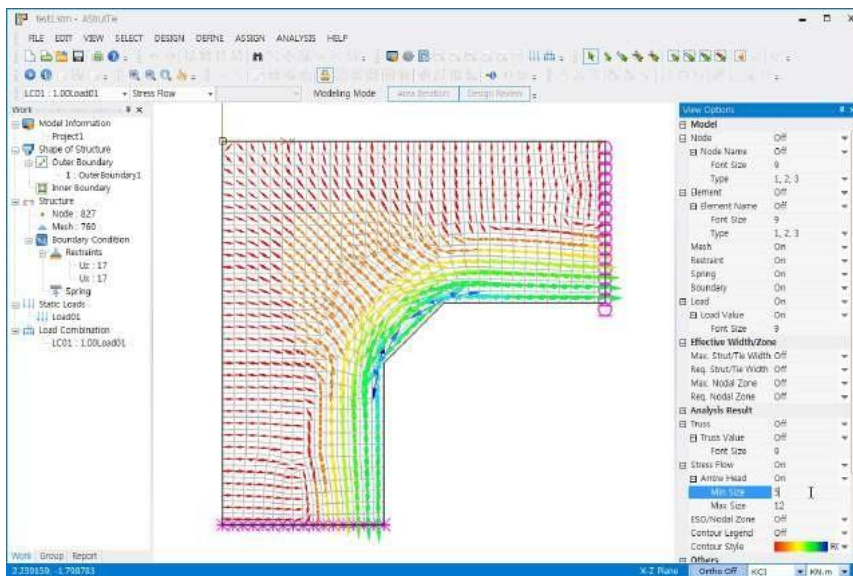


Figure 43. Results of the optimization are shown below.

After selecting the nodes on which restraints must be imposed, the boundary conditions are set up by clicking ASSIGN-Restraints. The structural analysis on the truss model is conducted by clicking ANALYSIS-Run Analysis. After the analysis, the results including element forces are shown on the truss model. This is in the following figure 44.

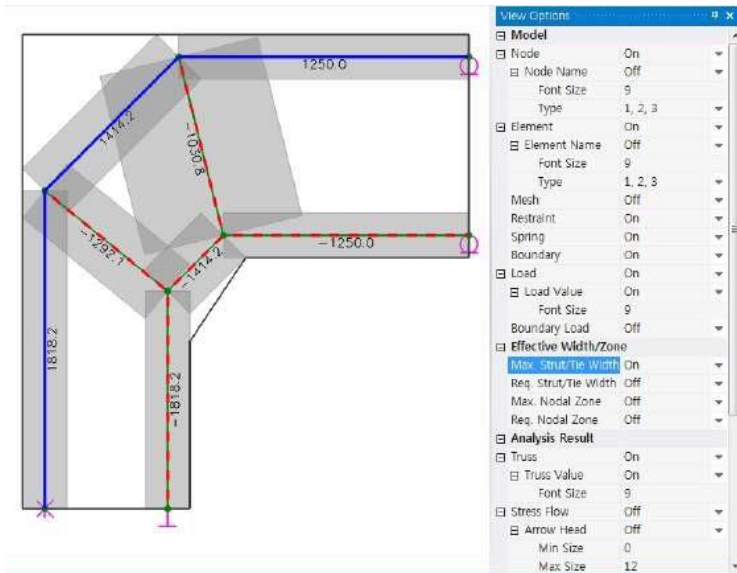
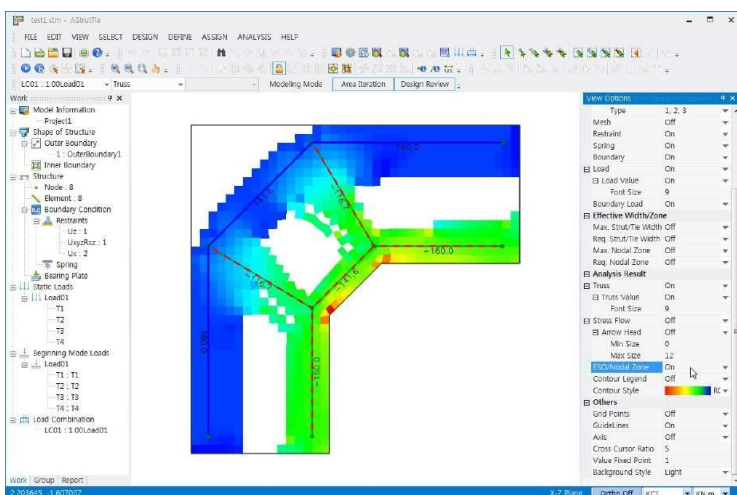


Figure 44. Results of the element forces.



EffectiveWidth/Zone

The available and required widths of struts, ties, and nodal zones are or are not displayed by clicking True or False in the View Options Window – Effective Width/Zone.

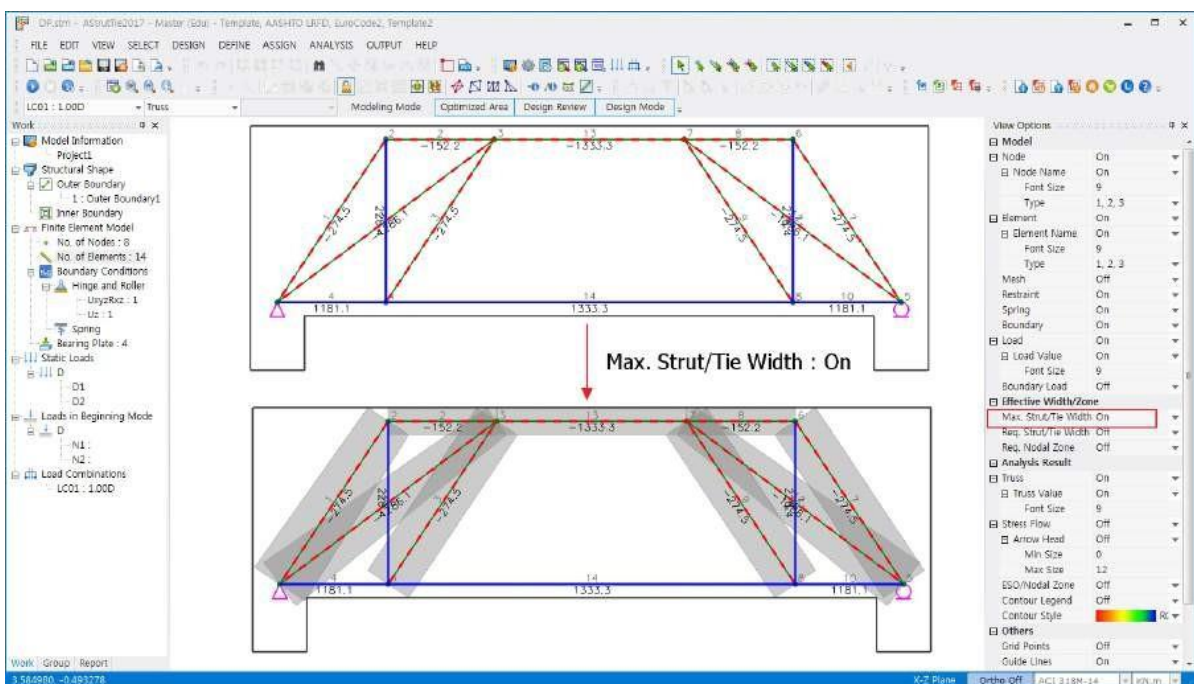
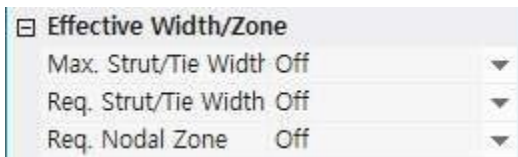
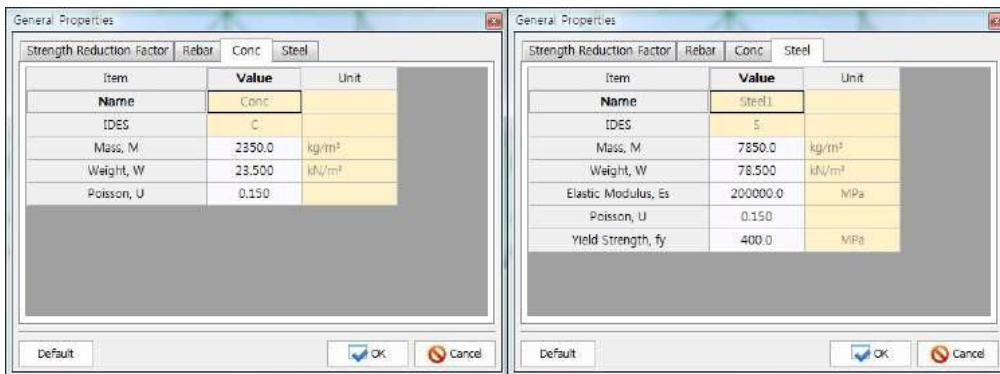
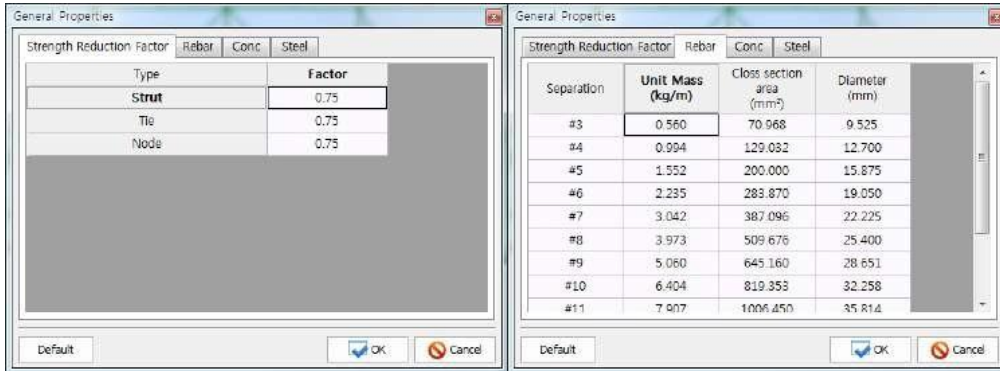


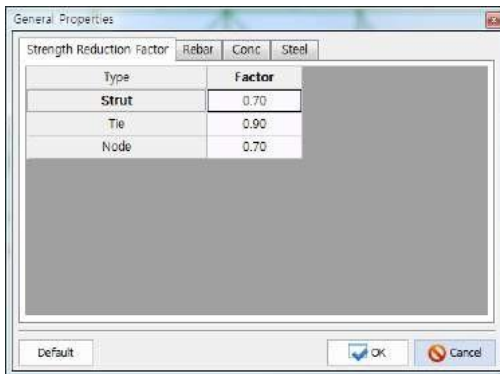
Figure 45. Results of the element forces.

The strength reduction factors of strut, tie, and node are assigned here. These sectional and material properties of reinforcing bars and concrete are also assigned. For different codes, the strength of the nodes varies. In figure 46, the safe factors are shown, for different codes.

ACI318M-14(2014)



AASHTOLFRD (2014)



EuroCode2(2004)

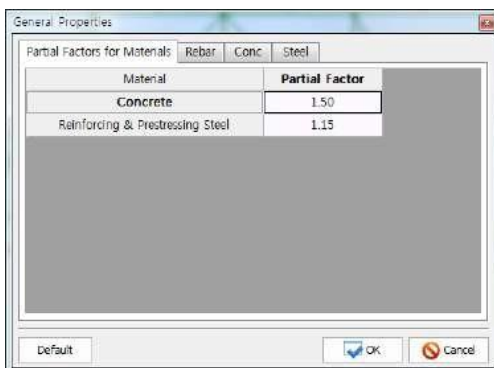


Figure 46. Safety factors, for different codes.

2.6.1 StrutTypes

Default types of concrete struts in a strut-tie model are defined here. More strut types can be added. In figure 47, the reduction factors of struts are shown.

ACI318M-14(2014)

| Name | β_s | λ |
|--|---------------|-----------|
| Prismatic Strut | 1.0 | - |
| Bottle Shape Strut (Satisfying ACI 318M-14 23.5.3) | 0.75 | - |
| Bottle Shape Strut (Not Satisfying ACI 318M-14 23.5.3) | 0.60λ | 1.0 |
| Strut in Tension Zones | 0.40 | - |
| All Other Cases | 0.60 | - |

AASHTO LRFD (2014)

| Option | Select |
|--|-----------|
| Strain of Steel Tie, ϵ_s | f_s/E_s |
| Minimum Effective Strength of Concrete Strut | 0.4 |

EuroCode2(2004)

| Name | v |
|----------------------------------|-------------------|
| Strut without Transverse Tension | 1.0 |
| Strut with Transverse Tension | $0.6(1-f_c'/250)$ |

Figure 47. Reduction factors, for different codes.

2.6.2 TieTypes

The steel ties in a strut-

tie model represent the main reinforcing bars, shear reinforcing bars, and supplementary reinforcing bars of a concrete member. Two different types of reinforcing bars in a horizontal layer and up to 4 vertical layers. The shear reinforcing bars can be divided into horizontal, vertical, and inclined reinforcing bars. The information on the shear reinforcing bars is required. For the horizontal or vertical supplementary reinforcing bars, the number of legs and layers must be assigned. These are shown in the following:

The dialog box 'Define Reinforcements: Ties' shows the configuration for a Main Rebar. The left sidebar has 'Main Rebar' selected. The central preview shows a square cross-section with five blue circles representing rebar at the bottom, with a label 'R.D' and a downward arrow. The right panel contains the following table:

| | |
|--------------------------|----------------|
| Rebar Name | Main Rebar |
| Rebar Type | Main Rebar |
| Main Rebar Type | Top Main Rebar |
| Total Layer | Layer 1 |
| Current Layer | Layer 1 |
| Centroid of Rebar (mm) | 0.0 |
| 1st Cycle Rebar Diameter | #3 |
| No. of 1st Cycle Rebar | 0 |
| 2nd Cycle Rebar Diameter | #3 |
| No. of 2nd Cycle Rebar | 0 |
| Material Type | Steel1 |

At the bottom, there are 'Add' and 'Delete' buttons, and 'Layer As:' and 'Total As:' fields, both set to 0 mm². 'OK' and 'Cancel' buttons are at the bottom right.

The dialog box 'Define Reinforcements: Ties' shows the configuration for a Shear Rebar. The left sidebar has 'Shear Rebar' selected. The central preview shows a square cross-section with five vertical blue lines representing rebar, with labels 'Rebar Dia.' and 'Rebar C.T.C'. The right panel contains the following table:

| | |
|------------------|----------------|
| Rebar Name | Shear Rebar |
| Rebar Type | Shear Rebar |
| Shear Type | Vertical Shear |
| Rebar Diameter | #3 |
| Number of Legs | 0 |
| Rebar C.T.C (mm) | 0.0 |
| Material Type | Steel1 |

At the bottom, there are 'Add' and 'Delete' buttons, and a 'Total As:' field set to 0 mm². 'OK' and 'Cancel' buttons are at the bottom right.

Figure 48. Defining reinforcement.

2.6.3 NodeTypes

Threetypesofnodesinastrut-tiemodelaredefinedhere(figure 49).Morenodetypescanbeadded.

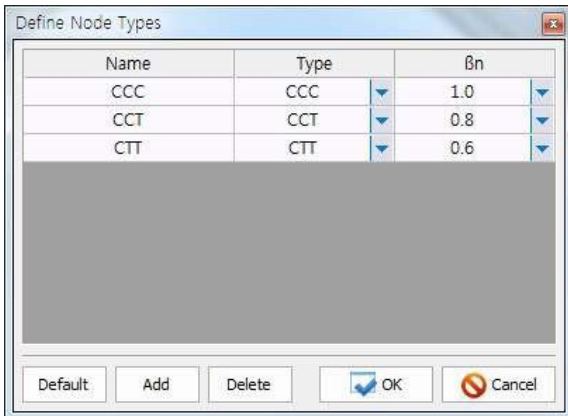


Figure 49. Node types.

Defaulttypesofloads and combinationsaredefinedhere in figure 50.

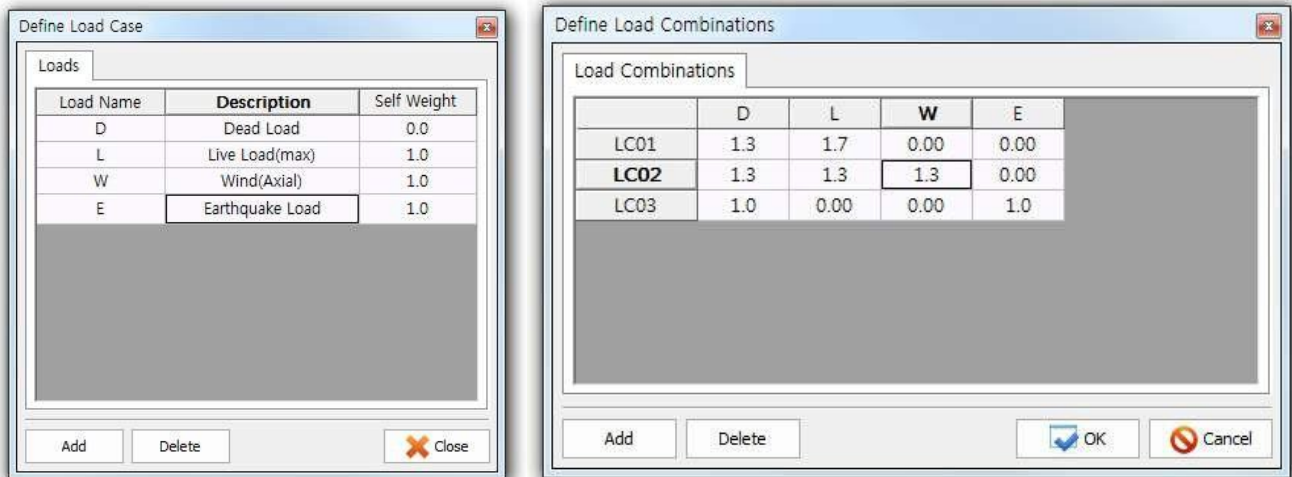
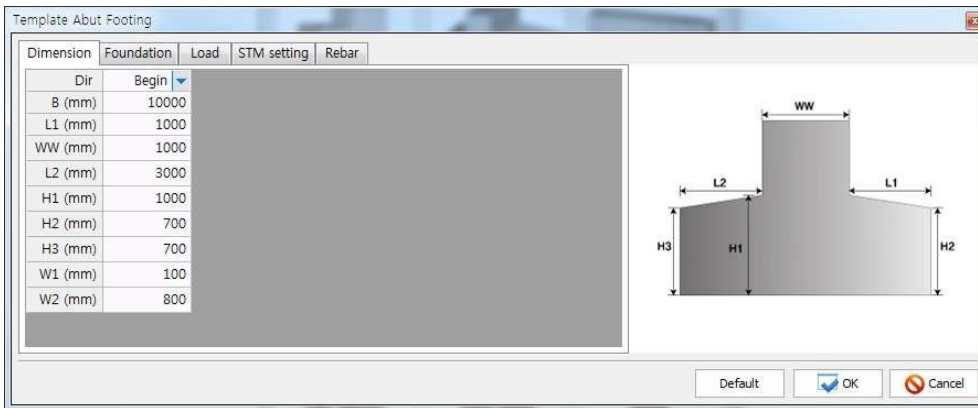


Figure 50. Defining reinforcement

2.7 Elements of the templates



Next, in the figures 51-55, some elements that are solved with the program are shown.

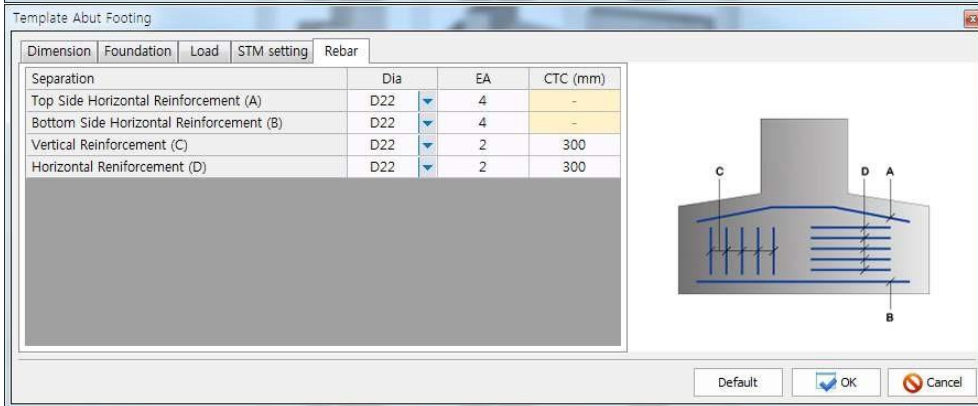
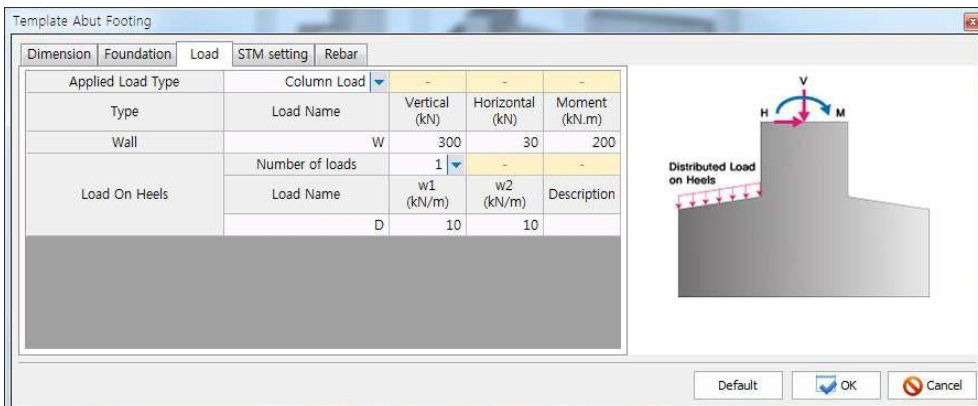


Figure 51. Foundation.

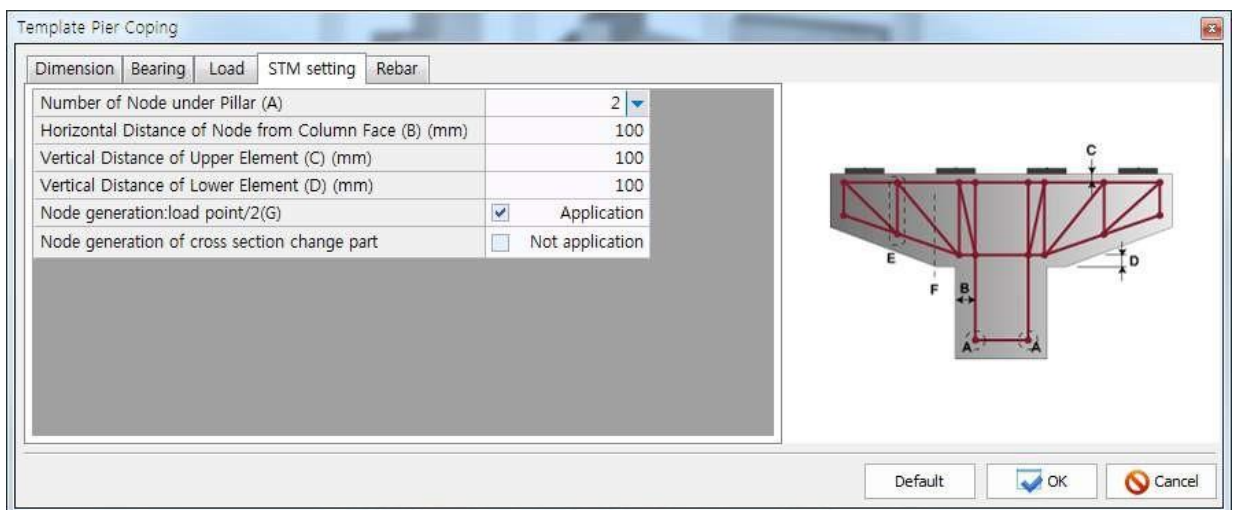
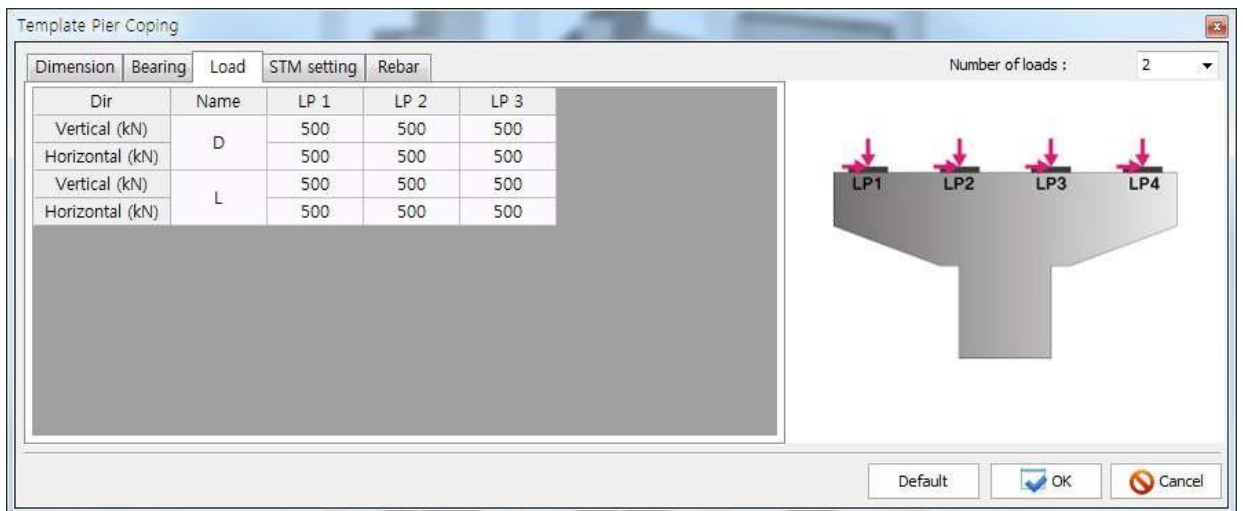
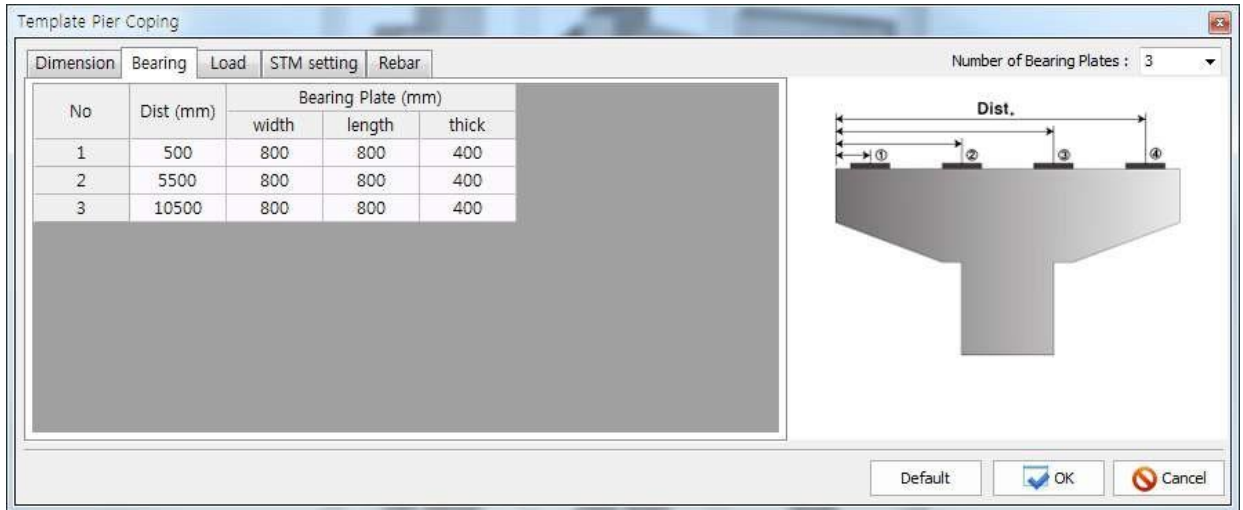


Figure 52. Two symmetric corbels.

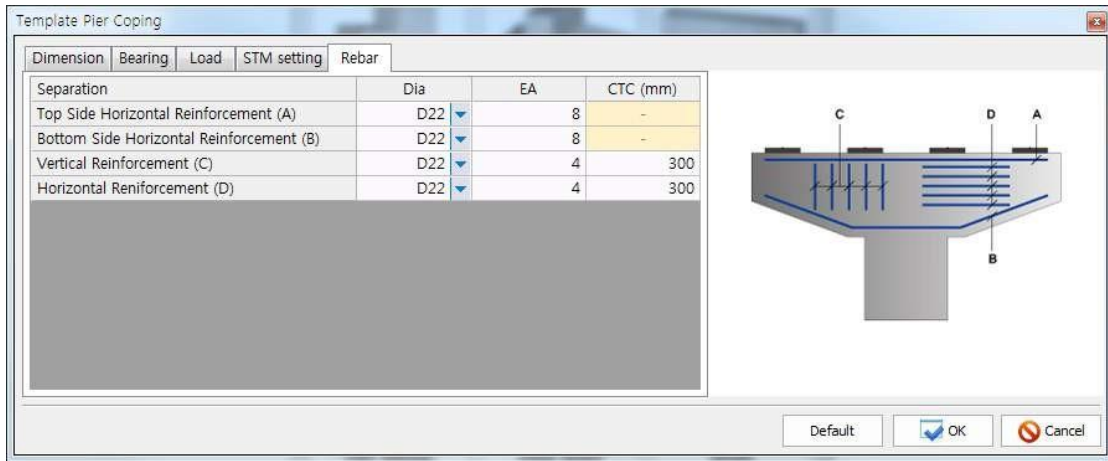


Figure 53. Reinforcement of tew symmetric corbels.

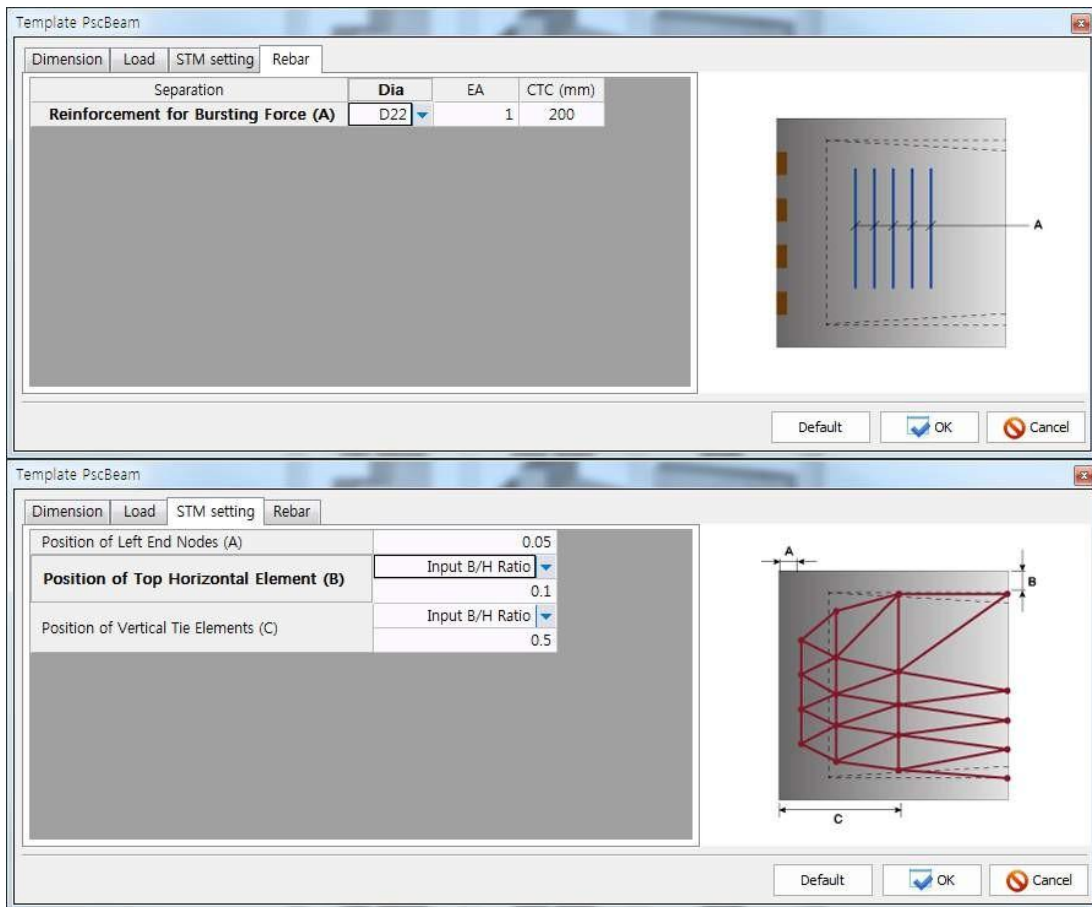


Figure 54. Prestressed concrete tenonds.

Template PscBox

Dimension Bearing Load STM setting Rebar

Type Solid

| | |
|---------|-------|
| B (mm) | 10000 |
| H1 (mm) | 300 |
| H2 (mm) | 2000 |
| H3 (mm) | 300 |
| H (mm) | 2600 |
| B1 (mm) | 5000 |
| B2 (mm) | 1000 |
| C1 (mm) | 2000 |
| C2 (mm) | 500 |
| T (mm) | 300 |

Default OK Cancel

Template PscBox

Dimension Bearing Load STM setting Rebar

Type Hollow

| | |
|---------|-------|
| B (mm) | 10000 |
| H1 (mm) | 300 |
| H2 (mm) | 2000 |
| H3 (mm) | 300 |
| H (mm) | 2600 |
| B1 (mm) | 5000 |
| B2 (mm) | 1000 |
| C1 (mm) | 2000 |
| C2 (mm) | 500 |
| T (mm) | 300 |
| X (mm) | 600 |

Default OK Cancel

Template PscBox

Dimension Bearing Load STM setting Rebar

| Dimension | Dia | EA | CTC (mm) |
|----------------------------|-----|----|----------|
| Horizontal Rebar (A) | #8 | 8 | - |
| Inclined Rebar (B) | #8 | 10 | - |
| Vertical Shear Rebar (C) | #5 | 2 | 200 |
| Horizontal Shear Rebar (D) | #5 | 4 | 150 |

Default OK Cancel

Figure 55. Concrete box.

Chapter 3

FEM Programm FE77

3.1 Introduction

This finite element program (FE), for structural concrete is used, in order to allow the analysis with crack closure in localized regions of structures. The model uses three-dimensional solid elements, while most of commercial programs use two-dimensional elements. The only material parameter that has to be defined in the program, is the uniaxial compressive strength of concrete. The steel bars are modeled as uniaxial elements and are considered as embedded in the concrete element. The proposed strategy has also a numerical procedure that is stable and efficient.

This program, considers both formation and closure of cracks, in the concrete structure. The numerical description of the crack process, involves the development of a procedure describing crack closure.

The characteristic feature of cracking is the discontinuity that arises in the structure. On the other hand, the FE model is essentially a continuum-mechanics technique. For this reason, the incompatibility between the problem and the model, requires special scheme, that will use the notation of continuity in the FE model, while will also consider sudden changes in the location of cracks. There are two basic schemes, that constitute the fundamentals alternatives to crack modeling, that are the discrete-crack approach and the smeared-crack approach.

The discrete-crack approach introduces an actual gap in the FE mesh at the location of the crack. It achieves this by doubling and separating the nodal coordinates lying along individual crack paths. This implies drastic changes in numbering of nodes, and the stiffness matrix.

The Smeared-cracking approach, describes the cracking in concrete structures within the framework of damage mechanics. A simple model has been developed by Kotsovos and Pavlovich, based on experimental tests of concrete under multiaxial stress states, as a complete sudden loss of stress. This model ignores any strain softening, that is considered to exist due to some interaction between the test specimen and the machine, in the course of testing. The only parameter that is needed for this model is the compressive test. For mesh dependency in connection to finer meshes, it is considered that the experimental conditions under which the constitutive relations show that the size of the elements in the FE analysis, should be no less than two or three times the size of the maximum aggregate in the concrete mix and therefore no consideration of finer meshes is needed.

A critical issue in the non-linear analysis of RC structure, is non-convergence, and in the case of convergence, it should be towards the realistic solution. In this program, a linear FE package called FINEL within an iterative procedure based on the Newton-Raphson method. The finite elements that are chosen, are called HX20 and HX27, that are the 20-node serendipity and the 27-node Lagrangian brick element for concrete modeling, respectively (*figure 56*). An element LM03 is a 3-node parabolic element, with only axial stiffness, is used for reinforcing bars. However, the main feature of the model is its heavy dependence on a description of the concrete behavior which sharply contrasts with those adopted by other FE structural-concrete models.

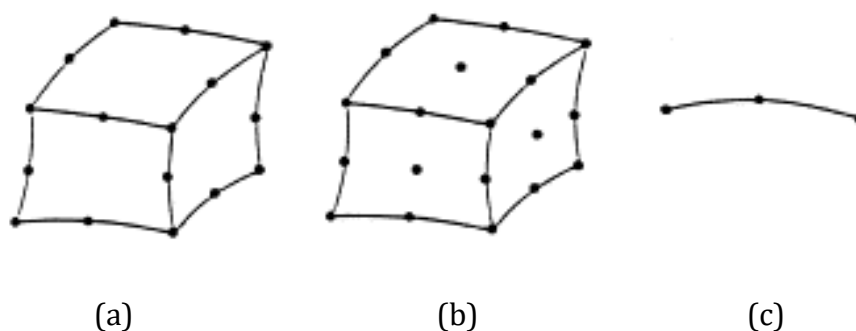


Figure 56. Selected 3-D finite elements (a) HX20, 20-node serendipity element (concrete); (b) HX27, 27 Lagrangian element (concrete); (c) LM03, 3-node uniaxial element (steel)

3.2 Concrete modeling

The constitutive relations for concrete comes from curves that best fit to valid experimental data on concrete behavior under triaxial states of stress. They describe concrete as a fully brittle medium in compliance with experimental information which indicates that “strain-softening” does not exist, for the reasons described before. It is also assumed that unloading from a given state, and then reloading is described by the initial elastic parameters (*figure 57*). The criterion for loading/unloading is based on the decomposition of the stress state into octahedral normal (σ_o) and shear (τ_o) stress components. As the component of the non-linear deformation of concrete under (τ_o) is considerably larger than that under (σ_o) only (τ_o) at a Gauss point at the start of every load step; if it is found larger, the Gauss point is consider to be in a state of loading; otherwise, it is consider to be in a state of unloading;

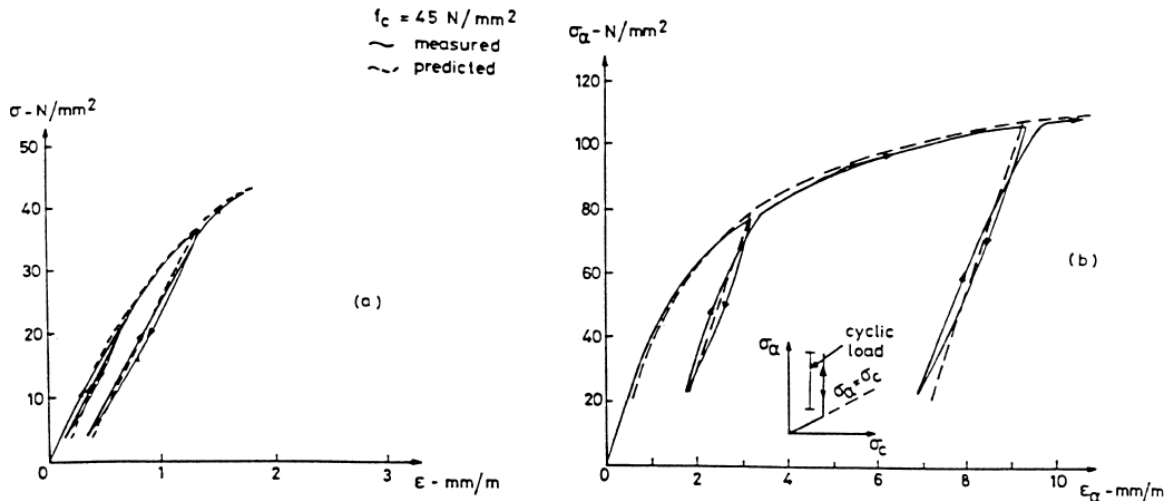


Figure 57. Measured and analytical stress-strain curves during loading and unloading/reloading for a typical concrete under (a) uniaxial and (b) triaxial compression.

The most important feature of the strength surface is the very significant effect of even small principal stresses on the strength in the third principal direction: Their effect is to significantly increase or decrease the ultimate-strength value depending on whether they are compressive or tensile in nature, respectively.

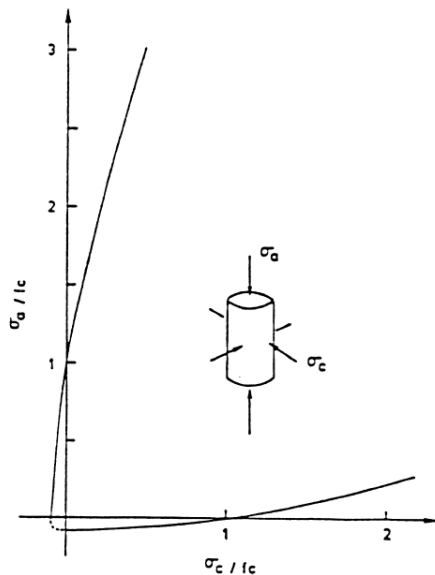


Figure 58. Measured and analytical stress-strain curves during loading and unloading/reloading for a typical concrete under (a) uniaxial and (b) triaxial compression.

3.3 Reinforcement steel modeling

The constitutive model of the reinforcing steel is shown in *figure 59*.

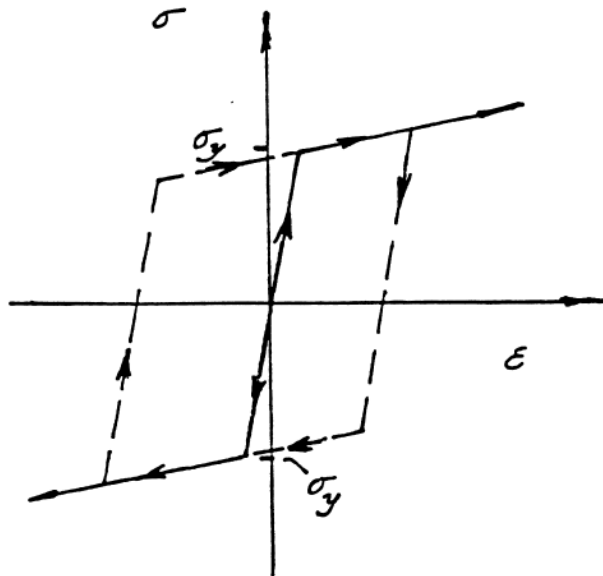


Figure 59. Constitutive model for steel.

The constitutive model for reinforcing steel is shown in *figure 59*. Unloading from any load level beyond yield is described by a straight line parallel to the initial elastic response. The same line describes reloading to the highest previous load level; when latter is exceeded, the steel response is described the bilinear stress-strain characteristics describing the response to a monotonically increased load.

3.4 Failure criterion

The following assumptions are made concerning their corresponding strains ϵ_0 and γ_0 .

Under pure hydrostatic stress, concrete only develops hydrostatic strains ϵ_{oh} .

Deviatoric stress-strain relationships are almost independent of the applied hydrostatic stress.

Under deviatoric stress, concrete also develops hydrostatic strains ϵ_{od} , the values of which depend on the level of hydrostatic stress. This is the only significant form of coupling between the deviatoric stress and volume change.

The behavior is essentially isotropic.

Unloading and subsequent reloading follow the initial stiffness slope (*figure 57*).

So the stress-strain relationship may be written in the following form:

$$\begin{aligned} \varepsilon_0 &= \varepsilon_{0h} + \varepsilon_{0d} = \frac{\sigma_0 + \sigma_{id}}{3K_s} \\ \gamma_0 &= \frac{\tau_0}{2G_s} \end{aligned} \quad (1)$$

where $\sigma_{id}(\sigma_0, \tau_0, f_c)$ is an anequivalent internal hydrostatic stress that accounts for the coupling and f_c is the uniaxial compressive strength of concrete; $K_s(\sigma_0, f_c)$ are secant bulk and shear moduli, respectively, should such a coupling not exist (i.e. they are obtained ignoring σ_{id}). Expressions for σ_{id} , K_s , and G_s may be derived through curve fitting of experimental data.

Since σ_{id} is a pure hydrostatic correction, expressions (1) are equivalent to the following relations in global co-ordinate directions:

$$\varepsilon_{ij} = \frac{\sigma_{ij} + \sigma_{id} \delta_{ij}}{2G_s} - \frac{3\nu_s}{E_s} (\sigma_0 + \sigma_{id}) \delta_{ij} \quad (2)$$

where $E_s(\sigma_0, \tau_0, f_c)$ and $\nu_s(\sigma_0, \tau_0, f_c)$ are secant Young's modulus and Poisson's ratio derived from K_s and G_s , using standard formulae of linear elasticity:

$$\begin{aligned} E_s &= \frac{9K_s G_s}{3K_s + G_s} \\ \nu_s &= \frac{3K_s - 2G_s}{6K_s + 2G_s} \end{aligned} \quad (3)$$

The component of the non-linear deformation of concrete under τ_0 is considerably larger than under σ_0 , if we denote by $\max \tau_0$ the deviatoric stress at each point on the stress-strain curve, then elastic unloading/reloading occurs whenever during a loading program the deviatoric stresses τ_0 become less than $\max \tau_0$.

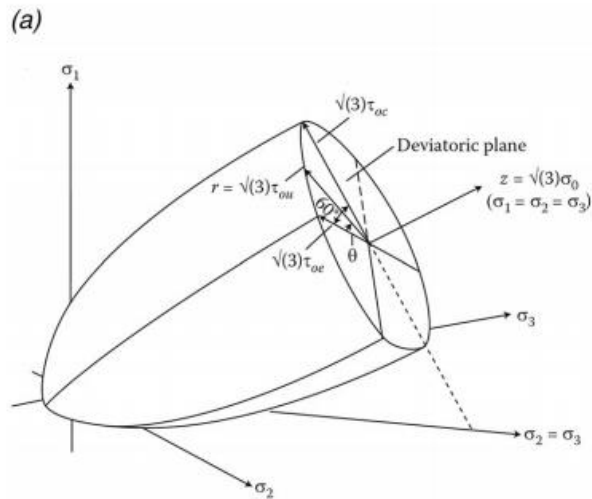


Figure 60. Concrete ultimate stress surface.

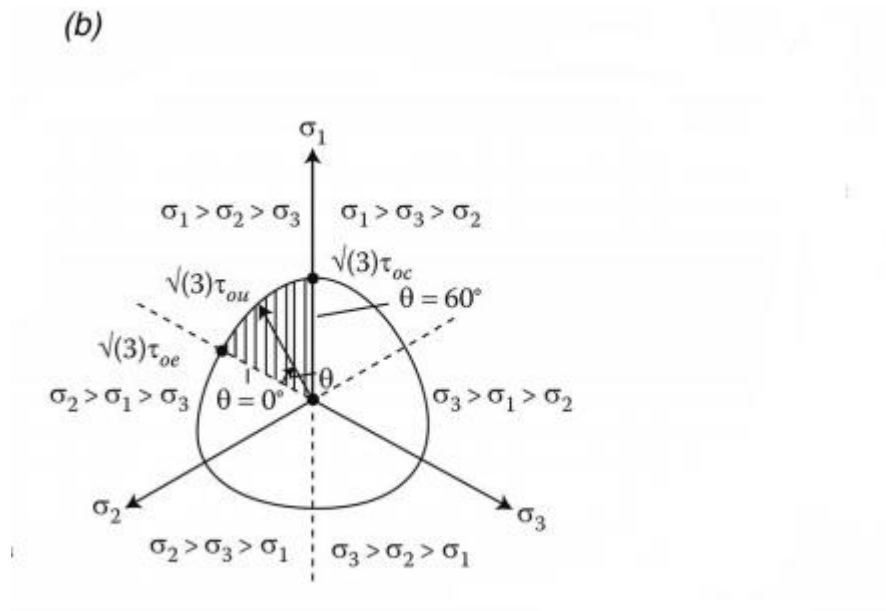


Figure 61. cross section of the stress surface under constant σ_0 .

The octahedral stresses also serve as a means to describe concrete failure which may be represented in the three-dimensional principal stress space by an open and convex failure surface. The form of such a failure surface can be seen in *figure 60*.

The projection of the failure surface on the deviatoric plane, results in a curve which is the locus of the ultimate deviatoric stress τ_{ou} . This ultimate stress may be calculated from σ_0 and θ , where θ is the rotational angle that the deviatoric stress,

taken as a vector, forms with one of the projected stress principal axes on the deviatoric plane.

For a given state of stress the quantities σ_0 , τ_0 , θ may be calculated:

$$\begin{aligned}\sigma_0 &= \frac{I_1}{3} \\ \tau_0 &= \sqrt{\left(2\sigma_0^2 - \frac{2}{3}I_2\right)} \\ \cos 3\theta &= -\frac{\sqrt{2}}{\tau_0^3} J_3\end{aligned}\tag{4}$$

where I_1 and I_2 are the first and second invariants of the stress tensor, whereas J_3 is the third invariant of the deviatoric stress tensor $s_{ij} = \sigma_{ij} - \sigma_0 \delta_{ij}$.

As has been experimentally shown, concrete starts due to concrete-homogeneity, and as a result concrete in localized region tends to expand against the surrounding material. So, the confined concrete therefore introduces in the localized region lateral compressive stresses, that, in turn, for equilibrium to be maintained, make the surrounding regions develop tensile stresses. This increases the strength of the localized region while the tensile stresses in the surrounding region eventually turn this state of stress into having one of its principal components tensile. This, as can be seen from *figure 58*, leads to the reduction of the strength of the surrounding region and macrocracking takes place.

Numerical modeling of cracking

A smeared fixed crack model within the framework of the finite element method is used to simulate the effect of cracking on the structure as the load is applied incrementally. Then, the increments of stresses and strains are related by the **D**-matrix adopted. Neglecting initial strains and stresses, its incremental counterpart is simply

$$\Delta\sigma = [\mathbf{D}]\Delta\varepsilon\tag{5}$$

For uncracked-concrete Gauss points, the **D**-matrix may be calculated by reference to a linearly-elastic isotropic material which is usually described in the following concise form

$$\sigma_{ij} = 2G\varepsilon_{ij} + 3\mu\varepsilon_0\delta_{ij}\tag{6}$$

Where G , and μ are the shear and Lamé's moduli, while the latter is also related to E and ν by the expression

$$\mu = \frac{\nu E}{(1+\nu)(1-2\nu)}$$

So for an uncracked Gauss point we have :

$$\begin{bmatrix} \Delta\sigma_x \\ \Delta\sigma_y \\ \Delta\sigma_z \\ \Delta\tau_{xy} \\ \Delta\tau_{xz} \\ \Delta\tau_{yz} \end{bmatrix} = \begin{bmatrix} 2G + \mu & \mu & \mu & 0 & 0 & 0 \\ \mu & 2G + \mu & \mu & 0 & 0 & 0 \\ \mu & \mu & 2G + \mu & 0 & 0 & 0 \\ 0 & 0 & 0 & G & 0 & 0 \\ 0 & 0 & 0 & 0 & G & 0 \\ 0 & 0 & 0 & 0 & 0 & G \end{bmatrix} \begin{bmatrix} \Delta\varepsilon_x \\ \Delta\varepsilon_y \\ \Delta\varepsilon_z \\ \Delta\gamma_{xy} \\ \Delta\gamma_{xz} \\ \Delta\gamma_{yz} \end{bmatrix} \quad (7)$$

Where $(\Delta\sigma_x, \Delta\sigma_y, \Delta\sigma_z, \Delta\tau_x, \Delta\tau_y, \Delta\tau_z)$ are the increments of direct and shear stresses in global coordinate, while G and μ are derived from tangent shear and bulk modulus. The coefficients of the D-matrix are functions of the state of stress, but, at the same time, it is worth noting that the constitutive matrix is isotropic throughout the microcracking regime and, hence, invariant with respect to any set of orthogonal axes.

Since the relations are in incremental form, the above material constants are tangent ones.

When the failure surface at a Gauss point has been exceeded for the first time a crack perpendicular to the maximum tensile stress is formed. Suppose that the plane of the crack is OAB (figure 62). Then for the local axis z' , which is perpendicular to this plane, the corresponding stiffnesses are zeroed, whereas a small shear is allowed to be transmitted in this plane denoted by βG . The shear retention factor β is set equal to 0.1, mainly for convergence, simulating, however, in a way, some 'aggregate interlock' that has also been verified experimentally. When the state of stress at a Gauss point reaches the triaxial envelope involving at least one principal tensile component for the first time, a crack plane is assumed to form in the direction orthogonal to the maximum principal tensile stress. As explained previously, such a tensile stress is set to zero and transformed into equivalent unbalanced forces, and the adopted incremental constitutive relationships in local axes are subsequently given the following matrix:

$$\begin{bmatrix} \Delta\sigma'_x \\ \Delta\sigma'_y \\ \Delta\sigma'_z \\ \Delta\tau'_{xy} \\ \Delta\tau'_{xz} \\ \Delta\tau'_{yz} \end{bmatrix} = \begin{bmatrix} 2G + \mu & \mu & \mu & 0 & 0 & 0 \\ \mu & 2G + \mu & \mu & 0 & 0 & 0 \\ \mu & \mu & 2G + \mu & 0 & 0 & 0 \\ 0 & 0 & 0 & G & 0 & 0 \\ 0 & 0 & 0 & 0 & G & 0 \\ 0 & 0 & 0 & 0 & 0 & G \end{bmatrix} \begin{bmatrix} \Delta\varepsilon'_x \\ \Delta\varepsilon'_y \\ \Delta\varepsilon'_z \\ \Delta\gamma'_{xy} \\ \Delta\gamma'_{xz} \\ \Delta\gamma'_{yz} \end{bmatrix} \quad (8)$$

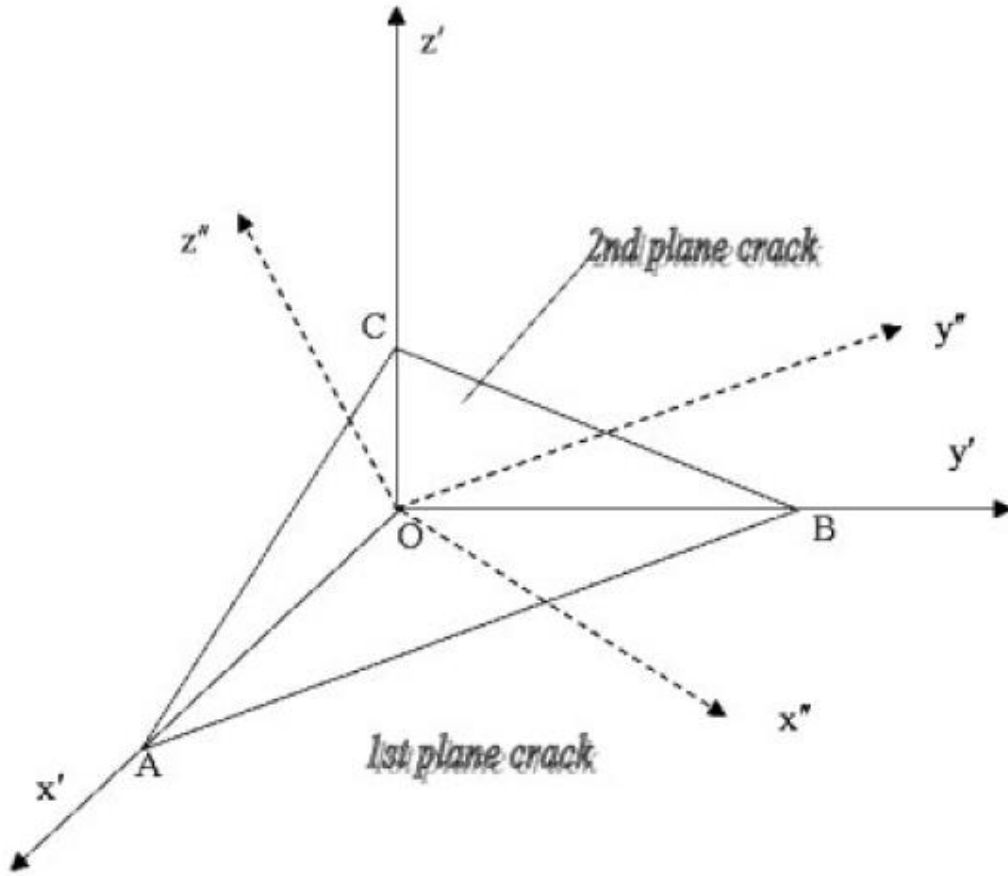


Figure 62. Local axes for one and two cracks at a Gauss point.

If the state of stress at a given Gauss point reaches the triaxial envelope in tension a second time, then a second crack plane is assumed to form. This new crack plane is now orthogonal to the current maximum tensile principal stress and, as a result, is not necessarily orthogonal to the first crack plane. The combination of the two fracture planes only leaves stiffness in the direction of the intersection of both planes. As for the one-crack case, some residual shear stiffness has to be kept on order to improve the conditioning of the crack stiffness matrices. Explicitly, the incremental constitutive relations adopted for this case are as follows

$$\begin{bmatrix} \Delta\sigma''_x \\ \Delta\sigma''_y \\ \Delta\sigma''_z \\ \Delta\tau''_{xy} \\ \Delta\tau''_{xz} \\ \Delta\tau''_{yz} \end{bmatrix} = \begin{bmatrix} 2G + \mu & \mu & \mu & 0 & 0 & 0 \\ \mu & 2G + \mu & \mu & 0 & 0 & 0 \\ \mu & \mu & 2G + \mu & 0 & 0 & 0 \\ 0 & 0 & 0 & G & 0 & 0 \\ 0 & 0 & 0 & 0 & G & 0 \\ 0 & 0 & 0 & 0 & 0 & G \end{bmatrix} \begin{bmatrix} \Delta\varepsilon''_x \\ \Delta\varepsilon''_y \\ \Delta\varepsilon''_z \\ \Delta\gamma''_{xy} \\ \Delta\gamma''_{xz} \\ \Delta\gamma''_{yz} \end{bmatrix} \quad (9)$$

Because of the crack induced anisotropy for the last two cases, the stress-strain matrix, is transformed to global orientations using standard co-ordinate system transformation laws.

If the new tensile stress occurs at the same time Gauss point for third time, then we have a complete loss of carrying capacity of the Gauss point.

3.5 Proposed Numerical strategy

A single crack approach (SCA) has been used by **Kotsovos and Spiliopoulos** in analyses of reinforced concrete structures with crack closure. According to this strategy, the load is applied in relatively large steps and for convergence reason only one crack is allowed to open or close inside a Newton–Raphson iteration. The check for the state of loading or unloading at a Gauss point is determined at the beginning of the load step and remains fixed until convergence. A single crack approach (SCA) has been used by Kotsovos and Spiliopoulos in analyses of reinforced concrete structures with crack closure. According to this strategy, the load is applied in relatively large steps and for convergence reason only one crack is allowed to open or close inside a Newton–Raphson iteration. The check for the state of loading or unloading at a Gauss point is determined at the beginning of the load step and remains fixed until convergence. According to the proposed procedure, if we denote by j an iteration inside an incremental load step we can get an increment of displacements, using the tangent stiffness matrix of the previous iteration.

Focusing on a Gauss point:

1. The increments of strains are evaluated from the increments of the displacements

$$\Delta \boldsymbol{\varepsilon}^{(j)} = \mathbf{B}_c \Delta \mathbf{u}^{(j)} \quad (10)$$

2. The total strains are calculated from the strains of the previous iteration

$$\boldsymbol{\varepsilon}^{(j)} = \boldsymbol{\varepsilon}^{(j-1)} + \Delta \boldsymbol{\varepsilon}^{(j)} \quad (11)$$

3. The prediction of stresses is made using the material of the previous iteration

$$\boldsymbol{\sigma}_{pr}^{(j)} = \boldsymbol{\sigma}^{(j-1)} + \mathbf{D}^{(j-1)} \Delta \boldsymbol{\varepsilon}^{(j)} \quad (12)$$

From the predicted state of stress the quantities $\tau_0^{(j)}$, $\sigma_0^{(j)}$ and $\tau_{0u}^{(j)}$ may be calculated. A correction of stress occurs depending on whether the Gauss point was at the previous iteration cracked or uncracked.

For an uncracked Gauss point, all the different possibilities may be traced in *figure 63*. If $\tau_0^{(j)}$ is found larger than $\tau_{0u}^{(j)}$, something which normally happens when tensile stresses have developed, a new crack forms normal to the maximum principal tensile stress σ_1 . This stress is put to zero without the other two principal stresses being affected. This has an effect to produce residual stresses:

$$\Delta\sigma_r = \mathbf{T}_\sigma^{-1} \begin{Bmatrix} -\sigma_1 \\ 0 \\ 0 \end{Bmatrix} \quad (13)$$

Where \mathbf{T}_σ^{-1} is the inverse transformation matrix from the principal stress axes to the initial x, y, z axes. At the same time the material matrix in terms of the local crack's axis is established using Equation (6). The transformation of this matrix to global axes, denoted by $\mathbf{D}_{cr}^{(j)}$, updates the material matrix $\mathbf{D}^{(j)}$ to be used in the next iteration.

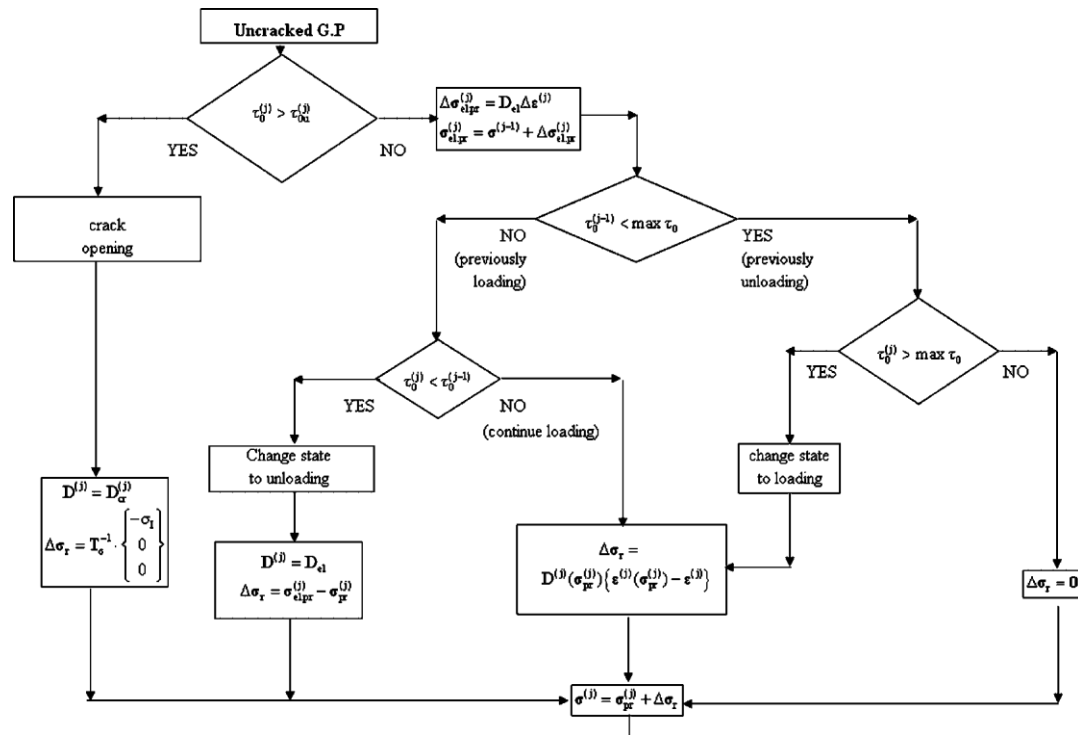


Figure 63. Flow chart for the stress correction at an uncracked Gauss point.

For a Gauss point that remains uncracked an elastic stress prediction is performed:

$$\Delta\sigma_{pr}^{(j)} = \mathbf{D}_{el} \Delta\boldsymbol{\varepsilon}^{(j)} \quad (14)$$

$$\boldsymbol{\sigma}_{el.pr}^{(j)} = \boldsymbol{\sigma}^{(j-1)} + \Delta\boldsymbol{\sigma}_{el.pr}^{(j)}$$

Where \mathbf{D}_{el} is the material matrix that contains the initial material constants.

Next it has to be determined whether the Gauss point is in a condition of previously loading ($\tau_0^{(j-1)} > \max \tau_0$) or unloading ($\tau_0^{(j-1)} < \max \tau_0$).

For a previously loading Gauss point that changes its state to loading ($\tau_0^{(j-1)} > \max \tau_0$)

or a previously unloading Gauss point that changes its state to loading ($\tau_0^{(j-1)} > \max \tau_0$), an initial stain method is applied and the stress is corrected according to

$$\Delta \sigma_r = \mathbf{D}^{(j)}(\sigma_{pr}^{(j)}) \{ \epsilon^{(j)}(\sigma_{pr}^{(j)}) - \epsilon^{(j)} \} \quad (15)$$

Where $\epsilon^{(j)}(\sigma_{pr}^{(j)})$ is computed according to equation (2). If a previously unloading

Gauss point continues to unload ($\tau_0^{(j-1)} < \max \tau_0$), then no stress

correction is needed ($\Delta \sigma_r = \mathbf{0}$).

In the last case where a previously loading uncracked Gauss point begins to unload ($\tau_0^{(j-1)} < \max \tau_0$), initial elastic properties are restored and the residual stresses are equal to the difference of the elastically predicted stresses and the tangent predicted stresses:

$$\Delta \sigma_r = \sigma_{el.pr}^{(j)} - \sigma_{pr}^{(j)} \quad (16)$$

For a *cracked* Gauss point the different possibilities may be found in Figure 6.

The total strains normal to all the existing crack directions $\epsilon_N^{(j)}$ are checked and if any one of them is found compressive, the crack is assumed to close, the material matrix in the local crack's direction is updated using Equations () and () and the transformed to the global stress directions $\mathbf{D}_{cr}^{(j)}$ is set equal to $\mathbf{D}^{(j)}$. At the same time the stresses are corrected using this matrix and the total strains:

$$\Delta \sigma_r = \mathbf{D}^{(j)} \epsilon^{(j)} \quad (17)$$

In case there is no crack closure the procedure checks whether we have a crack opening ($\tau_0^{(j)} > \tau_{0u}^{(j)}$). If this happens, then the stress correction may be done using Equation (); otherwise no stress correction is needed ($\Delta \sigma_r = \mathbf{0}$).

For both the cases of the cracked or uncracked Gauss points the stress corrections give rise to unbalanced forces that are implemented, in the standard way, as a new force vector applied in the next iteration.

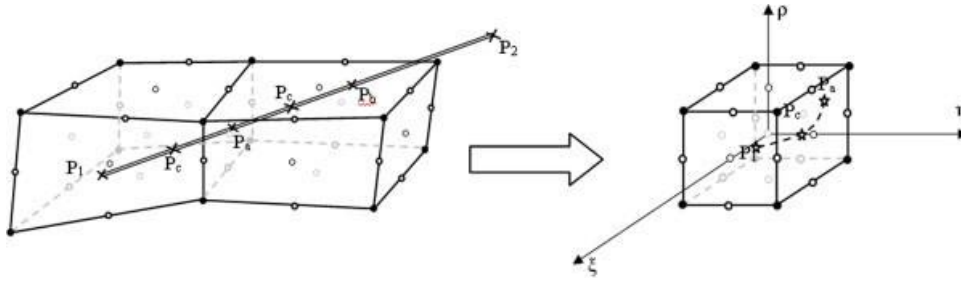


Figure 64. Embedding a straight steel bar inside concrete.

Twenty seven-node Lagrangian brick elements with 3x3x3 Gauss points were used for the finite element implementation of concrete behaviour. The well-known fact of mesh in- objectivity for brittle materials is circumvented using elements having a size of 5–20 cm that have proved to give realistic results. This is due to the fact that the size of the concrete specimens that were used to deduce the above-described concrete behaviour is roughly the same as the equivalent volume that corresponds to a Gauss point. This size of elements therefore serves as a means of a 'localization limiter'.

Steel bars are modelled as three-noded uniaxial truss elements. The Menegotto–Pinto model is adopted, a model that accommodates the Bauschinger effect, observed in steel, under large load reversals. Inside an iteration of an incremental step, in the standard way, the incremental strain along the steel bar is used to make an elastic prediction for the stress. If this stress is found to be larger than the current yield stress, a correction to the stress is made so that it is brought back on the true stress–strain curve. Equivalent nodal stresses are then applied so that equilibrium is restored. Steel bars may be considered to have arbitrary positions inside the concrete elements (Figure 64). A numerical procedure that takes into account the contribution of such an embedded reinforcement is used. With this procedure for each straight segment of reinforcement only the endpoint co-ordinates in the global axes need to be provided by the analyst. The concrete elements that contain a portion of the bar defined through the points P_1 and P_2 may be found with the aid of a reverse mapping from the global co-ordinates (x, y, z) to the element natural ones ξ, η, ρ . A Newton–Raphson procedure is utilized to make this conversion. The point P_1 is contained in a given concrete element if its co-ordinates $\xi_{P_1}, \eta_{P_1}, \rho_{P_1}$ satisfy

$$|\xi_{P_1}, \eta_{P_1}, \rho_{P_1}| \leq 1 \quad (18)$$

Once the element that contains P_1 is found, the use of analytic geometry determines the intersection point P_a of P_1P_2 with one of the possible six faces of the elements. After this has been established, P_1 becomes P_a and the algorithm is repeated.

Assuming a perfect bond between steel and concrete, the strain inside iteration

j of the incremental step along the steel bar with direction cosines l, m, n may easily be evaluated :

$$\Delta \varepsilon_{r.xx}^{(j)} = \Delta \varepsilon_{xx}^{(j)} l^2 + \Delta \varepsilon_{yy}^{(j)} m^2 + \Delta \varepsilon_{zz}^{(j)} n^2 + 2\Delta \varepsilon_{xy}^{(j)} lm + 2\Delta \varepsilon_{yz}^{(j)} mn + 2\Delta \varepsilon_{xz}^{(j)} ln$$

$$= \mathbf{T}_\varepsilon \Delta \boldsymbol{\varepsilon}^{(j)} = \mathbf{T}_\varepsilon \mathbf{B}_c \Delta \mathbf{u}^{(j)} = \mathbf{B}_r \Delta \mathbf{u}^{(j)} \quad (19)$$

The contribution to the stiffness matrix of a steel bar inside a concrete element is given by

$$\mathbf{K}_r^{(j)} = A_r E_r^{(j)} \int_S \mathbf{B}_r^T \mathbf{B}_r dS \quad (20)$$

Where $E_r^{(j)}$ and A_r are the tangential modulus of elasticity and the cross-sectional area of the steel bar. Thus, the total stiffness matrix of the reinforced concrete element is

$$\mathbf{K}^{(j)} = \mathbf{K}_c^{(j)} + \sum_{i=1}^{nrs} \mathbf{K}_c^{(j)} = \int_V \mathbf{B}_c^T \mathbf{D}^{(j)} \mathbf{B}_c dV + \sum_{i=1}^{nrs} \mathbf{K}_{r,i}^{(j)}$$

where nrs is the number of embedded reinforcements inside a brick element.

A highly modular finite element code (FE77) was used as a basis for the implementation of the above-described procedures. A new module was added in which the Newton-Raphson iterative procedure with the mathematical description of concrete behavior, together with the different approaches regarding the crack strategy were implemented.

Chapter 4

Abaqus Damage Plasticity Model (DPM)

4.1 Introduction

This model provides a general capability for modeling concrete and other quasi-brittle materials in all types of structures (beams, trusses, shells, and solids). It uses concepts of isotropic damaged elasticity in combination with isotropic tensile and compressive plasticity to represent the inelastic behavior of concrete, that can be used for plain concrete, even though it is intended primarily for the analysis of reinforced concrete structures. It can be used with rebar to model concrete reinforcement. The model is designed for applications in which concrete is subjected to monotonic, cyclic, and dynamic loading under low confining pressures, and consists of the combination of nonassociated multi-hardening plasticity and scalar (isotropic) damaged elasticity to describe the irreversible damage that occurs during the fracturing process. It allows user control of stiffness recovery effects during cyclic load reversals, and can be defined to be sensitive to the rate of straining. The model can be used in conjunction with a viscoplastic regularization of the constitutive equations in Abaqus to improve the convergence rate in the softening area and it requires that the elastic behavior of the material be isotropic and linear.

4.2 Mechanical behavior

The model is a continuum, plasticity-based, damage model for concrete. It assumes that the main two failure mechanisms are tensile cracking and compressive crushing of the concrete material. The evolution of the yield (or failure) surface is controlled by two hardening variables $\bar{\epsilon}_t^{pl}$ and $\bar{\epsilon}_c^{pl}$, linked to failure mechanisms under tension and compression loading, respectively. We refer to $\bar{\epsilon}_t^{pl}$ and $\bar{\epsilon}_c^{pl}$ as tensile and compressive equivalent plastic strains, respectively. The following sections discuss the main assumptions about the mechanical behavior of concrete.

4.3 Uniaxial tension and compression stress behavior

The model assumes that the uniaxial tensile and compressive response of concrete is characterized by damaged plasticity, as shown in figure 65.

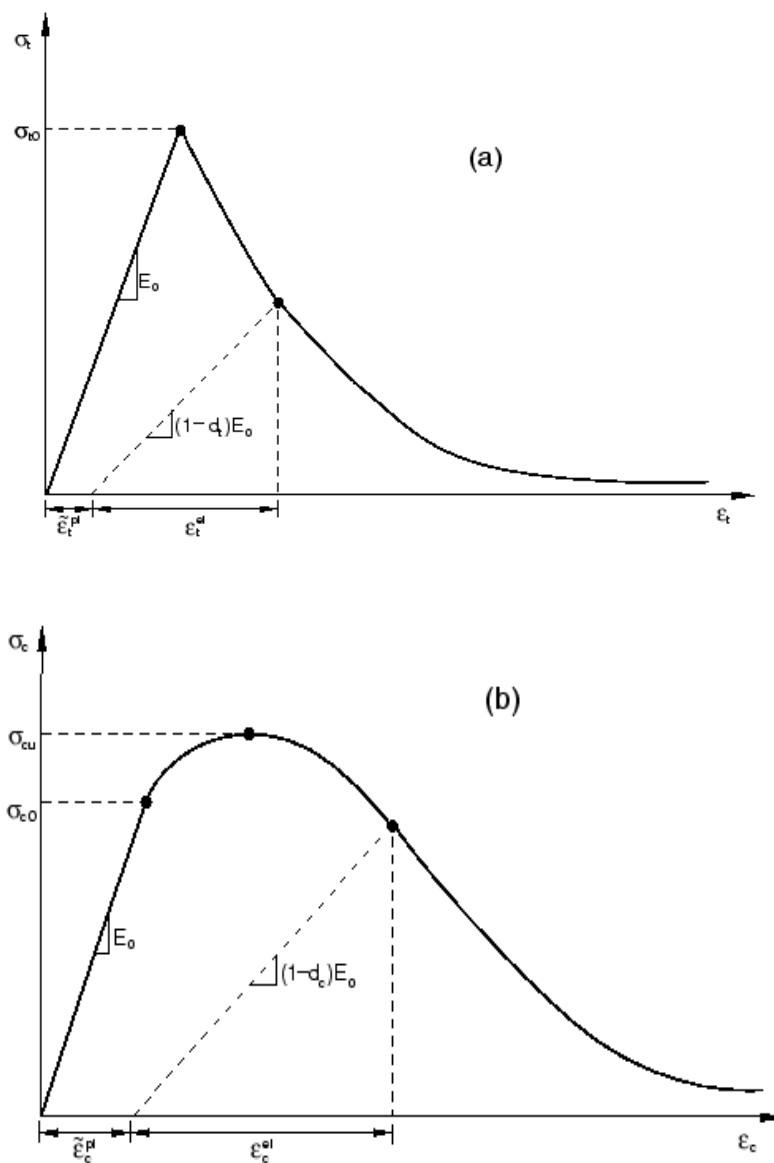


Figure 65. Response of concrete to uniaxial loading in tension (a) and compression (b).

Under uniaxial tension the stress-strain response follows a linear elastic relationship until the value of the failure stress σ_{to} , is reached. The failure stress corresponds to the onset of micro-cracking in the concrete material. Beyond the failure stress the formation of micro-cracks is represented macroscopically with a softening stress-strain response, which induces strain localization in the concrete structure. Under uniaxial compression the response is linear until the value of initial yield, σ_{to} . In the plastic regime the response is typically characterized by stress hardening followed by strain softening beyond the ultimate stress, σ_{cu} . This representation, although somewhat simplified, captures the main features of the response of concrete.

It is assumed that the uniaxial stress-strain curves can be converted into stress versus plastic-strain curves. Thus,

$$\sigma_t = \sigma_t(\bar{\varepsilon}_t^{pl}, \dot{\bar{\varepsilon}}_t^{pl}, \theta, f_i)$$

$$\sigma_c = \sigma_c(\bar{\varepsilon}_c^{pl}, \dot{\bar{\varepsilon}}_c^{pl}, \theta, f_i)$$

where the subscripts t and c refer to tension and compression,

respectively; $\bar{\varepsilon}_t^{pl}$ and $\bar{\varepsilon}_c^{pl}$ are the equivalent plastic strains, $\dot{\bar{\varepsilon}}_t^{pl}$ and $\dot{\bar{\varepsilon}}_c^{pl}$ are the equivalent plastic strain rates, θ is the temperature, and f_i are other predefined field variables.

As shown in *figure 1*, when the concrete specimen is unloaded from any point on the strain softening branch of the stress-strain curves, the unloading response is weakened. The elastic stiffness of the material appears to be damaged (or degraded). The degradation of the elastic stiffness is characterized by two damage variables, d_t and d_c , which are assumed to be functions of the plastic strains, temperature, and field variables:

$$d_t = d_t(\bar{\varepsilon}_t^{pl}, \theta, f_i); \quad 0 \leq d_t \leq 1,$$

$$d_c = d_c(\bar{\varepsilon}_c^{pl}, \theta, f_i); \quad 0 \leq d_c \leq 1.$$

The damage variables can take values from zero, representing the undamaged material, to one, which represents total loss of strength.

If E_0 is the initial (undamaged) elastic stiffness of the material, the stress-strain relations under uniaxial tension and compression loading are, respectively:

$$\sigma_t = (1 - d_t) E_0 (\varepsilon_t - \bar{\varepsilon}_t^{pl}),$$

$$\sigma_c = (1 - d_c) E_0 (\varepsilon_c - \bar{\varepsilon}_c^{pl}).$$

We define the “effective” tensile and compressive cohesion stresses as

$$\bar{\sigma}_t = \frac{\sigma_t}{(1-d_t)} = E_0(\epsilon_t - \bar{\epsilon}_t^{pl}) ,$$

$$\bar{\sigma}_c = \frac{\sigma_c}{(1-d_c)} = E_0(\epsilon_c - \bar{\epsilon}_c^{pl}) ,$$

The effective cohesion stresses determine the size of the yield (or failure) surface.

Uniaxial cyclic behavior

Under uniaxial cyclic loading conditions the degradation mechanisms are quite complex, involving the opening and closing of previously formed micro-cracks, as well as their interaction. Experimentally, it is observed that there is some recovery of the elastic stiffness as the load changes sign during a uniaxial cyclic test. The stiffness recovery effect, also known as the “unilateral effect,” is an important aspect of the concrete behavior under cyclic loading. The effect is usually more pronounced as the load changes from tension to compression, causing tensile cracks to close, which results in the recovery of the compressive stiffness.

The concrete damaged plasticity model assumes that the reduction of the elastic modulus is given in terms of a scalar degradation variable d as

$$E = (1-d)E_0,$$

where E_0 is the initial (undamaged) modulus of the material.

This expression holds both in the tensile ($\sigma_{11} > 0$) and the compressive ($\sigma_{11} < 0$) sides of the cycle. The stiffness degradation variable, d , is a function of the stress state and the uniaxial damage variables, d_t and d_c . For the uniaxial cyclic conditions, Abaqus assumes that

$$(1-d) = (1-s_t d_t)(1-s_c d_c)$$

where s_t and s_c are functions of the stress state that are introduced to model stiffness recovery effects associated with stress reversals. They are defined according to:

$$s_t = 1 - w_t r^*(\sigma_{11}) ; 0 \leq w_t \leq 1,$$

$$s_c = 1 - w_c (1 - r^*(\sigma_{11})) ; 0 \leq w_c \leq 1, \text{ where}$$

$$r^*(\sigma_{11}) = H(\sigma_{11}) = \begin{cases} 1 & \text{if } \sigma_{11} > 0 \\ 0 & \text{if } \sigma_{11} < 0 \end{cases}$$

The weight factors w_t and w_c , which are assumed to be material properties, control the recovery of the tensile and compressive stiffness upon load reversal.

To illustrate this, consider the example in *figure 66*, where the load changes from tension to compression.

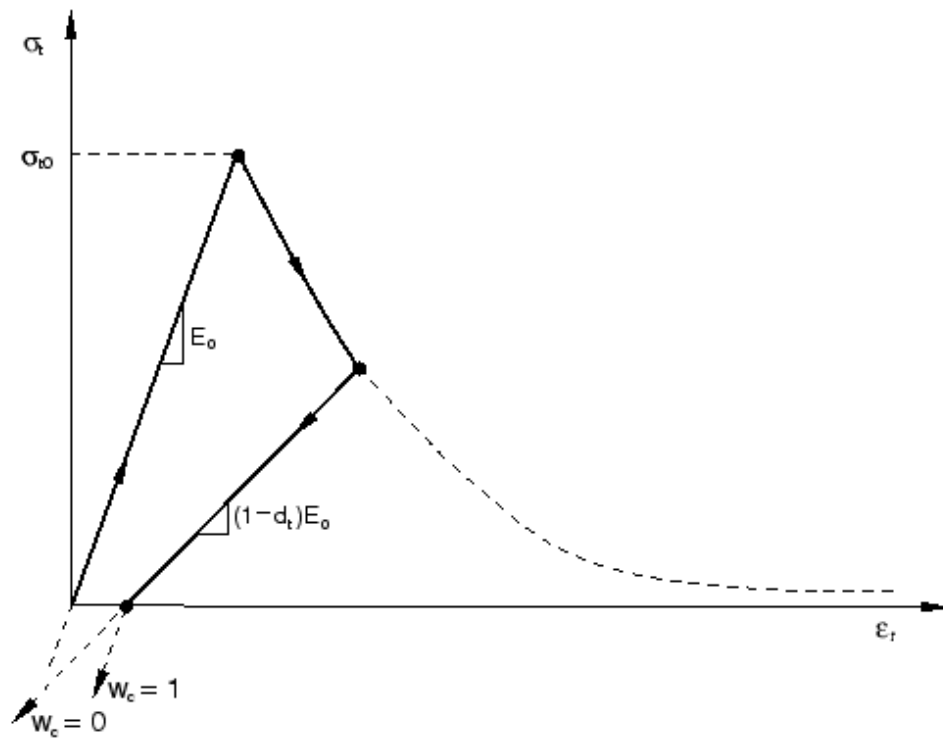


Figure 66. Illustration of the effect of the compression stiffness recovery parameter w_c .

Assume that there was no previous compressive damage (crushing) in the material; that is, $\bar{\epsilon}_c^{pl}$, and $d_c=0$

Then

$$(1-d)=(1-s_c d_t)=(1-(1-w_c(1-r^*))d_t).$$

In tension ($\sigma_{11}>0$), $r^*=1$; therefore, $d=d_t$ as expected.

In compression ($\sigma_{11}<0$), $r^*=0$, and $d=(1-w_c)d_t$.

If $w_c=1$, then $d=0$; therefore, the material fully recovers the compressive stiffness (which in this case is the initial undamaged stiffness, $E=E_0$). If, on the other hand, $w_c=0$, then $d=d_t$ and there is no stiffness recovery. Intermediate values of w_c result in partial recovery of the stiffness.

4.4 Multiaxial behavior

The stress-strain relations for the general three-dimensional multiaxial condition are given by the scalar damage elasticity equation:

$$\sigma = (1-d)D_0^{el}Q:(\varepsilon - \varepsilon^{pl})$$

where D_0^{el} is the initial (undamaged) elasticity matrix.

4.5 Reinforcement

In Abaqus reinforcement in concrete structures is typically provided by means of rebars, which are one-dimensional rods that can be defined singly or embedded in oriented surfaces. Rebars are typically used with metal plasticity models to describe the behavior of the rebar material and are superposed on a mesh of standard element types used to model the concrete. With this modeling approach, the concrete behavior is considered independently of the rebar. Effects associated with the rebar/concrete interface, such as bond slip and dowel action, are modeled approximately by introducing some “tension stiffening” into the concrete modeling to simulate load transfer across cracks through the rebar. Details regarding tension stiffening are provided below.

Defining the rebar can be tedious in complex problems, but it is important that this be done accurately since it may cause an analysis to fail due to lack of reinforcement in key regions of a model.

4.6 Defining tension stiffening

The postfailure behavior for direct straining is modeled with tension stiffening, which allows you to define the strain-softening behavior for cracked concrete. This behavior also allows for the effects of the reinforcement interaction with concrete to be simulated in a simple manner. Tension stiffening is required in the concrete damaged plasticity model. You can specify tension stiffening by means of a postfailure stress-strain relation or by applying a fracture energy cracking criterion.

4.7 Postfailure stress-strain relation

In reinforced concrete the specification of postfailure behavior generally means giving the postfailure stress as a function of cracking strain $\bar{\varepsilon}_t^{ck}$. The cracking strain is defined as the total strain minus the elastic strain corresponding to the undamaged material; that is,

$$\bar{\varepsilon}_t^{ck} = \varepsilon_t - \varepsilon_{0t}^{el}$$

Where $\varepsilon_{0t}^{el} = \sigma_t / E_0$, as illustrated in *figure 67*. To avoid potential numerical problems, Abaqus enforces a lower limit on the postfailure stress equal to 100 times of the initial failure stress: $\sigma_t \geq \sigma_{t0} / 100$.

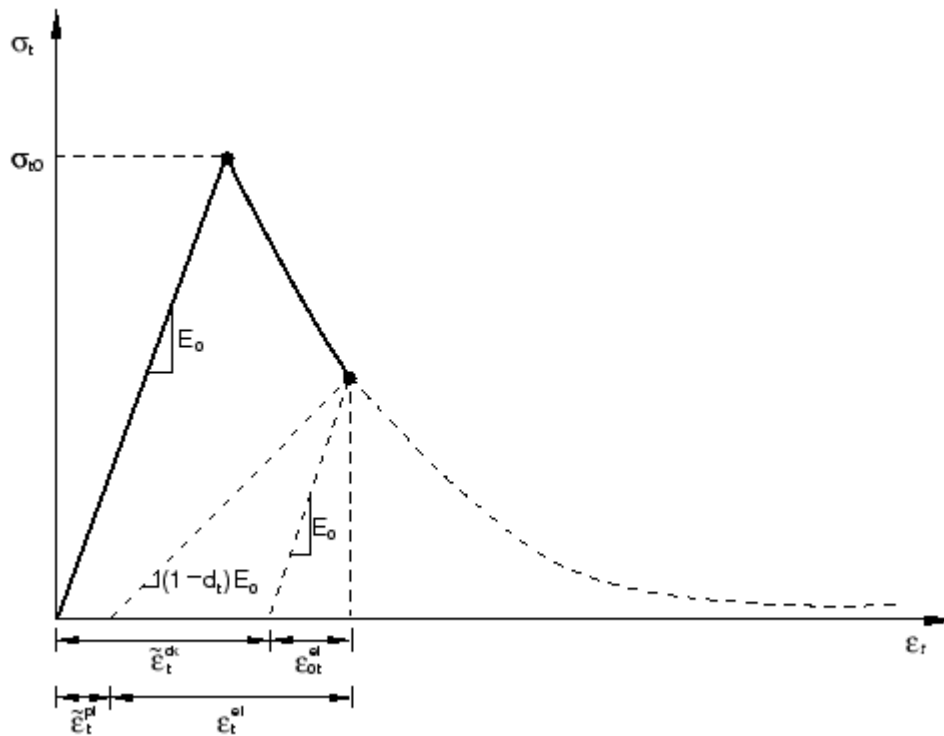


Figure 67. Illustration of the definition of the cracking strain $\bar{\varepsilon}_t^{ck}$ used for the definition of tension stiffening data.

Tension stiffening data are given in terms of the cracking strain, $\bar{\varepsilon}_t^{ck}$. When unloading data are available, the data are provided to Abaqus in terms of tensile damage curves, $d_t - \bar{\varepsilon}_t^{ck}$, as discussed below. Abaqus automatically converts the cracking strain values to plastic strain values using the relationship:

$$\bar{\varepsilon}_t^{pl} = \bar{\varepsilon}_t^{ck} - \frac{d_t \sigma_t}{(1-d_t) E_o}$$

Abaqus will issue an error message if the calculated plastic strain values are negative and/or decreasing with increasing cracking strain, which typically indicates that the tensile damage curves are incorrect. In the absence of tensile damage $\bar{\varepsilon}_t^{pl} = \bar{\varepsilon}_t^{ck}$.

In cases with little or no reinforcement, the specification of a postfailure stress-strain relation introduces mesh sensitivity in the results, in the sense that the finite element predictions do not converge to a unique solution as the mesh is refined because mesh refinement leads to narrower crack bands. This problem typically occurs if cracking failure occurs only at localized regions in the structure and mesh refinement does not result in the formation of additional cracks. If cracking failure is distributed evenly (either due to the effect of rebar or due to the presence of stabilizing elastic material, as in the case of plate bending), mesh sensitivity is less of a concern.

In practical calculations for reinforced concrete, the mesh is usually such that each element contains rebars. The interaction between the rebars and the concrete tends to reduce the mesh sensitivity, provided that a reasonable amount of tension stiffening is introduced in the concrete model to simulate this interaction. This requires an estimate of the tension stiffening effect, which depends on such factors as the density of reinforcement, the quality of the bond between the rebar and the concrete, the relative size of the concrete aggregate compared to the rebar diameter, and the mesh. A reasonable starting point for relatively heavily reinforced concrete modeled with a fairly detailed mesh is to assume that the strain softening after failure reduces the stress linearly to zero at a total strain of about 10 times the strain at failure. The strain at failure in standard concretes is typically 10^{-4} , which suggests that tension stiffening that reduces the stress to zero at a total strain of about 10^{-3} is reasonable. This parameter should be calibrated to a particular case.

The choice of tension stiffening parameters is important since, generally, more tension stiffening makes it easier to obtain numerical solutions. Too little tension stiffening will cause the local cracking failure in the concrete to introduce temporarily unstable behavior in the overall response of the model. Few practical designs exhibit such behavior, so that the presence of this type of response in the analysis model usually indicates that the tension stiffening is unreasonably low.

4.8 Fracture energy cracking criterion

When there is no reinforcement in significant regions of the model, the tension stiffening approach described above will introduce unreasonable mesh sensitivity into the results. However, it is generally accepted that Hillerborg's (1976) fracture energy proposal is adequate to allay the concern for many practical purposes. Hillerborg defines the energy required to open a unit area of crack, G_f , as a material parameter, using brittle fracture concepts. With this approach the concrete's brittle behavior is characterized by a stress-displacement response rather than a stress-strain response. Under tension a concrete specimen will crack across some section. After it has been pulled apart sufficiently for most of the stress to be removed (so that the undamaged elastic strain is small), its length will be determined primarily by the opening at the crack. The opening does not depend on the specimen's length.

This fracture energy cracking model can be invoked by specifying the postfailure stress as a tabular function of cracking displacement, as shown in *figure 68*.

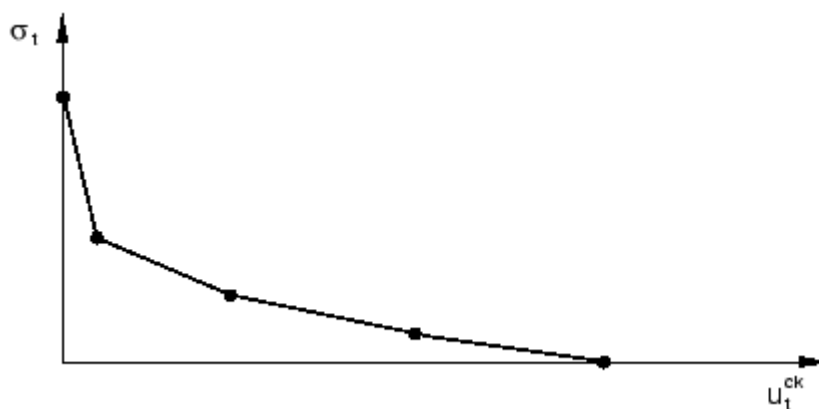


Figure 68. Postfailure stress-displacement curve.

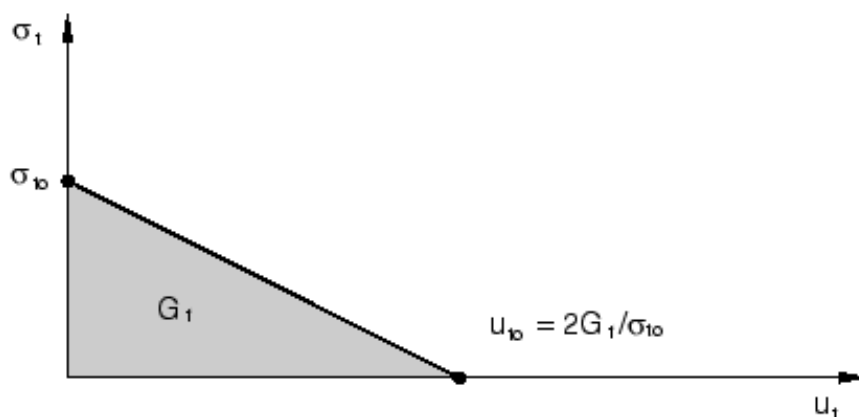


Figure 69. Postfailure stress-fracture energy curve.

The cracking displacement at which complete loss of strength takes place is, therefore, $u_{t0}=2G_f/\sigma_{t0}$. Typical values of G_f range from 40 N/m (0.22 lb/in) for a typical construction concrete (with a compressive strength of approximately 20 MPa, 2850 lb/in²) to 120 N/m (0.67 lb/in) for a high-strength concrete (with a compressive strength of approximately 40 MPa, 5700 lb/in²).

If tensile damage, d_t , is specified, Abaqus automatically converts the cracking displacement values to “plastic” displacement values using the relationship

$$\varepsilon_t^{pl} = \varepsilon_t^{ck} \frac{d_t}{(1-d_t)} \frac{\sigma_t l_0}{E_0}$$

where the specimen length, l_0 , is assumed to be one unit length $l_0=1$

4.9 Implementation

The implementation of this stress-displacement concept in a finite element model requires the definition of a characteristic length associated with an integration point. The characteristic crack length is based on the element geometry and formulation: it is a typical length of a line across an element for a first-order element; it is half of the same typical length for a second-order element. For beams and trusses it is a characteristic length along the element axis. For membranes and shells it is a characteristic length in the reference surface. For axisymmetric elements it is a characteristic length in the $r-z$ plane only. For cohesive elements it is equal to the constitutive thickness. This definition of the characteristic crack length is used because the direction in which cracking occurs is not known in advance. Therefore, elements with large aspect ratios will have rather different behavior depending on the direction in which they crack: some mesh sensitivity remains because of this effect, and elements that have aspect ratios close to one are recommended.

4.10 Defining compressive behavior

You can define the stress-strain behavior of plain concrete in uniaxial compression outside the elastic range. Compressive stress data are provided as a tabular function of inelastic (or crushing) strain, $\bar{\varepsilon}_c^{in}$, and, if desired, strain rate, temperature, and field variables. Positive (absolute) values should be given for the compressive stress and strain. The stress-strain curve can be defined beyond the ultimate stress, into the strain-softening regime.

Hardening data are given in terms of an inelastic strain, $\bar{\varepsilon}_c^{in}$, instead of plastic strain, $\bar{\varepsilon}_c^{pl}$. The compressive inelastic strain is defined as the total strain minus the

elastic strain corresponding to the undamaged material, $\bar{\varepsilon}_c^{in} = \varepsilon_c - \bar{\varepsilon}_{0c}^{el}$, as illustrated in figure 70.

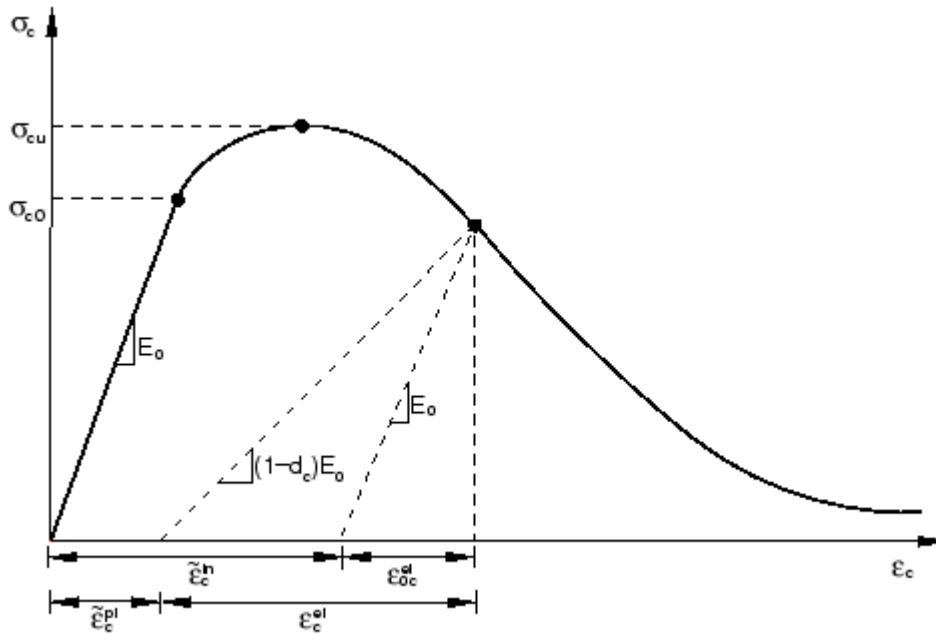


Figure 70. Definition of the compressive inelastic (or crushing) strain $\bar{\varepsilon}_c^{in}$ used for the definition of compression hardening data.

Unloading data are provided to Abaqus in terms of compressive damage curves, $d_c - \bar{\varepsilon}_c^{in}$, as discussed below. Abaqus automatically converts the inelastic strain values to plastic strain values using the relationship

$$\bar{\varepsilon}_c^{pl} = \bar{\varepsilon}_c^{in} - \frac{d_c}{(1-d_c)} \frac{\sigma_c}{E_0}$$

Abaqus will issue an error message if the calculated plastic strain values are negative and/or decreasing with increasing inelastic strain, which typically indicates that the compressive damage curves are incorrect. In the absence of compressive damage $\bar{\varepsilon}_c^{pl} = \bar{\varepsilon}_c^{in}$

4.11 Defining damage and stiffness recovery

Damage, d_t and/or d_c , can be specified in tabular form. In Abaqus the damage variables are treated as non-decreasing material point quantities. At any increment during the analysis, the new value of each damage variable is obtained as the maximum between the value at the end of the previous increment and the value

corresponding to the current state (interpolated from the user-specified tabular data); that is,

$$d_t|_{t+dt} = \max\{d_t|_t, d_t(\bar{\epsilon}_t^{pl}, \theta, f_i)\}$$

$$d_c|_{t+dt} = \max\{d_c|_t, d_c(\bar{\epsilon}_c^{pl}, \theta, f_i)\}$$

The choice of the damage properties is important since, generally, excessive damage may have a critical effect on the rate of convergence. It is recommended to avoid using values of the damage variables above 0.99, which corresponds to a 99% reduction of the stiffness.

It is strongly recommended that you specify the tabular definition of tensile and compressive damage variables for the same values of cracking and inelastic strains/displacements as those used in the tabular definitions of tension stiffening and compressive behavior, respectively. When the tensile stiffening response is defined directly in terms of failure stress and fracture energy (G_f), the definition of the tension damage variable should be such that it increases linearly as a function of the cracking displacement.

4.12.1 Tensile damage

You can define the uniaxial tension damage variable, d_t , as a tabular function of either cracking strain or cracking displacement.

4.12.2 Compressive damage

You can define the uniaxial compression damage variable, d_c , as a tabular function of inelastic (crushing) strain.

Stiffness recovery

As discussed above, stiffness recovery is an important aspect of the mechanical response of concrete under cyclic loading. Abaqus allows direct user specification of the stiffness recovery factors w_t and w_c .

The experimental observation in most quasi-brittle materials, including concrete, is that the compressive stiffness is recovered upon crack closure as the load changes from tension to compression. On the other hand, the tensile stiffness is not recovered as the load changes from compression to tension once crushing micro-cracks have developed. This behavior, which corresponds to $w_t=0$ and $w_c=1$, is the

Plastic flow

The concrete damaged plasticity model assumes nonassociated potential plastic flow. The flow potential G used for this model is the Drucker-Prager hyperbolic function:

$$\bar{q} = \sqrt{\varepsilon \sigma_{to} (\tan \psi)^2 + \bar{q} - \bar{p} (\tan \psi)}$$

where

$\psi(\theta, f_i)$, is the dilation angle measured in the p - q plane at high confining pressure;

$\sigma_{to}(\theta, f_i)$, is the uniaxial tensile stress at failure, taken from the user-specified tension stiffening data; and

$\varepsilon(\theta, f_i)$, is a parameter, referred to as the eccentricity, that defines the rate at which the function approaches the asymptote (the flow potential tends to a straight line as the eccentricity tends to zero).

This flow potential, which is continuous and smooth, ensures that the flow direction is always uniquely defined. The function approaches the linear Drucker-Prager flow potential asymptotically at high confining pressure stress and intersects the hydrostatic pressure axis at 90° . The default flow potential eccentricity is $\varepsilon = 0.1$, which implies that the material has almost the same dilation angle over a wide range of confining pressure stress values. Increasing the value of ε provides more curvature to the flow potential, implying that the dilation angle increases more rapidly as the confining pressure decreases. Values of ε that are significantly less than the default value may lead to convergence problems if the material is subjected to low confining pressures because of the very tight curvature of the flow potential locally where it intersects the p -axis.

Yield function

The model makes use of the yield function of Lubliner et. al. (1989), with the modifications proposed by Lee and Fenves (1998) to account for different evolution of strength under tension and compression. The evolution of the yield surface is controlled by the hardening variables, $\bar{\varepsilon}_t^{pl} = \bar{\varepsilon}_c^{pl}$. In terms of effective stresses, the yield function takes the form

$$F = \frac{1}{1-a} (\bar{q} - 3a\bar{p} + \beta(\bar{\varepsilon}^{pl}) < \hat{\sigma}_{max} > - \gamma < -\hat{\sigma}_{max} >) - \bar{\sigma}_c(\bar{\varepsilon}_c^{pl}) = 0$$

With

$$\alpha = \frac{\bar{\sigma}_c(\bar{\varepsilon}_c^{pl})^{-1}}{\bar{\sigma}_t(\bar{\varepsilon}_t^{pl})^{-1}}; 0 \leq \alpha \leq 0.5$$

$$\beta = \frac{\left(\frac{\sigma_{bo}}{\sigma_{co}}\right)^{-1}}{2\left(\frac{\sigma_{bo}}{\sigma_{co}}\right)^{-1}}(1-\alpha) - (1+\alpha),$$

$$\gamma = \frac{3(1-K_c)}{2K_c - 1}$$

Here,

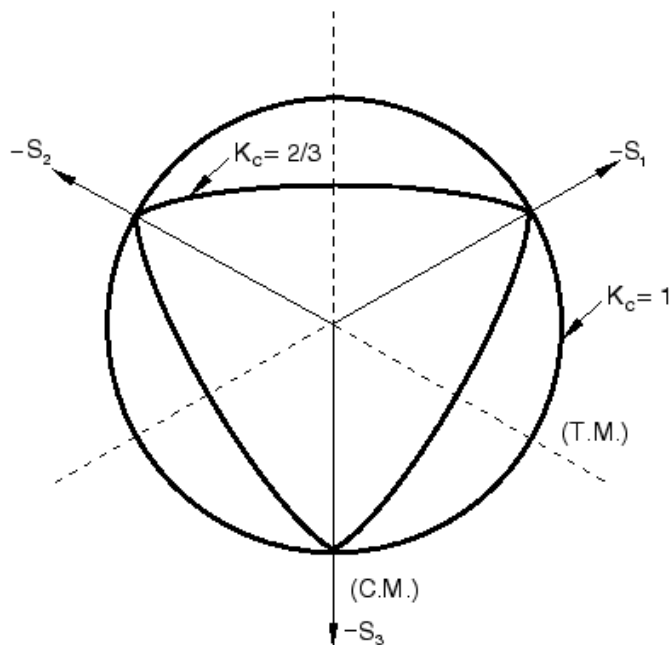
$\hat{\sigma}_{max}$ is the maximum principal effective stress;

$\sigma_{bo} / \sigma_{co}$ is the ratio of initial equibiaxial compressive yield stress to initial uniaxial compressive yield stress (the default value is 1.16);

K_c is the ratio of the second stress invariant on the tensile meridian, $q_{(TM)}$, to that on the compressive meridian, $q_{(CM)}$, at initial yield for any given value of the pressure invariant p such that the maximum principal stress is negative, $\hat{\sigma}_{max} < 0$ (Figure 72); it must satisfy the condition $0.5 < K_c \leq 1.0$ (the default value is 2/3);

$\bar{\sigma}_t(\bar{\varepsilon}_t^{pl})$ is the effective tensile cohesion stress;

and $\bar{\sigma}_c(\bar{\varepsilon}_c^{pl})$ is the effective compressive cohesion stress.



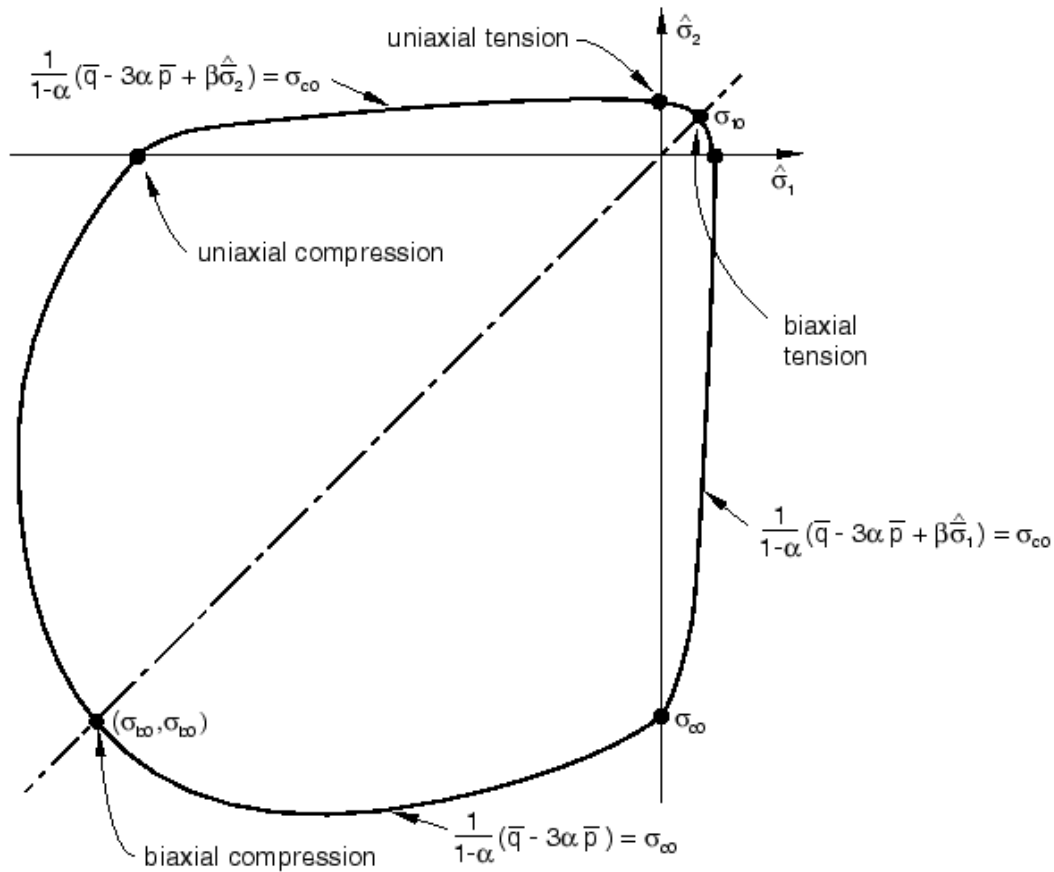


Figure 72. Yield surfaces in the deviatoric plane, corresponding to different values of Kc .

Nonassociated flow

Because plastic flow is nonassociated, the use of concrete damaged plasticity results in a nonsymmetric material stiffness matrix. Therefore, to obtain an acceptable rate of convergence in Abaqus/Standard, the unsymmetric matrix storage and solution scheme should be used. Abaqus/Standard will automatically activate the unsymmetric solution scheme if concrete damaged plasticity is used in the analysis. If desired, you can turn off the unsymmetric solution scheme for a particular step.

Viscoplastic regularization

Material models exhibiting softening behavior and stiffness degradation often lead to severe convergence difficulties in implicit analysis programs, such as Abaqus/Standard. A common technique to overcome some of these convergence difficulties is the use of a viscoplastic regularization of the constitutive equations,

which causes the consistent tangent stiffness of the softening material to become positive for sufficiently small time increments. The concrete damaged plasticity model can be regularized in Abaqus/Standard using viscoplasticity by permitting stresses to be outside of the yield surface. We use a generalization of the Duvaut-Lions regularization, according to which the viscoplastic strain rate tensor, $\dot{\varepsilon}_v^{pl}$, is defined as

$$\dot{\varepsilon}_v^{pl} = \frac{1}{\mu} (\varepsilon^{pl} - \varepsilon_v^{pl}).$$

Here μ is the viscosity parameter representing the relaxation time of the viscoplastic system, and ε^{pl} is the plastic strain evaluated in the inviscid backbone model.

Similarly, a viscous stiffness degradation variable, d_v , for the viscoplastic system is defined as

$$\dot{d}_v = \frac{1}{\mu} (d - d_v),$$

where d is the degradation variable evaluated in the inviscid backbone model. The stress-strain relation of the viscoplastic model is given as

$$\sigma = (1 - d_v) D_v^{pl} : (\varepsilon - \varepsilon_v^{pl}).$$

Using the viscoplastic regularization with a small value for the viscosity parameter (small compared to the characteristic time increment) usually helps improve the rate of convergence of the model in the softening regime, without compromising results. The basic idea is that the solution of the viscoplastic system relaxes to that of the inviscid case as $t/\mu \rightarrow \infty$, where t represents time. You can specify the value of the viscosity parameter as part of the concrete damaged plasticity material behavior definition. If the viscosity parameter is different from zero, output results of the plastic strain and stiffness degradation refer to the viscoplastic values, ε_v^{pl} and d_v . In Abaqus/Standard the default value of the viscosity parameter is zero, so that no viscoplastic regularization is performed.

Material damping

The concrete damaged plasticity model can be used in combination with material damping. If stiffness proportional damping is specified, Abaqus calculates the damping stress based on the undamaged elastic stiffness. This may introduce large artificial damping forces on elements undergoing severe damage at high strain rates.

Visualization of “crack directions”

Unlike concrete models based on the smeared crack approach, the concrete damaged plasticity model does not have the notion of cracks developing at the material integration point. However, it is possible to introduce the concept of an effective crack direction with the purpose of obtaining a graphical visualization of the cracking patterns in the concrete structure. Different criteria can be adopted within the framework of scalar-damage plasticity for the definition of the direction of cracking. Following Lubliner et. al. (1989), we can assume that cracking initiates at points where the tensile equivalent plastic strain is greater than zero, $\bar{\varepsilon}_t^{pl} > 0$, and the maximum principal plastic strain is positive. The direction of the vector normal to the crack plane is assumed to be parallel to the direction of the maximum principal plastic strain. This direction can be viewed in the Visualization module of Abaqus/CAE.

Chapter 5

Solution of beams with different ratios $\frac{a}{d}$ and $\frac{l}{h}$ with the Strut and Tie model

5.1 Case 1, $\frac{a}{d}=1.5$

Here we want to compare the experimental results with the results of the program STM. This beam has following geometry. The basic difference of this beam, is that it has a ratio a/d , equal to 1,0.

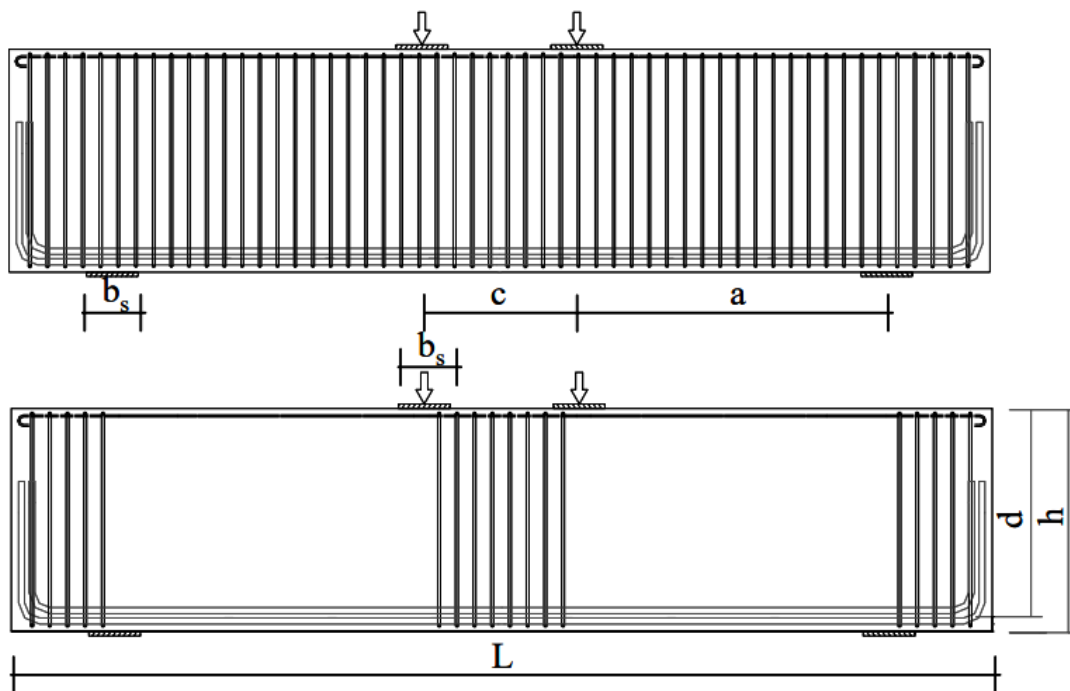


Figure 73. Geometry of the beam

Where

$L=1500\text{mm}$

$c=300\text{mm}$

$a=400\text{mm}$

$d=400\text{mm}$

$h=475\text{mm}$

$b=240\text{mm}$

$b_s=100\text{mm}$

The materials have the following properties:

$f_c=31.3\text{MPa}$

$f_y=500.0\text{MPa}$

The reinforcement of the beam is the following:

Tension reinforcement: 5D22

Compression reinforcement: 2D10

Stirrups: D6/65

The experimental results, gave a collapse load, equal to $P_{\max}=1181\text{KN}$.

The required rebars, for the main reinforcement, was found with the program, to be equal to $A_{s,\text{req}}=1205\text{mm}^2$. So the existantant reinforcement, that is 1900mm^2 , is enough.

(3) Strut and Tie Forces

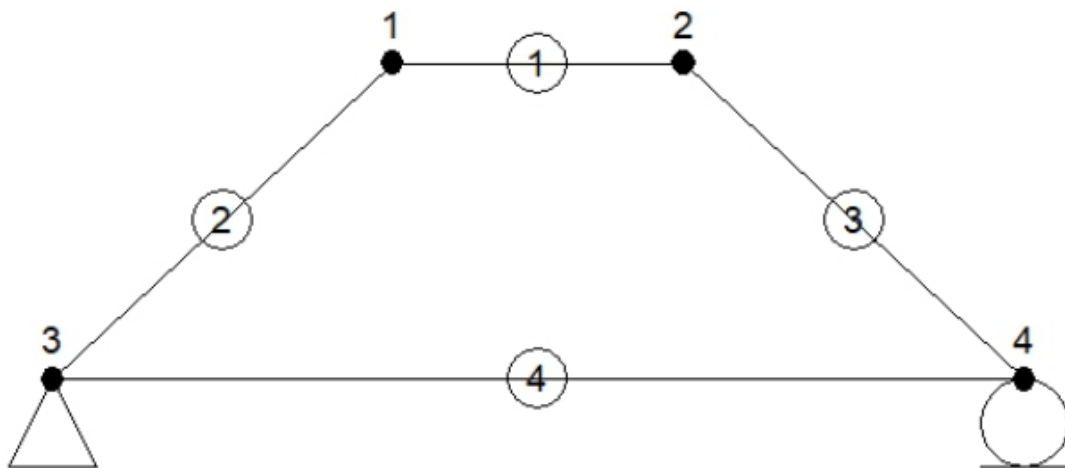


Figure 74. Truss model of the beam

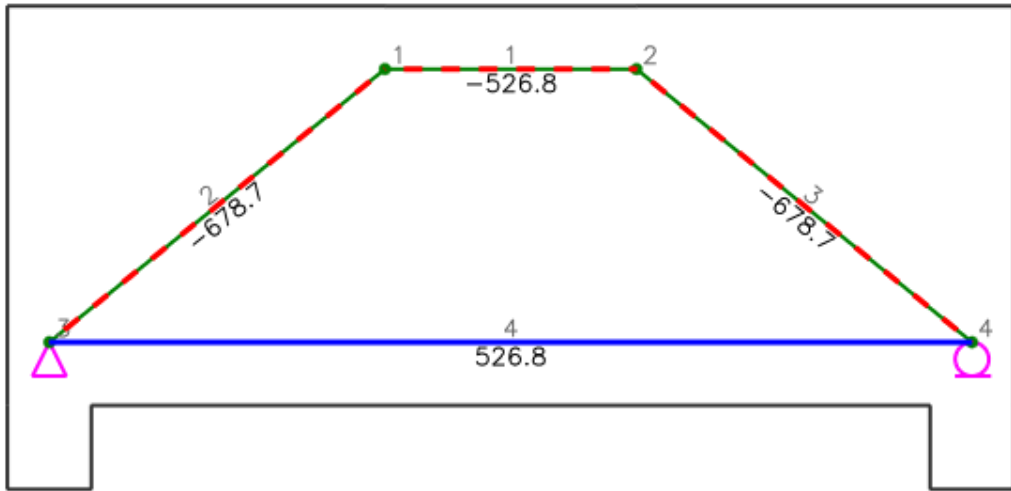


Figure 75. Analysis results

Following the same steps as previously, we find that:

For the required strength of struts, from the figure 76, the strength of the struts is enough.

| Elem. No. | i-width | j-width | Available Width | Elem. No. | i-width | j-width | Available Width |
|-----------|---------|---------|-----------------|-----------|---------|---------|-----------------|
| 1 | 150.0 | 150.0 | 150.0 | 2 | 179.5 | 179.5 | 179.5 |
| 3 | 179.5 | 179.5 | 179.5 | | | | |

(3) Strength of Struts

| Strut No. | Type | theta | Fu (kN) | b (mm) | Wreq (mm) | Wprov (mm) | Note |
|-----------|------|-------|---------|--------|-----------|------------|------|
| 1 | 1 | 0.0 | 526.8 | 240.0 | 52.6 | 150.0 | O.K |
| 2 | 2 | 39.1 | 678.7 | 240.0 | 129.1 | 179.5 | O.K |
| 3 | 2 | 39.1 | 678.7 | 240.0 | 129.1 | 179.5 | O.K |

Figure 76. Calculatios of strength and rebars

The W_{req} is found by the end area of each strut. Moreover, the strength of concrete is reduced by a factor $v=0.6$, considering tensile stresses vertical to the struts.

For the check of concentrated nodes, due to symmetry, it is enough to check the nodes 1 and 3.

For the node 1 (CCC)

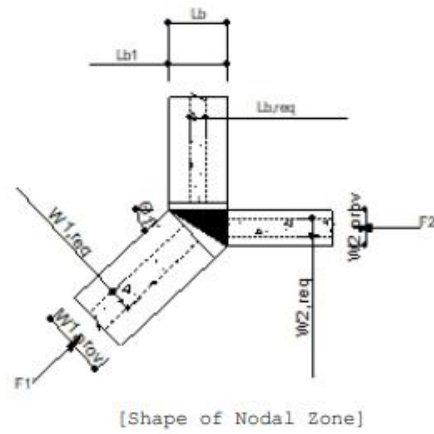
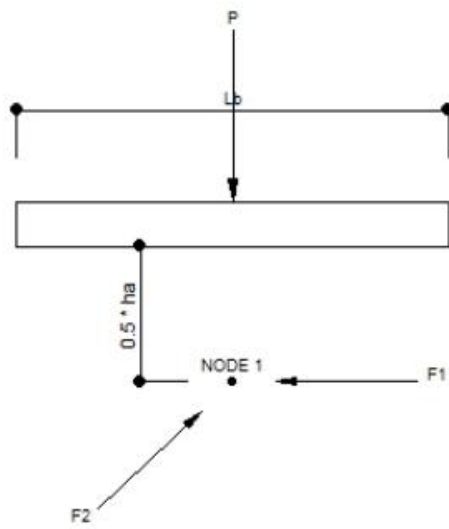


Figure77. Truss nodes

We have the following:

$$L_b=100\text{mm}$$

$$h_a=150\text{mm}$$

$$W_{1,prov}=180\text{mm}$$

$$P=428\text{KN}$$

For the node 3 (CCT)

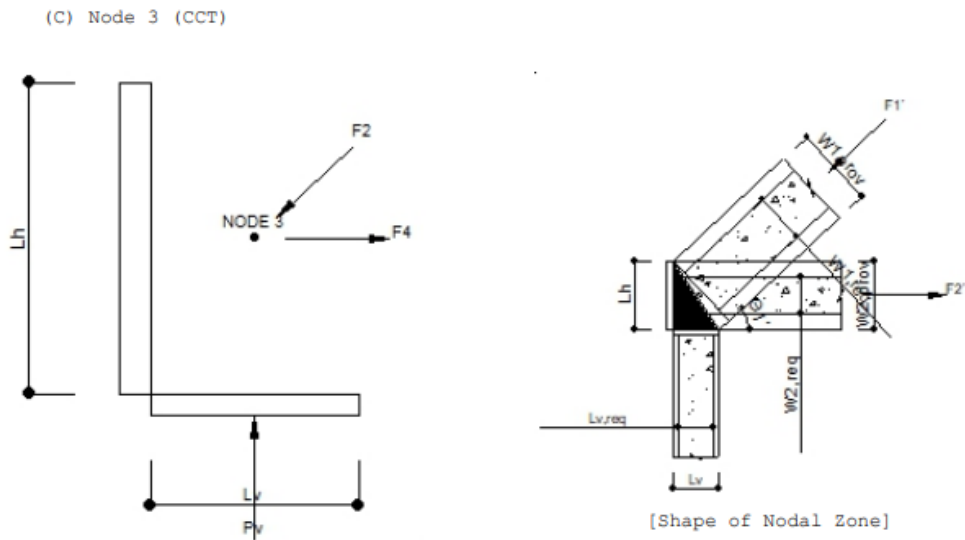


Figure 78. Geometry of node 3

We have the following:

$$L_v=100\text{mm}$$

$$L_h=150\text{mm}$$

$$W_{1,\text{prov}}=180\text{mm}$$

$$P=428\text{KN}$$

The results of the program ,are the following:

For the node 1

$$W_{1,\text{prov}}=180.3\text{mm}$$

$$W_{2,\text{prov}}=150.0\text{mm}$$

$$L_{1,\text{prov}}=100.0\text{mm}$$

$$W_{1,\text{req}}=78.6\text{mm} < W_{1,\text{prov}}=180.3\text{mm}$$

$$W_{2,\text{req}}=59.4\text{mm} < W_{2,\text{prov}}=150.0\text{mm}$$

$$L_{1,\text{req}}=48.9\text{mm} < L_{1,\text{prov}}=100.0\text{mm}$$

So, the strength of node 1 is enough.

For the node 3

$$W_{1,prov}=180.3\text{mm}$$

$$W_{2,prov}=150.0\text{mm}$$

$$L_{v,prov}=100.0\text{mm}$$

$$W_{1,req}=59.2\text{mm} < W_{1,prov}=178.0\text{mm}$$

$$W_{2,req}=76.8\text{mm} < W_{2,prov}=150.0\text{mm}$$

$$L_{1,req}=48.8\text{mm} < L_{1,prov}=100.0\text{mm}$$

So, the strength of node 3 is enough.

If we not use the safety factor for concrete, we find that the strength of the second strut is equal to the its force. So the total collapse load, is found to be equal :

$$F=2 \times 428 = 856\text{KN}$$

So, the collapse load is approximately 73% of the real collapse load, of the experiment.

The results, show that the Strut and Tie model, is very close to experimental results, for beams with small ratio a/d .

5.2 Case 2, $\frac{a}{d}=1.5$

Here we solve the same beam, using the program Fe77. This program uses, as we have presented later, the Kotsovo's model for concrete. This finite element program allows the analysis with crack closure in localized regions of structures, using three-dimensional solid elements.

The Force=Displacement curve, is shown in *figure 79*.

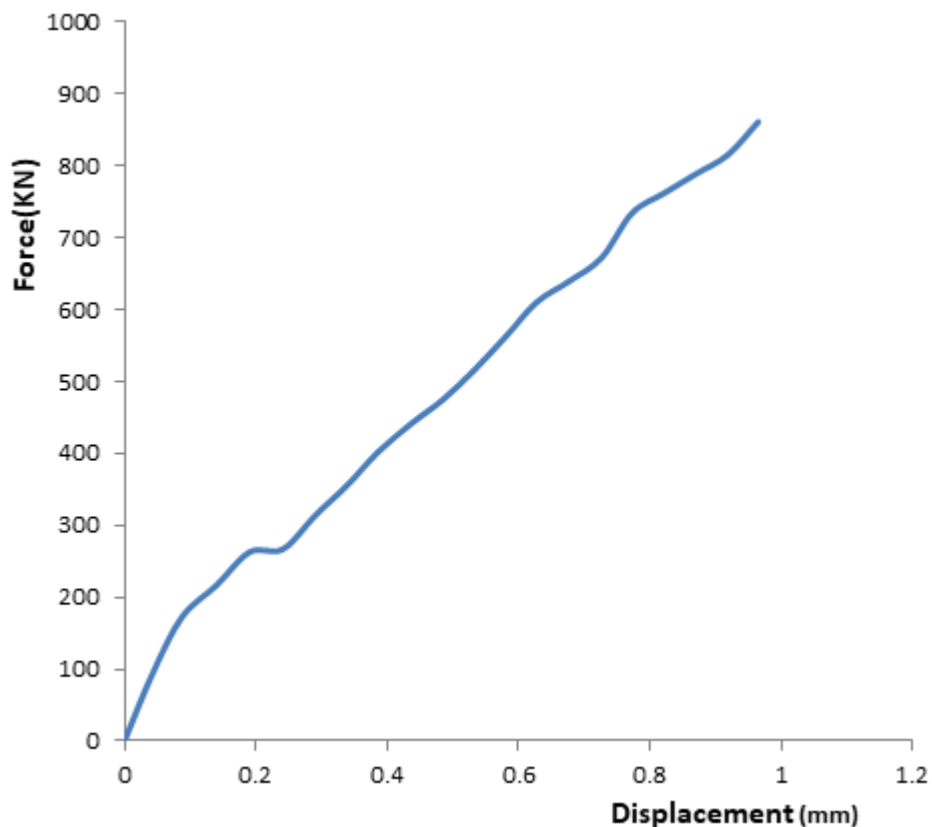


Figure 79. Force-Displacement curve

So, we find that the peak value of the curve reaches a value of $F=860\text{KN}$. From the experiment we had that the maximum value of the force is $F=1181\text{KN}$. So using the FEM program Fe77, we find a force that is approximately 73% of the experimental maximum load.

In figures 80-84, the deformation of the beam till collapse is presented.

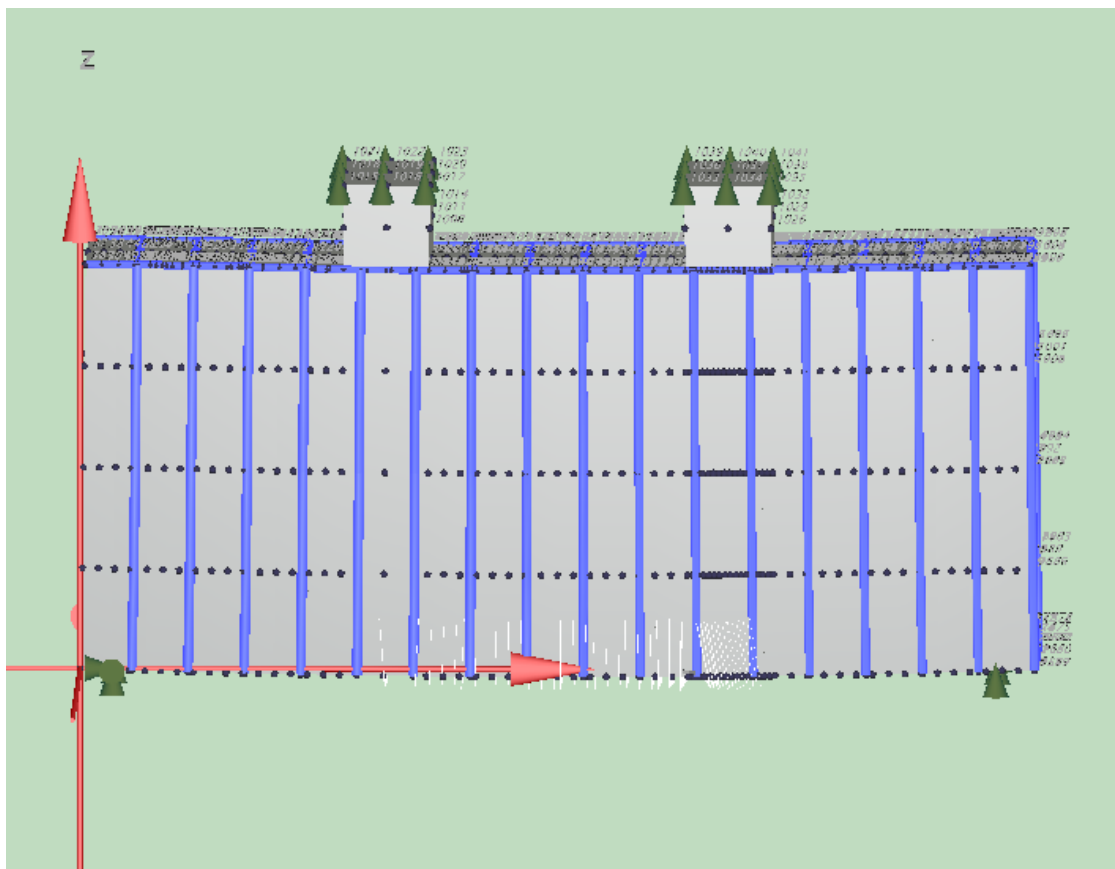
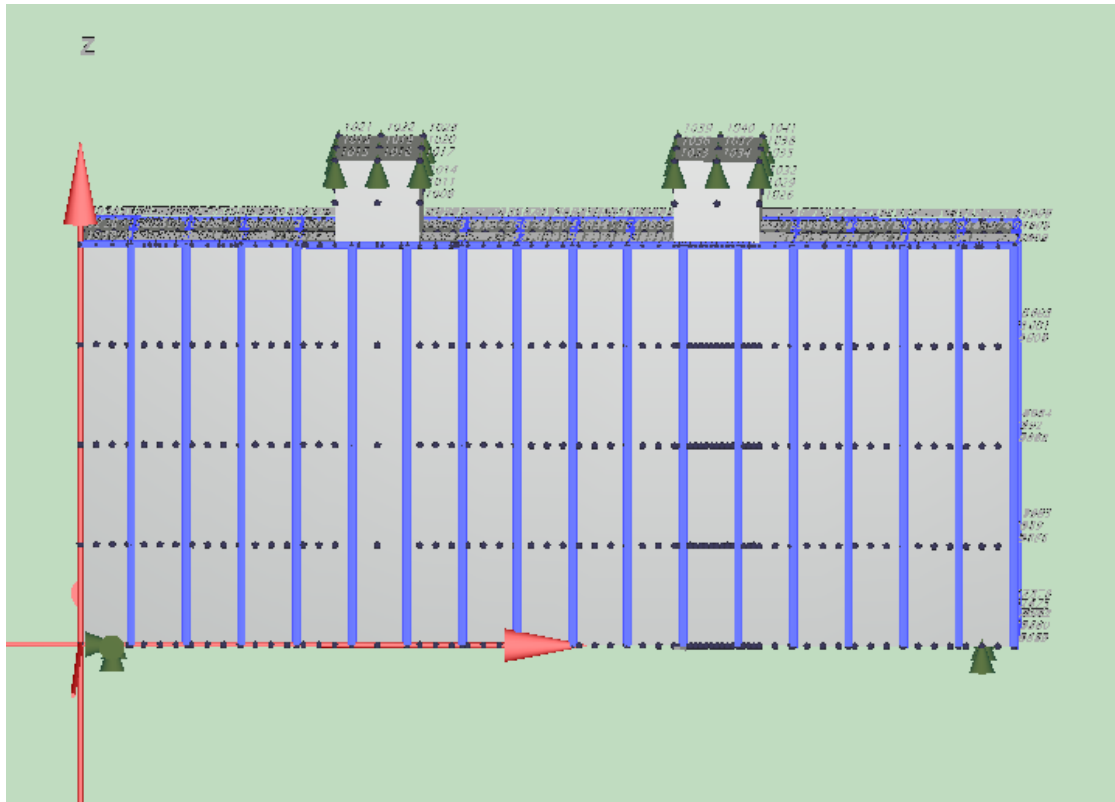


Figure 80. Geometry of the beam in Fe77

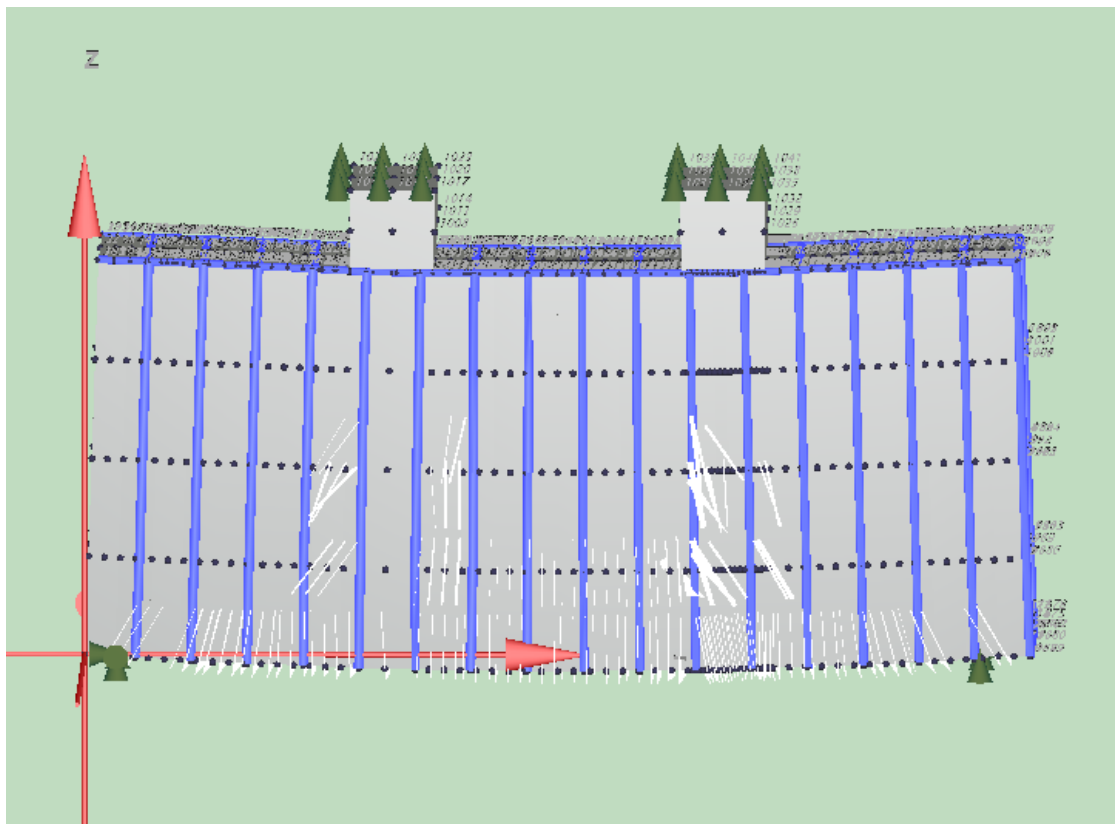
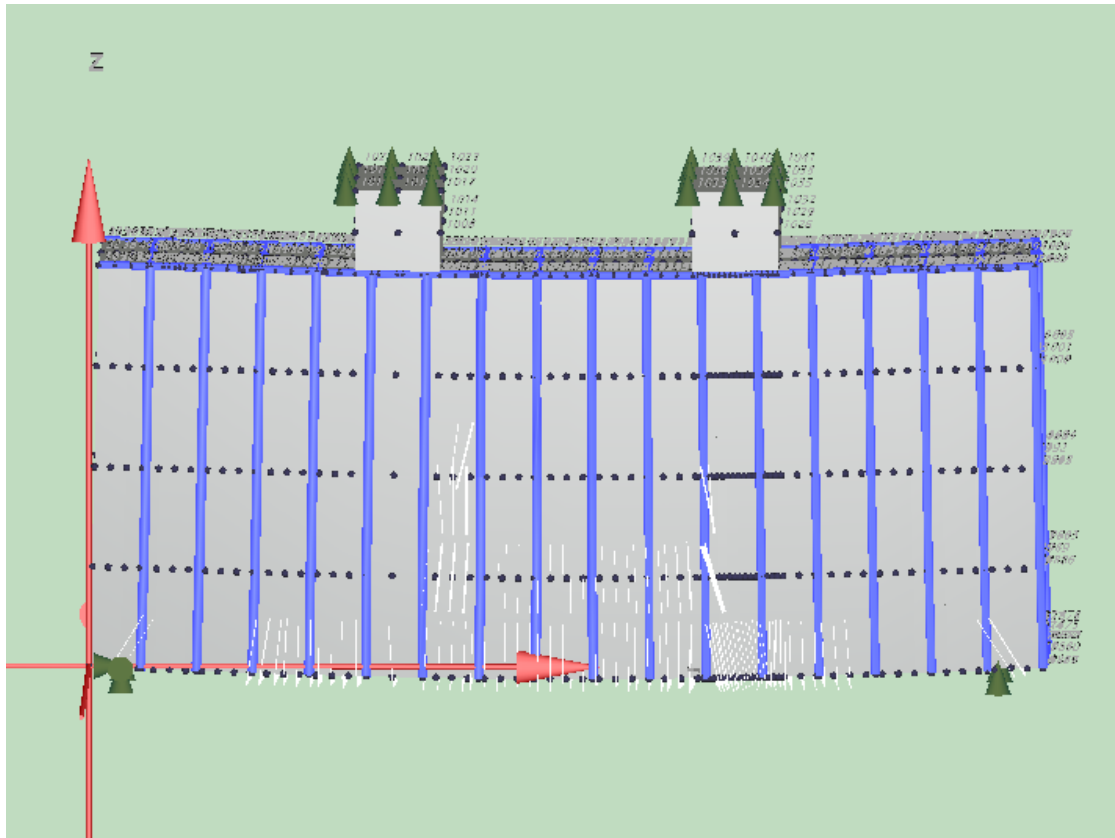


Figure 81. Initial cracking of the beam

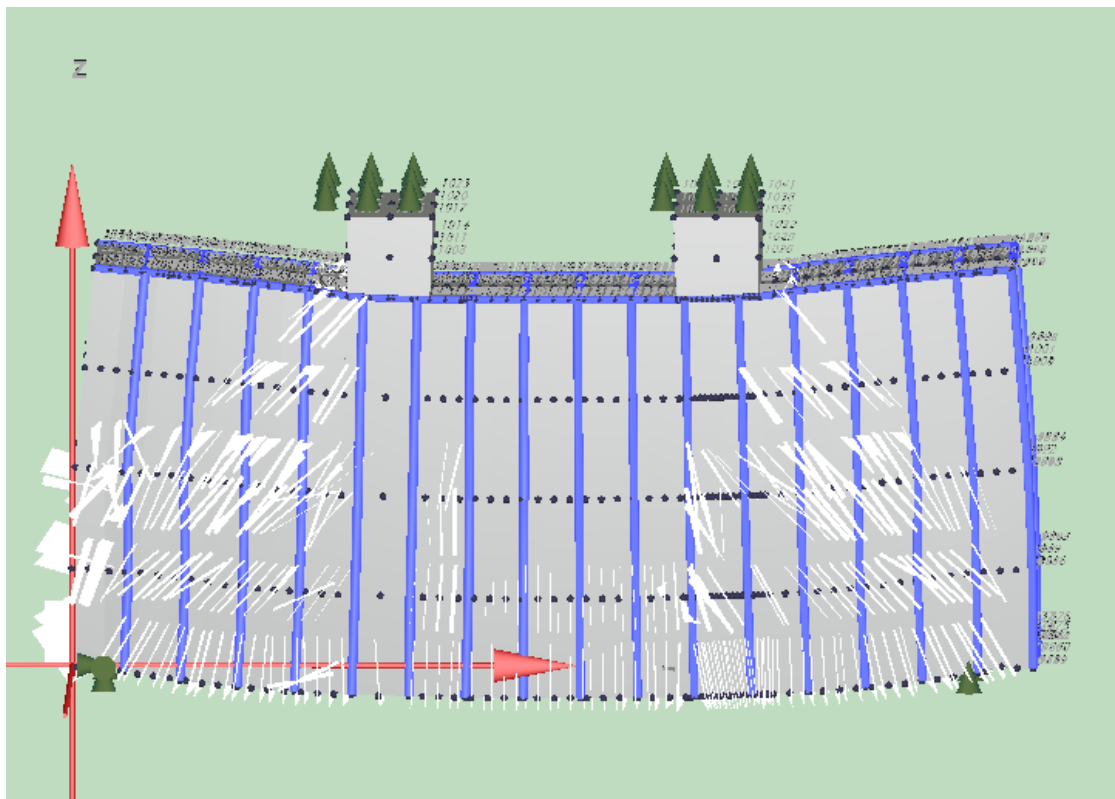
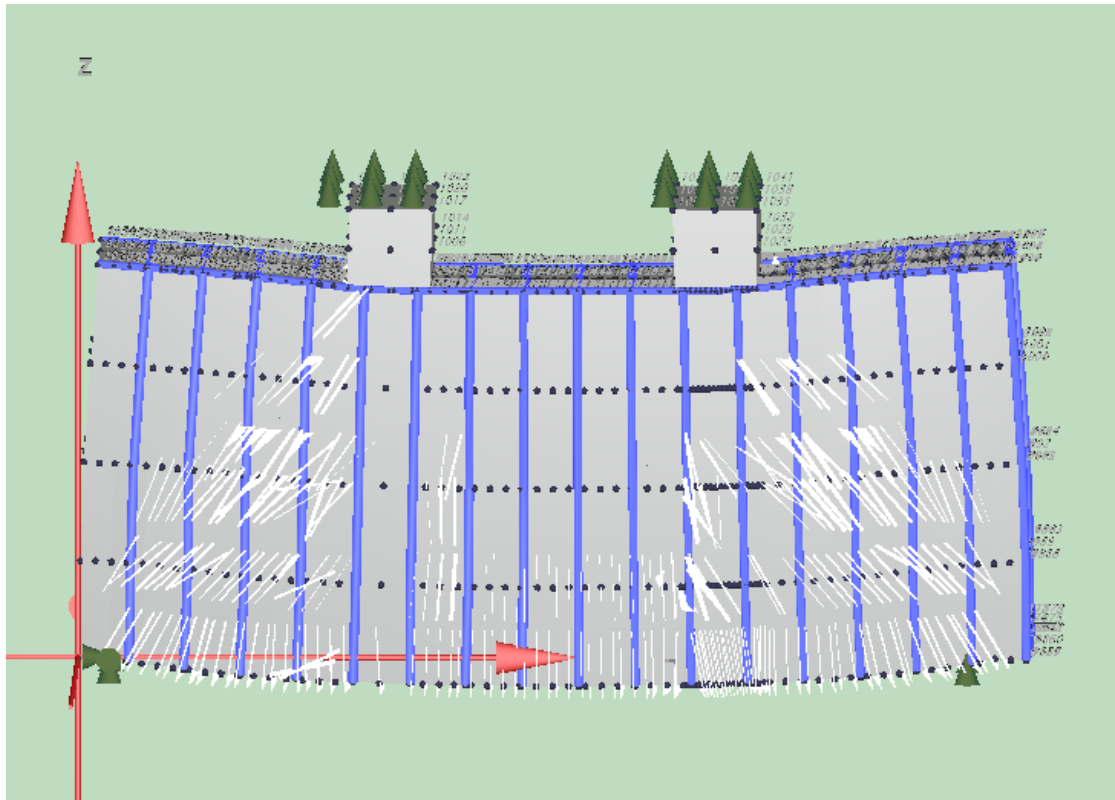


Figure 83. Forming of struts

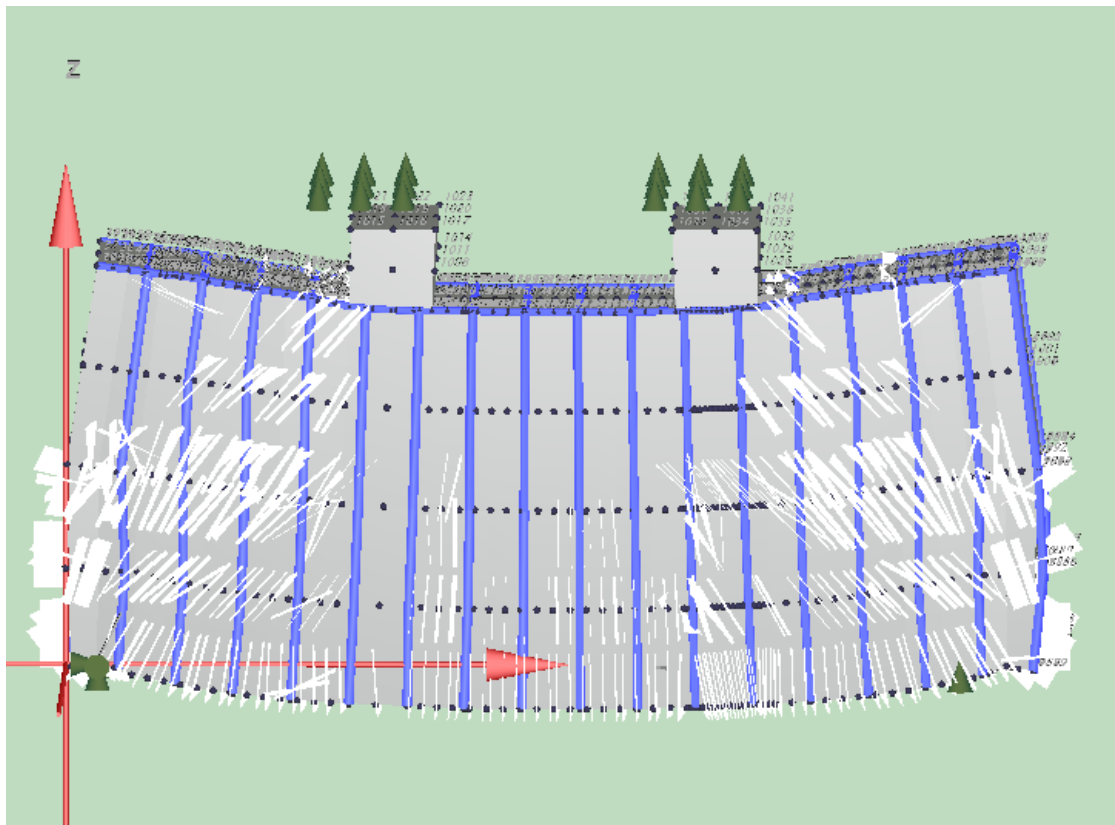
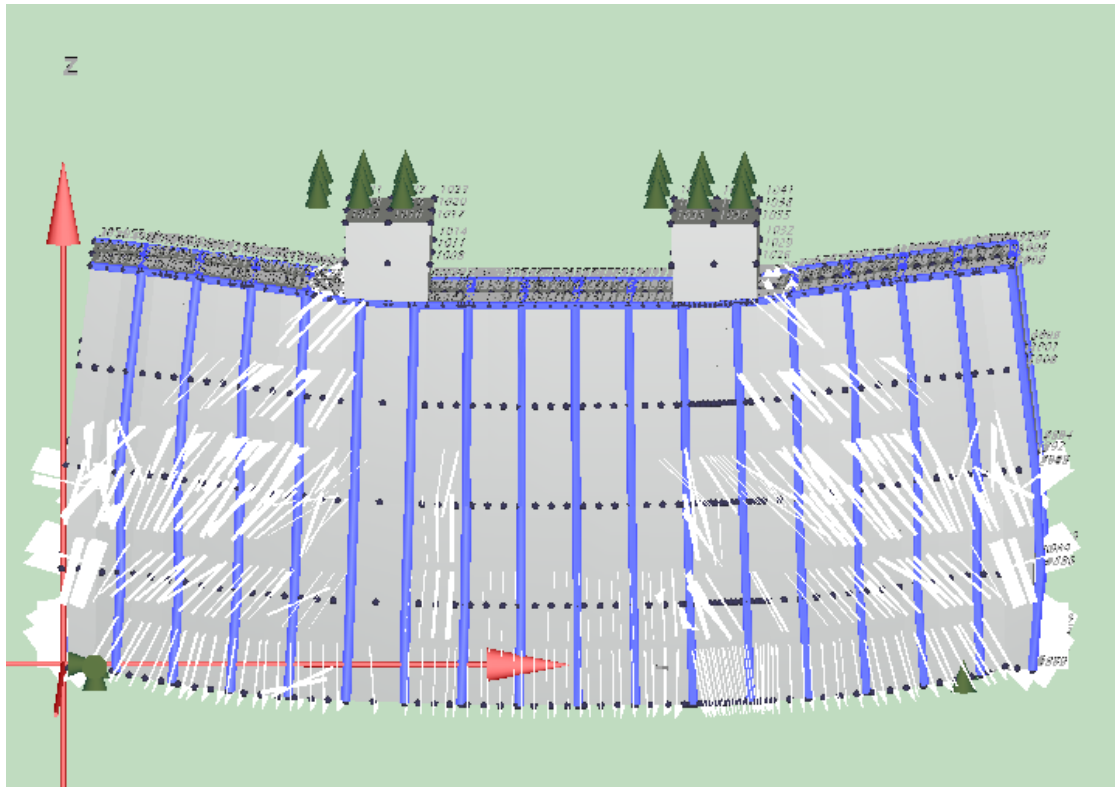


Figure 84. Deformation of the beam in collapse

5.3 Case 2, $\frac{a}{d}=1.0$

Here, we use some procedures, that were used last years, to find the collapse load, in order to compare the results with the EC2, the most current code to design deep beams. For this reason, we consider the beam B7 that we have from experimental results, that the collapse load is equal $F=1181\text{KN}$, and with the EC2, we found that $F=826\text{KN}$.

Here we use the Canadian Standards (CSA), to determine the strength of the beam.

The steps in design a distributed region, such as the deep beam, are:

1. Sketch flow of forces in distributed region and locate nodal zones which are regions bounded by struts, tension ties or bearing areas.
2. Choose dimensions of loading and reaction areas such that nodal stresses stay below permission limits (i.e., $0.85\phi_c f_c$ in nodal zones bounded by compressive struts and bearing areas, $0.75\phi_c f_c$ in nodal zones anchoring only one tension tie and $0.60\phi_c f_c$ in nodal zones anchoring tension ties in more than one direction).
3. Determine geometry of truss model and determine forces in struts and ties. If truss is statically indeterminate, estimate relative of truss members in order to solve forces in truss and ties.
4. Determine required areas of tension ties ($A_s = T/\phi_s f_y$) and check details of tension reinforcement to ensure adequate anchorage into nodal zones.
5. Check struts compressive stresses from $f_2 = C/\phi_c A_c$ where A_c is effective area of strut as determined by end anchorage conditions. Check that f_2 does not exceeds crushing strength, f_{2max} , of cracked concrete where :

$$f_{2max} = \frac{\lambda \phi_c f_c}{0.8 + 170 \epsilon_1} \leq 0.85 \phi_c f_c$$

$$\epsilon_1 = \epsilon_s + (\epsilon_s + 0.002) \cot^2 \alpha_s$$

where ϵ_1 is the required strain in tension tie (usually taken as ϵ_y) and α_s is the angle between the strut and the tie crossing the strut.

Step 1. Sketching the stress flow

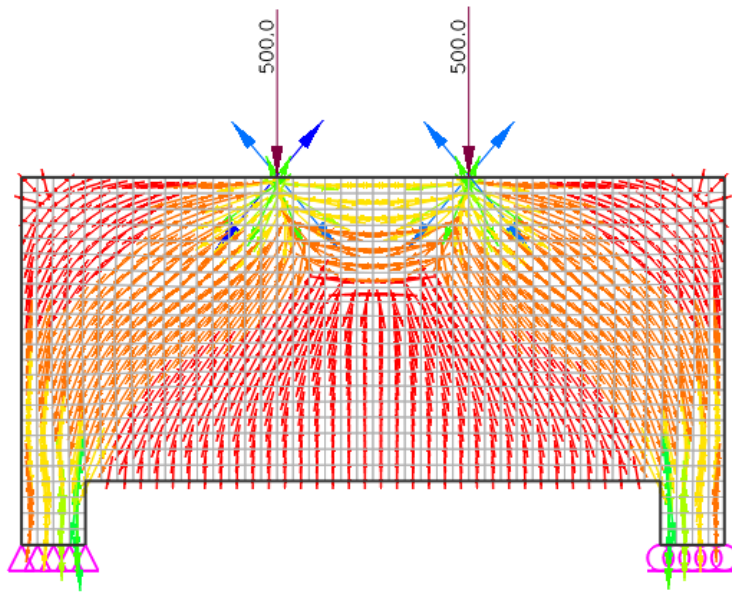


Figure 85. Flow of stresses

The way to find the provided width, is the same in EC2 and the Canadian Standards.

From the geometry, we have:

For the node 1

$$W_{1,prov}=180.3\text{mm}$$

$$W_{2,prov}=150.0\text{mm}$$

$$L_{1,prov}=100.0\text{mm}$$

For the node 3

$$W_{1,prov}=180.3\text{mm}$$

$$W_{2,prov}=150.0\text{mm}$$

$$L_{v,prov}=100.0\text{mm}$$

Step 2. Strength of nodes

Using the formulas of the CSA, we have the following strengths of nodal regions:

For a CCC node we have:

$$\sigma_{Rd,max1} = 0,85 * f_{ck} = 26.61 \text{MPa}$$

For a CCT node :

$$\sigma_{Rd,max2} = 0,75 * f_{ck} = 23.48 \text{MPa}$$

For a CTT node :

$$\sigma_{Rd,max3} = 0,60 * f_{ck} = 18.78 \text{MPa}$$

without considering any safety factor. So, the required widths for the nodes ,are:

$$W_{1,req} = \frac{T}{\sigma_{max} * b}$$

Step 3. Truss model

The truss model is the same as with the EC2, considering the stress flow of the beam.

Step 4. Requires rebars

Using the type $A_s = T / (\varphi_s f_y)$, to determine the required rebars, we find easily that the reinforcement is approximately the same as was found with the EC2, and is enough.

Step 5. Checking struts and nodes

So, for a total load of 1050KN we get:

For the node 1

$$W_{1,req} = 132.0 \text{mm}$$

$$W_{2,req} = 102.0 \text{mm}$$

$$W_{3,req} = 85.2 \text{mm}$$

For the node 3

$$W_{1,req}=150.0 \text{ mm}$$

$$W_{2,req}=116.0 \text{ mm}$$

$$W_{3,req}=96.5 \text{ mm}$$

So we have:

For the node 1

$$W_{1,req}=132.0 \text{ mm} < W_{1,prov}=180.0\text{mm}$$

$$W_{2,req}=102.0 \text{ mm} < W_{2,prov}=150.0\text{mm}$$

$$L_{1,req}=85.2 \text{ mm} < L_{1,prov}=100.0\text{mm}$$

For the node 3

$$W_{1,req}=150.0\text{mm} < W_{1,prov}=180.0\text{mm}$$

$$W_{2,req}=116.0\text{mm} < W_{2,prov}=150.0\text{mm}$$

$$L_{1,req}=96.5\text{mm} < L_{1,prov}=100.0\text{mm}$$

Finally, in order to check the compressive stresses, we have:

$$\varepsilon_1 = \varepsilon_s + (\varepsilon_s + 0.002) \cot^2 \alpha_s = 0.00347$$

$$f_{2max} = \frac{\lambda \varphi_c f_c}{0.8 + 170 \varepsilon_1} = \frac{1 \cdot 31.3}{0.8 + 170 \cdot 0.00347} = 22.77 \text{ MPa} \leq 0.85 \varphi_c f_c = 26.6 \text{ MPa}$$

So $f_{2max} = 22.6 \text{ MPa}$

The stresses of the struts are the following:

$$\sigma_1 = \frac{525 \cdot 10^3}{100 \cdot 240} = 21.8 \text{ MPa}$$

$$\sigma_2 = \frac{771 \cdot 10^3}{180 \cdot 240} = 17.8 \text{ MPa}$$

So, we have that:

$$\sigma_1, \sigma_2 \leq f_{2max}$$

So, the total load with this code is equal to 1050KN, as the five conditions that were described previously are checked, and the forces are very close to the strength. So, using this code we find a total load equal to 89% of the experimental collapse load.

Hear, we want to compare the results between the experimental results, the results of a FEM (finite element analysis) and the experimental results. For this reason we consider two deep beams, with two concentrated loads along the bottom of its length.

5.4 Case 3, $\frac{a}{d}=1.0$

Beam 1

Geometry and properties of the beam

Width: 720mm

Height: 1305mm

Length: 4500mm

Compressive strength of concrete: $f_c=27.0\text{Mpa}$

Reinforcement

Compression bars: 2D13

Tension bars: 18D35

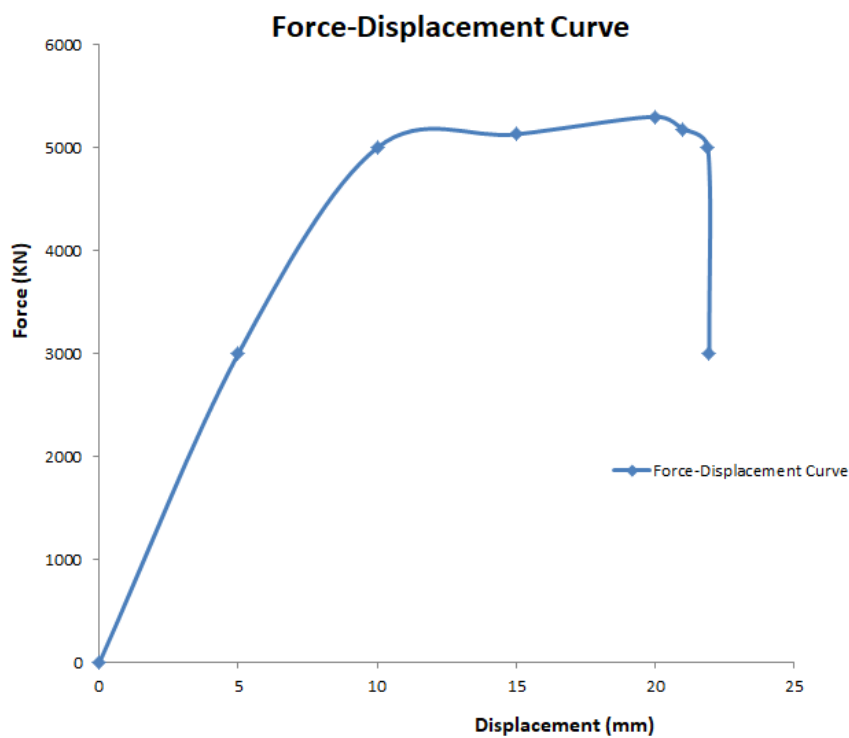


Figure 86. Force-Displacement Curve for the second beam, from experimental results

Experimental results, gave the Force-Displacement Curve from figure 86:

So, experiments gave a collapse load equal to $P_{exp} = 5325\text{KN}$, and a displacement equal to $\delta_{peak} = 11.3\text{mm}$.

Analysis with finite elements (FEA), using Abaqus, gave the following results, and Force-Displacement Curve, of figure 87.

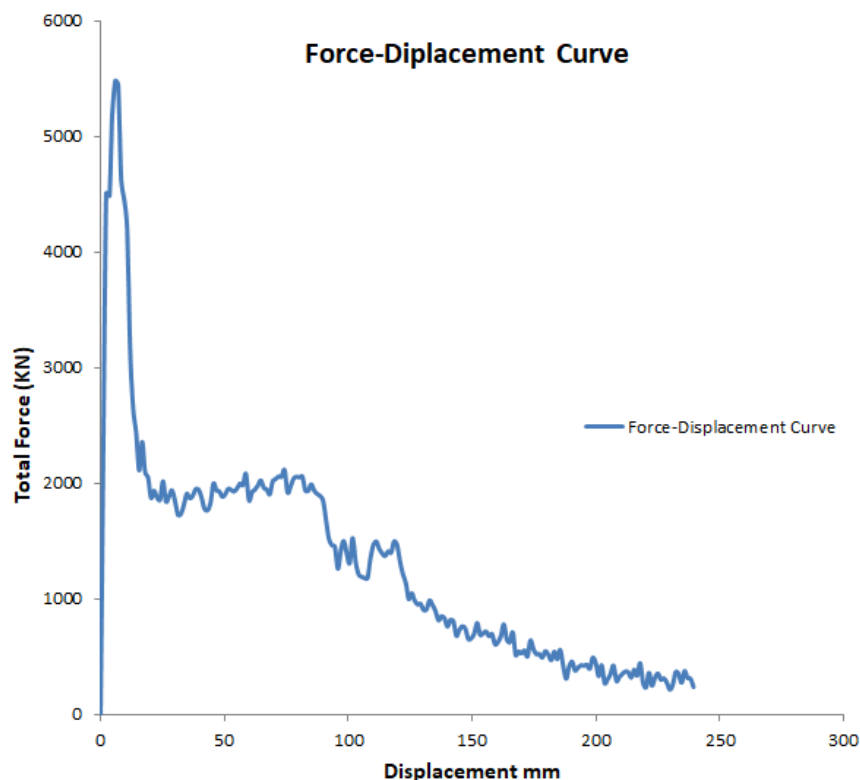


Figure 87. Force-Displacement Curve for the second beam, from FEA.

So, from the analysis we find that the collapse load is equal to collapse load equal to $P_{exp} = 5482\text{KN}$, and the peak displacement is equal to $\delta_{peak} = 5.91\text{mm}$.

So, analysis with finite elements, gave results that are very close to experimental results. In the following pictures, the cracks during initial loading and complete failure is presented (figures 88-91).

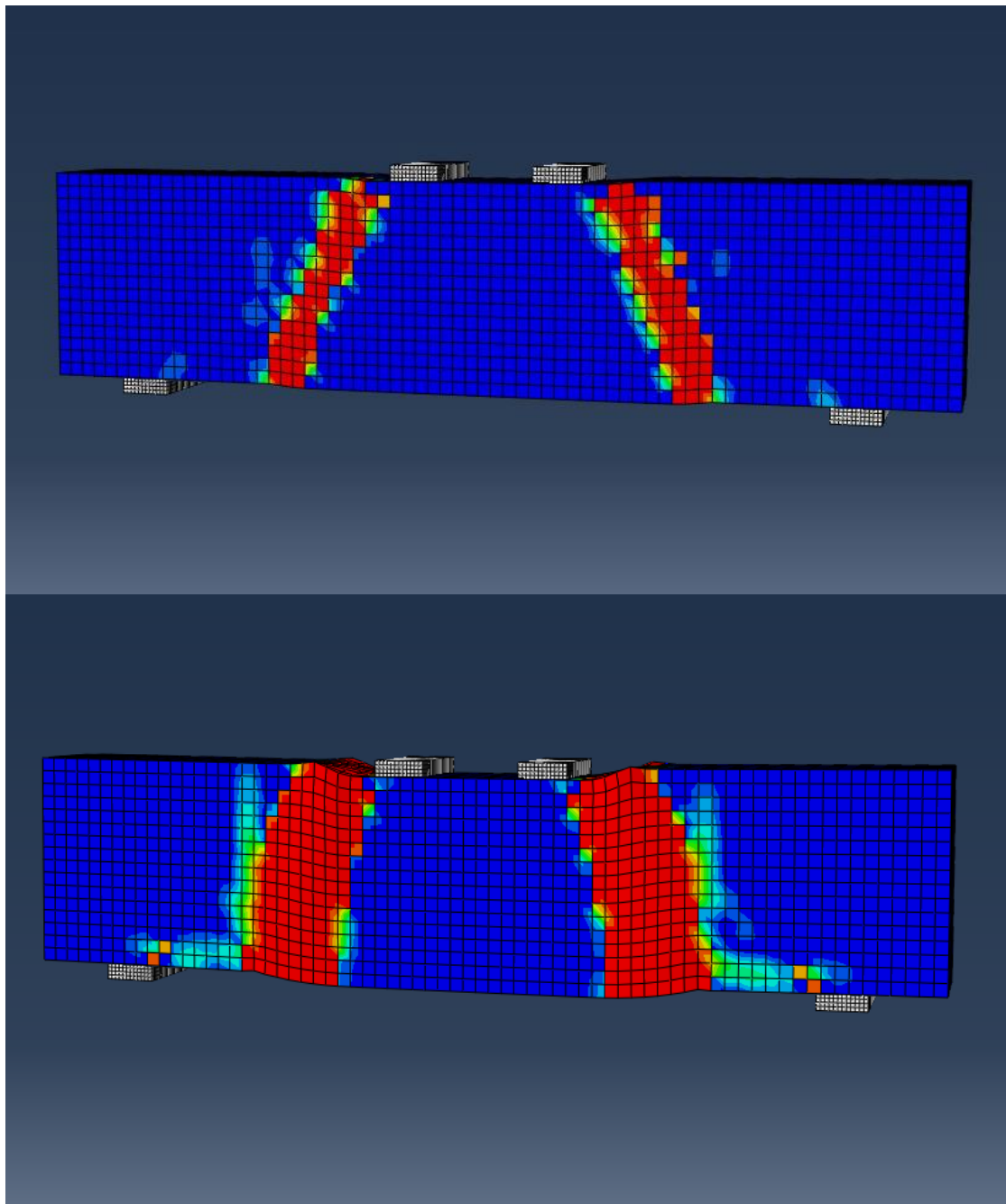


Figure 88. Initial formation of compressive cracks

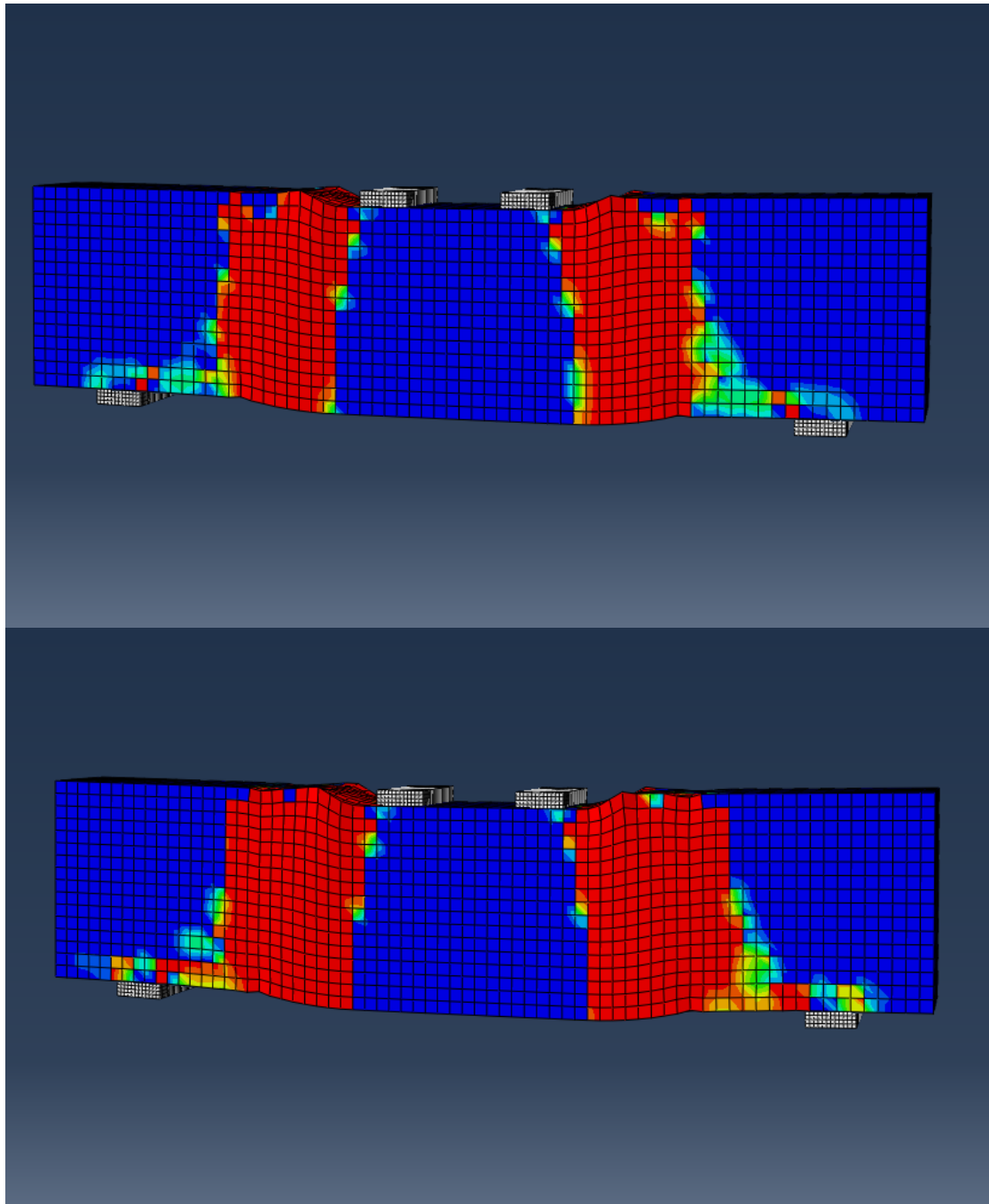


Figure 89. Compressive cracks at the failure of the beam

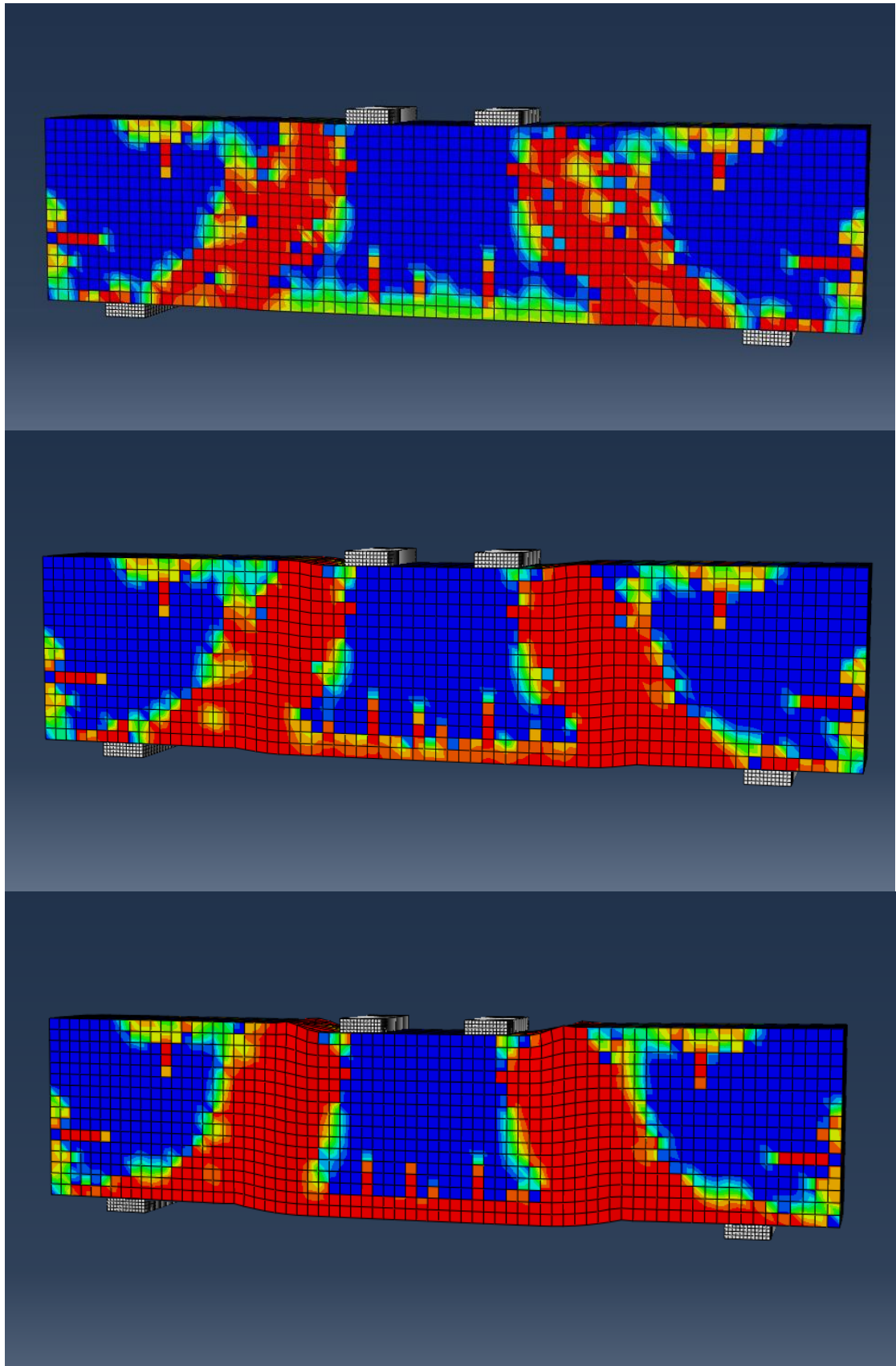


Figure 90. Formation of tensile cracks

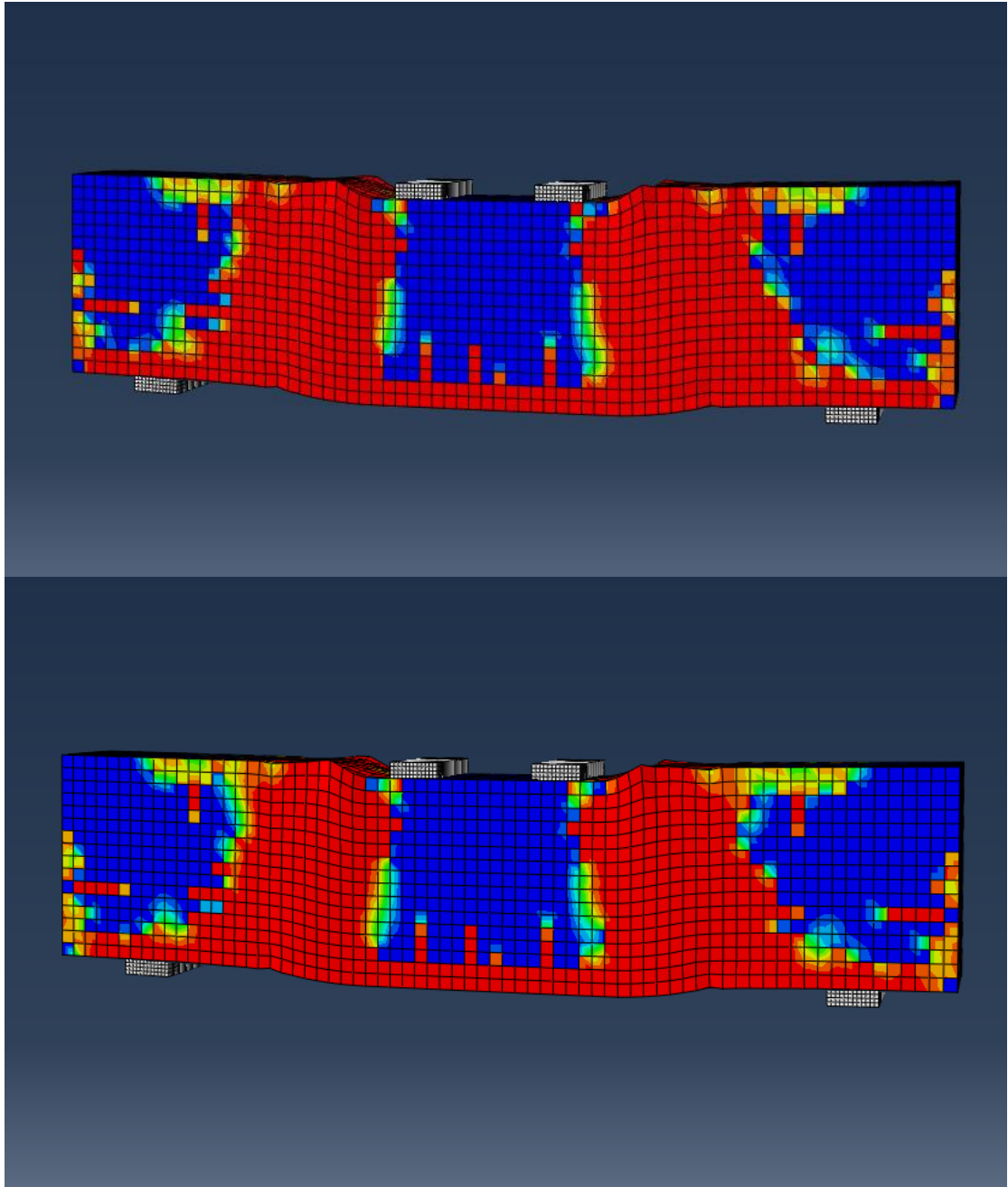


Figure 91. Tensile cracks at the failure of the beam

Case 4, $\frac{a}{d}=1.5$

Beam 2

Geometry and properties of the beam

Width: 360mm

Height: 675mm

Length: 2250mm

Compressive strength of concrete: $f_c=32.0\text{Mpa}$

Reinforcement

Compression bars: 2D16

Tension bars: 9D25

Experimental results, gave the following *Force-Displacement Curve*, of figure 92:

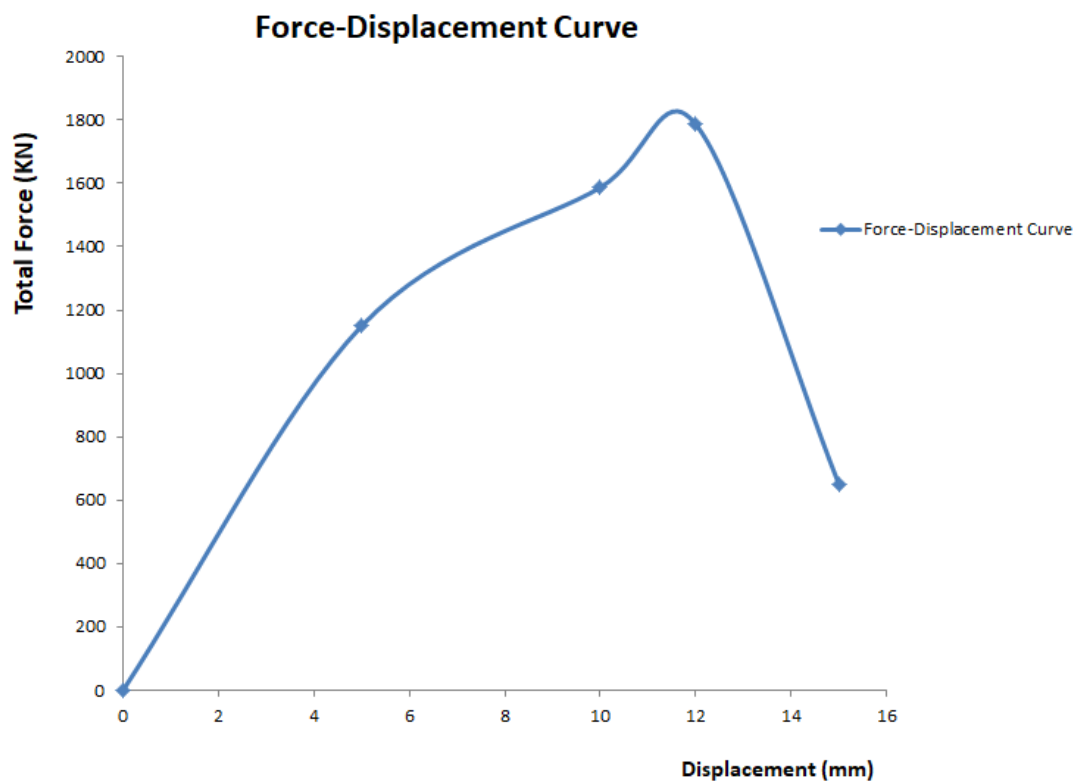


Figure 92. Force-Displacement Curve for the second beam, from experimental results

So, experiments gave a collapse load equal to $P_{exp}=1787\text{KN}$, and a displacement equal to $\delta_{peak}=8.62\text{mm}$.

Analysis with finite elements (FEM), using again Abaqus gave the following results, and *Force-Displacement Curve* in figure 93:

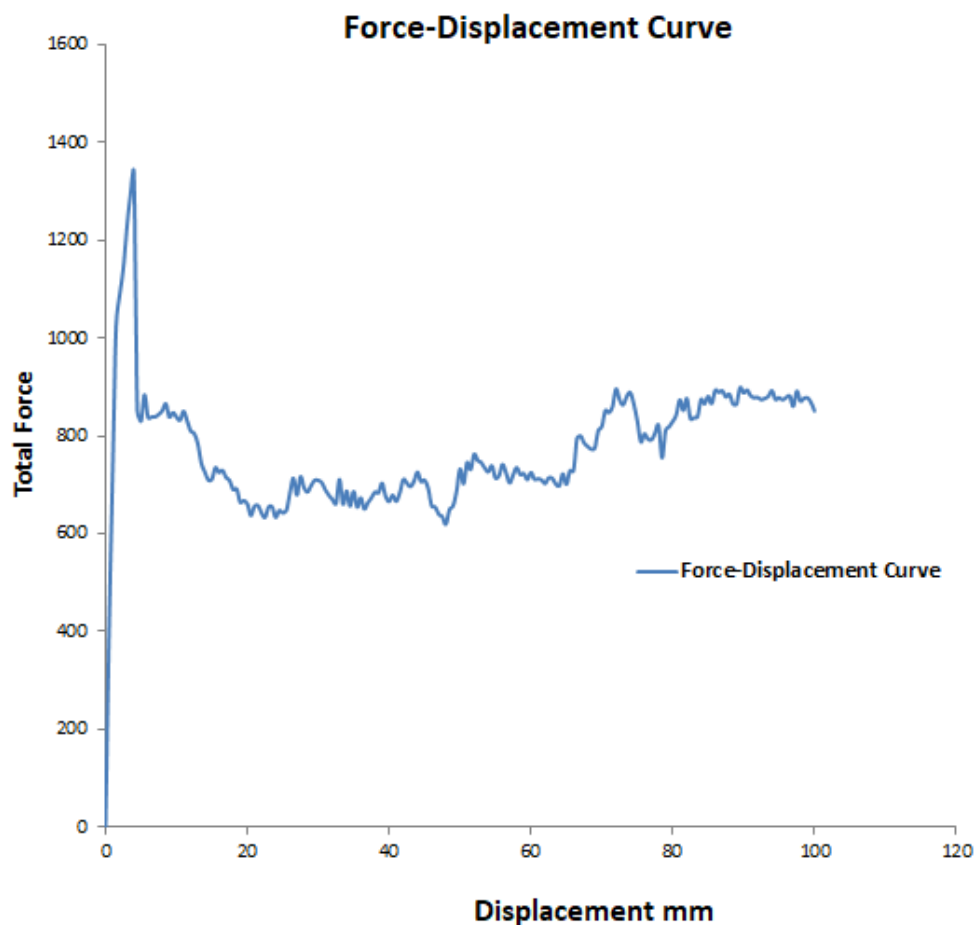


Figure 93. Force-Displacement Curve for the second beam, from FEA

So, from the analysis we find that the collapse load is equal to collapse load equal to $P_{exp}=1339.5\text{KN}$, and the peak displacement is equal to $\delta_{peak}=4.01\text{mm}$.

So, analysis with finite elements, gave also results that are very close to experimental results. In the following pictures, the cracks during initial loading and complete failure is presented, in figure 94-98.

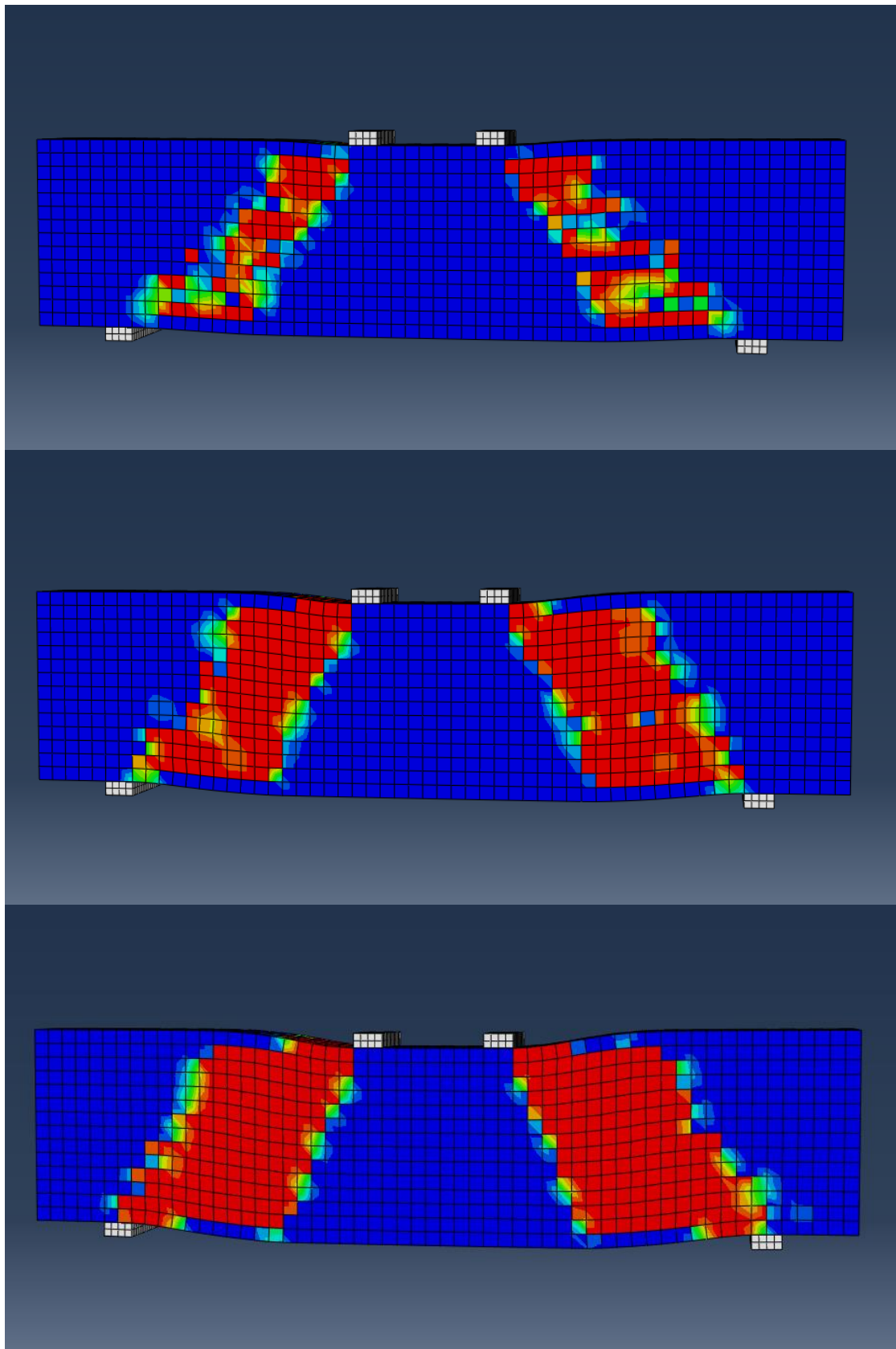


Figure 94. Initial formation of compressive cracks

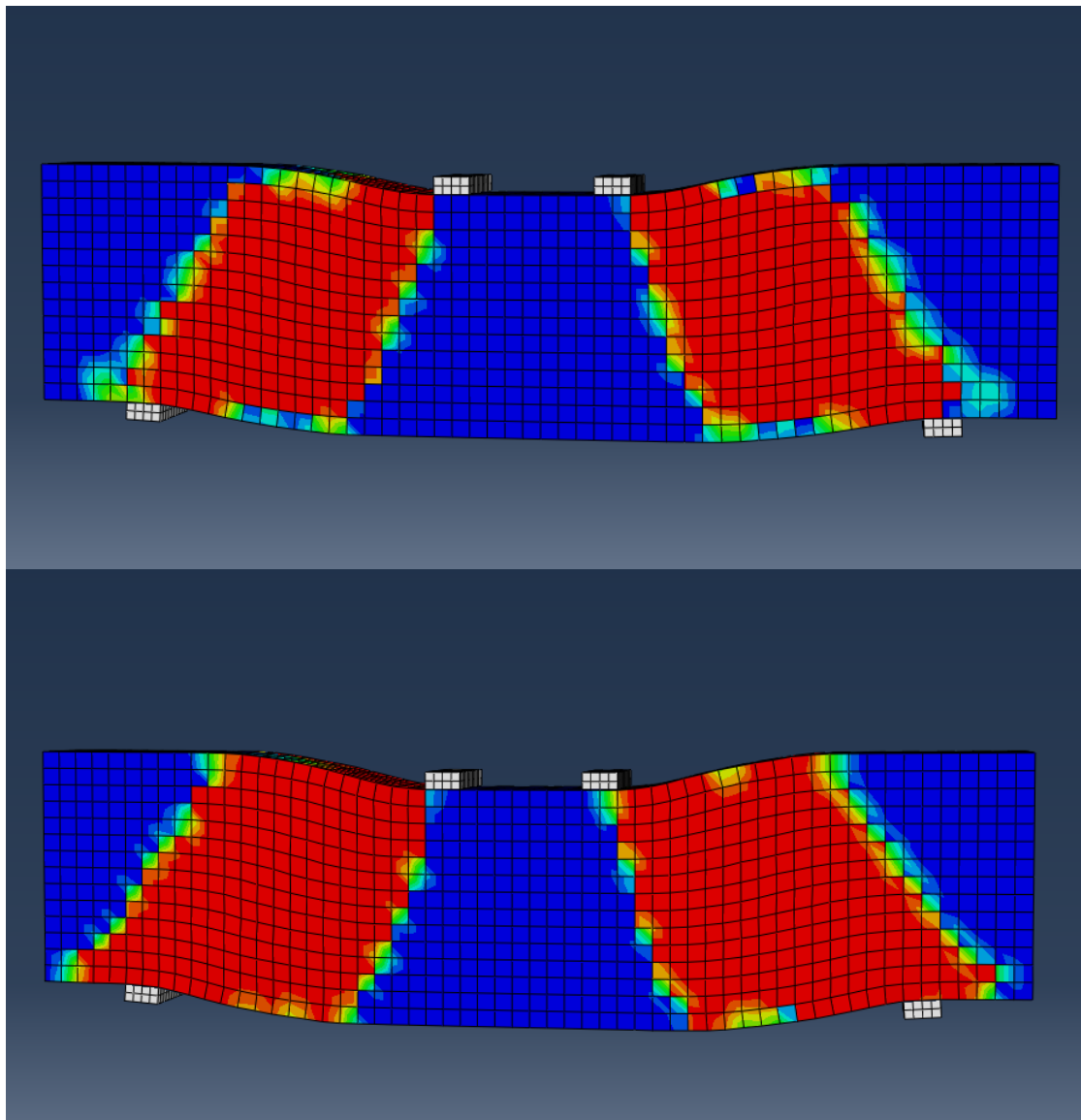


Figure 95. Compressive cracks at the failure of the beam

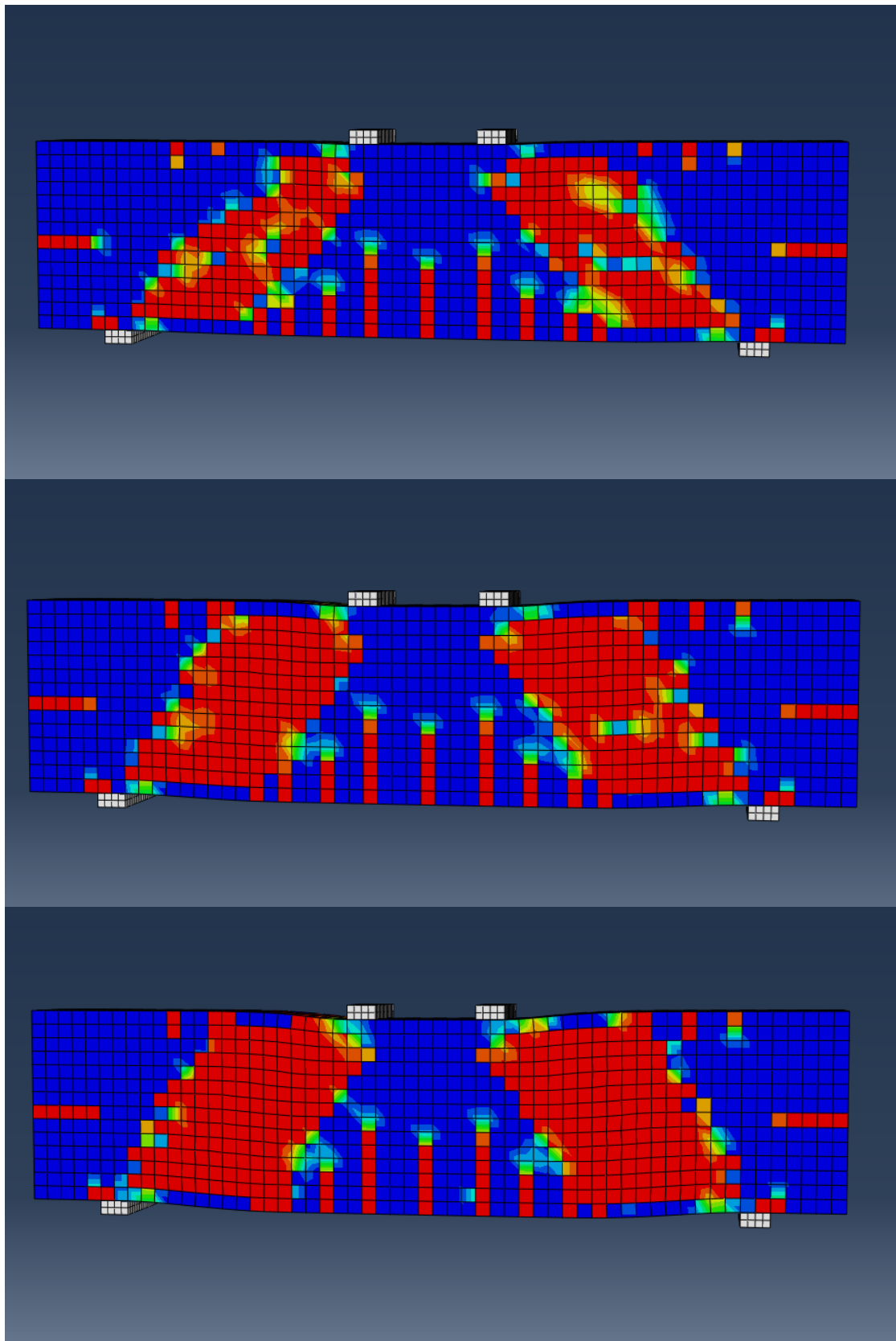


Figure 96. Initial formation of tensile cracks

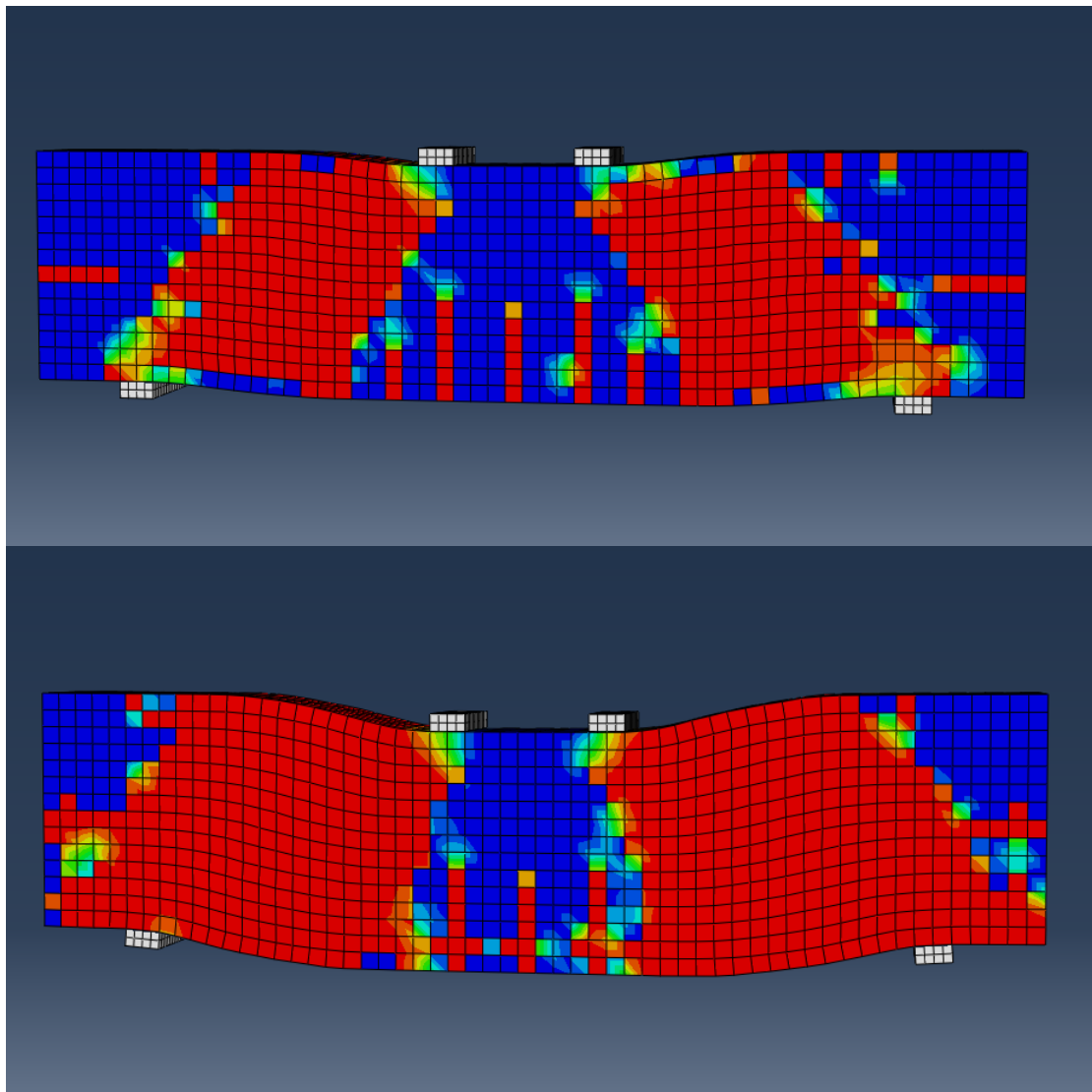


Figure 97. Tensile cracks at the failure of the beam

From the formed cracks, we can see that the cracks in experimental results, are very close to the results from FEA. It can be better seen, from diagonal cracks, that the failure is due to struts that are formed between the supports and the loading plates. It can be easily seen, comparing with the *figure 13*.

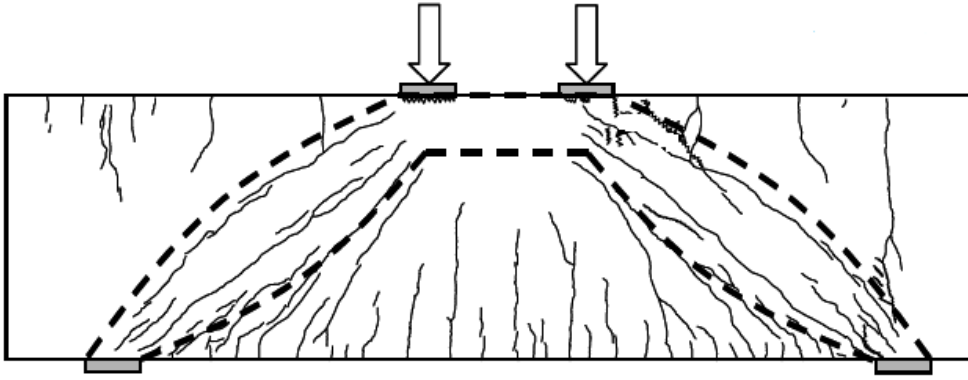


Figure 98. Cracks at the failure of the beam

5.5 Results from Strut and Tie modeling

Using the strut and tie model, we evaluate the collapse load, using the program AStrutTie.

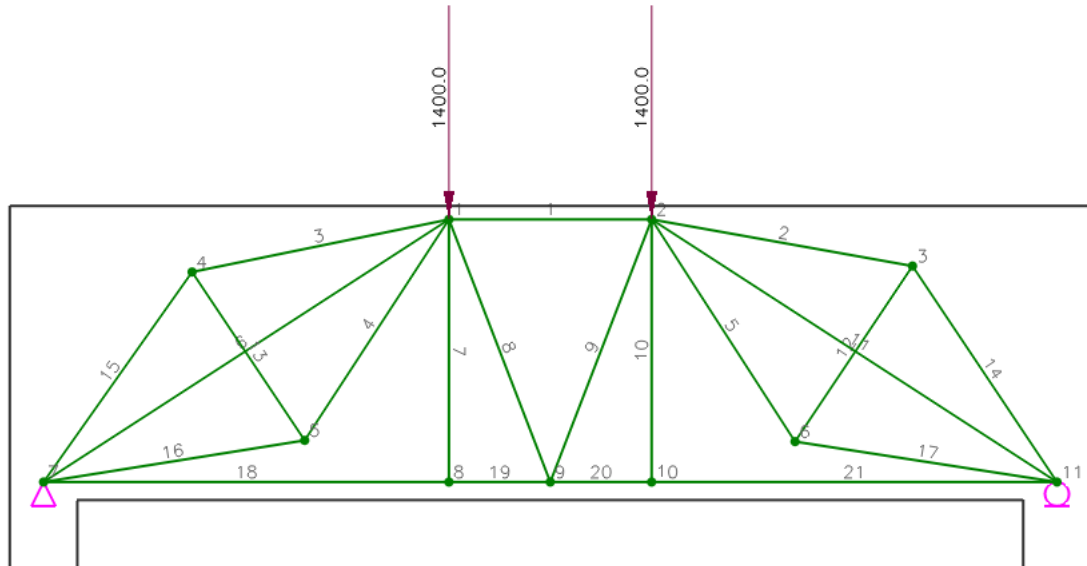


Figure 98. Strut and Tie model for the first beam

Here, we consider the appropriate load, in order to take the required reinforcement that we had from the experiment. This will be the collapse load.

Analysis from the program, gave the following results for the forces of the strut, in figure 99

| Elem. No. | Force (kN) |
|-----------|------------|-----------|------------|-----------|------------|-----------|------------|
| 1 | -2163.0 | 2 | -449.8 | 3 | -486.0 | 4 | -436.3 |
| 5 | -424.7 | 6 | -1725.0 | 7 | -0.0 | 8 | -0.1 |
| 9 | 0.1 | 10 | 0.0 | 11 | -1774.6 | 12 | 350.4 |
| 13 | 355.8 | 14 | -445.5 | 15 | -481.6 | 16 | -442.1 |
| 17 | -430.3 | 18 | 2163.0 | 19 | 2163.0 | 20 | 2162.9 |
| 21 | 2162.9 | | | | | | |

Figure 99. Resultant forces of the analysis

| Tie No. | Types | Fu (kN) | theta (deg.) | Rebars | As.req (mm ²) | As.used (mm ²) | Note |
|---------|-------|---------|--------------|--------|---------------------------|----------------------------|------|
| 12 | Top | 350.40 | 56.2 | 21-#10 | 1417 | 17163 | O.K |
| 13 | Top | 355.80 | 56.2 | 21-#10 | 1439 | 17163 | O.K |
| 18 | Top | 2162.99 | 0.0 | 21-#10 | 4867 | 17163 | O.K |

Figure 100. Required rebars of the beam

The required rebars, can be seen in the *figure 100*. The strength of the struts, can be seen in the following *figure 101*.

| Strut No. | Type | theta | Fu (kN) | b (mm) | Wreq (mm) | Wprov (mm) | Note |
|-----------|------|-------|---------|--------|-----------|------------|------|
| 1 | 1 | 0.0 | 2560.5 | 720.0 | 98.8 | 120.0 | O.K |
| 2 | 1 | 10.1 | 528.3 | 720.0 | 20.4 | 244.6 | O.K |
| 3 | 1 | 11.6 | 569.7 | 720.0 | 22.0 | 261.9 | O.K |
| 4 | 1 | 56.8 | 540.9 | 720.0 | 20.9 | 392.7 | O.K |
| 5 | 1 | 57.1 | 526.2 | 720.0 | 20.3 | 385.8 | O.K |
| 7 | 1 | 33.6 | 2048.4 | 720.0 | 79.0 | 249.2 | O.K |
| 12 | 1 | 33.6 | 2106.6 | 720.0 | 81.3 | 249.3 | O.K |
| 14 | 1 | 57.0 | 526.4 | 720.0 | 20.3 | 306.1 | O.K |
| 15 | 1 | 55.6 | 567.8 | 720.0 | 21.9 | 304.0 | O.K |
| 16 | 1 | 10.5 | 542.0 | 720.0 | 20.9 | 145.4 | O.K |
| 17 | 1 | 10.2 | 527.2 | 720.0 | 20.3 | 144.1 | O.K |

Figure 101. Strength of struts

The collapse load from experimental results was to found equal to $P_{exp}=5325\text{KN}$. So ,the strut and tie model, finds a collapse load 2800KN, that is approximately 53% over the real.

Now we use a different Truss, in order to design the beam again, and to see the differences. So, we consider the easiest truss model, that is in figure 102.

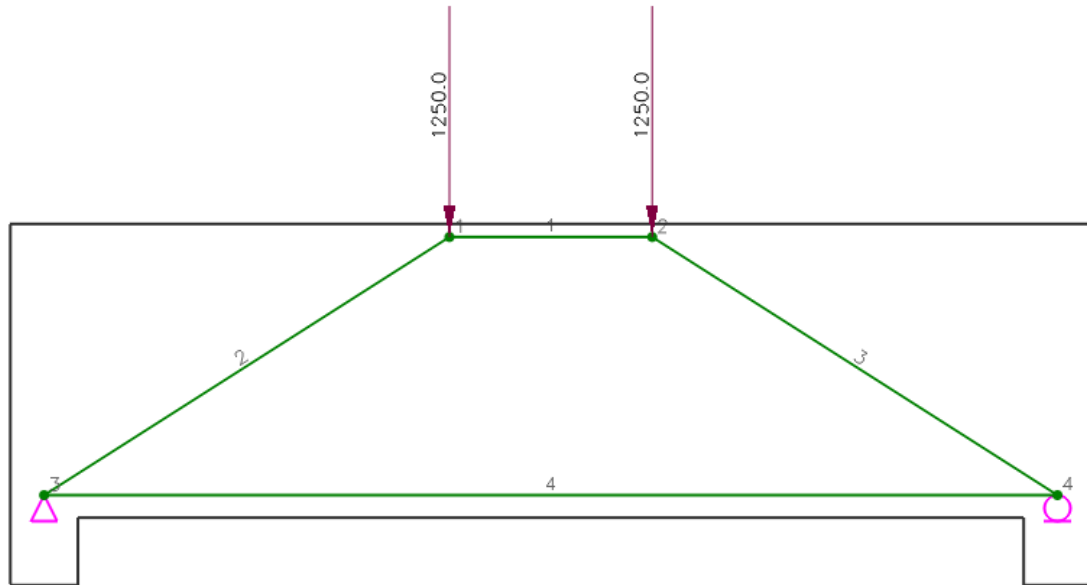


Figure 102. STM-model

This model for two concentrated loads, 1250KN each, gave the following results, for the reinforcement and strength of struts, in figure 103:

| Tie No. | Types | Fu (kN) | theta (deg.) | Rebars | As.req (mm ²) | As.used (mm ²) | Note |
|---------|-------|---------|--------------|--------|---------------------------|----------------------------|------|
| 4 | Top | 1961.36 | 0.0 | 27-#9 | 4413 | 17408 | O.K |

Figure 103. Results for required reinforcement and strength of struts.

From the results, we can see that the total load of 2500KN, is the ultimate load, as the W_{req} , is equal to W_{prov} . So the collapse load is equal to 2500KN. So it approximately 47% the collapse load, that we took from the experiment.

Using the strut and tie model, we evaluate the collapse load again, using the program AStrutTie, for the second beam.

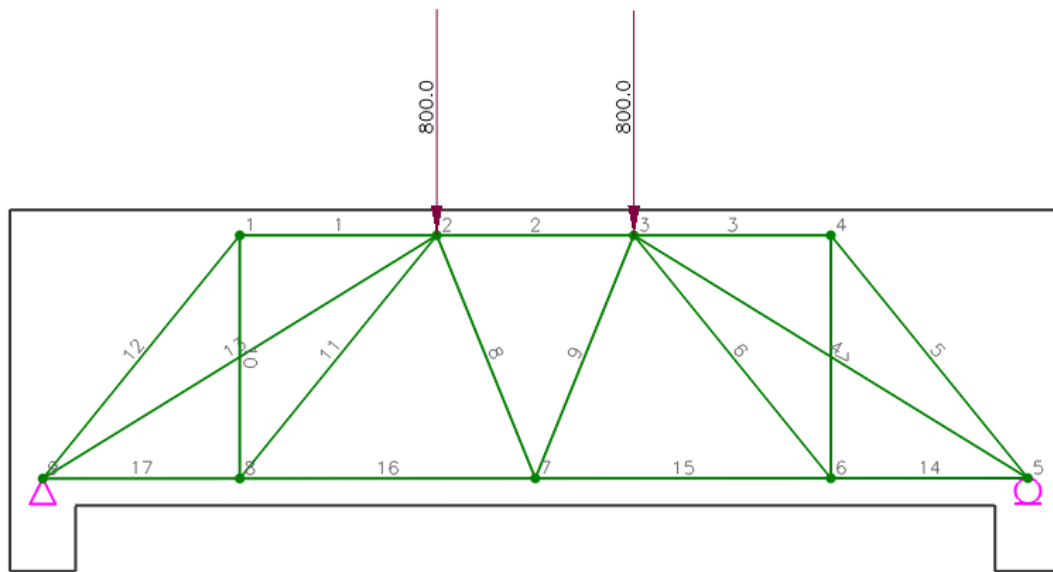
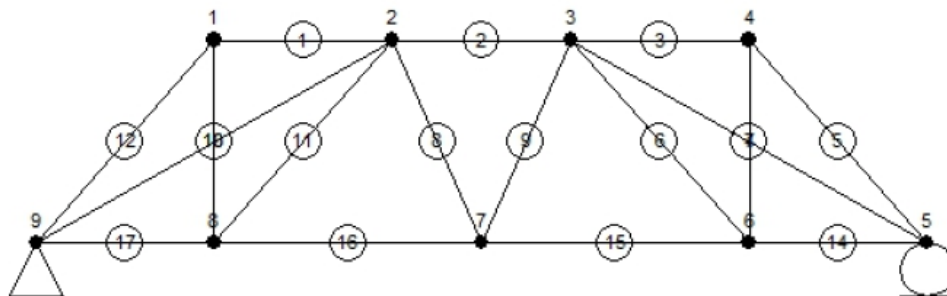


Figure 103. Strut and Tie model for the second beam

Analysis from the program, gave the following results for the forces of the strut in figure 104



| Elem. No. | Force (kN) |
|-----------|------------|-----------|------------|-----------|------------|-----------|------------|
| 1 | -315.4 | 2 | -1403.5 | 3 | -316.3 | 4 | -887.8 |
| 5 | -479.3 | 6 | -479.0 | 7 | 360.2 | 8 | 0.7 |
| 9 | -0.7 | 10 | 359.9 | 11 | -478.9 | 12 | -478.6 |
| 13 | -889.0 | 14 | 1087.8 | 15 | 1403.8 | 16 | 1403.2 |
| 17 | 1087.6 | | | | | | |

Figure 104. Resultant forces of the analysis

The required rebars, can be seen in the following figure 105

| Tie No. | Types | Fu (kN) | theta (deg.) | Rebars | As.req (mm ²) | As.used (mm ²) | Note |
|---------|-------|---------|--------------|--------|---------------------------|----------------------------|------|
| 14 | Top | 1087.78 | 0.0 | 11-#7 | 2447 | 4267 | O.K |
| 15 | Top | 1403.78 | 0.0 | 11-#7 | 3159 | 4267 | O.K |
| 16 | Top | 1403.24 | 0.0 | 11-#7 | 3157 | 4267 | O.K |

Figure 105. Strength verification and required rebars of the beam

The strength of struts, can be seen in the following figure 106

| Strut No. | Type | theta | Fu (kN) | b (mm) | Wreq (mm) | Wprov (mm) | Note |
|-----------|------|-------|---------|--------|-----------|------------|------|
| 1 | 1 | 0.0 | 315.4 | 360.0 | 20.5 | 200.0 | O.K |

| | | | | | | | |
|----|---|------|--------|-------|-------|-------|-----|
| 2 | 1 | 0.0 | 1403.5 | 360.0 | 91.4 | 200.0 | O.K |
| 3 | 1 | 0.0 | 316.3 | 360.0 | 20.6 | 200.0 | O.K |
| 4 | 2 | 29.7 | 887.8 | 360.0 | 110.5 | 182.8 | O.K |
| 5 | 2 | 48.7 | 479.3 | 360.0 | 59.6 | 195.2 | O.K |
| 6 | 2 | 48.7 | 479.0 | 360.0 | 59.6 | 188.9 | O.K |
| 9 | 2 | 66.3 | 0.7 | 360.0 | 0.1 | 308.7 | O.K |
| 11 | 2 | 48.8 | 478.9 | 360.0 | 59.6 | 187.2 | O.K |
| 12 | 2 | 48.8 | 478.6 | 360.0 | 59.6 | 193.9 | O.K |
| 13 | 2 | 29.7 | 889.0 | 360.0 | 110.6 | 181.2 | O.K |

Figure 106. Strength of struts

So with this strut and tie model, we find that the collapse load is equal to 1600KN.

So, the model gives a collapse load, equal to 90% of the real collapse load.

Now we use again a different truss, in order to design the beam. So, we consider the truss model, that is in *figure 107*.

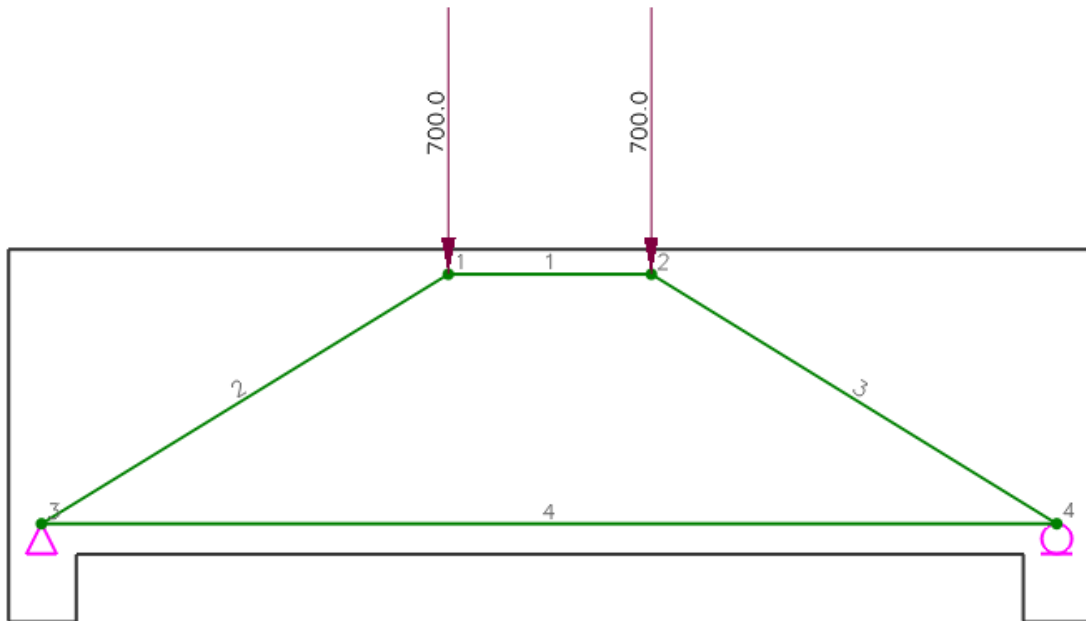


Figure 107. Truss model for the second beam

This model for two concentrated loads, 700kN each, gave the following results, for the reinforcement and strength of struts, in *figure 108*:

| Tie No. | Types | Fu (kN) | theta (deg.) | Rebars | As.req (mm ²) | As.used (mm ²) | Note |
|---------|-------|-------------|--------------|--------|---------------------------|----------------------------|------|
| 4 | Top | 1137.9 5 | 0.0 | 35-#4 | 2560 | 4434 | O.K |

| Strut No. | Type | theta | Fu (kN) | b (mm) | Wreq (mm) | Wprov (mm) | Note |
|-----------|------|-------|---------|--------|-----------|------------|------|
| 1 | 1 | 0.0 | 1130.3 | 360.0 | 73.6 | 110.0 | O.K |
| 2 | 2 | 31.5 | 1342.1 | 360.0 | 167.0 | 193.5 | O.K |
| 3 | 2 | 31.6 | 1334.0 | 360.0 | 166.0 | 193.6 | O.K |

Figure 108. Results for required reinforcement and strength of struts.

From the results, we can see that the total load of 1400kN, is the ultimate load, as the W_{req} , is equal to W_{prov} . So the collapse load is equal to 1400kN. So it approximately 78% the collapse load, that we took from the experiment.

From the results of STM models we can see that when new the simplest truss model, we take a collapse load that is lower than that we take from the experiments. On the other hand, when we use more complicating truss models, we take much biggest collapse loads. So the main characteristic for truss model ,in order to be safe and accurate, is to be the simplest that we can have to do the analysis.

Next, we give the information about how the program calculate the required rebars, and the strength verification of struts, and the strength of nodes.

(1) Required rebars

$$A_{s.req} = (F_u / \cos(\theta)) / (f_y / \gamma_s)$$

where,

F_u = member force of steel tie

γ_s = partial safety factor for steel tie

f_y = yield strength of steel

θ = angle of steel tie, measured from positive horizontal axis

So, having these as known quantities, the program calculates the required rebar.

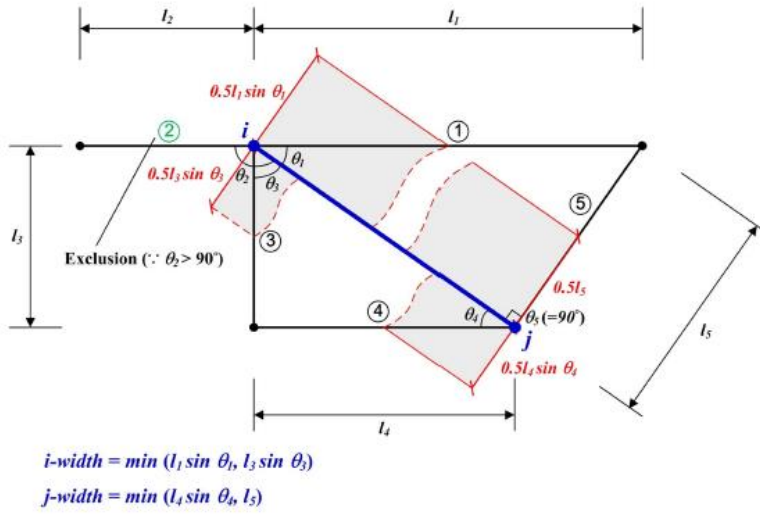
(2) Available Widths of Struts and nodal zones

In order to calculate the W_{prov} , the program calculates the provided width, as it is shown in the *figure 109*.

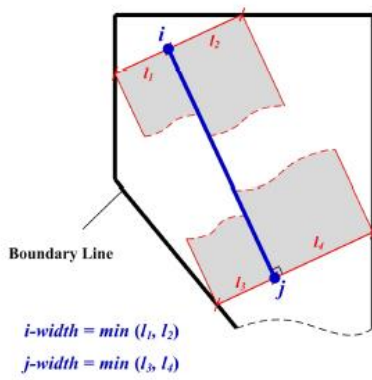
So, the program calculates the available widths in the two nodes of a strut, and gives the minimum, in the results.

The strength of a node is calculated using the definitions of the EC2. The verification of the nodal zone strength should be done through comparing the available nodal zone area with that required. In this report, if the thickness of the structural concrete is consistent, the verification will be done by comparing the available nodal zone width, W_{prov} , with that required, W_{req} . The verification of the nodal zone strength should be done through comparing the available nodal zone area with that required. In this report, if the thickness of the structural concrete is consistent, the verification will be done by comparing the available nodal zone width, W_{prov} , with that required, W_{req} .

[CASE 1]



[CASE 2]



[CASE 3]

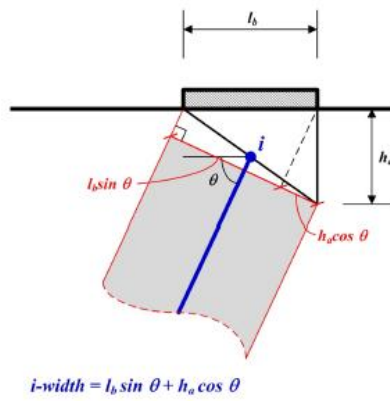


Figure 109. Available width in a node

For our example, we have the following

For the beam 1

For the case of the simplest truss, for the node 1 where the plate is located, we have that:

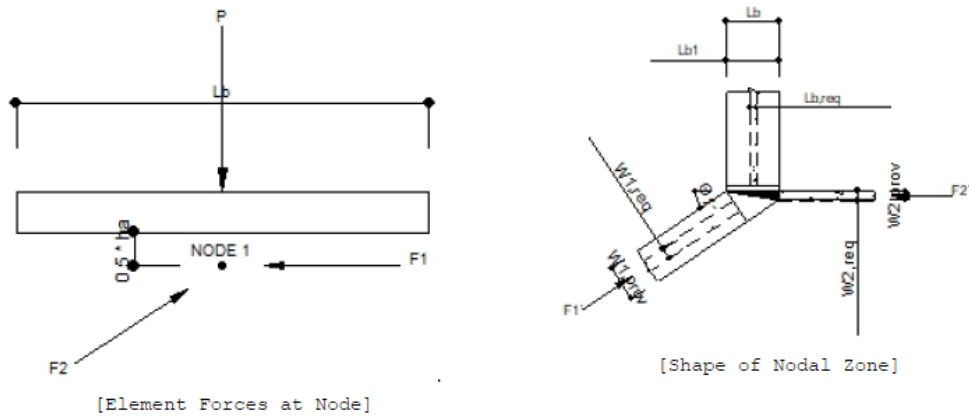


Figure 110. Element forces in node 1.

$L_b=720 \text{ mm}$

$h_a=116 \text{ mm}$

$P=1250 \text{ KN}$

For the forces we have

$F_1=2325.90 \text{ KN}$

$F_2=1961.64 \text{ KN}$

The angles that the struts form are:

Theta 1=32.5° and

Theta 2=0.0°

So, using figure 24, we calculate the W_{prov} , for the two struts that coincide to node 1. That is,

$W_{1,prov} = L_b \sin(\theta_1) + h_a \cos(\theta_1) = 720 \sin(32.5) + 116 \cos(32.5) = 484.7 \text{ mm}$

$W_{2,prov} = L_b \sin(\theta_2) + h_a \cos(\theta_2) = 0 \sin(0.0) + 116 \cos(0.0) = 116.0 \text{ mm}$

$L_{prov} = 720 \text{ mm}$

For the W_{req} , the program uses the EC2 and the following type:

$$W_{req} = \frac{F}{\left(1 - \frac{f_{ck}}{250}\right) * \frac{\alpha * f_{ck}}{\gamma} b}$$

Where

f_{ck} =strength of concrete

α =1,00

b =width of the beam

γ =safety factor=0.75

F =force of strut

So, using this, we have that:

$$W_{1,req} = 2326.89 * 1000 / \left(1.00 * \left(1 - \frac{27}{250}\right) * \frac{27}{0.75}\right) * 720 = 100.6 \text{ mm}$$

$$W_{2,req} = 1961.64 * 1000 / \left(1.00 * \left(1 - \frac{27}{250}\right) * \frac{27}{0.75}\right) * 720 = 84.8 \text{ mm}$$

$$L_{b,req} = 1250 * 1000 / \left(1.00 * \left(1 - \frac{27}{250}\right) * \frac{27}{0.75}\right) * 720 = 54.1 \text{ mm}$$

So, the node has enough strength, since we have:

$$W_{1,prov} = 484.7 \text{ mm} > 100.6 \text{ mm} = W_{1,req}$$

$$W_{2,prov} = 116.0 \text{ mm} > 84.8 \text{ mm} = W_{2,req}$$

$$L_{prov} = 720 \text{ mm} > 54.1 \text{ mm} = L_{b,req}$$

Hear, we used the equation for W_{req} , without the safety factor for concrete f_{ck} .

For the node 3, where the strut and the tie coincide, we have that:

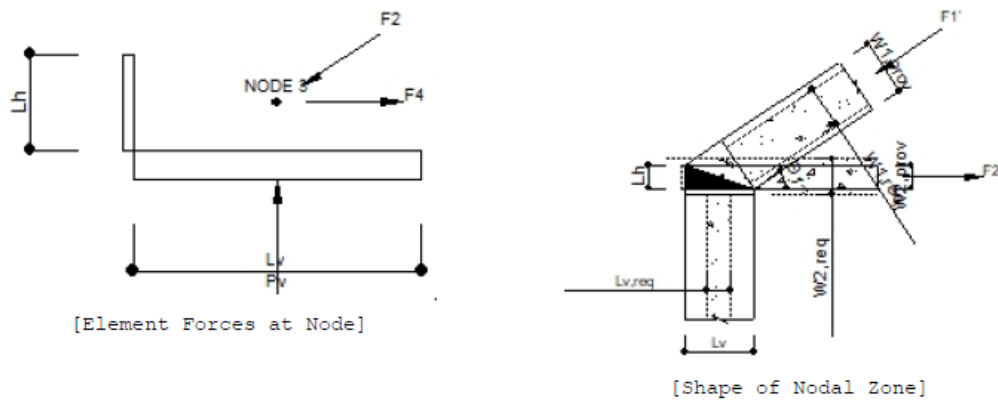


Figure 111. Element forces in node 3.

$$L_b = 300.0 \text{ mm}$$

$$L_h = 210.0 \text{ mm}$$

$$P = 1250 \text{ KN}$$

Again using *figure 24*, we calculate the W_{prov} , for the two struts that coincide to node 1. That is,

$$W_{1,prov} = L_v \sin(\theta_1) + L_h \cos(\theta_1) = 300 \sin(32.5) + 200 \cos(32.6) = 329.9 \text{ mm}$$

$$W_{2,prov} = L_v \sin(\theta_2) + L_h \cos(\theta_2) = 300 \sin(0.0) + 100.00 \cos(0.0) = 200.0 \text{ mm}$$

$$W_{1,req} = 1805.92 * 1000 / (0.85 * (1 - \frac{27}{250})^{\frac{27}{0.75}}) * 720 = 118.4 \text{ mm}$$

$$W_{2,req} = 1503.62 * 1000 / (0.85 * (1 - \frac{27}{250})^{\frac{27}{0.75}}) * 720 = 99.8 \text{ mm}$$

$$L_{v,req} = 1250.00 * 1000 / (0.85 * (1 - \frac{27}{250})^{\frac{27}{0.75}}) * 720 = 63.6 \text{ mm}$$

So, the node has enough strength, since we have:

$$W_{1,prov} = 249.4 \text{ mm} > 118.4 \text{ mm} = W_{1,req}$$

$$W_{2,prov} = 210.0 \text{ mm} > 100.0 \text{ mm} = W_{2,req}$$

$$L_{v,prov} = 300 \text{ mm} > 63.6 \text{ mm} = L_{v,req}$$

For the case of the more complicating truss, for the node 1 where the plate is located, we have that:

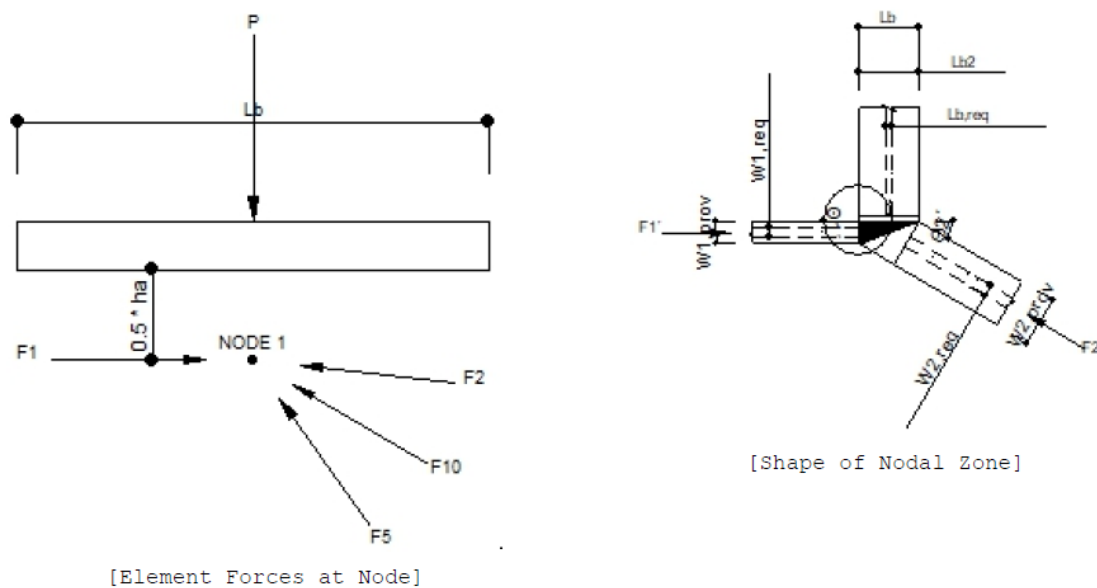


Figure 112. Element forces in node 1.

$$L_b = 720 \text{ mm}$$

$$h_a = 116 \text{ mm}$$

$$P = 1400 \text{ KN}$$

For the forces we have

$$F_1 = 2576.50 \text{ KN}$$

$$F_2 = 2162.97 \text{ KN}$$

The angles that the struts form are:

$$\text{Theta } 1 = 32.9^\circ \quad \text{and}$$

$$\text{Theta } 2 = 0.0^\circ$$

So, using *figure 24*, we calculate the W_{prov} , for the two struts that coincide to node 1.

That is,

$$W_{1,prov} = L_b \sin(\text{theta } 1) + h_a \cos(\text{theta } 1) = 720 \sin(32.9) + 116 \cos(32.9) = 491.9 \text{ mm}$$

$$W_{2,prov} = L_b \sin(\text{theta } 2) + h_a \cos(\text{theta } 2) = 0 \sin(0.0) + 116 \cos(0.0) = 120.0 \text{ mm}$$

$$L_{prov} = 720 \text{ mm}$$

For the W_{req} , the program uses the EC2 and the following type:

For the W_{req} , the program uses the EC2 and the following type:

$$W_{req} = \frac{F}{\left(1 - \frac{f_{ck}}{250}\right) * \frac{\alpha * f_{ck}}{\gamma} b}$$

So, using this, we have that:

$$W_{1,req} = 2162.97 * 1000 / \left(1.00 * \left(1 - \frac{27}{250}\right) * \frac{27}{0.75}\right) * 720 = 93.6 \text{ mm}$$

$$W_{2,req} = 2576.53 * 1000 / \left(1.00 * \left(1 - \frac{27}{250}\right) * \frac{27}{0.75}\right) * 720 = 111.4 \text{ mm}$$

$$L_{b,req} = 1250 * 1000 / \left(1.00 * \left(1 - \frac{27}{250}\right) * \frac{27}{0.75}\right) * 720 = 60.6 \text{ mm}$$

So, the node has enough strength, since we have:

$$W_{1,prov} = 491.9 \text{ mm} > 100.6 \text{ mm} = W_{1,req}$$

$$W_{2,prov} = 120.0 \text{ mm} > 84.8 \text{ mm} = W_{2,req}$$

$$L_{prov} = 720 \text{ mm} > 54.1 \text{ mm} = L_{b,req}$$

Hear, we used the equation for W_{req} , without the safety factor for concrete f_{ck} .

For the node 3, where the strut and the tie coincide, we have that:

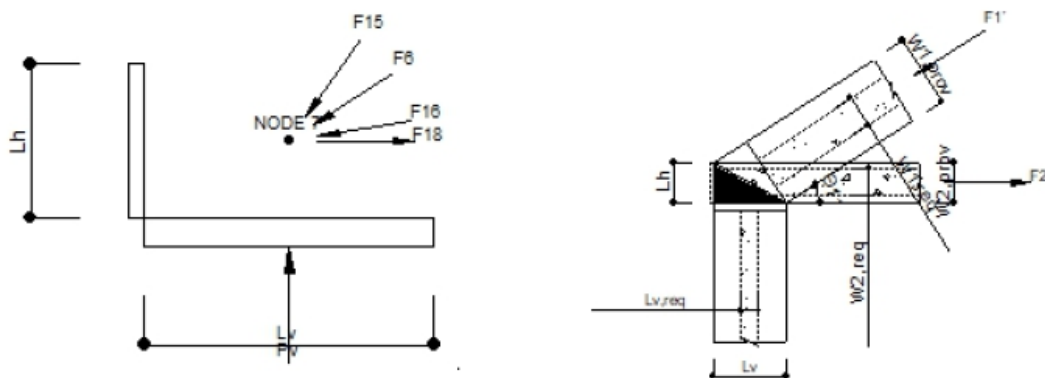


Figure 113. Element forces in node 7.

$$L_v = 300.0 \text{ mm}$$

$$L_h = 210.0 \text{ mm}$$

P = 1400 KN

Again using *figure 24*, we calculate the W_{prov} , for the two struts that coincide to node 1. That is,

$$W_{1,prov} = 297.3\text{mm}$$

$$W_{2,prov} = 200.0\text{mm}$$

$$W_{1,req} = 131.1\text{mm}$$

$$W_{2,req} = 110.1\text{mm}$$

$$L_{v,req} = 71.2\text{mm}$$

So, the node has enough strength, since we have:

$$W_{1,prov} = 297.3\text{mm} > 131.1\text{ mm} = W_{1,req}$$

$$W_{2,prov} = 160.0\text{mm} > 110.1\text{ mm} = W_{2,req}$$

$$L_{v,prov} = 210\text{mm} > 71.2\text{ mm} = L_{v,req}$$

The final results are shown in table 1.

| | BEAM 1 | BEAM2 |
|---------------------|---------------|--------------|
| EXPERIMENTAL | 5325 | 1787 |
| FEA | 5482 | 1340 |
| STM-1 | 2800 | 1600 |
| STM-2 | 2500 | 1400 |

1. Results of the analysis

5.6 Deep beam with Fe77 and with Strut and tie model, and comparisons

Here we compare the results of that the Strut and Tie model gives us, with the results of a finite element analysis, using the program Fe77, that are considered to be close to the real, for the collapse load.

Strut and Tie model analysis results

Here, we consider the deep beam of the figure 114

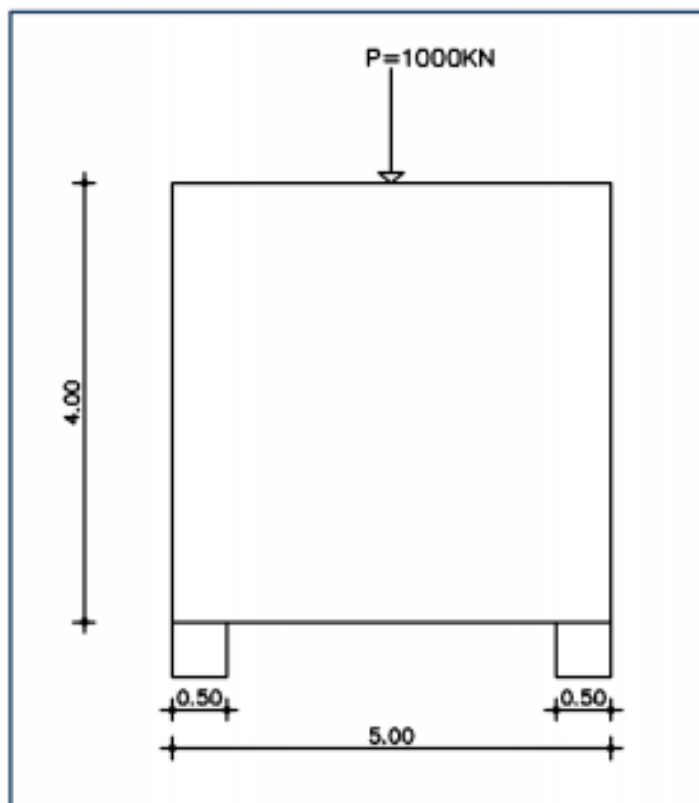


Figure 114. Geometry of the beam.

$$l=4.5\text{m}$$

$$h=4.0\text{m}$$

$$\frac{l}{h}=1.125$$

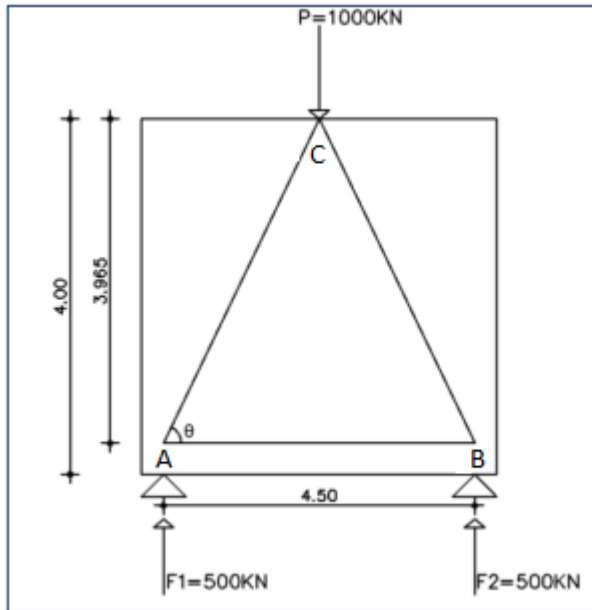


Figure 115. Truss model of the beam.

From the equilibrium of the truss, we find that

$$F_{AB} = -575 \text{KN}$$

$$F_{AC} = -284 \text{KN}$$

So, the reinforcement of the beam, is equal to:

$$A_s = \frac{F_{AB}}{f_{yd}} = 568 \text{mm}^2$$

So, 3 steel bars of 18mm diameter are placed as the main reinforcement of the beam. Next, the strength of nodal zones are calculated, in order to find if they fail or not.

In figure 116, the geometry of the nodal zone A is shown.

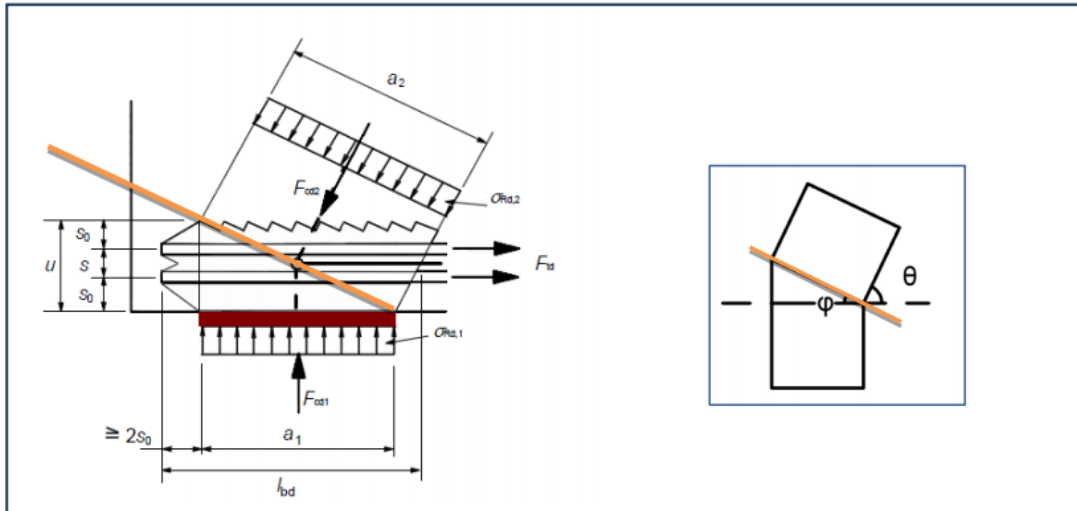


Figure 116. Geometry of nodal zone A.

Strength of nodal zone A

$$\sigma_{Rd} = 0.85 \left(1 - \frac{f_{ck}}{250}\right) f_{ck} = 0.85 \left(1 - \frac{30}{250}\right) 30 = 22.4 \text{ MPa}$$

The geometrical properties of nodal zones, are found using the dimensions of the column, and the theory that was described later.

Strength of nodal zone C

$$\sigma_{Rd} = 1.00 \left(1 - \frac{f_{ck}}{250}\right) f_{ck} = 0.85 \left(1 - \frac{30}{250}\right) 30 = 26.4 \text{ MPa}$$

Next, we find the stresses in zones, using the geometry of the nodes and the calculated loads:

$$\sigma_{c1} = \frac{1000000}{300 \cdot 870} = 3.83 \text{ MPa}$$

$$\sigma_{c2} = \frac{1000000}{300 \cdot 870} = 3.83 \text{ MPa}$$

It is clear that the strength of the nodal zones is enough. So, for the load of 1000KN, we have found that the reinforcement is equal to 568mm².

Fe77 analysis results

Hear, in *figure 117*, the deep beam is shown. Next, in *figures 118-120*, the deformation of the beam till collapse is shown. Next, the force- displacement diagram is constructed.

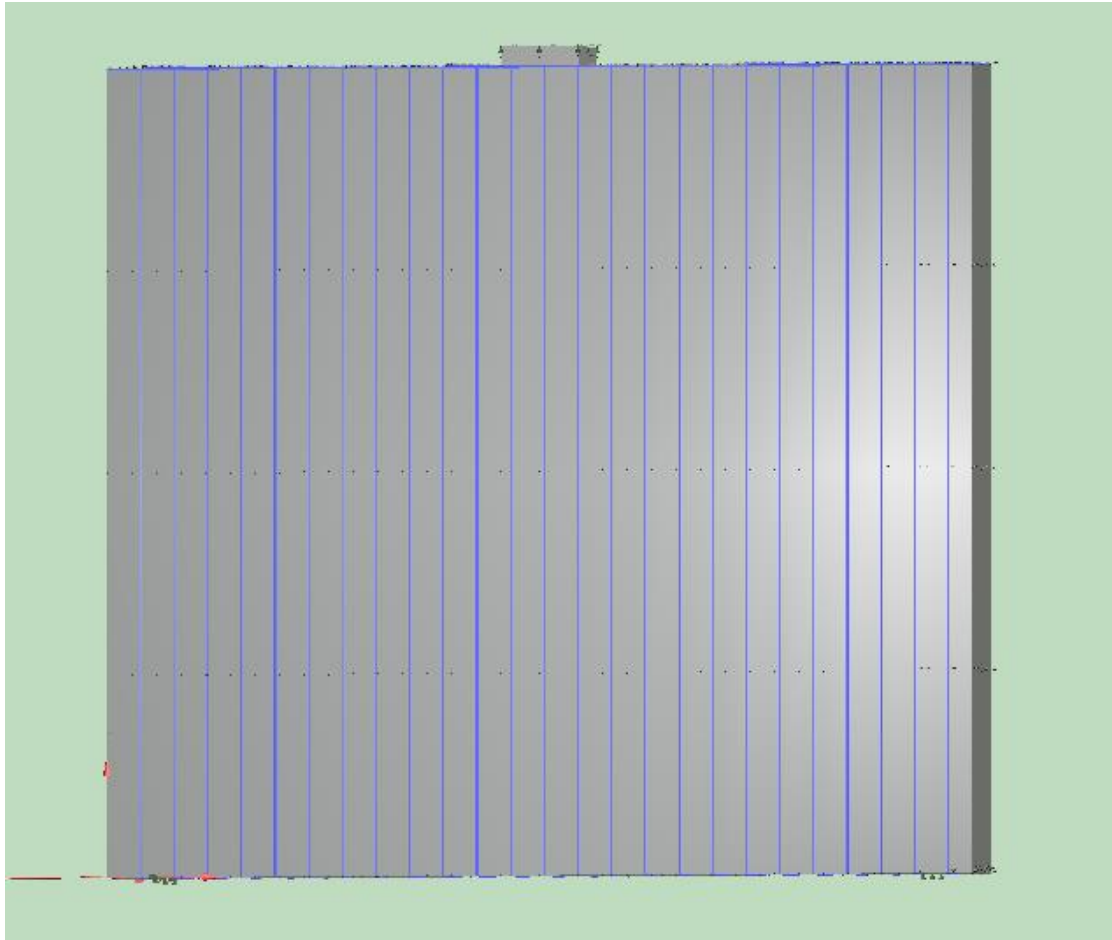


Figure 117. Deep beam geometry

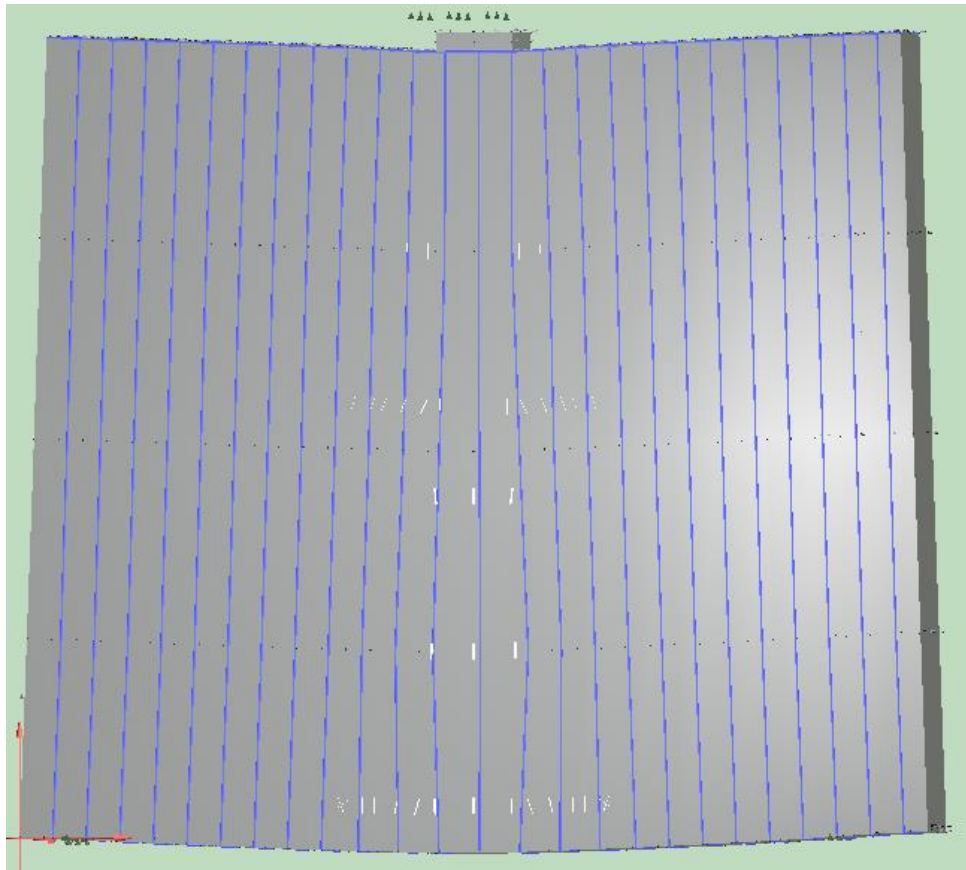


Figure 118. Initial deformation of the beam.

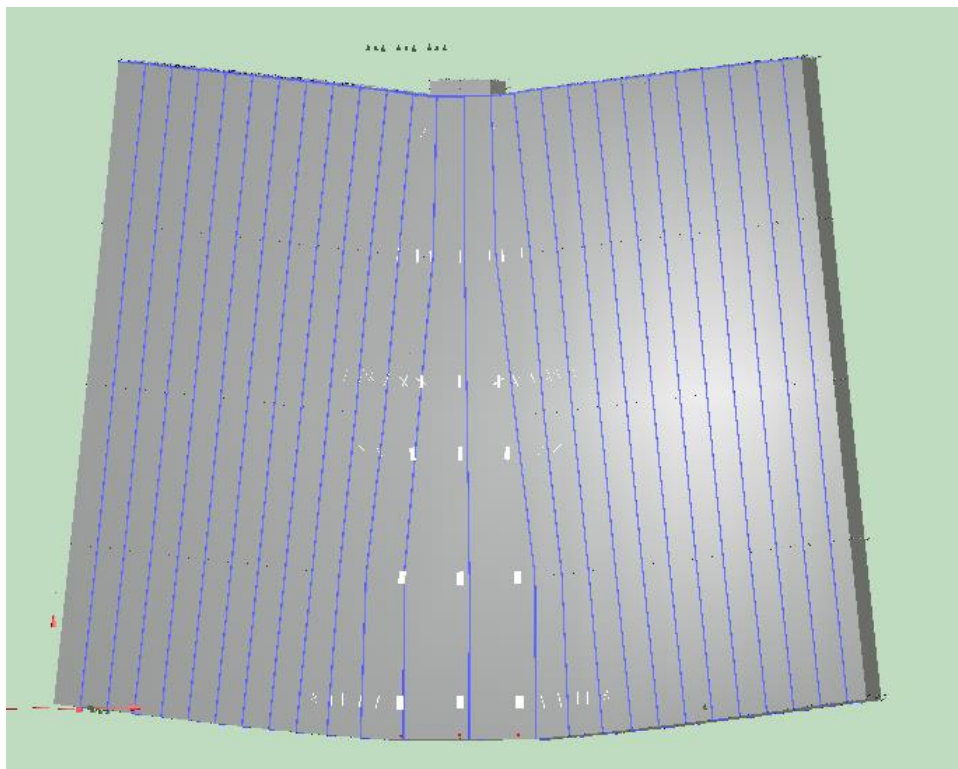


Figure 119. First yielding of the reinforcement

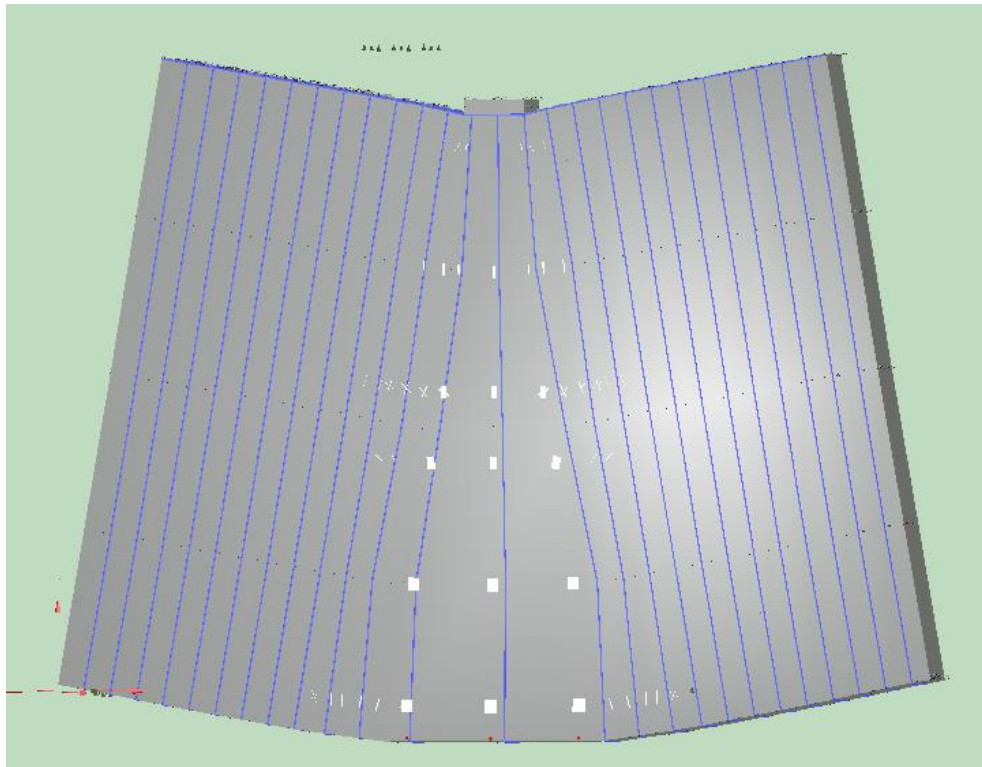


Figure 120. Deformation of the beam in collapse

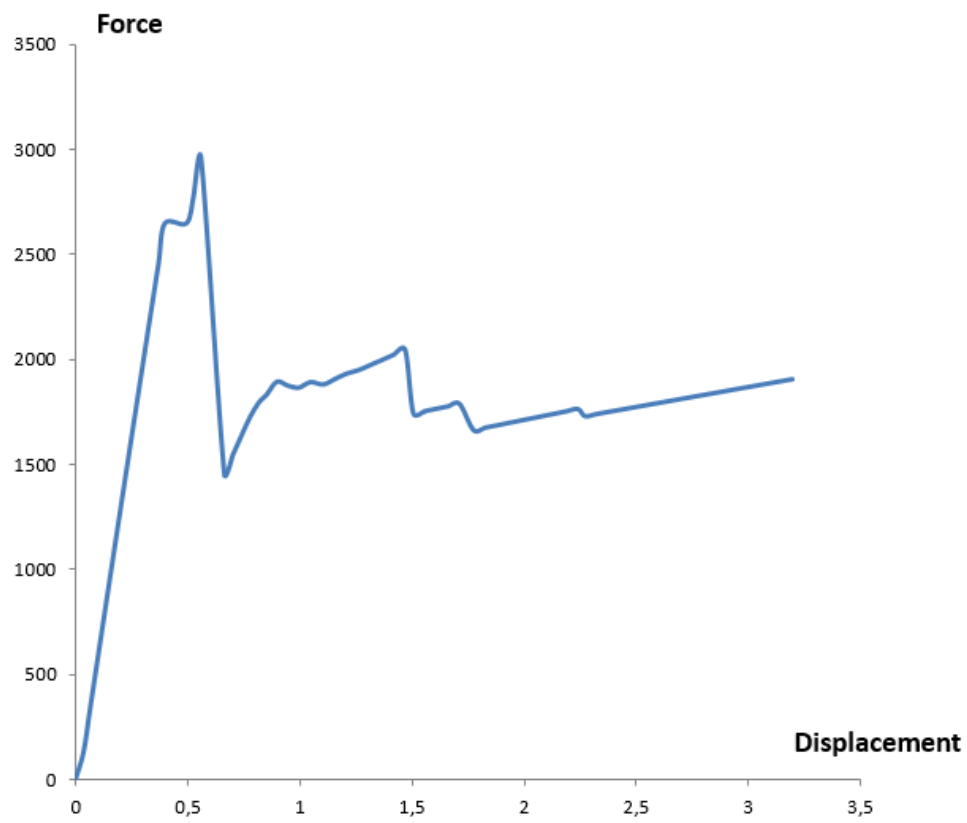


Figure 121. Force-displacement diagram.

From the analysis, it is shown that the collapse load is approximately equal to $P_{max}=3000KN$.

The results show that the collapse load that was calculated with the Strut and Tie model, is only 33%, of the total load.

Deep beam example

In the first example, we solve a deep beam ,with the following information and geometry of the *figure 122*:

Beam's of width: 0,35m

Column's width: 0,4m

Compressive strength of concrete: 23,5MPa

Yield modulus of steel: 400MPa

Concentrated load: 1000KN

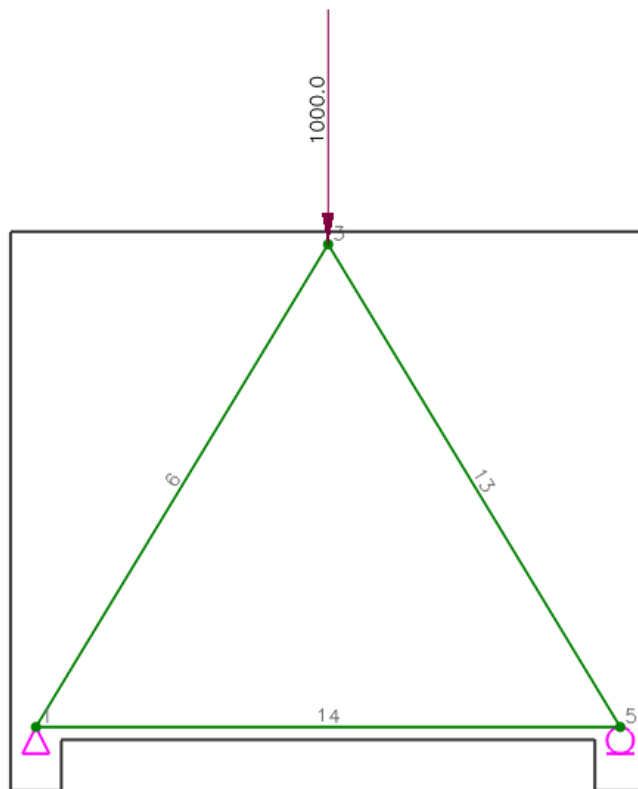


Figure 122. Truss model (a)

The bars 6,13 are the two concrete struts, while the bar 14 is the tie, that represents the steel bars. Using the program AStrutTie, the solution of the truss, gave the following results:

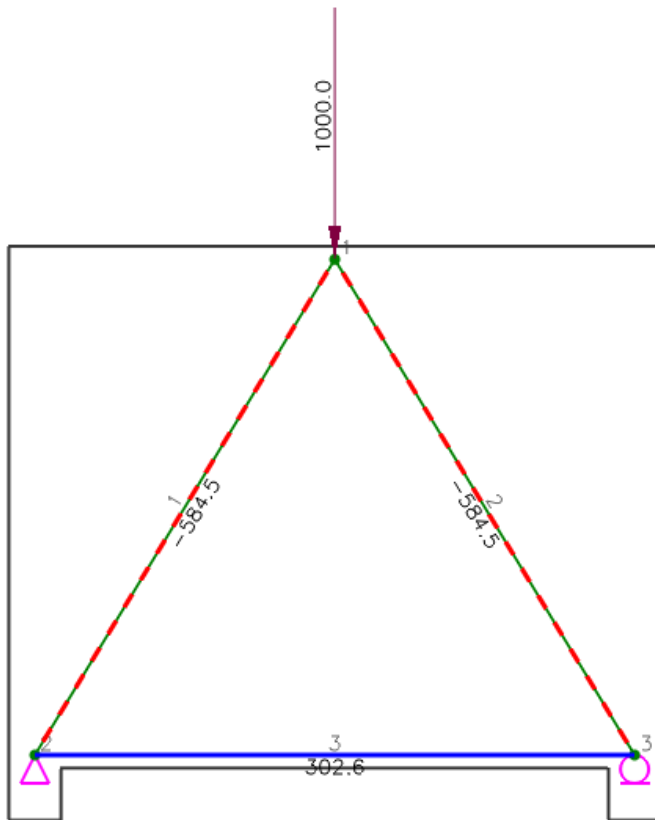


Figure 123. Analysis of truss model (a)

Using the program, we can see if the beam is safe or not. So, it can be seen from figure 3 if there is enough reinforcement, and if the w_{prov} is greater than the w_{req} .

| Tie No. | Types | Fu (kN) | theta (deg.) | Rebars | As.req (mm ²) | As.used (mm ²) | Note |
|---------|--------|---------|--------------|--------|---------------------------|----------------------------|------|
| 5 | Bottom | 302.63 | 0.0 | 8-#4 | 681 | 1013 | O.K |

| Strut No. | Type | theta | Fu (kN) | b (mm) | Wreq (mm) | Wprov (mm) | Note |
|-----------|------|-------|---------|--------|-----------|------------|------|
| 1 | 2 | 58.8 | 584.5 | 350.0 | 96.2 | 445.8 | O.K |
| 4 | 1 | 58.8 | 584.5 | 350.0 | 52.2 | 445.8 | O.K |

Figure 124. Calculations of truss model (a)

Form the tables of figure 125, it is shown that the beam is safe.

Next, the same beam is solved using a different STM, in order to show the difference in the results. In figure 124 shows the STM model

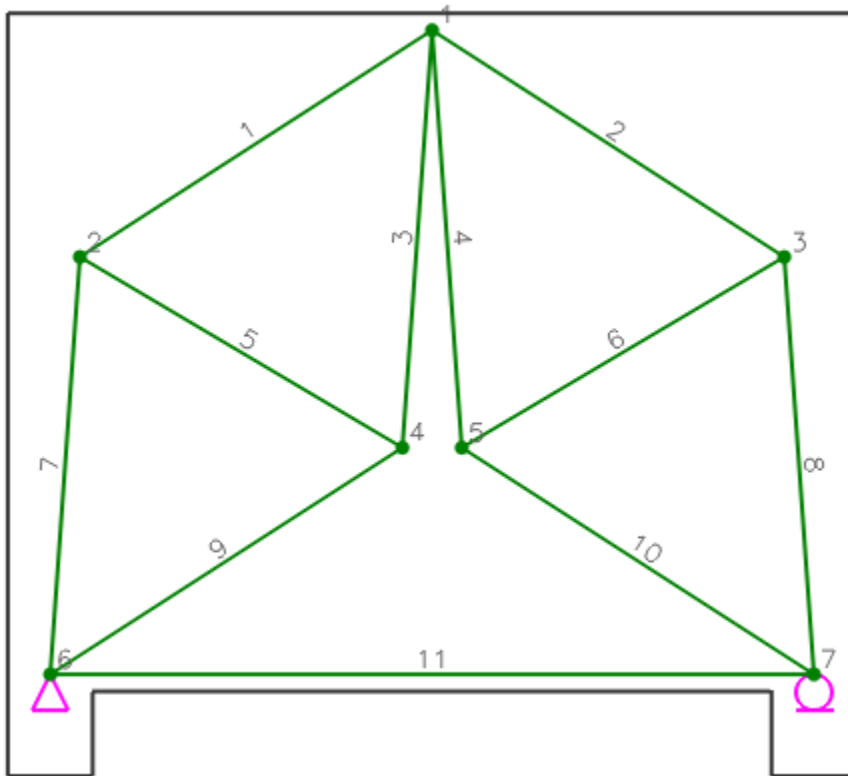


Figure 124. Truss model (b)

Here, bars 1,2,3,4,7,8,9,10 represent the concrete struts, while the tensile bars 5,6 represent the steel bars that may be grid reinforcement, horizontal and vertical, that may be placed also for crack control. The tensile bar 11 represent the tie, that is the main reinforcement of the beam. The solution of the bar gives the following result, in figure 125:

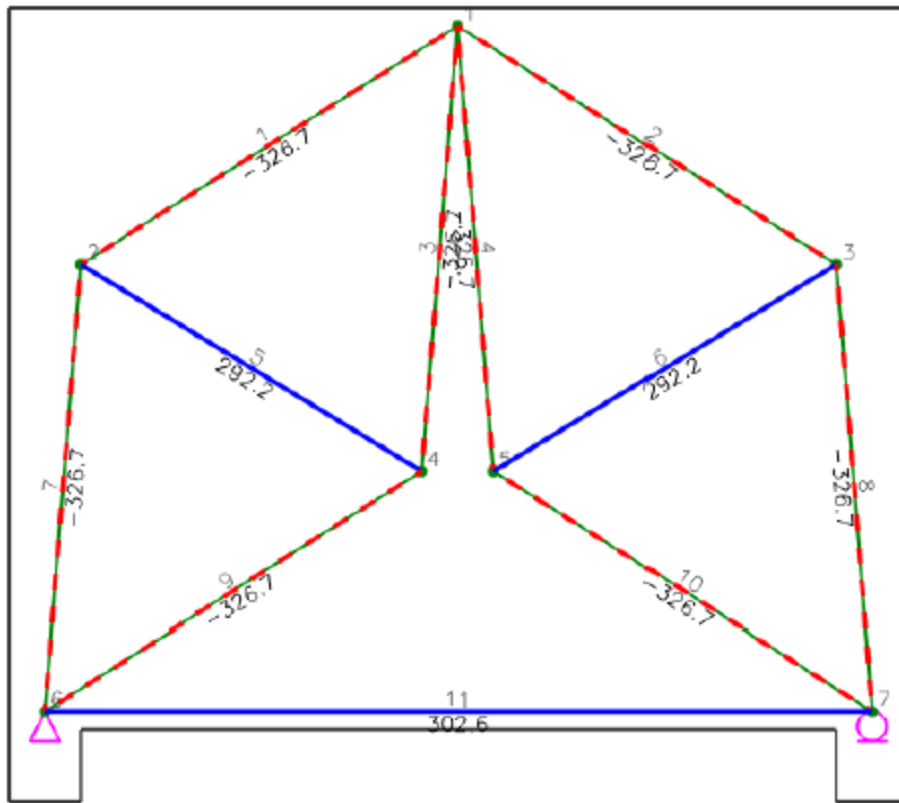


Figure 125. Analysis of truss model (b)

In the same way, it can be seen from figure 126 if there is enough reinforcement, and if the w_{prov} is greater than the w_{req} .

| Tie No. | Types | Fu (kN) | theta (deg.) | Rebars | As.req (mm ²) | As.used (mm ²) | Note |
|---------|--------|---------|--------------|--------|---------------------------|----------------------------|------|
| 5 | Top | 292.23 | 31.2 | 8-#4 | 769 | 1013 | O.K |
| 11 | Bottom | 302.63 | 0.0 | 8-#4 | 681 | 1013 | O.K |

| Strut No. | Type | theta | Fu (kN) | b (mm) | Wreq (mm) | Wprov (mm) | Note |
|-----------|------|-------|---------|--------|-----------|------------|------|
| 1 | 1 | 32.2 | 326.7 | 350.0 | 29.2 | 382.6 | O.K |
| 2 | 1 | 32.2 | 326.7 | 350.0 | 29.2 | 382.6 | O.K |

| | | | | | | | |
|----|---|------|-------|-------|------|-------|-----|
| 3 | 1 | 85.4 | 326.7 | 350.0 | 29.2 | 414.8 | O.K |
| 4 | 1 | 85.4 | 326.7 | 350.0 | 29.2 | 414.8 | O.K |
| 7 | 1 | 85.4 | 326.7 | 350.0 | 29.2 | 414.8 | O.K |
| 8 | 1 | 85.4 | 326.7 | 350.0 | 29.2 | 414.8 | O.K |
| 9 | 1 | 32.2 | 326.7 | 350.0 | 29.2 | 382.6 | O.K |
| 10 | 1 | 32.2 | 326.7 | 350.0 | 29.2 | 382.6 | O.K |

Figure 124. Calculations of truss model (b)

Form the tables of figure 126, it is shown that the beam is safe.

Then, we use the STM of figure 127, to solve the beam. The current model is the same with the pervious, with two more bars, so the corresponding truss is two times indetermined. Hear in figure 127 isthemodel:

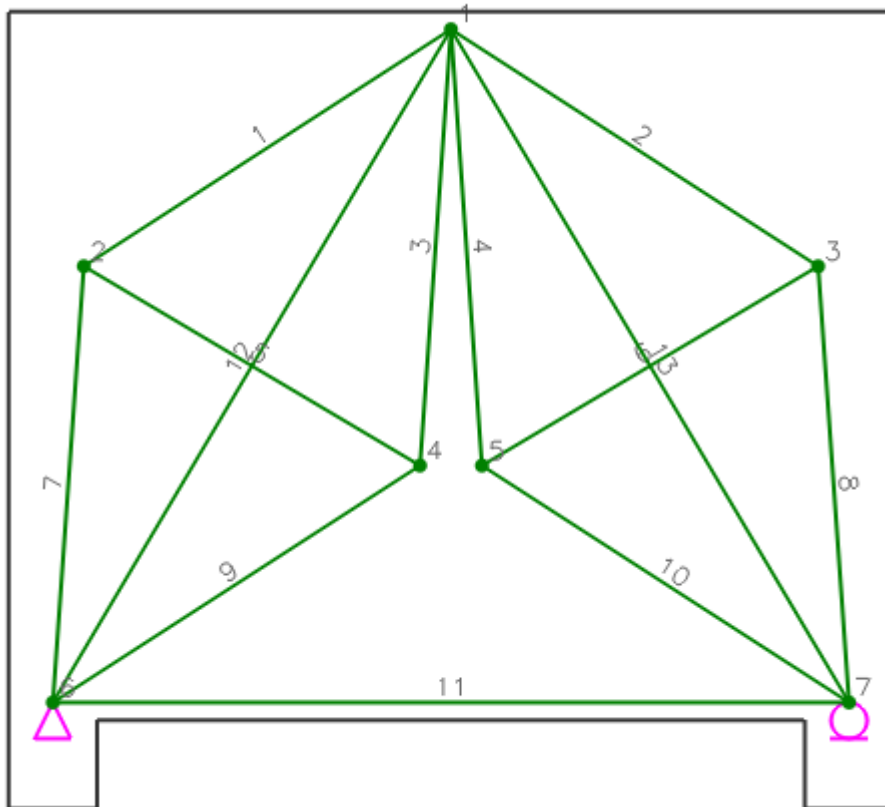


Figure 127. Truss model (c)

Hear, the struts are the same as before, with the additional 5,6 bars. The solution of the bar gives the following result, in figure 126:

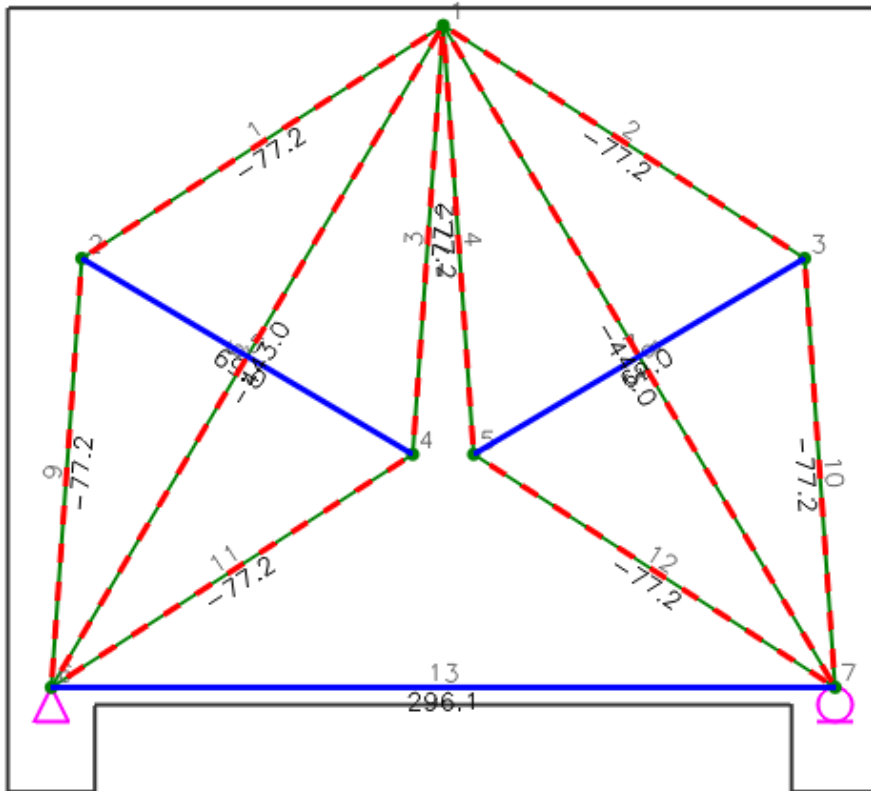


Figure 128. Analysis of truss model (c)

From figure 129, we can see if the beam is safe or not:

| Tie No. | Types | Fu (kN) | theta (deg.) | Rebars | As.req (mm ²) | As.used (mm ²) | Note |
|---------|--------|---------|--------------|--------|---------------------------|----------------------------|------|
| 5 | Top | 69.44 | 31.2 | 8-#4 | 183 | 1013 | O.K |
| 13 | Bottom | 302.63 | 0.0 | 8-#4 | 681 | 1013 | O.K |

| | | | | | | | |
|----|---|------|-------|-------|------|-------|-----|
| 2 | 1 | 32.2 | 77.6 | 350.0 | 6.9 | 382.6 | O.K |
| 3 | 1 | 85.4 | 77.6 | 350.0 | 6.9 | 414.8 | O.K |
| 4 | 1 | 85.4 | 77.6 | 350.0 | 6.9 | 414.8 | O.K |
| 6 | 1 | 58.8 | 445.6 | 350.0 | 39.8 | 445.8 | O.K |
| 8 | 1 | 58.8 | 445.6 | 350.0 | 39.8 | 445.8 | O.K |
| 9 | 1 | 85.4 | 77.6 | 350.0 | 6.9 | 414.8 | O.K |
| 10 | 1 | 85.4 | 77.6 | 350.0 | 6.9 | 414.8 | O.K |
| 11 | 1 | 32.2 | 77.6 | 350.0 | 6.9 | 382.6 | O.K |
| 12 | 1 | 32.2 | 77.6 | 350.0 | 6.9 | 382.6 | O.K |

Figure 129. Calculations of truss model (c)

From the tables of figure 129, it is shown that the beam is again safe.

Finally, we solve the beam with the above model of figure 130:

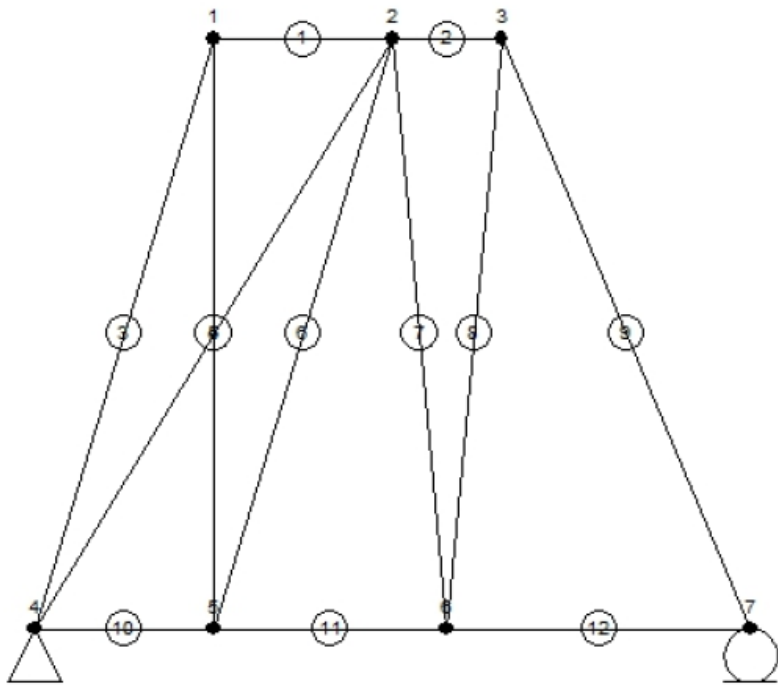


Figure 130. Truss model (d)

By solving the truss, we take the following forces of the bars:

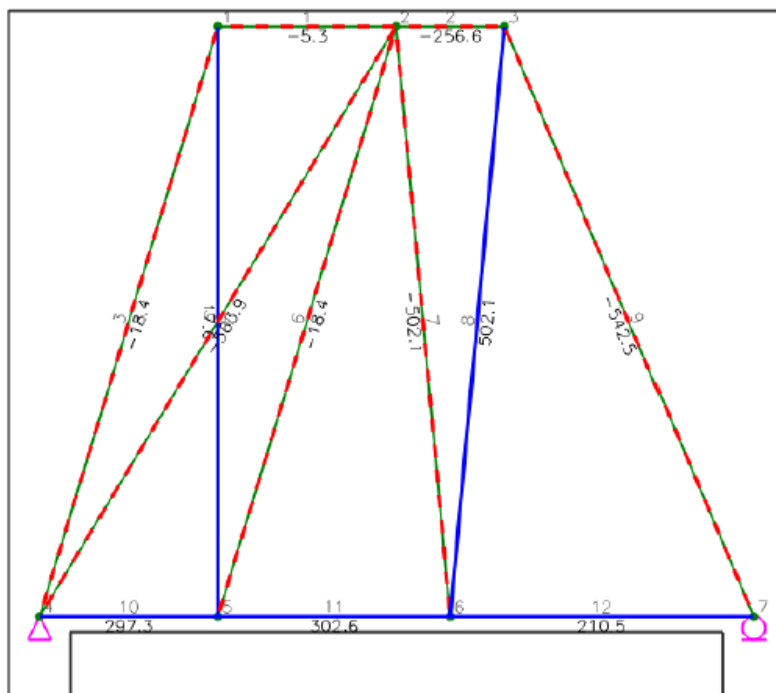


Figure 131. Analysis of truss model (d)

Form the tables of figure 12,we have the results of design.

| Tie No. | Types | Fu (kN) | theta (deg.) | Rebars | As.req (mm ²) | As.used (mm ²) | Note |
|---------|--------|---------|--------------|--------|---------------------------|----------------------------|------|
| 10 | Bottom | 297.31 | 0.0 | 8-#4 | 669 | 1013 | O.K |
| 11 | Bottom | 302.63 | 0.0 | 8-#4 | 681 | 1013 | O.K |
| 12 | Bottom | 210.53 | 0.0 | 8-#4 | 474 | 1013 | O.K |

| Tie No. | Fu (kN) | theta (deg.) | Rebars | W _{eff,tie} (mm) | S _{prov} (mm) | phi F _n (kN) | Note |
|---------|---------|--------------|--------|---------------------------|------------------------|-------------------------|------|
| 4 | 17.57 | 90.0 | 4-#4 | 1150.0 | 200.0 | 1294.9 | O.K |
| | | | 4-#4 | 1150.0 | 200.0 | | |
| 8 | 502.12 | 84.7 | 4-#4 | 416.7 | 200.0 | 1193.9 | O.K |
| | | | 4-#4 | 975.0 | 200.0 | | |

Figure 132. Calculations of truss model (c)

From figure 132, we get that the beam is again safe.

In all the four truss models, we try to present the differences between the results of each case. These differences are shown form the values of compressive stresses, on compressive struts, and also the required reinforcement. By comparison of the compressive stresses of the trusses **a** and **b**, we can see that both the W_{req} ,and W_{prov} are less than before. As for the ties, the requirement is the approximately the same, because the forces in the main tie remains the same.

Deep beam with uniform load with Fe77 and with Strut and tie model.

Here we compare the results of that the Strut and Tie model gives us, with the results of a finite element analysis, using the program Fe77, that are considered to be close to the real, for the collapse load.

Strut and Tie model analysis results

Here, we consider the deep beam of the figure 132

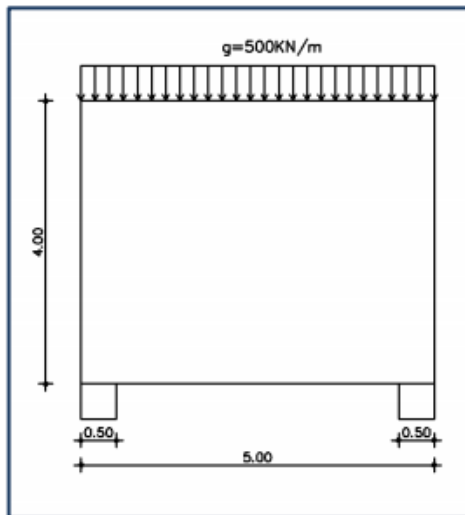


Figure 132. Geometry of the beam.

The truss model for this beam, is showed in figure 133.

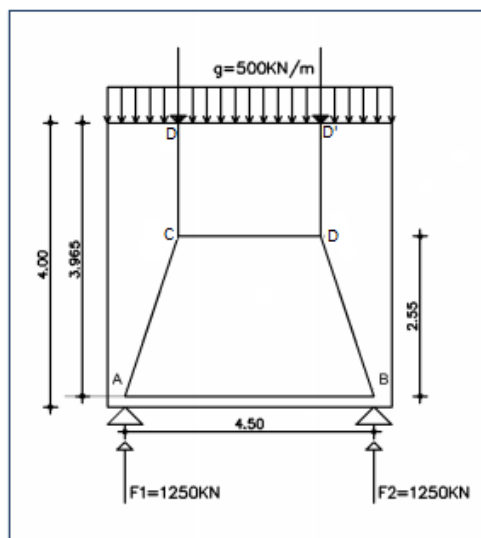


Figure 133. Truss model of the beam.

$$\frac{l}{h}=1.125 \text{ as previously.}$$

From the equilibrium of the truss, we find that

$$F_{AB}=568.08\text{KN}$$

$$F_{AC}=-1373\text{KN}$$

So, the reinforcement of the beam, is equal to:

$$A_s=\frac{F_{AB}}{f_{yd}}=1137\text{mm}^2$$

Strength of nodal zone A

$$\sigma_{Rd}=0.85\left(1-\frac{f_{ck}}{250}\right)f_{ck}=0.85\left(1-\frac{30}{250}\right)30=22.4\text{MPa}$$

The geometrical properties of nodal zones, are found using the dimensions of the column, and the theory that was described later.

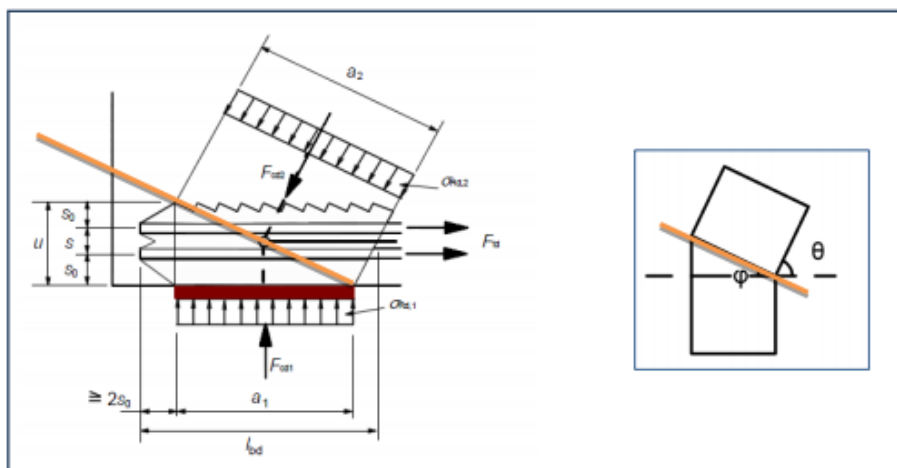


Figure 134. Geometry of node A

Width of beam: $b=0.3\text{m}$

Width of column: $b=0.5\text{m}$

$u=0.12h=0.48\text{m}$

$a_2=693\text{mm}$

$$\sigma_{c1}=\frac{F_{AB}}{(b*\alpha_1)}=3.34\text{MPa}$$

$$\sigma_{c2} = \frac{F_{AC}}{(b \cdot \alpha_1)} = 6.6 \text{ MPa}$$

$$\sigma_{c,\max} = 6.6 < \sigma_{Rd} = 22.4 \text{ MPa}$$

So the node A has enough strength.

Strength of nodal zone C'

We consider a plate with dimensions 300x500mm

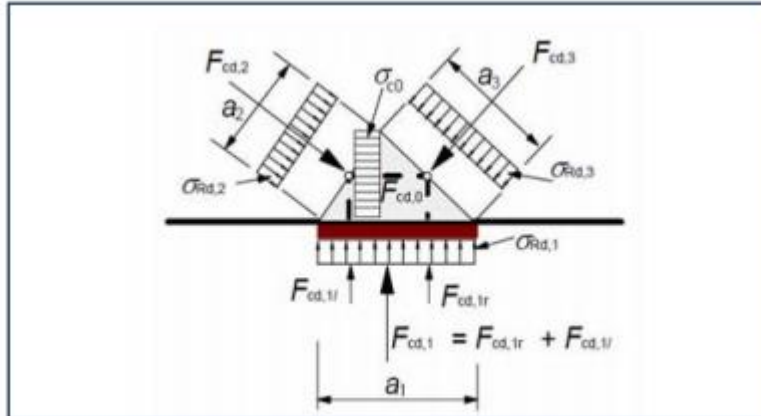
$$a_1 = 500 \text{ mm}$$

$$\sigma_{c1} = \frac{F_{AB}}{(b \cdot \alpha_1)} = 8.33 \text{ MPa}$$

$$\sigma_{Rd} = 1.00 \left(1 - \frac{f_{ck}}{250}\right) f_{ck} = 0.85 \left(1 - \frac{30}{250}\right) 30 = 26.35 \text{ MPa}$$

$$\sigma_{c,\max} = 8.33 < \sigma_{Rd} = 26.35 \text{ MPa}$$

So, the node C' has enough strength.



Strength of nodal zone C

$$\sigma_{c1} = \frac{1250000}{300 \cdot 500} = 8.33 \text{ MPa}$$

$$\sigma_{c2} = \frac{1373000}{300 \cdot 693} = 6.6 \text{ MPa}$$

$$\sigma_{c3} = \frac{568000}{300 \cdot 480} = 3.95 \text{ MPa}$$

$$\sigma_{c,\max} = 8.33 < \sigma_{Rd} = 26.35 \text{ MPa}$$

So the node C has enough strength.

Next, we find the stresses in zones, using the geometry of the nodes and the calculated loads:

$$\sigma_{c1} = \frac{1000000}{300 \cdot 870} = 3.83 \text{ MPa}$$

$$\sigma_{c2} = \frac{1000000}{300 \cdot 870} = 3.83 \text{ MPa}$$

It is clear that the strength of the nodal zones is enough. So, for the load of 1000KN, we have found that the reinforcement is equal to 568mm².

Fe77 analysis results

Hear, in *figure 135*, the deep beam is shown. Next, in *figures 136-138* the deformation of the beam till collapse is shown. Next, the force- displacement diagram is constructed.

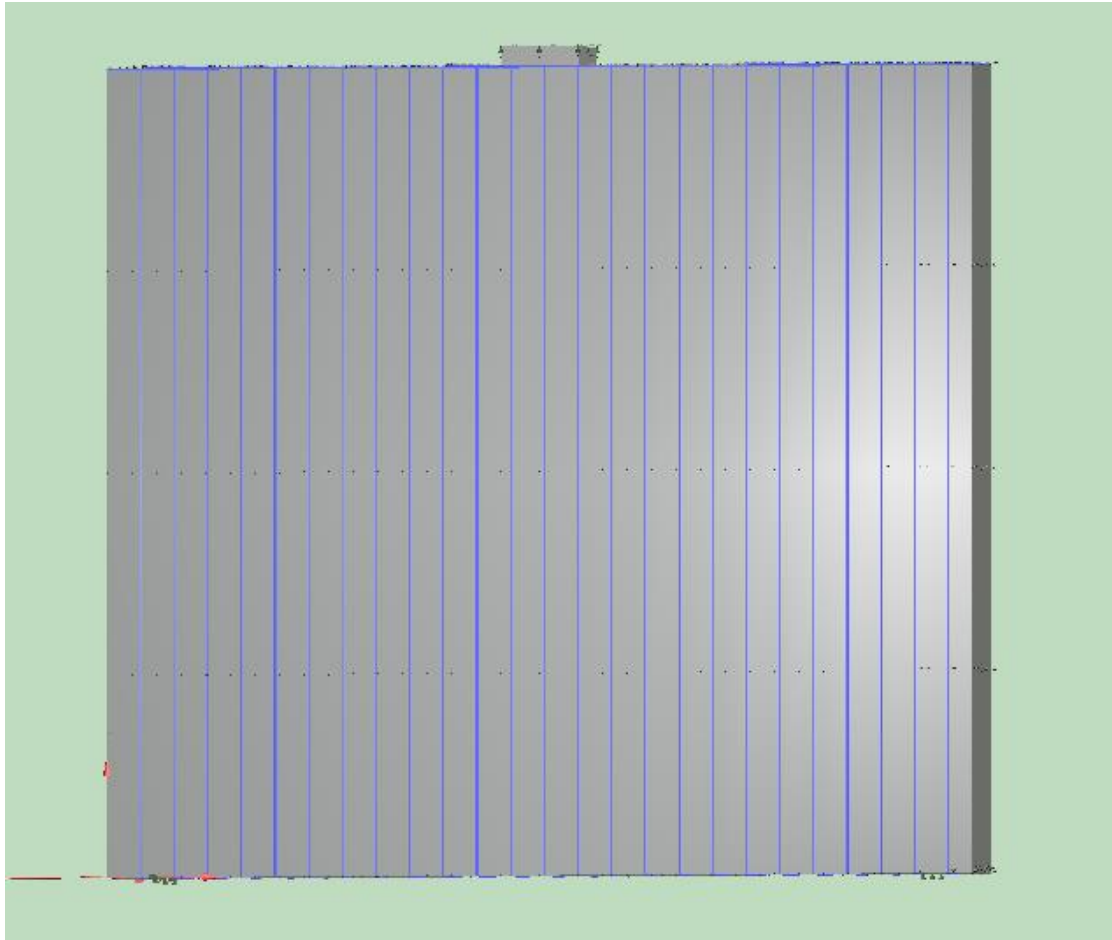


Figure 135. Deep beam geometry

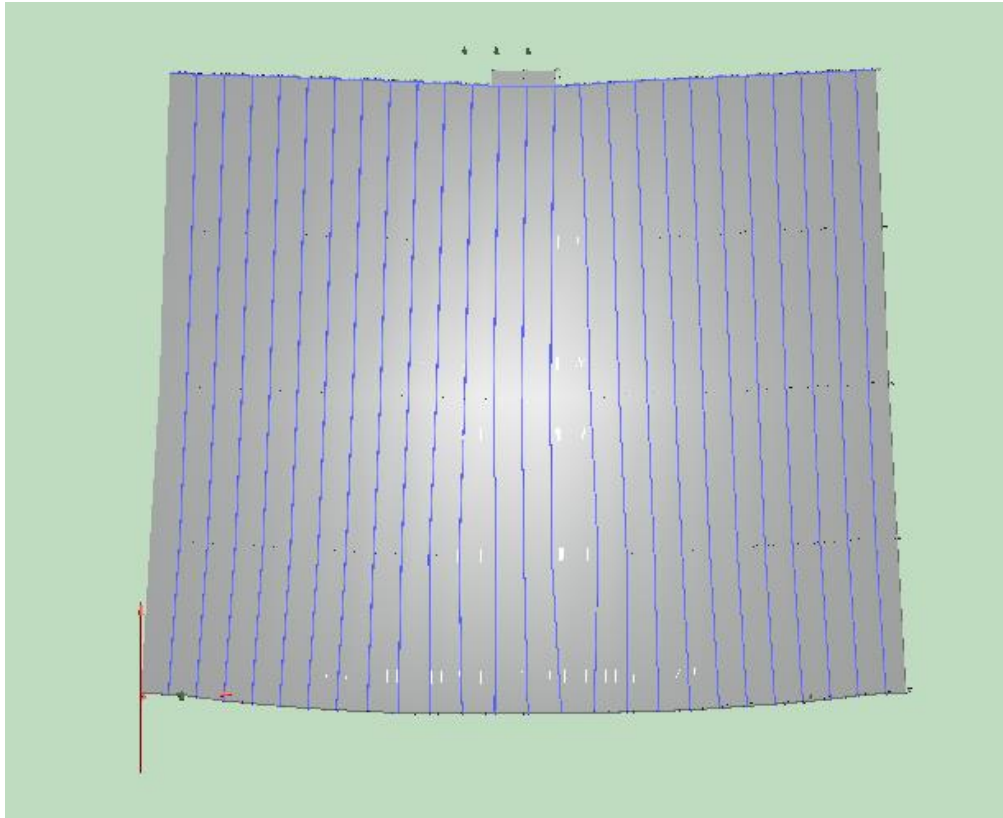


Figure 136. Initial deformation of the beam

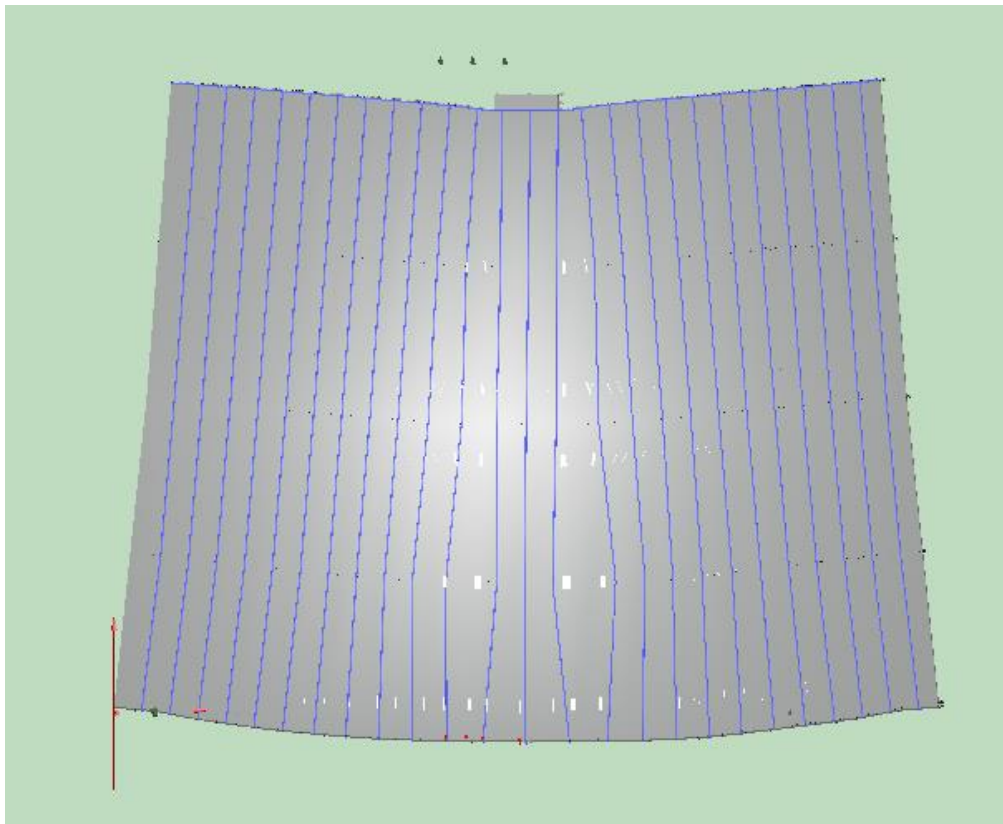


Figure 137. First yielding of the reinforcement

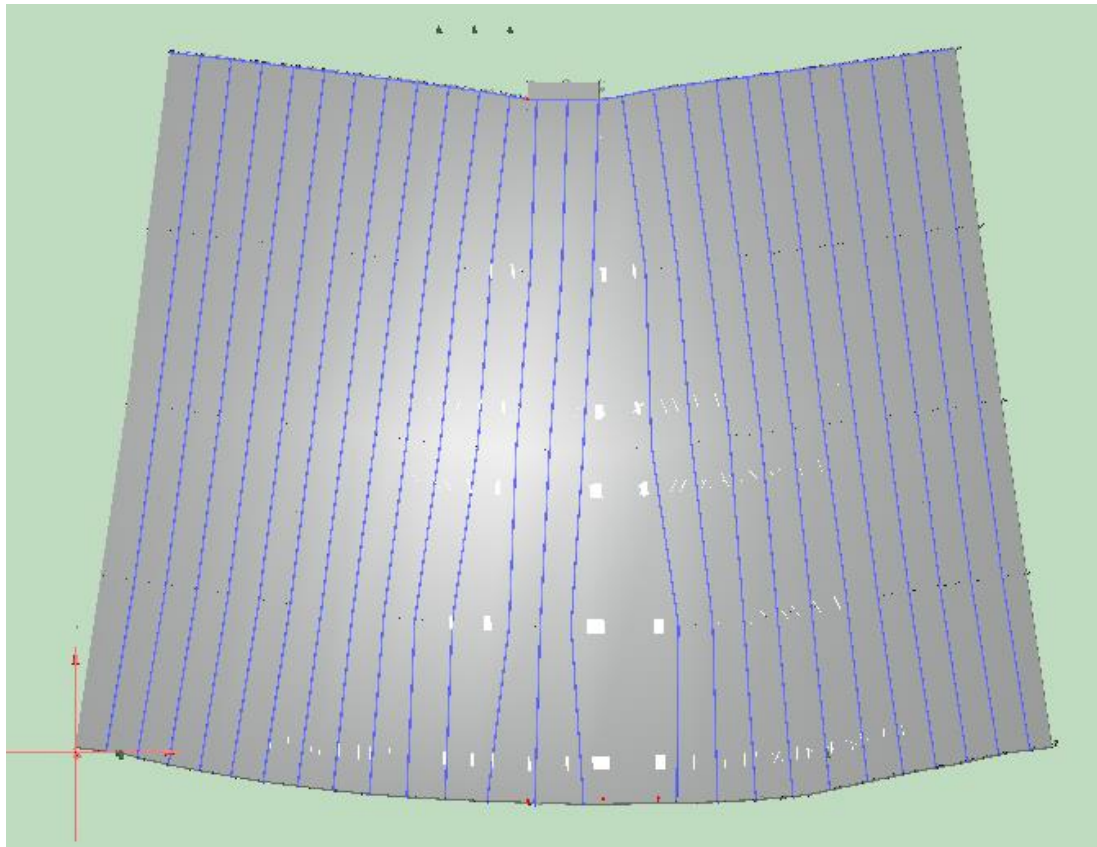


Figure 138. Deformation of the beam in collapse

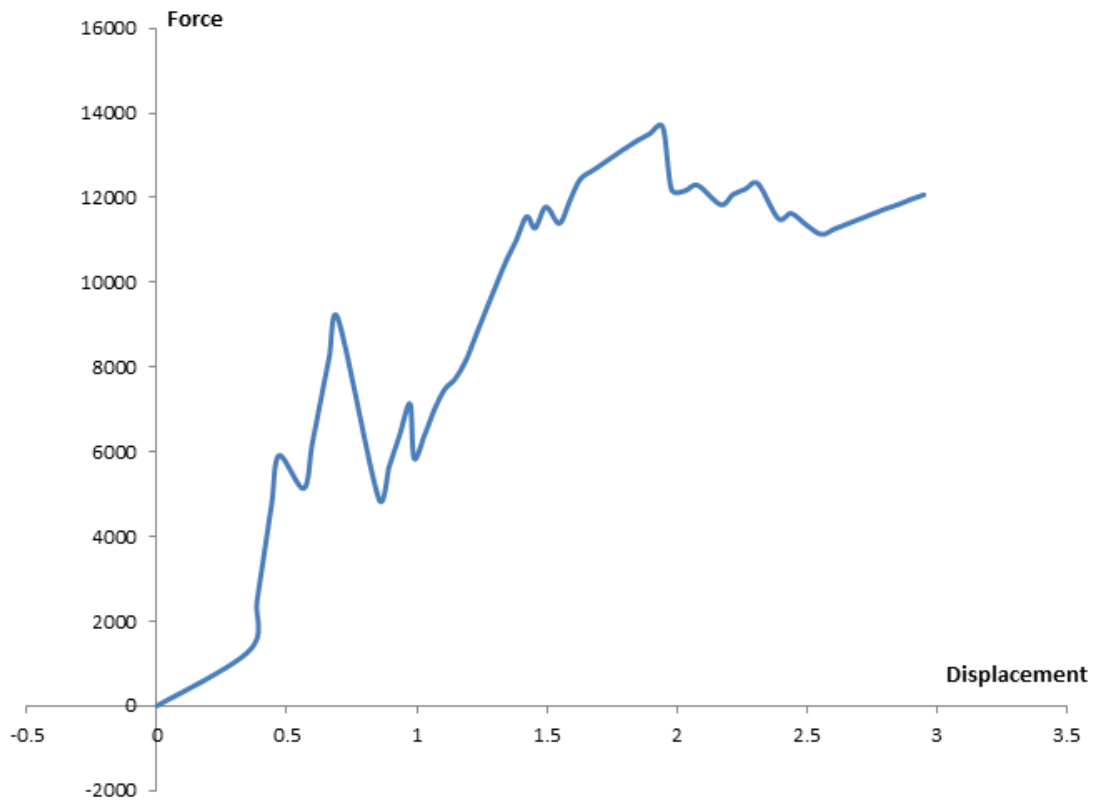


Figure 139. Force-displacement diagram.

From the analysis, it is shown that the collapse load is approximately equal to $P_{max}=14000KN$.

The results show that the collapse load that was calculated with the Strut and Tie model, is only 18%, of the total load.

5.7 Flexural beam with Fe77 and comparison with Strut and tie model.

Here we compare the results of that the Strut and Tie model gives us, with the results of a finite element analysis, using the program Fe77, for a flexural beam, in order to see how close are the results to the real, for this case, for the collapse load.

Beam properties

Length: 3.0m

Height: 0.262m

Width: 0.16

Concrete compressive strength: $f_c=52\text{MPa}$

Steel yield strength: $f_y=500\text{MPa}$

Tensile reinforcement: $A_s=3\phi 18$

Compressive reinforcement: $A_s=2\phi 12$

Firstly, we find the collapse load, using finite elements, and the program **Fe77**. Then, with this collapse load, we find the collapse load, using the Strut and Tie model, and the program **AStrutTie**.

Fe77 analysis results

Hear, in *figure 140*, the flexural beam is shown. Next, in *figures 141-142* the deformation of the beam till collapse is shown. Next, the force- displacement diagram is constructed. The monitor point is selected to be at the bottom of the middle section.

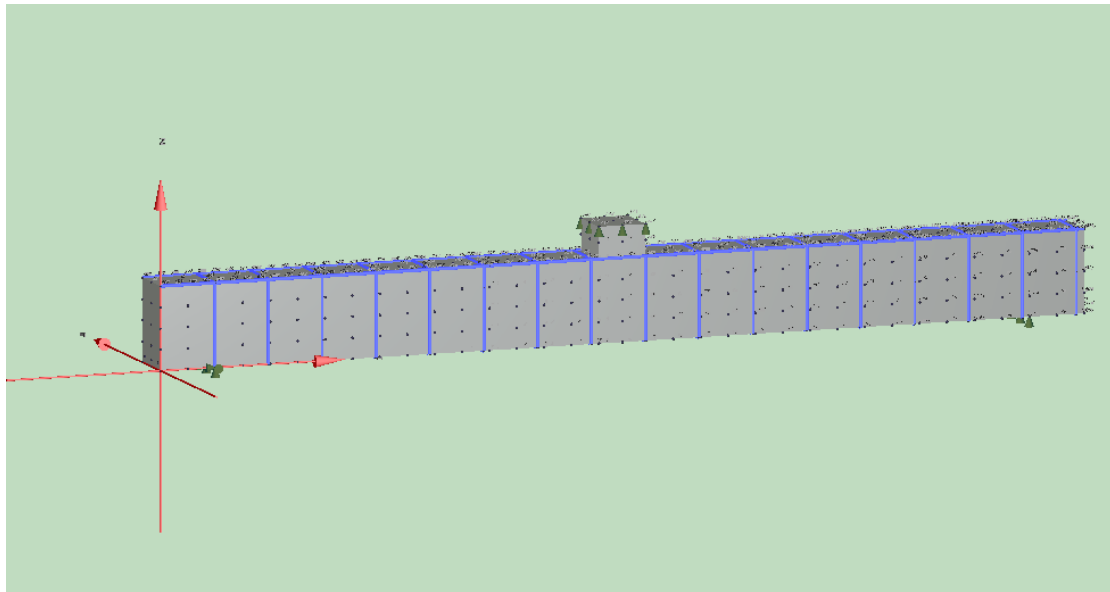


Figure 140. Flexural beam geometry



Figure 141. Initial deformation of the beam.



Figure 142. Deformation of the beam in collapse

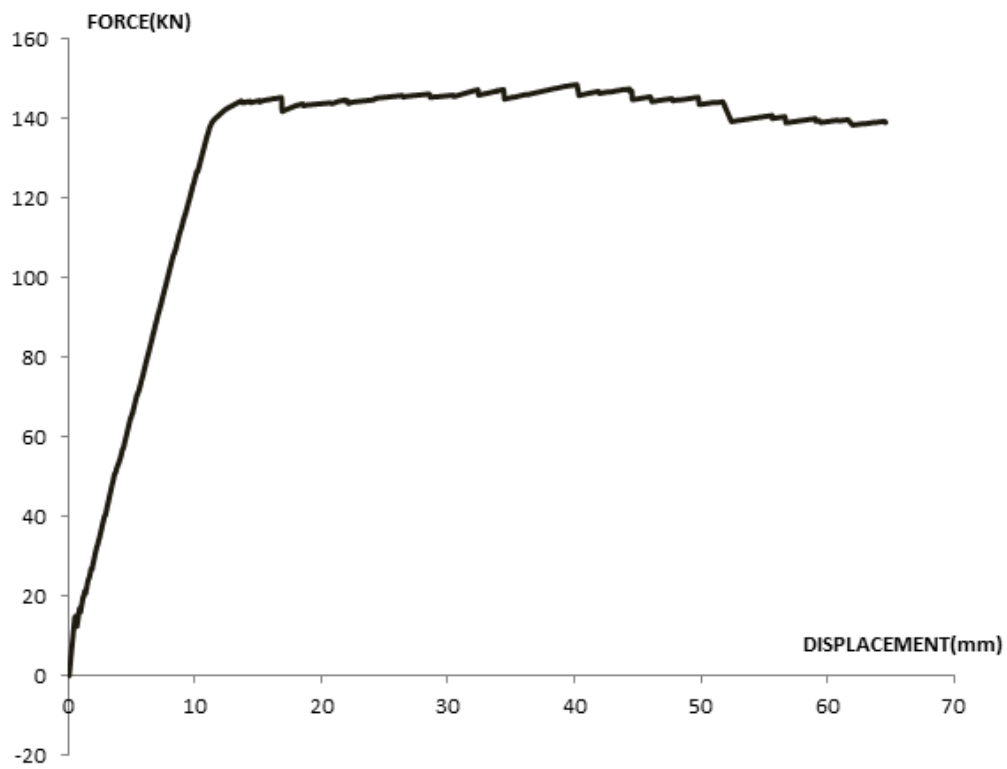


Figure 143. Force-displacement diagram.

From the analysis (figure 143), it is shown that the collapse load is approximately equal to $P_{max}=144KN$.

Then, with this reinforcement, we find the collapse load, using the strut and tie model. We check also, if the nodes have enough compressive strength.

Strut and Tie model analysis results

The strut and tie model, for this beam, is show in figure 144, below.

1) Construction of Strut-Tie Model

(1) Constructed Strut-Tie Model

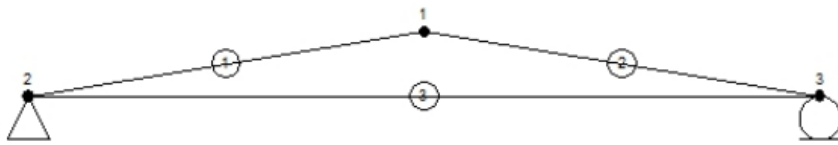


Figure 144. Strut and tie model of the beam.

After the selection of the truss model, we check the strength of the nodes and find the required rebars. In this case, we had initially the required rebars, and we have to find the collapse load, with repetitions. For the total amount of $A_s=763\text{mm}^2$, we find a corresponding load $F_{\max}=158$

(1) Required Area of Rebars

We have that

$$A_{s,\text{req}} = (F_u / \cos(\theta)) / (f_y / \gamma_s)$$

Using this type, for the required reinforcement, we find that for a load equal to $F=157\text{KN}$, the required rebars have total area $A_s=763\text{mm}^2$.

(2) Available Widths of Struts and Nodal Zones

The nodes that will be checked, are shown below

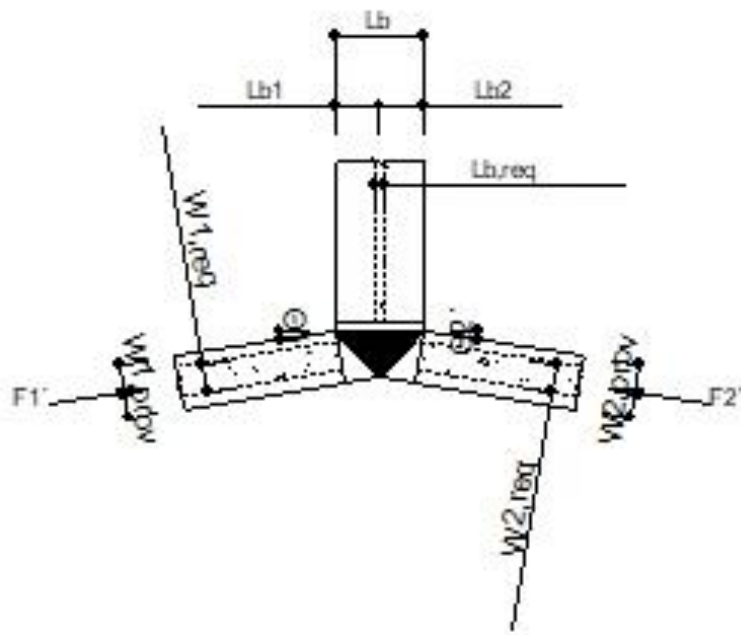


Figure 145. Geometry of the node 1

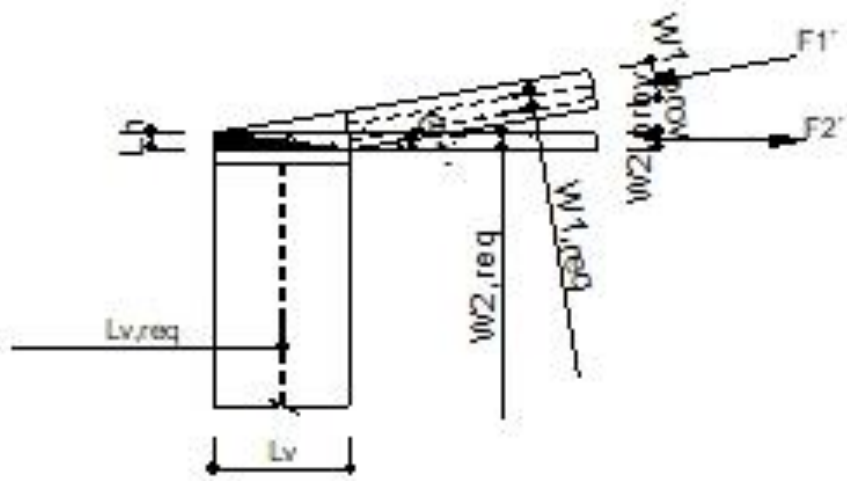


Figure 146. Geometry of the node 2

(A) Node 1 (CCC)

$$L_b = 160.0 \text{ mm } h_a = 83.7 \text{ mm } P = 144.00 \text{ kN}$$

$$L_b = 200 \text{ mm}$$

$$L_{b1} = 80 \text{ mm}$$

$$L_{b2} = 80 \text{ mm}$$

$$L_{b,req} =$$

$$L_{b,prov} =$$

$$W_{1,prov} = 95.4 \text{ mm}$$

$$W_{1,req} = 95.4 \text{ mm}$$

$$W_{2,prov} = L_b \sin(\theta/2) + h_a \cos(\theta/2) = 80.00 \sin(9.2) + 83.71 \cos(9.2) = 95.4 \text{ mm}$$

$$W_{2,req} = 95.4 \text{ mm}$$

(B) Node 2 (CCT)

$$L_b = 160.0 \text{ mm } h_a = 83.7 \text{ mm } P = 144.00 \text{ kN}$$

$$L_b = 200 \text{ mm}$$

$$L_{b1} = 80 \text{ mm}$$

$$L_{b2} = 80 \text{ mm}$$

$$L_{b,req} =$$

$$L_{b,prov} =$$

$$W_{1,prov} = 95.4 \text{ mm}$$

$$W_{1,req} = 95.4 \text{ mm}$$

$$W_{2,prov} = L_b \sin(\theta/2) + h_a \cos(\theta/2) = 80.00 \sin(9.2) + 83.71 \cos(9.2) = 95.4 \text{ mm}$$

$$W_{2,req} = 95.4 \text{ mm}$$

So, the corresponding collapse load for the beam, is 9% under the real, and so the truss model is not suitable, because it is against safety.

Chapter 6

Nonlinear Cyclic Truss Model for Reinforced Concrete Structures

6.1 Introduction

A strut-and-tie model (STM) is a discrete representation of the stress field developed within a concrete structure when subjected to external actions. Representation of structures with STMs allow analysis and design of reinforced concrete structural types to be performed in a rational manner. Within a STM, uniaxially stressed struts and ties having finite dimensions are used to represent the actual compressive and tensile stress fields respectively. The pin connections joining the struts and ties together correspond to the biaxially or triaxially stressed nodal zones. The strut-and-tie modelling technique has traditionally been employed in design practice to predict strength and to examine equilibrium of the applied loads, reactions, and internal forces for disturbed (D) regions of structures with irregular geometry where the internal flow of force is not well known. Typically, such an investigation enables determination of suitable reinforcement detailing for the D-regions.

In this chapter, a nonlinear truss modeling of shear-critical reinforced concrete structures, subjected to cyclic loading, is presented. Nonlinear steel and concrete truss elements are used to represent steel reinforcement and concrete areas, respectively, in the vertical and horizontal directions. Nonlinear concrete trusses are used in the diagonals, accounting for the biaxial effect on the compression behavior. Tension stiffening and softening effects are modeled for all concrete truss elements, accounting for mesh size effects and fracture energy, and the effects of strain penetration are modeled. Flexure-shear interaction is modeled explicitly through the coupling of these elements. The model is validated by comparing experimentally measured and numerically results, using the program Fe77, both characterized by significant flexure-shear interaction effects and softening of the concrete in the diagonal direction. The overall force-deformation response is presented including significant strength degradation. In addition, the effects of the diagonal truss angle and concrete biaxial relationship on the response are studied. This approach is based on the work of M. Panagiotou, Y. Lu and S.C. Girgin.

Modeling approaches for RC elements, considering flexure-shear interaction for reinforced concrete columns can be categorized as (i) lumped plasticity models, (ii) fiber - section beam - column element models, (iii) macro models, (iv) truss or strut-and-tie models. This study presents a nonlinear truss modeling approach for shear-critical reinforced concrete elements, subjected to cyclic loading. The nonlinear concrete truss elements accounts for tension softening for the biaxial effect on the compression behavior in the diagonal direction and tension stiffening in the vertical and horizontal directions developed by Lu and Panagiotou (2013) are used. In

addition, this model considers strain penetration effects resulted by longitudinal reinforcement slip from anchorage of column to foundation. Flexure-shear interaction is modeled explicitly through the coupling of these elements. The model is validated by comparing measured and computed responses of two RC columns tested and both characterized by significant flexure-shear interaction effects.

Truss or strut-and-tie models have been proposed in the literature to capture the strength and stiffness characteristics of RC members during cyclic reversals. Kim and Mander (1999) improved a truss model for monotonic and cyclic behavior of RC columns. Miki and Niwa (2004) proposed a three dimensional lattice model for biaxial responses of RC members. Park and Eom (2007) improved a truss model consisting composite elements of concrete and rebar for RC members. These models didn't account for the mesh size effects for concrete material models. Zimmerman et al. (2013) used nonlinear truss model for numerical modeling for shear failure of RC columns with considering strain penetration effects. This model didn't consider biaxial effect for concrete diagonals in compression.

6.2 Nonlinear truss modeling approach

The truss modeling approach in this chapter uses nonlinear truss elements in the vertical, horizontal and diagonal directions. Nonlinear concrete truss elements accounts for tension softening for the biaxial effect on the compression behavior in the diagonal direction and tension stiffening in the vertical and horizontal directions are used. The RC wall section considered in non-seismically designed RC structures is shown in Figure 1(a). The clear height of the column is H . Column section width and height is B_c and H_c , respectively. Figure 1(b) shows the truss model of the column. Vertical and horizontal truss elements representing reinforcing bars and concrete, and their effective areas. The diagonal truss elements representing concrete only are also shown in the same figure. The cross-section area of the diagonal truss elements is the product of the section width B_c and effective width b_{eff} of the column. Strain penetration effects due to anchorage deformations are considered using truss elements for reinforcement and concrete with a length of $L_{sp}=16d_{bl}$ is assumed for all case studies, in which d_{bl} is the longitudinal bar diameter (Figure 1). Strain penetration concrete truss elements have larger areas than the vertical concrete truss elements to account for the stiffness of the beams, while the area of steel truss elements are same with the vertical steel trusses. The diagonal truss angle θ is considered to be ranged between 420 and 520 in the case, as used by Panagiotou et al (2013).

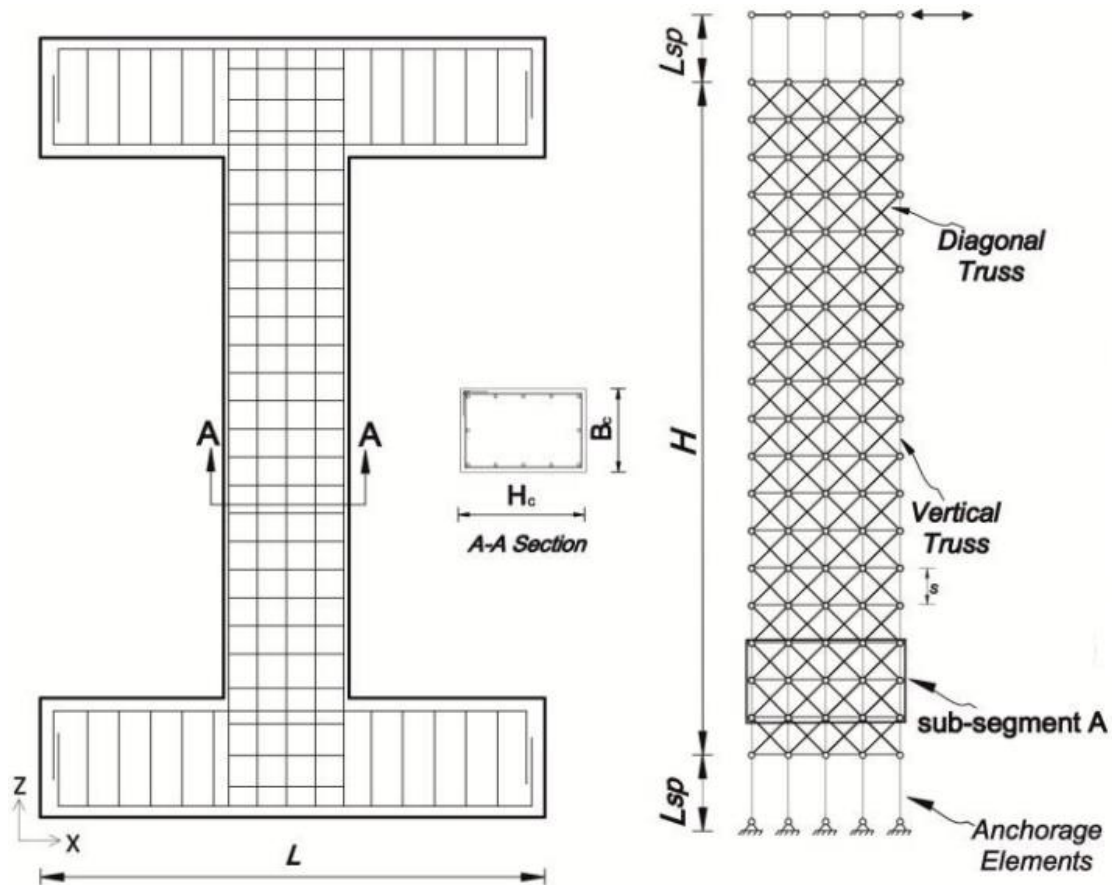


Figure 147. Nonlinear truss modeling approach for a RC wall specimen

6.3 Constitutive stress-strain relationships

Reinforcing Steel Material Model a number of Giuffr -Menegotto-Pinto (GMP) steel material models are used to define the stress-strain relationship used for the reinforcing steel. A single GMP model is shown in Figure 2, where f_y is the yield strength, ϵ_y the corresponding yield strain, E_s the elastic modulus. For the case studies presented in this paper, five to six GMP models are used in each parallel steel material model and the material parameters are chosen to match the experimentally reported steel behavior. A uniaxial material **SteelMPF** is used, which represents the well-known uniaxial constitutive nonlinear hysteretic material model for steel proposed by Menegotto and Pinto (1973), and extended by Filippou et al. (1983) to include isotropic strain hardening effects. The relationship is in the form of curved transitions (Figure 147), each from a straight-line asymptote with slope E_0 (modulus of elasticity) to another straight-line asymptote with slope $E_1 = bE_0$ (yield modulus) where b is the strain hardening ratio. The curvature of the transition curve between the two asymptotes is governed by a cyclic curvature parameter R , which permits the Bauschinger effect to be represented, and is dependent on the absolute strain

difference between the current asymptote intersection point and the previous maximum or minimum strain reversal point depending on whether the current strain is increasing or decreasing, respectively. The strain and stress pairs (ϵ_r, σ_r) and (ϵ_0, σ_0) shown on Figure 148 are updated after each strain reversal. The model allows calibration of isotropic hardening parameters in both compression and tension through optional input variables a_1 and a_2 for isotropic strain hardening in compression, and a_3 and a_4 for isotropic strain hardening tension, and uses default values of $a_1 = a_3 = 0.0$ and $a_2 = a_4 = 1.0$ that yield no isotropic strain hardening for either compression or tension. To incorporate isotropic strain hardening in compression, the recommended parameters are $a_1 = 0.01$ and $a_2 = 7.0$. To incorporate isotropic strain hardening in tension, the recommended parameters are $a_3 = 0.01$ and $a_4 = 7.0$.

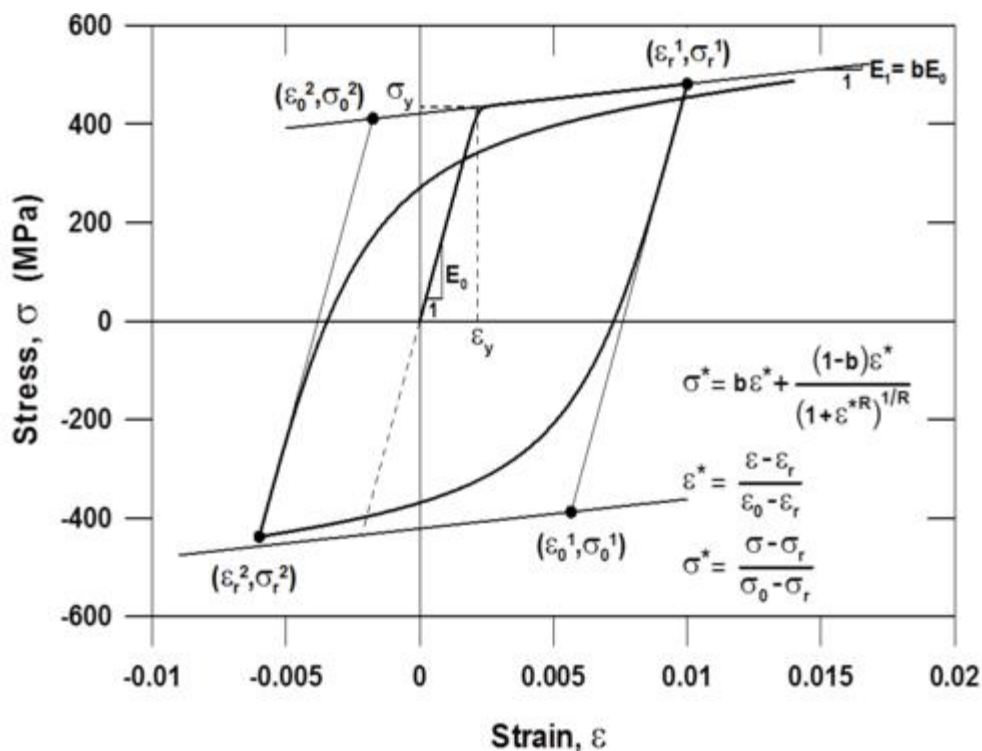


Figure 148. (a) Stress-strain relationship of the GMP steel material model

6.4.1 Concrete Model for Vertical and Horizontal Truss Elements

The compressive stress-strain relation is based on the Fujii concrete model (Hoshikuma et al. 1997). The stress-strain relation for concrete developed by Lu and Panagiotou(2013) is used for the models and shown in Figure 149, where f_c is the compressive strength of unconfined concrete occurring at strain $\epsilon = 0.2\%$. The initial

concrete modulus was $E_c = 2f_c / \varepsilon_0$. The value of ε_u accounted for mesh-size effects based on the notion of concrete fracture energy in compression (Bazant and Planas 1998). The reference length (L_R) based on the panel studies in Vecchio and Collins (1986) is taken and for $L = L_R = 600$ mm, $\varepsilon_u = 0.4\%$. The tension stress-strain relationship during loading is linear until it reaches the tensile strength of concrete $f_t = 0.33\sqrt{f_c}$ in MPa. After this point, the concrete softens in accordance to the tension stiffening equation of Stevens et al. (1991), which has parameters for the bar diameter and steel ratio in the direction of the bar. Upon unloading from a compressive strain, the tangent modulus is $E_u = 0.5E_c + 0.5(f/\varepsilon)$ until reaching zero stress, which then reloads linearly to the point with the largest tensile strain that occurred before. The unloading from a tensile strain is linear with a tangent modulus E_c until reaching zero stress. After this, the material loads in compression and targets a stress equal to $\alpha \cdot f_t$ at zero strain with $\alpha = 0.5$.

6.4.2 Concrete Model for Diagonal Truss Elements

The concrete material model used for the diagonal truss elements accounts for the bi-axial strain field on the concrete compressive behavior as described by Vecchio and Collins (1986). For truss element e1 extending from node 1 to node 2 [shown in Figure 4(a)], the normal strain, ε_n , is computed using the zero-stiffness gauge element extending from the mid-length of the element to nodes 3 and 4, g1 and g2, respectively. The instantaneous compressive stress of element e1 is multiplied by the factor β determined from the instantaneous normal strain ε_n , which is the average of the strain measured with the gauge elements g1 and g2. When $\varepsilon_n > 0$, the relationship between β and ε_n is tri-linear, as shown in Figure 4(b).

For this study, the relation between β and ε_n depends on the length of the gauge elements, as first proposed by Panagiotou et al. (2013). Here, $\varepsilon_{int} = (600 / L_g) = 1\%$ and $\varepsilon_{res} = (600 / L_g) 2.5\%$, where L_g is the total length of gauge elements g1 and g2, as shown in Figure 4(a). The value of $\beta_{int} = 0.3$ and $\beta_{res} = 0.1$ was chosen to be similar to that developed by Vecchio and Collins (1986). Concrete model for diagonals in tension has $f_{t,res} = 0.02f_t$ at tensile strain ε_{tres} . Element length effect is accounted for ε_{tres} , and $\varepsilon_{tres} = 75\varepsilon_{cr}(L_R/L_D)$ as a function of diagonal element length (L_D) for $L_R = 600$ mm.

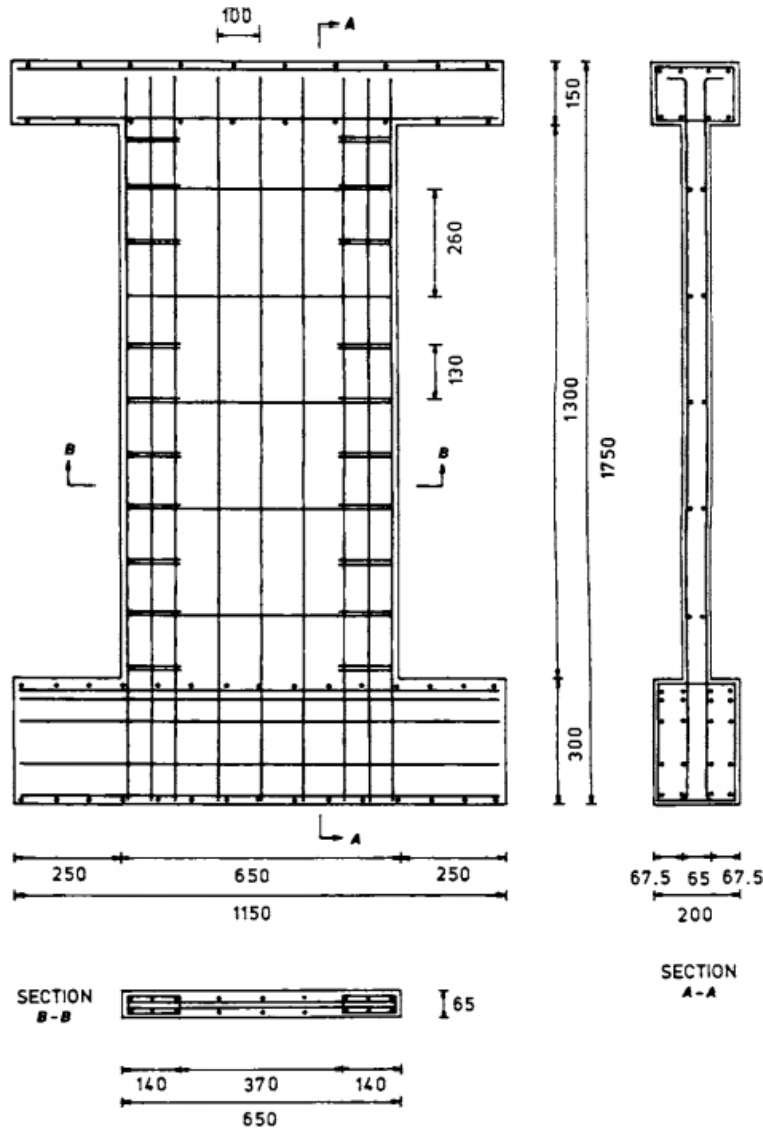


Figure 4. (a) Geometry of the concrete wall

6.6 Wall details

The walls tested were 650 mm wide, 1300 mm high, and 65 mm thick. In all cases they were monolithically connected to an upper and lower beam; the former functioned both as the element through which vertical and horizontal loads were applied on the walls, as well as a cage for anchoring the vertical bars, while the latter was utilized to clamp down the specimen to the laboratory floor, simulating a rigid foundation. The nominal dimensions of the specimens, together with the arrangement of vertical and horizontal reinforcement, are shown in *figure 150*. The vertical and horizontal reinforcement comprised high-tensile deformed steel bars of 8 and 6.25 mm diameter, respectively. Additional reinforcement in the form of stirrups confined the wall edges. Mild steel bars of 4 mm diameter were used for this purpose. The yield f_s , and ultimate strength f_{su} characteristics of the steel bars used

are summarized in Table 1. While the vertical reinforcement was designed in compliance with the recommendations of the ACI Building Code 11 for a given bending moment at the base of the wall, the design of the horizontal reinforcement was based on the results obtained from previous work, which indicated that for the case of the walls investigated in the present program, the provision of almost nominal reinforcement was sufficient to safeguard against brittle failure. The preceding design solution has been preferred because it lacks the ambiguity that characterizes the code recommendations, for the case of plastic hinge regions, where wide flexural cracks occur due to ductile flexural response under the combined action of a horizontal and a relatively low vertical load.

6.7 Results and discussion

It is shown in the following *figure 151*, that and numerically computed responses using nonlinear truss modeling approach give very satisfactory results in comparison with finite element analysis data. The effect of angle of inclination of diagonal truss elements on the response are studied. It was shown by **Panagiotou et al**, that the angle should be between the values 42 and 57°. The commands from program Opensees, are discussed in the appendix 1.

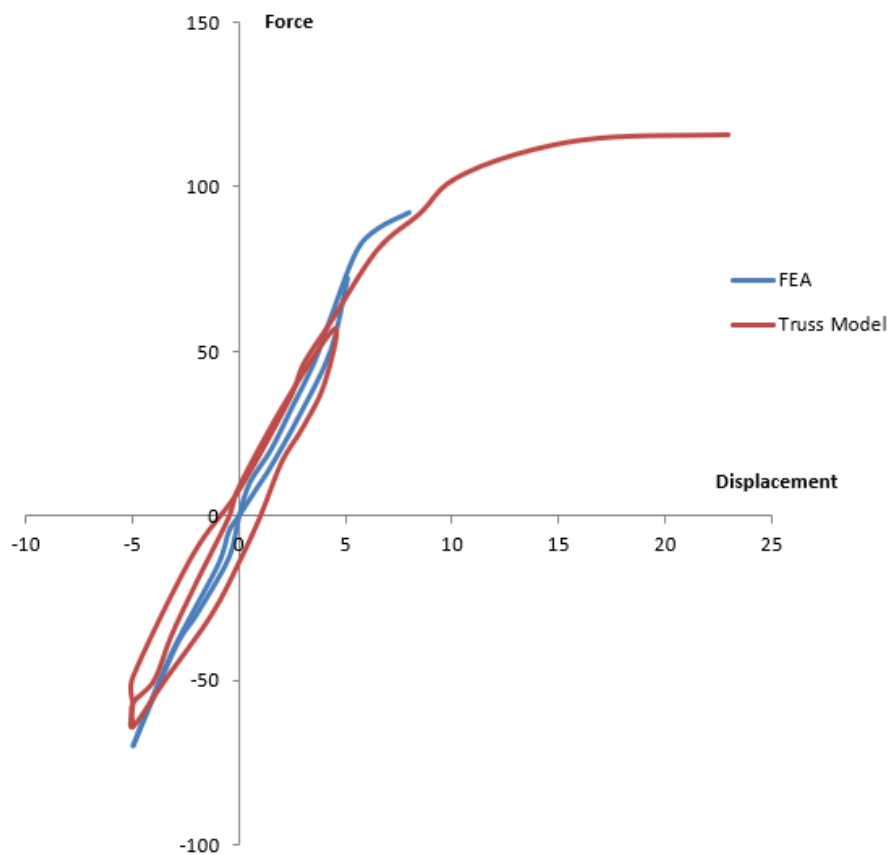


Figure 151. (a) Finite element and truss model results

Bibliography

- [1]. Experimental Study on the Cyclic Performance of Reinforced Concrete Shear Walls Exposed to Fire
- [2]. Ioannis Lefas, BEHAVIOUR OF REINFORCED CONCRETE WALLS AND ITS IMPLICATION FOR ULTIMATE LIMIT STATE DESIGN,
- [3]. Qing Zhi ,Zhengxing Guo, Quandong Xiao, Fu Yuan, Jingran Song Quasi-static test and strut-and-tie modeling of precast concrete shear walls with grouted lap-spliced connection
- [4]. Maria K. Kardala Student & Konstantinos V. Spiliopoulos, A More Realistic Estimation of Ductility in Reinforced Concrete Beams Through Three Dimensional Finite Elements
- [5]. M.R. Salamy, H. Kobayashi and Sh. Unjoh, EXPERIMENTAL AND ANALYTICAL STUDY ON RC DEEP BEAMS
- [6]. K.V. Spiliopoulos and G.Ch. Lykidis, An efficient three-dimensional solid finite element dynamic analysis of reinforced concrete structures
- [7]. Kotsovos M, Pavlovic M, Structural Concrete, Finite Element Analysis for Limit State Design. Thomas Telford: London, 1995.
- [8]. To1 , Sri Sritharan2 M.ASCE, Jason M. Ingham3 3 M.ASCE Nicholas H.T.To, Sri Sritharan M.ASCE, STRUT-AND-TIE NONLINEAR CYCLIC ANALYSIS OF CONCRETE FRAMES
- [9]. Vecchio, Frank J. and Collins, Michael P., The Modified Compression-Field Theory for reinforced concrete elements subjected to shear, ACI Journal, 1986, Vol.83, No.2, March-April, pp. 219-231.
- [10]. Chopra AK. Dynamics of Structures—Theory and Applications to Earthquake Engineering.
- [11]. James K White and James G MacGreror, Reinforced Concrete: Mechanics and Design
- [12]. K. J. Bathe, J. Walczak, A. Welch and N. Mistry, "Nonlinear analysis of concrete structures", *Computers & Structures*, 32(3/4):563-590, 1989
- [13]. M. D. Kotsovos and K. V. Spiliopoulos, "Modeling of crack closure for finite-element analysis of structural concrete", *Computers & Structures*, 69:383–398, 1998.
- [14]. A. Carpinteri, S. Valente, G. Ferrara and L. Imperato, "Experimental and numerical fracture modeling of a gravity dam", *Proceedings of the First International Conference on Fracture Mechanics of Concrete Structures* ed. Z. P. Bazant, 351-360, 1992.
- [15]. Marios Panagioyou Yuan Lu, Three-Dimensional Cyclic Beam-Truss Model for Nonplanar Reinforced Concrete Walls

- [16]. Aly Said, M. Elmersi and M. Nehdi, Nonlinear Model for Reinforced Concrete under Cyclic Loading
- [17]. Richard Fenwick and Rajesh P. Dhakal, Material Strain Limits for Seismic Design of Concrete Structures
- [18]. Park R. and Paulay T, Reinforced concrete, Published John Wiley and Sons, 1975.
- [19]. Popov, E. P. Bertero, V. V. and Krawinkler, H., Cyclic behaviour of three concrete flexural members with high shear, Earthquake Engineering Research Center, University of California, Berkeley, Report no. EERC 72-5, Oct. 1972.
- [20]. Vecchio, F. G. and Collins, M.P. (1986). The modified compression field theory for reinforced concrete elements subjected to shear, Journal of the American Concrete Institute, 83(2), 219-231.
- [21]. Panagiotou, M., Restrepo, J.I., Schoettler, M., and Kim G. (2012). Nonlinear cyclic truss model for reinforced concrete walls. ACI Structural Journal, 109(2), 205-214.
- [22]. Mergos PE, Kappos AJ. A (2008). A distributed shear and flexural flexibility model with shear–flexure interaction for R/C members subjected to seismic loading. Earthquake Engineering and Structural Dynamics, 37:1349–1370
- [23]. Filippou, F. C., Popov, E. P., and Bertero, V. V. (1983). Effects of bond deterioration on hysteretic behavior of reinforced concrete joints. Report EERC 83-19, Earthquake Engineering Research Center, University of California, Berkeley.
- [24]. Bazant, Z. P. and Planas, J. (1998). Fracture and size effect in concrete and other quasibrittle materials. Boca Raton, FL: CRC Press.
- [25]. Xu, S., and Zhang, J. (2011). Hysteretic shear–flexure interaction model of reinforced concrete columns for seismic response assessment of bridges, Earthquake Engineering and Structural Dynamics, 40:315-337.
- [26]. Park, H., and Eom, T. (2007). Truss model for nonlinear analysis of RC members subject to cyclic loading, Journal of Structural Engineering, 133(10), 1351-1363.
- [27]. Building Code Requirements for Structural Concrete (ACI 318-14)
- [28]. Eurocode 2: Design of concrete structures - Part 1-1 : General rules and rules for buildings
- [29]. Panagiotakos T, Fardis M. Deformations of reinforced concrete members at yielding and ultimate. ACI Struct J. 2001; 98(2): 135–148.

- [30]. [15] Code of Interventions (KAN.EPE.), Earthquake Planning and Protection Organization, Athens, 2017.
- [31]. Massone Sanchez, L. M. (2006). "RC Wall Shear—Flexure Interaction: Analytical and Experimental Responses." PhD thesis, University of California, Los Angeles, Los Angeles, CA, 398 pp.
- [32].Filippou, F. C., Popov, E. P., Bertero, V. V. (1983). "Effects of Bond Deterioration on Hysteretic Behavior of Reinforced Concrete Joints". Report EERC 83-19, Earthquake Engineering Research Center, University of California, Berkeley.
- [33]. Stevens, N. J., Uzumeri, S. M., Collins, M. P., and Will, T. G. (1991). "Constitutive model for reinforced concrete finite element analysis." *ACI Structural Journal*, 88(1), 49-59.
- [34].Mestyaneck, J. M. (1986). "The earthquake resistance of reinforced concrete structural walls of limited ductility." ME thesis. University of Canterbury.
- [35].Massone Sanchez, L. M. (2006). "RC Wall Shear—Flexure Interaction: Analytical and Experimental Responses." PhD thesis, University of California, Los Angeles, Los Angeles, CA, 398 pp.
- [36].Hoshikuma, J., Kawashima, K., Nagaya, K., and Taylor, A. W. (1997). "Stress-strain model for confined reinforced concrete in bridge piers." *Journal of Structural Engineering*, 123(5), 624-633.
- [37]. Beyer, K., Dazio, A., and Priestley, M. J. N.(2008). "Quasi-Static Cyclic Tests of Two U-Shaped Reinforced Concrete Walls." *Journal of Earthquake Engineering*, 12:7, 1023-1053.
- [38]. Lu, Y., Panagiotou, M, and Koutromanos, I. (2014). "Three-dimensional beam-truss model for reinforced concrete walls and slabs subjected to cyclic static or dynamic loading." Report PEER 2014/18, Pacific Earthquake Engineering Research Center, University of California, Berkeley, Berkeley, CA.
- [39]. ABAQUS/CAE User's Manual
- [40].AStrutTie2017, Strut-Tie Model Analysis/Design of Structural Concrete
- [41]. Schlaich, J.; Schaefer, K.; and Mattias, M., "Toward a Consistent Design of Structural Concrete," *Special Report of PCI Journal*, V. 32, No. 3, 1987, pp. 75-150.
- [42]. Zimmerman, R. B., Panagiotou, M., Mahin, S. (2013). Numerical Modeling and Seismic Retrofit for Shear Failure in Reinforced Concrete Columns. UCB/SEMM Report 2013/03 Earthquake Engineering Research Center, University of California, Berkeley.
- [43].Xu,S., and Zhang, J. (2011). Hysteretic shear–flexure interaction model of reinforced concrete columns for seismic response assessment of bridges, *Earthquake Engineering and Structural Dynamics*, 40:315-337.
- [44]. Stevens, N. J., Uzumeri, S. M., Collins, M. P., and Will, T. G. (1991). Constitutive model for reinforced concrete finite element analysis, *ACI Structural Journal*, 99 (10), 2109-2122.

- [45]. Sezen, H., and Moehle, J. (2006). Seismic tests of concrete columns with light transverse reinforcement, *ACI Structural Journal*, 103 (6), 842-849.
- [46]. Priestley, M. J. N., Seible, F., Xiao, Y., and Verma, R. (1994). Steel jacket retrofitting of reinforced concrete bridge columns for enhanced shear strength – Part 1: Theoretical considerations and test design , *ACI Structural Journal*, 91 (4), 394-405.
- [47]. Park, H., and Eom, T. (2007). Truss model for nonlinear analysis of RC members subject to cyclic loading , *Journal of Structural Engineering*, 133(10), 1351-1363.
- [48]. Kim, J. H., and Mander, J. B. (1999). Truss modeling of reinforced concrete shear – flexure behaviour, MCEER Report 99-0005, University at Buffalo, State University of New York.
- [49]. Lee, D. H., and Alnashai, A. S. (2001). Seismic analysis of RC bridge columns with flexure-shear interaction, *Journal of Structural Engineering*, 127(5), 546:553.
- [50]. Lodhi, M. S., and Sezen, H. (2012). Estimation of monotonic behavior of reinforced concrete columns considering shear-flexure-axial load interaction, *Earthquake Engineering and Structural Dynamics*, 41:2159- 2175.
- [51]. https://opensees.berkeley.edu/wiki/index.php/Truss_Model_Example_-_Squat_RC_Wall
- [52]. 51. Bentz, E. C., “Explaining the Riddle of Tension Stiffening Models for Shear Panel Experiments,” *Journal of Structural Engineering*, ASCE, V. 114, No. 9, 2005, pp. 1422-1425.
- [53]. https://opensees.berkeley.edu/wiki/index.php/Truss_Model_Example_-_Squat_RC_Wall
- [54]. https://opensees.berkeley.edu/wiki/index.php/Truss_Element
- [55]. https://opensees.berkeley.edu/wiki/index.php/Steel02_Material_-_Giuffr%C3%A9-Menegotto-Pinto_Model_with_Isotropic_Strain_Hardening